



Peptidoglycan Synthesis and Rod Shape Maintenance in Mycobacteria

Permanent link

<http://nrs.harvard.edu/urn-3:HUL.InstRepos:40050005>

Terms of Use

This article was downloaded from Harvard University's DASH repository, and is made available under the terms and conditions applicable to Other Posted Material, as set forth at <http://nrs.harvard.edu/urn-3:HUL.InstRepos:dash.current.terms-of-use#LAA>

Share Your Story

The Harvard community has made this article openly available.
Please share how this access benefits you. [Submit a story](#).

[Accessibility](#)

HARVARD UNIVERSITY

Graduate School of Arts and Sciences



DISSERTATION ACCEPTANCE CERTIFICATE

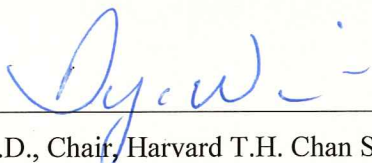
The undersigned, appointed by the
Committee on Higher Degrees in Biological Sciences in Public Health
have examined a dissertation entitled

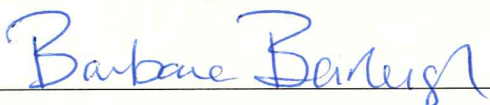
“Peptidoglycan Synthesis and Rod Shape Maintenance in Mycobacteria”

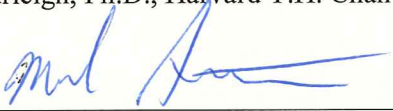
presented by

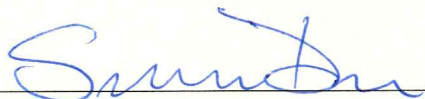
Catherine Baranowski

candidate for the degree of Doctor of Philosophy
and hereby certify that it is worthy of acceptance.

Signature 
Dr. Dyann Wirth, Ph.D., Chair, Harvard T.H. Chan School of Public Health

Signature 
Dr. Barbara Burleigh, Ph.D., Harvard T.H. Chan School of Public Health

Signature 
Dr. Michael Starnbach, Ph.D., Harvard Medical School

Signature 
Dr. Simon Dove, Ph.D., Harvard Medical School

Date: April 2, 2018

Peptidoglycan Synthesis and Rod Shape Maintenance in Mycobacteria

A dissertation presented

by

Catherine Baranowski

to

The Committee on Higher Degrees in Biological Sciences in Public Health

in partial fulfillment of the requirements

for the degree of

Doctor of Philosophy

in the subject of

Biological Sciences in Public Health

Harvard University

Cambridge, Massachusetts

April 2018

© Catherine Baranowski
All rights reserved.

Peptidoglycan Synthesis and Rod Shape Maintenance in Mycobacteria

Abstract

Bacteria surround themselves with a cell wall whose foundation is a layer called peptidoglycan. Peptidoglycan is a mesh of linear glycan strands that are linked together by short peptide side chains. As a crucial bacterial polymer, peptidoglycan is the target of numerous antibiotics. My thesis has focused on features of peptidoglycan in mycobacteria, a genus including the formidable human pathogen *Mycobacterium tuberculosis*.

In comparison to other well-studied rod-shaped bacteria like *Escherichia coli* and *Bacillus subtilis*, mycobacteria are unique. First, the peptidoglycan of mycobacteria is highly enriched for specific linkages called 3-3 crosslinks. Second, mycobacteria grow via insertion of new peptidoglycan at the poles of the bacillus. This occurs at unequal rates depending on the age of the pole. While the lateral mode of growth in *E. coli* and *B. subtilis* ensures that new and old cell wall are constantly intermingled, mycobacterial polar growth segregates peptidoglycan by age whereby the newest material is at the poles and the oldest material is located toward mid-cell.

L,D-transpeptidases are PG synthesis enzymes that catalyze 3-3 crosslinks. As these crosslinks are rare in the model bacterial species from which we have garnered much of our knowledge about peptidoglycan, the role of this crosslink is not well understood. I discovered that 3-3 crosslinks are required to maintain rod shape at sites of aging cell wall in *Mycobacterium smegmatis*. Moreover, I found that uneven polar growth, and the subsequent spatial segregation of aging peptidoglycan, leads to an asymmetric distribution of peptidoglycan chemistries and enzymes, like penicillin binding proteins and L,D-transpeptidases, within a

single cell. Lastly, I demonstrated that in the absence of L,D-transpeptidases, mycobacterial cells rely more heavily on penicillin binding proteins, peptidoglycan synthases that catalyze 4-3 crosslinks.

Current first line therapies for tuberculosis target the mycobacterial cell wall, however they do not yet target the peptidoglycan layer. Non-carbapenem β -lactams (with β -lactamase inhibitors) and carbapenems, drugs that inhibit peptidoglycan synthases like penicillin binding proteins and L,D-transpeptidases, have garnered recent interest for the treatment of tuberculosis. My work on the spatial and genetic relationship between penicillin binding proteins and L,D-transpeptidases suggests details on the mechanism by which the combination of these antibiotics may kill tuberculosis faster than these drugs do alone. As resistance to current tuberculosis therapies continues to be a problem, it is critical that we gather mechanistic insights into the action of therapies to both aid in the rational combination of drugs, and to prepare ourselves for the putative mechanisms of resistance that will likely arise.

Table of Contents

Title page.....	i
Copyright page	ii
Abstract	iii
Table of Contents.....	v
Dedication	vii
Acknowledgements.....	viii
Chapter 1: Introduction.....	1
Section 1.1 The dream of a mycobacterium- a review of mycobacterial cell division.....	2
Section 1.2 References	29
Chapter 2: Identifying mycobacterial divisome factors	40
Section 2.1 Characterization of novel and conserved septal factors in <i>Mycobacterium smegmatis</i>	41
Section 2.2 Materials and methods.....	66
Sections 2.3 References.....	71
Chapter 3: Mycobacterial peptidoglycan synthesis and the role of L,D- transpeptidase mediated crosslinks in rod shape maintenance	79
Section 3.1 Overview of peptidoglycan synthesis and L,D-transpeptidases in mycobacteria	80
Section 3.2 Maturing mycobacterial peptidoglycan requires non-canonical crosslinks to maintain shape	87

Section 3.3 Characterization of fluorescent D-amino acid probes in <i>Mycobacterium smegmatis</i>	100
Section 3.4 Materials and methods	107
Section 3.5 References	119
Chapter 4: Pathways and networks of peptidoglycan synthesis in <i>Mycobacterium tuberculosis</i>	128
Section 4.1 Peptidoglycan synthesis in <i>Mycobacterium tuberculosis</i> is organized into networks with varying drug susceptibility	129
Section 4.2 Materials and methods	151
Section 4.3 References	155
Chapter 5: Discussion	159
Section 5.1 Abstract	160
Section 5.2 Summary of results and implications for understanding and targeting mycobacterial growth	161
Section 5.3 Future Directions	171
Section 5.4 References	186
Appendices	193
Appendix 1: Supplementary data for Chapter 3	194
Appendix 2: BlaR, a protein canonically implicated in β -lactam sensing, is critical for <i>Mycobacterium tuberculosis</i> fitness in low iron conditions	215

Dedication

My thesis is dedicated to my parents, Tosiek and Ela, whose constant barrage of homemade smoked meat and various pickled delights helped me make friends and kept me more than well fed throughout my PhD.

Acknowledgements

I need to start by acknowledging Dr. Eric Rubin, my thesis advisor, for his scientific mentorship and emotional support. Eric, beyond the science, you've given me an example of someone who is endlessly generous and caring. And, you've helped me master word puns! It has been a privilege being in your lab. Thank you!

I want to thank the Rubin lab, past and present, for creating an intellectually stimulating, supportive and ridiculously funny environment to work in. I want to acknowledge Cara, Karen, Justin and Andrej for their guidance as well as Skye and Jeff for being hilarious. I would like to thank Hesper for taking me under her wing. Hesper, your mentorship has been invaluable.

Thank you to the Bernhardt, Rudner, Hochschild, Kolter, Beckwith, Fortune and Walker labs. Every time I walked into these labs, I could find whatever help I was looking for. The generosity of the scientists I have been surrounded by has taught me that kindness is the most valuable currency.

My dissertation advisory committee members have been incredibly helpful throughout the years. Thank you to Dr. Matthew Waldor, Dr. Thomas Bernhardt and Dr. Dyann Wirth. I would to thank my defense committee, Drs. Dyann Wirth, Simon Dove, Barbara Burleigh and Michael Starnbach for their time and effort. Thank you to Deirdre and Andi for your support!

Thank you to all of my friends - your support has meant so much to me. Thank you to fellow BPHers- Jemila, Lear, Perrine and Sheena. And, to my 'phages crew'- your friendship brings me joy.

Finally, I want to thank my family. My parents, Ela and Tosiek, deserve all the credit. Thank you to Monika, Brad, Danny and Catie for your love and support. Lastly, thank you to Pusia for always splitting a chicken finger sub with me.

Chapter 1: The dream of a mycobacterium- a review of mycobacterial cell division and growth

Section 1.1: The dream of a mycobacterium

Overview: This chapter consists of a review written as a book chapter/*Microbiology Spectrum* article for "Gram-Positive Pathogens, Third Edition" published by ASM press.

Attributions: CB wrote this manuscript with significant input and editing from EHR and EJR.

Catherine Baranowski¹, E. Hesper Rego² and Eric J. Rubin^{1,3,*}

¹ Department of Immunology and Infectious Disease, Harvard T. H. Chan School of Public Health, Boston, MA 02115

² Department of Microbial Pathogenesis, Yale University School of Medicine, New Haven, Connecticut, 06510

³ Department of Microbiology and Immunobiology, Harvard Medical School, Boston, MA 02115

* Corresponding author: erubin@hsph.harvard.edu

Abstract

How do mycobacteria, a genus including the human pathogens *M. tuberculosis* and *M. leprae*, divide? While cell division has been studied extensively in the model rod-shaped bacteria *Escherichia coli* and *Bacillus subtilis*, much less is understood about mycobacterial cell division. Bacterial cell division requires cell elongation, chromosome replication and segregation, construction of a septal wall, and the subsequent splitting of that wall to create two daughter cells. Here, we describe distinct stages of cell division in *Bacillus subtilis* and follow with the current knowledge of this process in mycobacteria. Mycobacteria are quite different than *Bacillus subtilis*

and thus, for many described proteins in BS, mycobacteria either lack homologues or use unique factors and protein interactions to fill these voids. So, while the fundamental challenge of spatially and temporally organizing cell division is shared between these rod-shaped bacteria, the approach taken to address this challenge can be vastly distinct.

Introduction

“A toutes ces activités, il faut une cohésion rigoureuse pour que puisse se réaliser **le rêve de la bactérie: produire deux bactéries.**” [*To all these activities, it takes a rigorous cohesion to realize the dream of the bacterium : produce two bacteria.*] -- François Jacob, 1965 (1)

Bacterial psychology is a challenging field. Like many psychologists, Jacob impressed the bacterium with our own value system. And part of that is defining what it is to be alive. As microbiologists we generally define bacterial life as the ability to form progeny, to become two bacteria through cell division. Like all reproductive processes, bacterial division uses a combination of mechanics and mystery. Here we will focus on the mechanics (and mystery) of cell division in acid-fast mycobacteria, a genus that includes the major human pathogens *M. tuberculosis* and *M. leprae*.

From the 1968 study where Hirota, Ryter and Jacob classified temperature sensitive mutants blocked for various steps of cell division in *Escherichia coli* (2), to the discovery of the FtsZ ring (Z-ring) in 1991 by Bi and Lutkenhaus, microbiologists have launched into an era of genetic, microscopic, biochemical and structural work to understand bacterial cell growth and division (3). (For a review on the history of cell division research see (4)). This topic has been studied most in the model rod-shaped bacteria - the Gram-negative *E.coli* and the Gram-positive *Bacillus subtilis* (BS). Work on cell growth and division in mycobacteria is not as extensive as in

E.coli or BS. However, mycobacteria face the same challenge as these other organisms: organizing, both spatially and temporally, the factors that are responsible for making two cells from one. This process requires the concerted effort of many molecules to elongate the cell, replicate and separate the chromosome, build the septal cell wall that separates the two daughter cells, and separate the now distinct daughter cells. As you will see in this chapter, one common theme in the nascent field of mycobacterial cell division is that mycobacteria have often solved these challenges differently, sometimes, vastly so, than either *E.coli* or BS.

We will take a comparative approach. Throughout this chapter, we will describe distinct stages of cell division in *Bacillus subtilis* (BS) and follow with the current knowledge of this process in mycobacteria. Mycobacteria are quite different than BS and for many described proteins in BS, mycobacteria either lack homologues or use unique factors and protein interactions to fill these voids.

Cell elongation and division are intimately associated processes that require both synthesis and remodeling of the complex mycobacterial cell wall. The mycobacterial cell wall consists of covalently linked layers of fatty acids (mycolic acid), a carbohydrate polymer known as arabinogalactan, and an inner-most layer of peptidoglycan (PG) (5). The envelope of most other bacteria, like BS, is comprised of PG but these other polymers are unique to mycobacteria and related bacteria. We favor a model whereby the synthesis and remodeling of the distinct layers is coordinated, but there is currently little direct evidence to support this model.

Mycobacterial growth: a different ballgame

The first obvious difference between BS and mycobacteria is in the geometry of cell division. To increase in size, mycobacteria insert new wall at or near their poles, rather than along

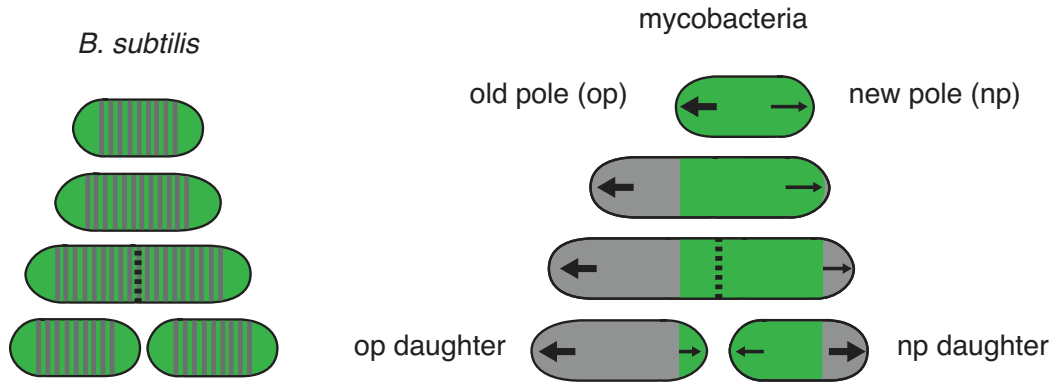


Figure 1.1: Characteristics of growth and division in *B. subtilis* and mycobacteria

Bacillus subtilis grows by adding new cell wall along the lateral cell body, here marked with grey lines. Mycobacteria grow only at the polar regions, and do so at unequal amounts depending on the identity (age) of the pole. This is observed by using a cell wall dye (green) to stain existing cell wall and observe outgrowth of newly synthesized, unstained cell wall (7). Arrows=location of new cell wall synthesis; black dotted line= septum; green portion=dye stained (old) cell wall, grey portion=location of new growth.

their side walls (Figure 1.1) like BS and *E.coli*. However, where *exactly* cell wall synthesis is occurring is still unclear. Many cell wall synthetic enzymes localize to the peri-polar region (6), but pulse chase experiments with dyes that covalently bind the cell wall suggest that that new cell wall material is being inserted at the very distal end of the cell (Figure 1.2 bottom panel) (7). Supporting this last observation are labeling experiments with dyes that incorporate into different layers of the cell wall via enzymatic processes. These dyes brightly label the cell poles (8-10) (Figure 1.2 top panel), as does a fluorescent analog of vancomycin (11, 12) which labels unprocessed, un-crosslinked PG. Thus, it seems most likely that mycobacteria insert new cell wall at the distal ends of the poles. But how that is coordinated by enzymes that are most abundant at adjacent cellular regions will need to be reconciled in future research.

In general, polar growth leads to a different set of challenges not encountered by side-wall growers. First, the site of division in pole growers will become the site of elongation. This means that division and elongation might need to be more tightly controlled temporally in mycobacteria than in BS, so that growth from the new poles does not occur before the cells completely divide.

This raises a question: are the components of the mycobacterial division complex (divisome) distinct from those of the elongation machinery (elongasome)? Throughout this review, you will see that mycobacterial cells blocked in certain points of division are elongated and form ectopic poles suggesting that division and elongation can be uncoupled. This doesn't necessarily mean that the divisome and elongasome contain mutually exclusive proteins, however it does support a model where division and elongation are temporally, and potentially spatially, separate. Therefore, assigning proteins to either the divisome or elongasome based on localization at a single time-point could be misleading, as factors involved in elongation will also localize to the site of division/new pole.

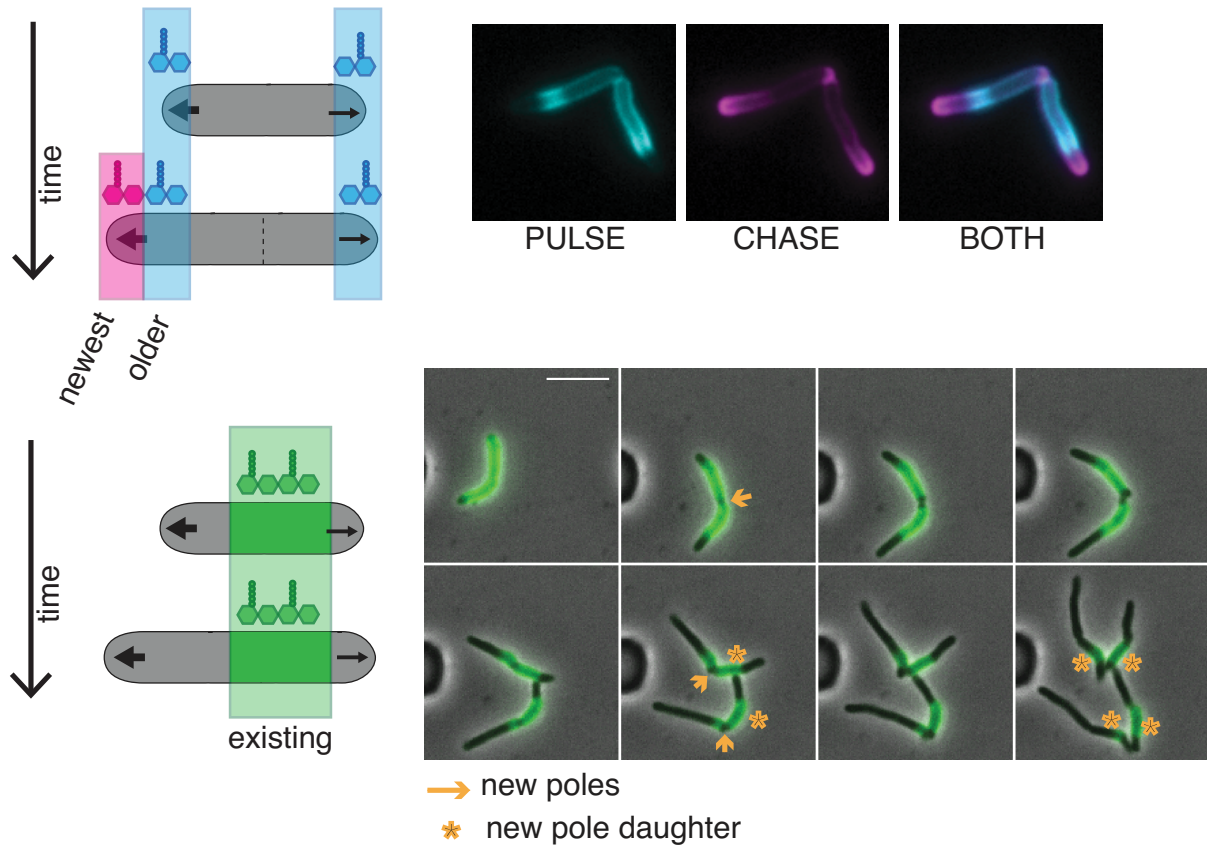


Figure 1.2: Polar growth segregates the cell wall based on age

(TOP) Fluorescent D-amino acids are thought to incorporate into nascent PG. Pulse chase with these FDAAs (shown in magenta and cyan) illustrates how new and old cell wall are spatially segregated in *M. smegmatis*. (Baranowski, Rego, and Rubin - unpublished images). Cells were pulsed with the first FDAAs (cyan), allowed to grow out, then chased with the second FDAAs (magenta). (BOTTOM) Alexa-488 NHS ester stains the existing cell wall (green). New cell wall is unstained and can be monitored using time-lapse microscopy. After 2 divisions, the oldest cell wall is inherited by the new pole daughter cells (marked with an orange asterisk) in *M. smegmatis*. (Baranowski, Rego, and Rubin - unpublished images, 7). New poles are highlighted with an orange arrow.

Second, polar growth leads to the spatial segregation of cell wall with different ages while lateral cell growth leads to the mixing of new and old material (7, 10, 13) (Figure 1.2). In *M. smegmatis*, it has been shown that the daughter cell inheriting the pole created at the most recent division, the so-called new pole, inherits the oldest cell wall (7) (Figure 1.2 bottom panel). The functional consequence of this remains unknown, however it may contribute to the distinct characteristics of the daughter cells.

Lastly, the manner by which mycobacteria maintain rod shape in the face of turgor pressure must be completely different than in the model rod-shaped organisms BS and *E. coli*. In BS, MreB, a homolog of eukaryotic actin, dictates the location of new cell wall synthesis along the side wall, incorporating new material at sites of negative curvature to aid in rod shape maintenance as the cell grows (14). This rod shape propagates in an MreB dependent manner along the greatest membrane curvature (circumferentially around the cell) (15). Not only do mycobacteria lack an obvious homolog of MreB, they also grow from a much smaller portion of the cell (11). It remains a mystery how cell shape can be maintained across the entire cell. However, we do have a few clues. Mycobacteria encode a homolog of BS DivIVA called Wag31. In BS, depletion of DivIVA results in elongated cells that cannot divide, indicating a role in division (16). In contrast, depletion of Wag31 in mycobacteria leads to cells that lose their rod shape first at the pole, and eventually throughout the entire cell, resulting in a spherical cell. Further, dysregulation of Wag31 results in polar growth from incorrect sites (6). Thus, it appears that Wag31 in mycobacteria works to establish the site of polar growth, unlike its counterpart in BS which has a role in dictating septum placement. Additionally, depletion of enzymes responsible for synthesizing or remodeling PG result in loss of rod shape either at the cell poles (17, 18) or along mid-cell (6). So, it may be that Wag31 is responsible for directing formation of the poles, and that the structure and rigidity of the

cell wall itself, established at the time of cell wall synthesis at the pole, aids in shape maintenance as the cell grows.

The mystery and mechanics of division

Once a cell grows, it must divide to make two cells. The factors involved in cell division are referred to collectively as the divisome, and they work in concert at mid-cell. The purpose of the divisome is to (1) identify mid-cell for Z-ring placement; (2) recruit Z-ring anchors, stabilizers and regulators; (3) build the septal cell wall; and, (4) split the two halves of the partitioned cell. The bacterial chromosome must be replicated and segregated in concert with cell division; however, this process will not be covered in this review.

Identifying mid-cell for Z-ring placement

FtsZ, a tubulin homolog, polymerizes into a ring (Z-ring) at mid-cell via GTP hydrolysis to begin cell division (3) (reviewed in (19)). The mid-cell placement and stabilization of the Z-ring are the critical first stages of bacterial cell division. Recent work using metabolic labeling of PG, the crucial inner-most cell wall layer, as well as fluorescent fusions to FtsZ and other well-characterized septal proteins in BS shows that FtsZ treadmilling directs septal synthesis in an inward-spiral fashion (you can also imagine a bullseye) (20). Thus, the Z-ring is the figurative and literal ringleader of bacterial cell division. Once placed, the Z-ring recruits a cascade of factors, both structural and enzymatic, required for both synthesizing and splitting the septum (which will become the new cell poles) to create two daughter cells. (For review of FtsZ see-(19, 21).)

(An (a)side on (a)symmetry). BS grows along the lateral cell body and divides at mid-cell with striking precision (22), resulting in two nearly identical daughter cells. On the other hand,

many observers (though not all) have observed that, on average, mycobacteria grow asymmetrically, with growth occurring in unequal amounts from the two poles (5). Multiple reports show that the old pole continues to grow during and after septation, but that the new pole - the pole established at septation - takes some time before it grows. Thus, the overall amount of elongation from the poles in one cell cycle is different. This can easily be visualized by staining existing cell wall with a dye and following the outgrowth of new, unstained cell wall (6, 7, 23, 24). Likewise, the amount of incorporated PG-specific fluorescent D-amino acids supports this finding (10) (Figure 1.2). While the total amount of growth appears different between the poles, the *rate* of cell wall addition may be the same between the poles at the end of division (10, 25, 26).

Besides potential differences in growth from the distinct poles, divisome placement may also be asymmetric. Fluorescent fusions to FtsZ show septal placement in mycobacteria occurs over a range of mid-cell, skewed toward the new pole (26-28). As a result of asymmetry in growth and Z-ring placement, mycobacterial daughter cells are phenotypically distinct – cells inheriting the new pole are smaller while old pole daughters are larger (5). The consequences and molecular details of this heterogeneity are poorly understood. Recently however, a mycobacterial specific protein, LamA (Loss of Asymmetry Mutant A) was found to actively promote asymmetry by inhibiting growth at the new pole (23). Loss of LamA leads to a population of cells that can be more uniformly killed by certain antibiotics suggesting that heterogeneity generated through cell growth and division confers a survival advantage in some conditions.

Identifying mid-cell for Z-ring placement (continued)

FtsZ is highly conserved in all bacteria, including mycobacteria. One unique feature of mycobacterial FtsZ is that its polymerization can be inhibited, at least *in vitro*, via phosphorylation

by the serine/threonine protein kinase, PknA (29, 30). In general, phosphorylation by PknA and PknB, both of which are essential for growth, plays a key role in regulating many mycobacterial divisome components. Depletion of either of these kinases results in elongated cells, implying a defect in division (31). Throughout this review, we will highlight specific ways in which division is regulated via phosphorylation by these kinases.

Where not to put the Z-ring: over the chromosome and at the poles. [See also (32)]. Division occurring over the chromosome is lethal, and creation of a daughter cell without DNA is not useful. Therefore, mechanisms exist to prevent Z-ring formation over the chromosome and at the poles. BS has two systems that prevent Z-ring formation from occurring at these non-optimal locations – Noc and Min. The Noc protein (nucleoid occlusion) binds along the chromosome, avoiding the replication terminus (which ends up orienting at mid-cell) (32). It then spreads from primary sites and associates with the membrane to inhibit Z-ring formation over the nucleoid (32). The Min system prevents the Z-ring from forming at the poles. The BS Min system is comprised of MinC, D J and DivIVA. MinC is recruited and activated by membrane bound MinD, to interact with and inhibit FtsZ. This MinCD complex is recruited to the poles by the DivIVA interacting partner, MinJ (33). DivIVA is believed to localize to septum/new pole late during division (at sites of negative membrane curvature) where it begins the recruitment of the Min system (34). To date, the mycobacterial DivIVA homolog, Wag31, has no described function in septal placement and, instead, functions in late septation/early pole establishment through interactions with non-Min related septal and polar machinery.

Mycobacteria do not have a known Noc homologue, and there has been only one report of a single Min protein distantly related to MinD (Ssd). Cells over-expressing *ssd* are longer and

transcriptional profiling shows numerous genes involved in growth and division to be repressed (35). However, we do not yet know whether this protein acts in a system akin to BS Min.

While the exact molecular mechanism of septal placement in mycobacteria remains unknown, it appears that the mycobacterial cell wall again plays a role. A recent study utilizing atomic force microscopy identified troughs on the mycobacterial cell surface that formed at the poles and, eventually, became the sites of division one or two generations later. This suggests that potential Z-ring placement sites are created and inherited well before division has begun, the earliest described marker of Z-ring placement in bacteria to date. The nature of the troughs and the mechanism of their formation are not yet known, but this might represent a novel Z-ring placement strategy in bacteria (28).

Recruitment of Z-ring anchors, stabilizers and regulators

FtsZ resides in the cytoplasm yet must trigger events occurring outside of the plasma membrane. Accordingly, it must be anchored to the membrane, an action achieved through various “early” interacting proteins. Once the Z-ring is anchored, the septal wall must be synthesized and daughter cells must then be split. Thus, the “late” divisome is comprised of structural proteins that recruit PG synthesis enzymes, and these enzymes themselves. While in BS, there is clear distinction between the early and late divisome, ~20% of the cell cycle passes between recruitment of these portions of the complex, this distinction is less well defined in mycobacteria but only perhaps due to lack of data (36).

Early divisome. The goal in the early steps of divisome assembly is to help the Z-ring polymerize and to anchor it to the membrane. The FtsZ ring is dynamic and requires both stabilizing and de-stabilizing proteins to function most properly (21). Division in BS begins with

Z ring formation at mid-cell which recruits FtsA (37), SepF, ZapA and EzrA (21). FtsA, an actin homolog, and SepF help anchor the Z-ring to the membrane (21). ZapA interacts with FtsZ and promotes its polymerization and stability (21, 32). A mutant of the transmembrane protein EzrA produces extra Z-rings (hence the name). The resultant mutant cells are longer, suggesting negative regulation of the Z-ring by EzrA is necessary for successful division. This protein has been shown to inhibit Z-ring polymerization *in vitro* (21, 34). EzrA also works to recruit PBP1, a PG synthase to the divisome (38).

Thus far, only SepF from BS's early, FtsZ-interacting, divisome has been identified in mycobacteria. BS SepF localizes to the septum in an FtsZ-dependent fashion, and anchors and stabilizes the Z-ring (21, 39). In addition, in BS, *sepF* is synthetically lethal with *ftsA* and *ezrA*, perhaps due to overlapping functions (21). Likewise, mycobacterial SepF localizes to the septum in an FtsZ-dependent manner. Depletion and over-expression of *sepF* leads to filaments and branching – canonical phenotypes of cell division inhibition in mycobacteria (39).

In BS, ClpX, the ATPase chaperone/substrate recognition portion of the ClpXP protease, inhibits FtsZ assembly. Intriguingly, this appears independent of its ATPase function (40, 41). Similarly, mycobacterial ClpX interacts directly (*in vivo*) and inhibits FtsZ polymerization (*in vitro*). Over-expression of ClpX leads to multi-nucleate, elongated cells suggesting a defect in septal assembly and division (42).

Connecting the cytoplasmic steps to the periplasmic steps. After the early BS divisome is assembled (the Z-ring anchored and stabilized), “late” divisome proteins are recruited (43). These proteins connect the cytoplasmic steps of division to the periplasmic steps required to build the septal cell wall (reviewed in (21)). To summarize decades of work briefly: a complex of structural proteins – FtsQ (DivIB), FtsL and FtsB (DivIC), transmembrane proteins that are critical

in connecting Z-ring formation to septal synthesis – as well as FtsW, a PG transglycosylase, localize to the septum to recruit other PG synthases. The timing and dependency of septal protein localization in BS reveals interdependency between members of the QLB complex, FtsW and Pbp2B (a monofunctional PG transpeptidase) (36). This is in contrast to the more linear dependency of localization in *E.coli*: FtsK->FtsQLB->FtsW->PBP3 (34).

Mycobacterial homologs of the essential *ftsL* and *ftsB* have been identified and experimentally validated through localization, depletion and *in silico* structural predictions (44). Intriguingly, these homologs have substantial N- and C-terminal expansions compared to their BS counterparts, presumably for mycobacterial specific interaction partners. In mycobacteria, depletion of either *ftsL* or *ftsB* causes cells to filament and branch, a phenocopy of known septal protein depletions (*ftsZ*, *pbpB*). FtsL and B, along with FtsQ and FtsK (a DNA translocase), localize to the septum. Depletion studies allow inferred localization dependencies of these structural divisome components in mycobacteria. Localization of FtsK, FtsQ, FtsL or FtsB depend upon FtsZ. FtsK localization does not require FtsQ, L or B. FtsQ can partially localize in the depletion of FtsL or FtsB supporting a preliminary dependency hierarchy: FtsZ->FtsK->FtsQ->FtsLB (44). Thus, finding counterparts to known BS divisome members provides a handle to identify and study previously uncharacterized mycobacterial-specific divisome proteins (Figure 1.3, brown dashed lines) .

One potential mycobacterial “work-around” in the absence of canonical Z-ring anchors like FtsA is the unique interaction between mycobacterial FtsZ and FtsW. FtsW is the divisome-specific homolog of the SEDs (shape, elongation, division, sporulation) family protein RodA, whose function is to polymerize glycan strands of PG through its transglycosylase function (45). Mycobacterial FtsW and FtsZ have non-canonical C-terminal extensions that are proposed to

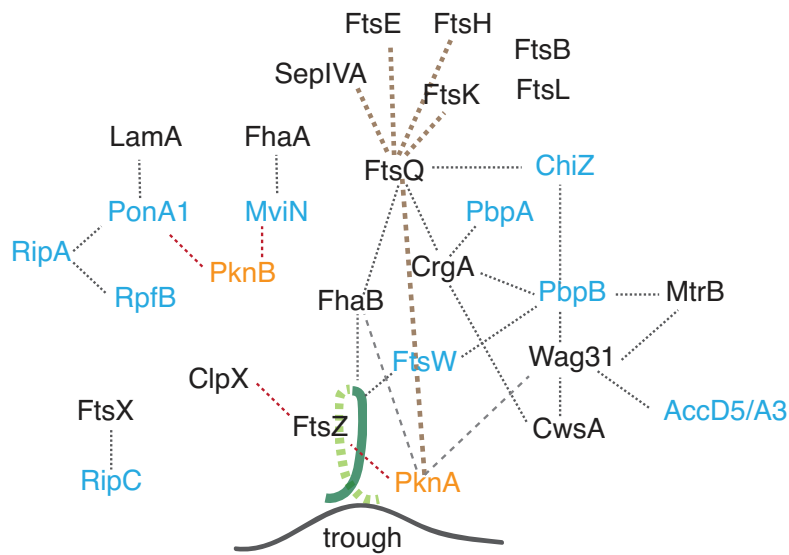


Figure 1.3: Mycobacterial divisome interactions

A schematic of mycobacterial divisome protein interactions. Note that interactions are not necessarily direct given the available data. Grey dotted lines=physical interactions; Red dotted lines= negative regulation; Brown lines=FtsQ pulldown proteins (44); Blue text= Cell wall enzymes; Orange text=kinases.

facilitate their interaction (46). They localize at the septum in a manner suggesting that FtsZ localizes before FtsW (47). FtsW also interacts with and appears to recruit PbpB, a monofunctional PG transpeptidase, to the septum (48). In cells depleted for FtsW, FtsZ localizes between nucleoids, but these cells are not proficient at division (48). By interacting with early divisome founding FtsZ and late divisome septal PG synthase PbpB, FtsW appears to link beginning cytoplasmic steps with late periplasmic wall synthesis steps in mycobacteria.

In actinomycetes, the cascade of interactions is facilitated by the small transmembrane protein, CrgA. CrgA is involved in nearly all steps of cell division: from the start of division, to septal wall synthesis, to establishment of the new growth poles. CrgA interacts with FtsZ, and two PG transpeptidases, PbpA and PbpB. It localizes to the septum after the Z-ring and may be required for proper recruitment of PbpB, similarly to FtsW (49). CrgA also interacts with the mycobacterial specific CwsA, a transmembrane protein that interacts with Wag31 (50). Expression of *cwsA* is directly linked to Wag31 abundance at poles, suggesting it is an important factor in either recruiting or maintaining Wag31 at the poles. (50) Since Wag31 is associated with new polar growth, the information flow from CrgA through CwsA to Wag31 may coordinate establishing the new pole at the site of division.

Another transmembrane protein, FhaB, (also called FipA) interacts with FtsZ. This relationship depends on phosphorylation of FhaB by PknA. FhaB is required for interactions between FtsZ and FtsQ during oxidative stress, a condition that pathogenic mycobacteria experience in the host, suggesting that it may be a signal transducing interaction between the Z-ring and the structural divisome protein FtsQ during intracellular division (5, 30).

While these examples are understood in some detail, several other proteins produce morphologic changes when disrupted. Loss of proteins such as the *whiB2* homolog *whmD*, and the

MinD like protein Ssd result in branching and chaining morphologies, phenotypes associated with disrupted cell division (35, 51). The functions of these proteins remain unknown.

Call to arms: septal cell wall synthetic machinery to build a wall

Constructing the septal wall. Division requires synthesis of a wall between two halves of the cell and physical separation of the two halves into independent daughter cells. The cell wall of mycobacteria is multi-faceted, consisting of linked layers of peptidoglycan (PG), arabinogalactan (AG) and mycolic acids (MA) (5). The coordination between layers seems likely, however evidence for this is currently slim. The discussion of septal cell wall synthesis will focus on the peptidoglycan layer.

PG, a netlike structure comprised of disaccharide chains crosslinked by peptide bridges, is located outside of the plasma membrane. PG synthesis begins in the cytoplasm where the disaccharide backbone and pentapeptide side chain are linked to a lipid and flipped across the membrane by the lipidII flippase, MurJ (MviN, in mycobacteria) (52) (Figure 1.4). This unit is added to the existing glycan strand by the transglycosylase function (TG) of bi-functional penicillin binding proteins (“class A PBPs” or aPBPs) and by SEDS proteins like RodA (45, 53). To covalently close the PG network into a cage-like molecule, the peptide bridges are cross-linked between either the 4th and 3rd (4-3) or the 3rd and 3rd (3-3) residues of opposite PG strand. 4-3 crosslinks, those commonly found in most well studied PG, are catalyzed by the transpeptidation (TP) function of aPBPs and/or by mono-functional class B PBPs (bPBPs), which possess only transpeptidase activity(53). 3-3 crosslinks, a variety of connection rare in the PG of other model rods but highly enriched in mycobacteria, are made by L,D-transpeptidases (5, 54, 55). (Figure 1.4)

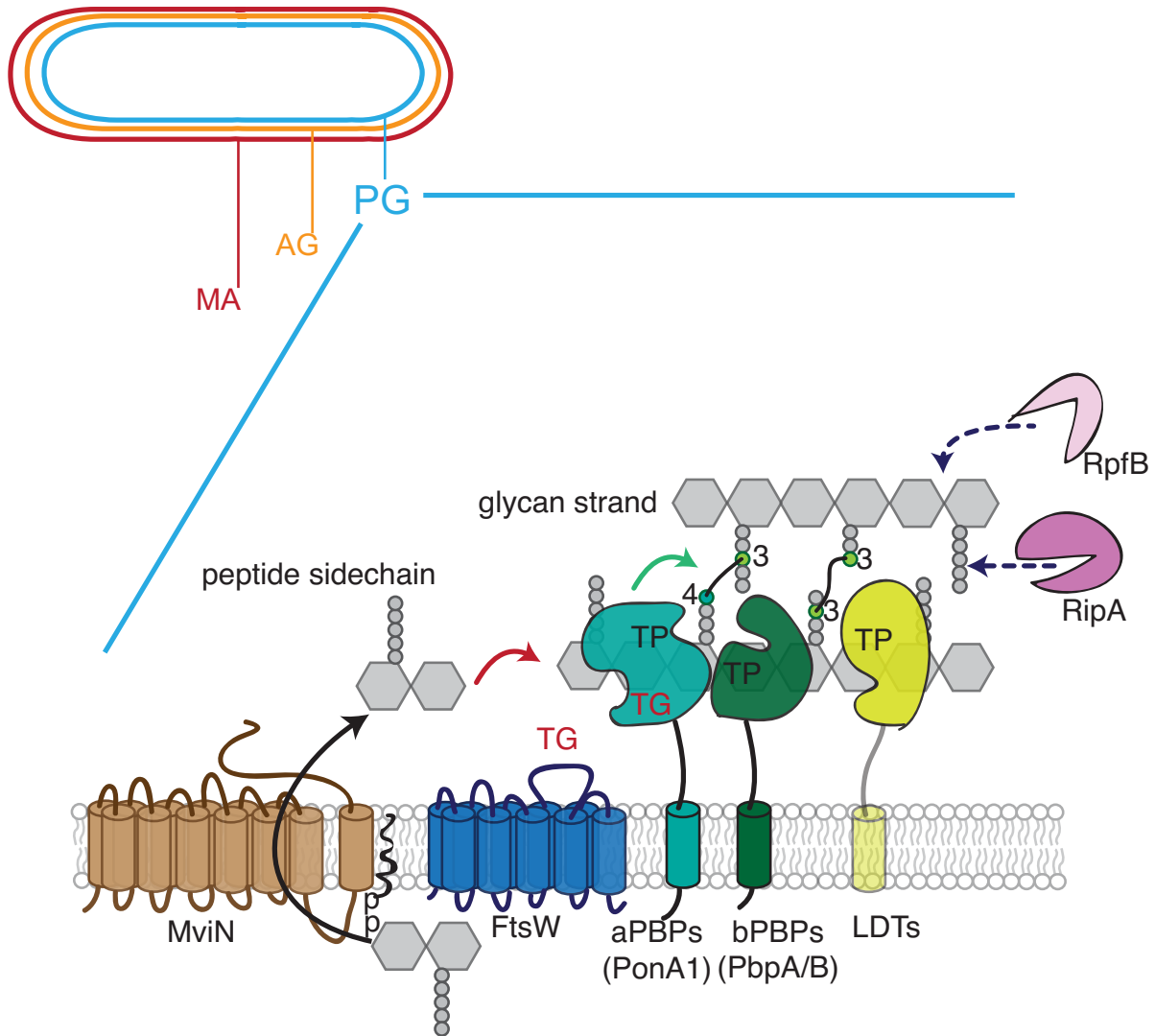


Figure 1.4: Peptidoglycan synthesis and the mycobacterial cell wall

The mycobacterial cell wall is comprised of linked layers of peptidoglycan (PG), arabinogalactan (AG) and mycolic acids (MA). Newly flipped PG (by flippase MviN) is added via its glycan strand into existing PG via transglycosylation (TG) by RodA/FtsW or aPBPs like PonA1, and then crosslinked to adjacent strands through its peptide sidechains by transpeptidases (TP) like the aPBPs, bPBPs and L,D-transpeptidases (LDTs). PG is cleaved for both growth and division to occur. RpfB and RipA are known to cleave PG for division related cell separation. Note that this schematic does not illustrate protein-protein interactions.

Mycobacteria encode homologs of the BS proteins that perform the essential cytoplasmic steps of PG synthesis but there are important differences in their regulation. For example, the first committed step of PG synthesis, performed in the cytoplasm by MurA, is regulated by CwlM, a degenerate PG amidase homolog (56). Phosphorylation of CwlM by PknB results in binding and activation of MurA to initiate PG synthesis. This regulatory cascade functions in times of starvation when CwlM is dephosphorylated, resulting in a halt of PG synthesis and reductive cell division.

Another difference is MviN, which is also regulated via phosphorylation in mycobacteria. MviN's phosphorylation by PknB recruits FhaA to a pseudokinase domain of MviN. Depletion of MviN causes cells to arrest PG synthesis as measured by precursor abundance in the cytoplasm. FhaA depletion leads to an accumulation of PG illustrated with a fluorescent derivative of vancomycin. FhaA localizes to the poles and septum. Together, these data suggest that FhaA may work to inhibit PG synthesis at the MviN step. Alternatively, FhaA may be required for a PG processing event required to remove the substrate for fluorescent vancomycin binding (57).

After lipid II is flipped across the plasma membrane, it must be incorporated into the existing PG network by both transglycosylases and transpeptidases. In BS, it is possible to delete all of the aPBPs, suggesting the presence of another glycosyltransferase (58). In BS, this was recently identified to be RodA in the elongation complex (45), and is likely FtsW, a homolog of RodA, in the division complex. In mycobacteria, the story again appears slightly different. PonA1, an aPBP, is an essential member of the *M. smegmatis* elongation complex, and is synthetically lethal with PonA2, another aPBP, in *M. tuberculosis* (59). PonA1 is essential because of its TG activity (24). RodA is not annotated essential in either organism. On the other hand, FtsW is essential and localizes to the site of division. Thus, these data suggest that, in contrast to BS, the

bi-functional PBPs are the major transglycosylases involved in elongation in mycobacteria. During division, the story may be more similar to BS, with FtsW fulfilling the major transglycosylase role.

Working in concert with the PG transglycosylases are transpeptidases. Again, this role can be filled by either aPBPs or bPBPs. There are 2 main divisome-associated bPBPs in BS - Pbp1 and Pbp2B. Pbp2B (also known as FtsI or PbpB in mycobacteria) localizes to the septum in an FtsQLB dependent manner (60) and works in partnership with FtsW (21, 36). Pbp1 is thought to shuttle in a cell cycle dependent manner between old septa (poles), to the sidewall, and then to the division complex by GspB by interacting with EzrA (38, 61).

In mycobacteria, there is evidence for both an aPBP (PonA1) and bPBPs (PbpB, PbpA) being involved in division. PbpB interacts with divisome members - FtsW, MtrB, CrgA (see above, Figure 1.3). Depletion of *pbpB* leads to branching, filamenting cells, clearly blocked in cell division (44, 62). Cells lacking *pbpA* are longer than WT and PbpA may localize to the septum (63). While PonA1 plays a critical role in elongation, it may also have a role during division. The best evidence for this is that PonA1 localizes to both the septum and poles, and interacts with RipA a PG hydrolase important for daughter cell separation (64). However, given the difficulty with assigning proteins to the division or elongation complex based on protein localization at a single timepoint (See Mycobacterial Growth: A Different Ballgame), it could be that PonA1's appearance at the septum reflects recruitment to the site of the nascent poles. Indeed, genetic modulation of PonA1's function results in elongation defects rather than canonical cell division defects (24). Further, its overexpression results in the appearance of atopic poles, suggesting an early role in the establishment of polar elongation.

Breaking the cell wall. Once the wall is made between the two halves of the cell, it must be split to create two independent daughter cells. This is achieved in BS through hydrolysis of PG

by LytC, D, E and F (65-67). Localization studies find LytE and LytF of BS at the septum and poles (68).

Currently, three PG hydrolases have been implicated in mycobacterial cell division - RipA, ChiZ and Ami1. RipA is a D,L-endopeptidase, that cleaves within PG peptide sidechains (69). It interacts with resuscitation promoting factor B (RpfB), a lytic transglycosylase, as well as PonA1. RipA localizes to the poles and the septum (64, 70). Cells depleted for *ripA* chain and branch - septa are made but not cleaved, suggesting RipA is required for daughter cell separation. RipA PG cleavage is synergistic with RpfB (71). Intriguingly, RipA and PonA1 interact in the same domain as RipA/RpfB. Adding PonA1 to a mixture of RipA and RpfB reduces the rate PG hydrolysis by the RipA/RpfB complex but does not inhibit RipA activity alone suggesting that the interaction of RipA with PonA1 and RpfB helps coordinate the synthesis and breakdown of the septal wall (5, 17).

ChiZ, like many PG hydrolases, contains a LysM domain known to bind peptidoglycan (72). ChiZ shares some similarities with BS YneA, a protein whose expression is induced by DNA damage, which curbs division by inhibiting the Z-ring and cell separation (73, 74). Overexpression of *yneA* leads to filaments but, intriguingly these filaments can be bypassed by a *divIB* (*ftsQ*) mutation further linking YneA with cell division (74). Similarly, overexpression of *chiZ* leads to filamentation and Z-ring assembly appears partially defective; some normal Z-rings appear to form but much of FtsZ appears distributed throughout the cell. ChiZ does not appear to inhibit FtsZ polymerization *in vitro* (73). It interacts with PbpB and FtsQ but does not appear to affect their localization (75). The mechanism by which ChiZ and YneA act in division remains unclear.

Ami1, a putative PG amidase, was recently found to be involved in mycobacterial division. In Δ *ami1* cells, division is blocked leading to filamentation and lateral/polar branching. Stability

of Z-rings appears compromised in these cells and lysis at the site of attempted septation is observed (76).

Notably, PG hydrolysis is a dangerous game for a bacterial cell, so hydrolase enzymes must be carefully regulated. FtsEX, an ABC transporter complex, is required for proper cell division in *E. coli* through recruitment of EnvC, a regulator of PG amidases at the septum and also through interaction with early divisome anchor FtsA (77, 78). However, FtsEX appears to regulate the CwIO hydrolase during cell elongation and not division in BS (79). In mycobacteria it has been shown that FtsX interacts with a RipA homolog, RipC, but the role of these proteins in division is yet to be explored (80).

Physical separation of daughter cells in BS occurs slowly. In contrast, mycobacterial cell separation has been described as “V-snapping” where daughter cells literally snap away from each other at the septum, but often retain a point of contact (like the quick opening of a door) (81). High-speed imaging has recently revealed that actinobacteria, like mycobacteria, split rapidly, in approximately 10 milliseconds (82). While some mycobacterial cells V-snap, some cells quickly push away from each other at the septum, but fail to V-snap; rather, they “straight” snap. This is likely due to the complexity of the mycobacterial cell wall that must be quickly sheared for full V-snapping (82). In fact, all layers of the cell wall, including PG, arabinogalactan (AG) and mycolic acids (MA), are present at the site of the septum by metabolic labeling (8, 10).

The circle of life: creating a new growth pole

In BS, the late septum, post-separation, becomes a synthesis-inert pole. In stark contrast, the pole created at division in mycobacteria becomes the location of cell wall synthesis, the hub of growth for these bacteria.

As previously mentioned, BS DivIVA is a cooperative partner of the Min system to prevent septation over the nucleoid. This can be classified as an early division inhibitor at the stage of Z-ring placement. Conversely, mycobacterial DivIVA homologue, known as Wag31 or Antigen84, plays a critical role in late stage septation/new pole establishment. It is essential for survival and its mis-regulation results in distinct division and elongation impairment phenotypes - branching cells in *wag31* over-expression (83) and polar bulges when depleted (6, 12). Like BS DivIVA, the N-terminus appears to direct Wag31 to polar curvature that may help it localize to the poles (6). Wag31 is phosphorylated by PknA/B (31, 84), but it is unclear how phosphorylation regulates its function (62, 84).

Wag31 localizes primarily to the old poles (i.e., the pole that existed before the most recent division- Figure 1) and is observed at the very late septum after the membrane has come down and separated daughter cells (12, 26). This post-membrane septal localization may indicate a role for Wag31 in the transition from a septum to a pole (26). In line with this, Wag31 interacts with members of both division (septal PG synthase PbpB (62, 85), MtrB-discussed below) and elongation (CwsA) machinery. The interaction of Wag31 and PbpB prevents protease cleavage of PbpB in oxidative stress conditions like growth in macrophages. This highlights a critical link between *in vivo* stresses and cell division (85).

In addition, Wag31 has been shown to interact with the mycolic acid synthesis enzymes AccA3 and AccD5 (6) supporting the notion of coordination between the mycobacterial layers. Interestingly, these enzymes localize in a manner like Wag31- primarily at the old pole, but also at the transitioning septum (6), again suggesting that Wag31 may be involved in the creation of new poles at the site of division.

Wag31 is not an enzyme and yet, must somehow coordinate cell wall synthases to the pole.

How this is accomplished is unknown. We do know that one major PG synthase involved in elongating the cells, PonA1, is also regulated by phosphorylation in mycobacteria. PonA1 is phosphorylated by PknB, an essential Ser/Thr eukaryotic-like kinase (24). A phosphoablative mutation in PonA1 *increases* the rate of cell elongation. Thus, PonA1's activity is negatively regulated by phosphorylation (24). PonA1 further interacts, either directly or indirectly, with LamA, a mycobacterial specific protein that actively inhibits growth from the new pole to create asymmetry in polar growth, at the late divisome (23). (See section: *An (a)side on (a)symmetry.*) Like FtsZ ring assembly, there may be both stimulatory and repressive forces at play to maintain balance in cell wall synthesis.

Does slow and steady win the race?: Mycobacterial growth rate

Many laboratory bacteria are famous for their ability to rapidly multiply. Mycobacteria, however, grow and divide relatively slowly or, in some cases, not at all under laboratory conditions. There is diversity even among the mycobacterial genus. For example, soil-dwelling *M. smegamatis* are “fast-growers” dividing once every ~2.5 hours. On the other side of the spectrum are the human pathogens *M. tuberculosis* and *M. leprae*, which grow extremely slowly during infection (between 20 hours to a few days for *M. tuberculosis* and ~2 weeks (!) for *M. leprae* (86)). Cultured *M. tuberculosis* grows at a similar rate (~20 hours) (87), suggesting that slow growth is not simply a matter of host restriction. Why do mycobacteria grow slowly? The short answer is that we do not know, but that will not stop us from speculating!

One possibility is that polar growth leads to a different set of rules governing bacterial growth. At what point does a bacterium divide? Is it based on time, on size, or on amount of growth? These three hypotheses are known as the sizer, the timer, and the adder models,

respectively. Recent work supports the idea that bacteria like *E.coli*, *Caulobacter crescentus* and BS may adhere to the adder model, whereby cells add a constant amount of volume during a cell cycle, independent of cells size (88, 89).

The adder model relies on exponential growth. In lateral growers like BS this is an easy feat to accomplish: as new cell wall is inserted along the entirety of the cell body, the area of new addition also grows. Polar growth, however, does not so simply allow for exponential addition as expansion is restrained to a specific, and proportionally small geographic, area of the cell. Indeed, at first it seemed that mycobacteria might be governed by a different principle. Early work suggested that mycobacteria employ a timer mechanism, dividing after a certain amount of time independent of cell size (7). However, two recent studies strongly suggest that mycobacteria are governed by the same adder principle as other bacteria, albeit with modifications (90, 91). One surprising conclusion from these studies is that single mycobacterial cells appear to grow exponentially (26, 91).

Another possible factor in slow-growth is the formidable nutrient barrier provided by the mycobacterial cell wall. And, of course, there is a strong causal relationship between nutrient availability and growth rate: in nutrient-rich environments, bacteria grow faster and, to an extent, become larger. Is the availability of nutrients rate-limiting in mycobacteria? *M. smegmatis*, the most well-studied fast-growing mycobacteria, encodes a porin, MspA, which aids in the uptake of nutrients across the myco-membrane. Notably, MspA is absent in *M. tuberculosis* (92). Expressing *mspA* in BCG, a slow-growing mycobacteria naturally lacking *mspA*, caused the cells to slightly but reproducibly increase their doubling rate, supporting a link between nutrient uptake and growth rate in mycobacteria (92-94). Likewise, porin knockdowns in the fast growing mycobacteria *M. fortuitum*, lead to a decrease in colony size, suggesting that nutrient uptake plays some role in

growth rate (95). However, this must only be part of the story as expression of MspA only marginally increased the growth rate of BCG.

An additional putative factor in the slow growth of mycobacteria is the rate of DNA replication. In many other species, the demands of fast growth necessitate multi-fork DNA replication because DNA replication is slower than the process of growth and division in nutrient rich conditions (96). Until recently, it was thought that mycobacteria were not capable of multi-fork DNA replication, thus decreasing the potential to increase growth rate beyond this rate limiting step. However, a recent study challenges this idea, showing multi-fork replication using time-lapse microscopy and fluorescent reporters of replication related proteins (97). Intriguingly, the authors found that multi-fork replication occurred in nutrient rich and nutrient poor conditions. Thus, it remains unclear what role multi-fork replication plays in mycobacteria. Perhaps mycobacterial DNA polymerization is inherently slow? *M. smegmatis* has an estimated DNA synthesis rate of 400 bases/second. This is quite rapid compared to *M. tuberculosis* with a proposed rate of 50 bases/second (97, 98). However, these rates are sluggish in relation to the 600-1000 bases/second that *E. coli* and BS can accomplish (99). DNA-replication, the so-called “C” period of the cell cycle, comprises ~75% of the *M. smegmatis* cell cycle (26, 97). Oddly, the *in vitro* rate of nucleotide incorporation by mycobacterial DNA polymerase DnaE1 is faster than that of *E. coli* PolIII α (100). This suggests that conditions within the cell, for example, limited nucleotide pools, are restricting the rate of new chromosomal synthesis (99).

Yet another possibility is that the construction of the intricate cell wall itself limits the growth rate of mycobacteria. Supporting this idea is the recent *E. coli* study by Vadia *et al* (101). They propose an “outside-in” model, in which *E. coli* cell size is limited by fatty-acid synthesis so that cell volume does not increase at a rate faster than can be accommodated by the cell envelope.

Certainly, cell wall fatty acid synthesis could be a contributing factor to mycobacterial slow growth since mycobacteria must synthesize their complex and long mycolic acids, and there are substantial cell wall differences between fast and slow growing mycobacteria (92).

More deep thoughts on mycobacterial division

While bacteria dream of dividing, pathogens dream of dividing within the host. And mycobacteria seem to be exquisitely tuned for doing so: *M. tuberculosis* is an obligate pathogen with essentially no environmental niche. And it is highly successful. In 2016 there were over 10 million new cases estimated, and nearly 2 million deaths (102). Thus, an important part of thinking about growth of this organism is to consider its adaptations to the host. The slow growth rate is likely optimized for surviving in humans, though why this should be remains unclear. And the ability to survive for decades as an asymptomatic infection, perhaps growing slowly or not at all, permits a reservoir of infection that assures the long-term survival of the species. The cell wall is appropriately adapted to interface with the host (5). And, while the pattern of growth has been inherited from the soil-dwelling organisms from which it has likely evolved, *M. tuberculosis* takes full advantage of it to avoid clearance during infection.

The outcome of these adaptations is crucial when we consider therapy for tuberculosis. The thick cell wall and its multiple embedded efflux pumps create a formidable barrier for many drugs that are effective against other bacteria (103). At the same time, it creates new opportunities to target structures and processes that are absent in model organisms. For example, antibiotics like ethambutol and isoniazid that inhibit the formation of arabinogalactan and mycolic acid synthesis respectively, are absolute mainstays of tuberculosis therapy. With a better understanding of

underlying molecular mechanisms, other unique aspects of mycobacterial cell division could provide effective and specific targets for tuberculosis therapy.

Those of us who study mycobacteria are indebted to the groundbreaking research conducted in BS and *E. coli* - work that has created a template on which to base our thinking about our own organisms. But mycobacteria create their own, unique paradigms. Model bacteria might dream alike, but each unusual bacterium dreams in its own way. C'est la vie!

Section 1.2: References

1. **Jacob F.** 1965. Leçon inaugurale: faite le vendredi 7 mai, 1965.
2. **Hirota Y, Ryter A, Jacob F.** 1968. Thermosensitive mutants of *E. coli* affected in the processes of DNA synthesis and cellular division. *Cold Spring Harb Symp Quant Biol* **33**:677–693.
3. **Bi EF, Lutkenhaus J.** 1991. FtsZ ring structure associated with division in *Escherichia coli*. *Nature* **354**:161–164.
4. **Blaauwen den T, Hamoen LW, Levin PA.** 2017. The divisome at 25: the road ahead. *Current Opinion in Microbiology* **36**:85–94.
5. **Kieser KJ, Rubin EJ.** 2014. How sisters grow apart: mycobacterial growth and division. *Nature Publishing Group* **12**:550–562.
6. **Meniche X, Otten R, Siegrist MS, Baer CE, Murphy KC, Bertozzi CR, Sasseti CM.** 2014. Subpolar addition of new cell wall is directed by DivIVA in mycobacteria. *Proc Natl Acad Sci USA* **111**:E3243–51.
7. **Aldridge BB, Fernandez-Suarez M, Heller D, Ambravaneswaran V, Irimia D, Toner M, Fortune SM.** 2012. Asymmetry and aging of mycobacterial cells lead to variable growth and antibiotic susceptibility. *Science* **335**:100–104.
8. **Foley HN, Stewart JA, Kavunja HW, Rundell SR, Swarts BM.** 2016. Bioorthogonal Chemical Reporters for Selective In Situ Probing of Mycomembrane Components in Mycobacteria. *Angew Chem Int Ed Engl* **55**:2053–2057.
9. **Siegrist MS, Whiteside S, Jewett JC, Aditham A, Cava F, Bertozzi CR.** 2013. d-Amino Acid Chemical Reporters Reveal Peptidoglycan Dynamics of an Intracellular Pathogen. *ACS Chem Biol* **8**:500–505.
10. **Botella H, Yang G, Ouerfelli O, Ehrt S, Nathan CF, Vaubourgeix J.** 2017. Distinct Spatiotemporal Dynamics of Peptidoglycan Synthesis between *Mycobacterium smegmatis* and *Mycobacterium tuberculosis*. *mBio* **8**:e01183–17.
11. **Daniel RA, Errington J.** 2003. Control of cell morphogenesis in bacteria: two distinct ways to make a rod-shaped cell. *Cell* **113**:767–776.

12. **Kang C-M, Nyayapathy S, Lee J-Y, Suh J-W, Husson RN.** 2008. Wag31, a homologue of the cell division protein DivIVA, regulates growth, morphology and polar cell wall synthesis in mycobacteria. *Microbiology* **154**:725–735.
13. **Cameron TA, Zupan JR, Zambryski PC.** 2015. The essential features and modes of bacterial polar growth. *Trends Microbiol* **23**:347–353.
14. **Ursell TS, Nguyen J, Monds RD, Colavin A, Billings G, Ouzounov N, Gitai Z, Shaevitz JW, Huang KC.** 2014. Rod-like bacterial shape is maintained by feedback between cell curvature and cytoskeletal localization. *Proc Natl Acad Sci USA* **111**:E1025–34.
15. **Hussain S, Wivagg CN, Szwedziak P, Wong F, Schaefer K, Izore T, Renner LD, Sun Y, Bisson Filho AW, Walker S, Amir A, Löwe J, Garner EC.** 2017. MreB Filaments Create Rod Shape By Aligning Along Principal Membrane Curvature.
16. **Edwards DH, Errington J.** 1997. The *Bacillus subtilis* DivIVA protein targets to the division septum and controls the site specificity of cell division. *Molecular Microbiology* **24**:905–915.
17. **Hett EC, Chao MC, Rubin EJ.** 2010. Interaction and Modulation of Two Antagonistic Cell Wall Enzymes of Mycobacteria. *PLoS Pathog* **6**:e1001020–14.
18. **Sanders AN, Wright LF, Pavelka MS.** 2014. Genetic characterization of mycobacterial L,D-transpeptidases. *Microbiology (Reading, Engl)* **160**:1795–1806.
19. **Haeusser DP, Margolin W.** 2016. Splitsville: structural and functional insights into the dynamic bacterial Z ring. *Nature Publishing Group* **14**:305–319.
20. **Bisson-Filho AW, Hsu Y-P, Squyres GR, Kuru E, Wu F, Jukes C, Sun Y, Dekker C, Holden S, VanNieuwenhze MS, Brun YV, Garner EC.** 2017. Treadmilling by FtsZ filaments drives peptidoglycan synthesis and bacterial cell division. *Science* **355**:739–743.
21. **Adams DW, Errington J.** 2009. Bacterial cell division: assembly, maintenance and disassembly of the Z ring. *Nature Publishing Group* **7**:642–653.
22. **Migocki MD, Freeman MK, Wake RG, Harry EJ.** 2002. The Min system is not required for precise placement of the midcell Z ring in *Bacillus subtilis*. *EMBO Rep* **3**:1163–1167.

23. **Rego EH, Audette RE, Rubin EJ.** 2017. Deletion of a mycobacterial divisome factor collapses single-cell phenotypic heterogeneity. *Nature* **546**:153–157.
24. **Kieser KJ, Boutte CC, Kester JC, Baer CE, Barczak AK, Meniche X, Chao MC, Rego EH, Sassetti CM, Fortune SM, Rubin EJ.** 2015. Phosphorylation of the Peptidoglycan Synthase PonA1 Governs the Rate of Polar Elongation in Mycobacteria. *PLoS Pathog* **11**:e1005010.
25. **Wakamoto Y, Dhar N, Chait R, Schneider K, Signorino-Gelo F, Leibler S, McKinney JD.** 2013. Dynamic persistence of antibiotic-stressed mycobacteria. *Science* **339**:91–95.
26. **Dhar N, Bousbaine D, Wakamoto Y, McKinney JD, Santi I.** 2013. Single-cell dynamics of the chromosome replication and cell division cycles in mycobacteria. *Nature Communications* **4**:1–10.
27. **Joyce G, Williams KJ, Robb M, Noens E, Tizzano B, Shahrezaei V, Robertson BD.** 2012. Cell division site placement and asymmetric growth in mycobacteria. *PLoS ONE* **7**:e44582.
28. **Eskandarian HA, Odermatt PD, Ven JXY, Hannebelle MTM, Nievergelt AP, Dhar N, McKinney JD, Fantner GE.** 2017. Division site selection linked to inherited cell surface wave troughs in mycobacteria. *Nat Microbiol* **2**:17094.
29. **Thakur M, Chakraborti PK.** 2006. GTPase activity of mycobacterial FtsZ is impaired due to its transphosphorylation by the eukaryotic-type Ser/Thr kinase, PknA. *Journal of Biological Chemistry* **281**:40107–40113.
30. **Sureka K, Hossain T, Mukherjee P, Chatterjee P, Datta P, Kundu M, Basu J.** 2010. Novel role of phosphorylation-dependent interaction between FtsZ and FipA in mycobacterial cell division. *PLoS ONE* **5**:e8590.
31. **Kang C-M, Abbott DW, Park ST, Dascher CC, Cantley LC, Husson RN.** 2005. The Mycobacterium tuberculosis serine/threonine kinases PknA and PknB: substrate identification and regulation of cell shape. *Genes Dev* **19**:1692–1704.
32. **Wu LJ, Errington J.** 2011. Nucleoid occlusion and bacterial cell division. *Nature Publishing Group* **10**:8–12.
33. **Patrick JE, Kearns DB.** 2008. MinJ (YvjD) is a topological determinant of cell division

in *Bacillus subtilis*. *Molecular Microbiology* **70**:1166–1179.

34. **Egan AJF, Vollmer W.** 2012. The physiology of bacterial cell division. *Annals of the New York Academy of Sciences* **1277**:8–28.
35. **England K, Crew R, Slayden RA.** 2011. Mycobacterium tuberculosis septum site determining protein, Ssd encoded by rv3660c, promotes filamentation and elicits an alternative metabolic and dormancy stress response. *BMC Microbiol* **11**:79.
36. **Gamba P, Hamoen LW, Daniel RA.** 2016. Cooperative Recruitment of FtsW to the Division Site of *Bacillus subtilis*. *Front Microbiol* **7**:1808.
37. **Feucht A, Lucet I, Yudkin MD, Errington J.** 2001. Cytological and biochemical characterization of the FtsA cell division protein of *Bacillus subtilis*. *Molecular Microbiology* **40**:115–125.
38. **Claessen D, Emmins R, Hamoen LW, Daniel RA, Errington J, Edwards DH.** 2008. Control of the cell elongation-division cycle by shuttling of PBP1 protein in *Bacillus subtilis*. *Molecular Microbiology* **68**:1029–1046.
39. **Gola S, Munder T, Casonato S, Manganelli R, Vicente M.** 2015. The essential role of SepF in mycobacterial division. *Molecular Microbiology* **97**:560–576.
40. **Haeusser DP, Lee AH, Weart RB, Levin PA.** 2009. ClpX inhibits FtsZ assembly in a manner that does not require its ATP hydrolysis-dependent chaperone activity. *Journal of Bacteriology* **191**:1986–1991.
41. **Weart RB, Nakano S, Lane BE, Zuber P, Levin PA.** 2005. The ClpX chaperone modulates assembly of the tubulin-like protein FtsZ. *Molecular Microbiology* **57**:238–249.
42. **Dziedzic R, Kiran M, Plocinski P, Ziolkiewicz M, Brzostek A, Moomey M, Vadrevu IS, Dziadek J, Madiraju M, Rajagopalan M.** 2010. Mycobacterium tuberculosis ClpX interacts with FtsZ and interferes with FtsZ assembly. *PLoS ONE* **5**:e11058.
43. **Gamba P, Veening JW, Saunders NJ, Hamoen LW, Daniel RA.** 2009. Two-Step Assembly Dynamics of the *Bacillus subtilis* Divisome. *Journal of Bacteriology* **191**:4186–4194.

44. **Wu KJ, Zhang J, Baranowski C, Leung V, Rego EH, Morita Y, Rubin EJ, Boutte CC.** Characterization of conserved and novel septal factors in *Mycobacterium smegmatis*. *Journal of Bacteriology*.
45. **Meeske AJ, Riley EP, Robins WP, Uehara T, Mekalanos JJ, Kahne D, Walker S, Kruse AC, Bernhardt TG, Rudner DZ.** 2016. SEDS proteins are a widespread family of bacterial cell wall polymerases. *Nature* **537**:634–638.
46. **Datta P.** 2002. Interaction between FtsZ and FtsW of *Mycobacterium tuberculosis*. *Journal of Biological Chemistry* **277**:24983–24987.
47. **Rajagopalan M, Maloney E, Dziadek J, Poplawska M, Lofton H, Chauhan A, Madiraju MVVS.** 2005. Genetic evidence that mycobacterial FtsZ and FtsW proteins interact, and colocalize to the division site in *Mycobacterium smegmatis*. *FEMS Microbiology Letters* **250**:9–17.
48. **Datta P, Dasgupta A, Singh AK, Mukherjee P, Kundu M, Basu J.** 2006. Interaction between FtsW and penicillin-binding protein 3 (PBP3) directs PBP3 to mid-cell, controls cell septation and mediates the formation of a trimeric complex involving FtsZ, FtsW and PBP3 in mycobacteria. *Molecular Microbiology* **62**:1655–1673.
49. **Plocinski P, Ziolkiewicz M, Kiran M, Vadrevu SI, Nguyen HB, Hugonnet J, Veckerle C, Arthur M, Dziadek J, Cross TA, Madiraju M, Rajagopalan M.** 2011. Characterization of CrgA, a new partner of the *Mycobacterium tuberculosis* peptidoglycan polymerization complexes. *Journal of Bacteriology* **193**:3246–3256.
50. **Plocinski P, Arora N, Sarva K, Blaszczyk E, Qin H, Das N, Plocinska R, Ziolkiewicz M, Dziadek J, Kiran M, Gorla P, Cross TA, Madiraju M, Rajagopalan M.** 2012. *Mycobacterium tuberculosis* CwsA interacts with CrgA and Wag31, and the CrgA-CwsA complex is involved in peptidoglycan synthesis and cell shape determination. *Journal of Bacteriology* **194**:6398–6409.
51. **Gomez JE, Bishai WR.** 2000. whmD is an essential mycobacterial gene required for proper septation and cell division. *Proc Natl Acad Sci USA* **97**:8554–8559.
52. **Sham L-T, Butler EK, Lebar MD, Kahne D, Bernhardt TG, Ruiz N.** 2014. Bacterial cell wall. MurJ is the flippase of lipid-linked precursors for peptidoglycan biogenesis. *Science* **345**:220–222.
53. **Typas A, Banzhaf M, Gross CA, Vollmer W.** 2011. From the regulation of

peptidoglycan synthesis to bacterial growth and morphology. *Nature Publishing Group* **10**:123–136.

54. **Lavollay M, Arthur M, Fourgeaud M, Dubost L, Marie A, Veziris N, Blanot D, Gutmann L, Mainardi JL.** 2008. The Peptidoglycan of Stationary-Phase *Mycobacterium tuberculosis* Predominantly Contains Cross-Links Generated by L,D-Transpeptidation. *Journal of Bacteriology* **190**:4360–4366.
55. **Kumar P, Arora K, Lloyd JR, Lee IY, Nair V, Fischer E, Boshoff HIM, Barry CE III.** 2012. Meropenem inhibits D,D-carboxypeptidase activity in *Mycobacterium tuberculosis*. *Molecular Microbiology* **86**:367–381.
56. **Boutte CC, Baer CE, Papavinasundaram K, Liu W, Chase MR, Meniche X, Fortune SM, Sassetti CM, Ioerger TR, Rubin EJ.** 2016. A cytoplasmic peptidoglycan amidase homologue controls mycobacterial cell wall synthesis. *eLife* **5**:a021113.
57. **Gee CL, Papavinasundaram KG, Blair SR, Baer CE, Falick AM, King DS, Griffin JE, Venghatakrishnan H, Zukauskas A, Wei J-R, Dhiman RK, Crick DC, Rubin EJ, Sassetti CM, Alber T.** 2012. A phosphorylated pseudokinase complex controls cell wall synthesis in mycobacteria. *Sci Signal* **5**:ra7–ra7.
58. **Meeske AJ, Sham L-T, Kimsey H, Koo B-M, Gross CA, Bernhardt TG, Rudner DZ.** 2015. MurJ and a novel lipid II flippase are required for cell wall biogenesis in *Bacillus subtilis*. *Proc Natl Acad Sci USA* **112**:6437–6442.
59. **Kieser KJ, Baranowski C, Chao MC, Long JE, Sassetti CM, Waldor MK, Sacchettini JC, Ioerger TR, Rubin EJ.** 2015. Peptidoglycan synthesis in *Mycobacterium tuberculosis* is organized into networks with varying drug susceptibility. *Proc Natl Acad Sci USA* **112**:13087–13092.
60. **Donovan C, Bramkamp M.** 2014. Cell division in *Corynebacterineae*. *Front Microbiol* **5**:132.
61. **Tavares JR, de Souza RF, Meira GLS, Gueiros-Filho FJ.** 2008. Cytological characterization of YpsB, a novel component of the *Bacillus subtilis* divisome. *Journal of Bacteriology* **190**:7096–7107.
62. **Plocinska R, Martinez L, Gorla P, Pandey E, Sarva K, Blaszczyk E, Dziadek J, Madiraju MV, Rajagopalan M.** 2014. *Mycobacterium tuberculosis* MtrB sensor kinase interactions with FtsI and Wag31 proteins reveal a role for MtrB distinct from that

- regulating MtrA activities. *Journal of Bacteriology* **196**:4120–4129.
63. **Dasgupta A, Datta P, Kundu M, Basu J.** 2006. The serine/threonine kinase PknB of *Mycobacterium tuberculosis* phosphorylates PBPA, a penicillin-binding protein required for cell division. *Microbiology* **152**:493–504.
 64. **Chao MC, Kieser KJ, Minami S, Mavrici D, Aldridge BB, Fortune SM, Alber T, Rubin EJ.** 2013. Protein complexes and proteolytic activation of the cell wall hydrolase RipA regulate septal resolution in mycobacteria. *PLoS Pathog* **9**:e1003197.
 65. **Smith TJ, Blackman SA, Foster SJ.** 2000. Autolysins of *Bacillus subtilis*: multiple enzymes with multiple functions. *Microbiology* **146 (Pt 2)**:249–262.
 66. **Ohnishi R, Ishikawa S, Sekiguchi J.** 1999. Peptidoglycan hydrolase LytF plays a role in cell separation with CwlF during vegetative growth of *Bacillus subtilis*. *Journal of Bacteriology* **181**:3178–3184.
 67. **Ishikawa S, Hara Y, Ohnishi R, Sekiguchi J.** 1998. Regulation of a new cell wall hydrolase gene, *cwlF*, which affects cell separation in *Bacillus subtilis*. *Journal of Bacteriology* **180**:2549–2555.
 68. **Scheffers D-J, Pinho MG.** 2005. Bacterial cell wall synthesis: new insights from localization studies. *Microbiol Mol Biol Rev* **69**:585–607.
 69. **Böth D, Schneider G, Schnell R.** 2011. Peptidoglycan remodeling in *Mycobacterium tuberculosis*: comparison of structures and catalytic activities of RipA and RipB. *J Mol Biol* **413**:247–260.
 70. **Hett EC, Chao MC, Steyn AJ, Fortune SM, Deng LL, Rubin EJ.** 2007. A partner for the resuscitation-promoting factors of *Mycobacterium tuberculosis*. *Molecular Microbiology* **66**:658–668.
 71. **Hett EC, Chao MC, Deng LL, Rubin EJ.** 2008. A mycobacterial enzyme essential for cell division synergizes with resuscitation-promoting factor. *PLoS Pathog* **4**:e1000001.
 72. **Buist G, Steen A, Kok J, Kuipers OP.** 2008. LysM, a widely distributed protein motif for binding to (peptido)glycans. *Molecular Microbiology* **68**:838–847.

73. **Chauhan A, Lofton H, Maloney E, Moore J, Fol M, Madiraju MVVS, Rajagopalan M.** 2006. Interference of Mycobacterium tuberculosis cell division by Rv2719c, a cell wall hydrolase. *Molecular Microbiology* **62**:132–147.
74. **Mo AH, Burkholder WF.** 2010. YneA, an SOS-induced inhibitor of cell division in *Bacillus subtilis*, is regulated posttranslationally and requires the transmembrane region for activity. *Journal of Bacteriology* **192**:3159–3173.
75. **Vadrevu IS, Lofton H, Sarva K, Blasczyk E, Plocinska R, Chinnaswamy J, Madiraju M, Rajagopalan M.** 2011. ChiZ levels modulate cell division process in mycobacteria. *Tuberculosis (Edinb)* **91 Suppl 1**:S128–35.
76. **Senzani S, Li D, Bhaskar A, Ealand C, Chang J, Rimal B, Liu C, Joon Kim S, Dhar N, Kana B.** 2017. An Amidase_3 domain-containing N-acetylmuramyl-L-alanine amidase is required for mycobacterial cell division. *Sci Rep* **7**:1140.
77. **Du S, Pichoff S, Lutkenhaus J.** 2016. FtsEX acts on FtsA to regulate divisome assembly and activity. *Proc Natl Acad Sci USA* **113**:E5052–E5061.
78. **Yang DC, Peters NT, Parzych KR, Uehara T, Markovski M, Bernhardt TG.** 2011. An ATP-binding cassette transporter-like complex governs cell-wall hydrolysis at the bacterial cytokinetic ring. *Proc Natl Acad Sci USA* **108**:E1052–60.
79. **Meisner J, Montero Llopis P, Sham L-T, Garner E, Bernhardt TG, Rudner DZ.** 2013. FtsEX is required for CwlO peptidoglycan hydrolase activity during cell wall elongation in *Bacillus subtilis*. *Molecular Microbiology* **89**:1069–1083.
80. **Mavrici D, Marakalala MJ, Holton JM, Prigozhin DM, Gee CL, Zhang YJ, Rubin EJ, Alber T.** 2014. Mycobacterium tuberculosis FtsX extracellular domain activates the peptidoglycan hydrolase, RipC. *Proc Natl Acad Sci USA* **111**:8037–8042.
81. **Thanky NR, Young DB, Robertson BD.** 2007. Unusual features of the cell cycle in mycobacteria: polar-restricted growth and the snapping-model of cell division. *Tuberculosis* **87**:231–236.
82. **Zhou X, Halladin DK, Theriot JA.** 2016. Fast Mechanically Driven Daughter Cell Separation Is Widespread in Actinobacteria. *mBio* **7**:e00952–16.
83. **Nguyen L, Scherr N, Gatfield J, Walburger A, Pieters J, Thompson CJ.** 2007. Antigen

- 84, an effector of pleiomorphism in *Mycobacterium smegmatis*. *Journal of Bacteriology* **189**:7896–7910.
84. **Jani C, Eoh H, Lee JJ, Hamasha K, Sahana MB, Han J-S, Nyayapathy S, Lee J-Y, Suh J-W, Lee SH, Rehse SJ, Crick DC, Kang C-M.** 2010. Regulation of polar peptidoglycan biosynthesis by Wag31 phosphorylation in mycobacteria. *BMC Microbiol* **10**:327.
85. **Mukherjee P, Sureka K, Datta P, Hossain T, Barik S, Das KP, Kundu M, Basu J.** 2009. Novel role of Wag31 in protection of mycobacteria under oxidative stress. *Molecular Microbiology* **73**:103–119.
86. **Cole ST, Eiglmeier K, Parkhill J, James KD, Thomson NR, Wheeler PR, Honoré N, Garnier T, Churcher C, Harris D, Mungall K, Basham D, Brown D, Chillingworth T, Connor R, Davies RM, Devlin K, Duthoy S, Feltwell T, Fraser A, Hamlin N, Holroyd S, Hornsby T, Jagels K, Lacroix C, Maclean J, Moule S, Murphy L, Oliver K, Quail MA, Rajandream MA, Rutherford KM, Rutter S, Seeger K, Simon S, Simmonds M, Skelton J, Squares R, Squares S, Stevens K, Taylor K, Whitehead S, Woodward JR, Barrell BG.** 2001. Massive gene decay in the leprosy bacillus. *Nature* **409**:1007–1011.
87. **Gill WP, Harik NS, Whiddon MR, Liao RP, Mittler JE, Sherman DR.** 2009. A replication clock for *Mycobacterium tuberculosis*. *Nature Medicine* **15**:211–214.
88. **Campos M, Surovtsev IV, Kato S, Paintdakhi A, Beltran B, Ebmeier SE, Jacobs-Wagner C.** 2014. A constant size extension drives bacterial cell size homeostasis. *Cell* **159**:1433–1446.
89. **Taheri-Araghi S, Bradde S, Sauls JT, Hill NS, Levin PA, Paulsson J, Vergassola M, Jun S.** 2015. Cell-Size Control and Homeostasis in Bacteria. *Current Biology* **25**:385–391.
90. **Priestman M, Thomas P, Robertson BD, Shahrezaei V.** 2017. Mycobacteria Modify Their Cell Size Control under Sub-Optimal Carbon Sources. *Front Cell Dev Biol* **5**:100–17.
91. **Logsdon MM, Ho P-Y, Papavinasasundaram K, Richardson K, Cokol M, Sasseti CM, Amir A, Aldridge BB.** 2017. A Parallel Adder Coordinates Mycobacterial Cell-Cycle Progression and Cell-Size Homeostasis in the Context of Asymmetric Growth and Organization. *Curr Biol* **27**:3367–3374.e7.

92. **Hett EC, Rubin EJ.** 2008. Bacterial growth and cell division: a mycobacterial perspective. *Microbiol Mol Biol Rev* **72**:126–56– table of contents.
93. **Sharbati-Tehrani S, Meister B, Appel B, Lewin A.** 2004. The porin MspA from *Mycobacterium smegmatis* improves growth of *Mycobacterium bovis* BCG. *Int J Med Microbiol* **294**:235–245.
94. **Mailaender C, Reiling N, Engelhardt H, Bossmann S, Ehlers S, Niederweis M.** 2004. The MspA porin promotes growth and increases antibiotic susceptibility of both *Mycobacterium bovis* BCG and *Mycobacterium tuberculosis*. *Microbiology* **150**:853–864.
95. **Sharbati S, Schramm K, Rempel S, Wang H, Andrich R, Tykiel V, Kunisch R, Lewin A.** 2009. Characterisation of porin genes from *Mycobacterium fortuitum* and their impact on growth. *BMC Microbiol* **9**:31.
96. **Wang JD, Levin PA.** 2009. Metabolism, cell growth and the bacterial cell cycle. *Nature Publishing Group* **7**:822–827.
97. **Trojanowski D, Ginda K, Pióro M, Hołówka J, Skut P, Jakimowicz D, Zakrzewska-Czerwińska J.** 2015. Choreography of the *Mycobacterium* replication machinery during the cell cycle. *mBio* **6**:e02125–14.
98. **Nair N, Dziedzic R, Greendyke R, Muniruzzaman S, Rajagopalan M, Madiraju MV.** 2009. Synchronous replication initiation in novel *Mycobacterium tuberculosis* dnaA cold-sensitive mutants. *Molecular Microbiology* **71**:291–304.
99. **Ditse Z, Lamers MH, Warner DF.** 2017. DNA Replication in *Mycobacterium tuberculosis*. *Microbiol Spectr* **5**.
100. **Rock JM, Lang UF, Chase MR, Ford CB, Gerrick ER, Gawande R, Coscolla M, Gagneux S, Fortune SM, Lamers MH.** 2015. DNA replication fidelity in *Mycobacterium tuberculosis* is mediated by an ancestral prokaryotic proofreader. *Nat Genet* **47**:677–681.
101. **Vadia S, Tse JL, Lucena R, Yang Z, Kellogg DR, Wang JD, Levin PA.** 2017. Fatty Acid Availability Sets Cell Envelope Capacity and Dictates Microbial Cell Size. *Curr Biol* **27**:1757–1767.e5.

102. 2017. Global Tuberculosis Report 2017 1–262.
103. **Pule CM, Sampson SL, Warren RM, Black PA, van Helden PD, Victor TC, Louw GE.** 2016. Efflux pump inhibitors: targeting mycobacterial efflux systems to enhance TB therapy. *J Antimicrob Chemother* **71**:17–26.

Chapter 2: Identifying mycobacterial divisome factors

Section 2.1: Characterization of conserved and novel septal factors in *Mycobacterium smegmatis*

Overview: This chapter consists of a manuscript published in the Journal of Bacteriology in January 2018 (1).

Attributions: CB constructed the GFPmut3-FtsL vector and helped perform time-lapse microscopy experiments in Figure 2.2. CB constructed the FtsL truncation series and performed the experiment depicted in Figure 2.1A (essentiality of FtsL extensions). KJW and CCB wrote the manuscript. CB provided edits.

Authors: Katherine J. Wu¹, Jenna Zhang¹, Catherine Baranowski¹, Vivian Leung¹, E. Hesper Rego², Yasu S. Morita³, Eric J. Rubin^{1,4} and Cara C. Boutte^{1,5,*}

¹Department of Immunology and Infectious Disease, Harvard TH Chan School of Public Health, Boston MA.²Department of Microbial Pathogenesis, Yale University, New Haven, CT.

³Department of Microbiology, University of Massachusetts, Amherst, MA. ⁴ Department of Microbiology and Immunobiology, Harvard Medical School, Boston, MA. ⁵ Current address:

Department of Biology, University of Texas at Arlington, Arlington, TX

*corresponding author: cara.boutte@uta.edu

Abstract

Septation in bacteria requires coordinated regulation of cell wall biosynthesis and hydrolysis enzymes so that new septal cross-wall can be appropriately constructed without compromising the integrity of the existing cell wall. Bacteria with different modes of growth and different types of cell wall require different regulators to mediate cell growth and division

processes. Mycobacteria have both a cell wall structure and mode of growth that are distinct from well-studied model organisms and use several different regulatory mechanisms. Here, using *Mycobacterium smegmatis*, we identify and characterize homologs of the conserved cell division regulators FtsL and FtsB, and show that they appear to function similarly to their homologs in *E. coli*. We identify a number of previously undescribed septally-localized factors which could be involved in cell wall regulation. One of these, SepIVA, has a DivIVA domain, is required for mycobacterial septation and is localized to the septum and the intracellular membrane domain. We propose that SepIVA is a regulator of cell wall precursor enzymes that contribute to construction of the septal cross-wall, similar to the putative elongation function of the other mycobacterial DivIVA homolog, Wag31.

Importance

The enzymes that build bacterial cell walls are essential for cell survival, but can cause cell lysis if misregulated; thus their regulators are also essential. The number and nature of these regulators is likely to vary in bacteria that grow in different ways. The mycobacteria are a genus that have a cell wall whose composition and construction varies greatly from that of well-studied model organisms. In this work, we identify and characterize some of the proteins that regulate the mycobacterial cell wall. We find that some of these regulators appear to be functionally conserved with their structural homologs in evolutionarily distant species such as *E. coli*, but other proteins have critical regulatory functions that may be unique to the actinomycetes.

Introduction

Division of rod-shaped bacteria is a tightly regulated process that requires new cell wall to be built in the middle of the cell orthogonal to the elongation axis. For decades, bacterial cell biologists have been occupied with questions about how periplasmic enzymes can be regulated in coordination with chromosome segregation (2) and how the cell wall can be bisected at each division event without compromising its integrity. Much of our understanding comes from the model organisms *Escherichia coli* and *Bacillus subtilis*, in which large protein complexes are required to properly regulate septal enzymes (3), and information is passed from the cytoplasm to the periplasmic enzymes through conformational changes in the transmembrane factors in these complexes (4, 5).

E. coli and *B. subtilis* are both rod-shaped bacteria that extend along their lateral walls via intercalary growth; however, a number of rod-shaped species from far-flung phyla grow at the cell poles (6-15), including the mycobacteria, a genus which includes *Mycobacterium tuberculosis* and other pathogens. In *Mycobacterium smegmatis* (*Msmeg*), a non-pathogenic relative of *M. tuberculosis* (*Mtb*), septation is thought to be broadly similar to the process in other rod-shaped bacteria. The mycobacterial septation apparatus contains homologs of many well-described septal factors from *E. coli* and *B. subtilis*, including FtsZ, PBP3, FtsW and FtsQ. However, many essential septal factors are unaccounted for in the current annotations of mycobacterial genomes. These missing factors include FtsA and ZipA, which in *E. coli* are required for Z ring stabilization and recruitment of FtsK (16), and ZapA, which recruits and (17) stabilizes the Z ring. Some missing factors can be accounted for because a function can be filled through alternative mechanisms. For instance, mycobacteria have SepF (18), which is present in many bacterial species that lack FtsA and is thought to perform the function of FtsA and EzrA in anchoring FtsZ to the membrane and recruiting it to the midcell (19). Mycobacterial FtsZ may also be anchored to

the membrane through a direct interaction with the intermembrane transglycosylase FtsW (20, 21) which, in turn, interacts with PBP3 (22), thus apparently cutting out some middlemen such that FtsZ may directly regulate the septal enzymes. Other missing canonical septal factors include FtsN, which is thought to initiate septation upon its late association with the cell division apparatus (divisome), and FtsB and FtsL, which are part of a trimer that includes FtsQ and are thought to be involved in regulating the initiation of septation (4, 23).

In addition to identifying the factors that perform the same septal functions that have been identified in *E. coli* and *B. subtilis*, we expect that mycobacteria will have septation factors that do not exist in these model species. These unidentified factors are likely to be involved in either: 1) coordinating between septal and polar growth or 2) coordinating the insertion of the arabinogalactan and mycolic acid layers of the cell wall.

In lateral wall growers, the functions of cell elongation and cell septation are largely temporally and spatially separated and mediated by separate factors (24). In pole-growing species, septal and polar growth are temporally separated but overlap spatially: septation produces the cell poles, which then become critical for orienting the peripolar elongation complex (25). Septation in these species must leave the newly formed cell poles in a state that allows elongation (26). This septum-to-growth pole remodeling must require regulatory factors that do not exist in the lateral-wall growing model organisms.

Mycobacteria and other actinomycetes have an acid-fast cell wall, in which layers of arabinogalactan and mycolic acids are covalently affixed to the peptidoglycan layer. The enzymes that build these extra cell wall layers likely require septation-specific and elongation-specific regulatory factors to control their activity and coordinate it with the synthesis of the peptidoglycan. One of these elongation-specific regulators is the DivIVA homolog Wag31. Wag31 localizes to

the cytoplasmic side of the inner membrane at the cell pole (27), is absolutely required for polar growth (25, 27) and interacts with (25, 28) and appears to regulate enzymes that make precursors for the mycolic acid layer of the cell wall at the growing poles (28). A similar system is likely to exist to help coordinate cell wall precursor production during septation.

Here we sought to identify and characterize mycobacterial homologs for the known septal factors FtsB and FtsL, and to identify novel septal factors that could be involved in functions specific to pole-growing or acid-fast bacteria. We identify predicted structural homologs of FtsB and FtsL and show that they are septal proteins and appear to be recruited to the septum in a fashion similar to that observed in *E. coli*. We also find that FtsQ associates with novel factors that localize to the divisome. We further characterize one of these newly identified septal proteins, which we have named SepIVA. SepIVA has a conserved DivIVA domain, localizes to the division site and the Intracellular Membrane Domain (IMD) and is required for cell division in *M. smegmatis*.

Results

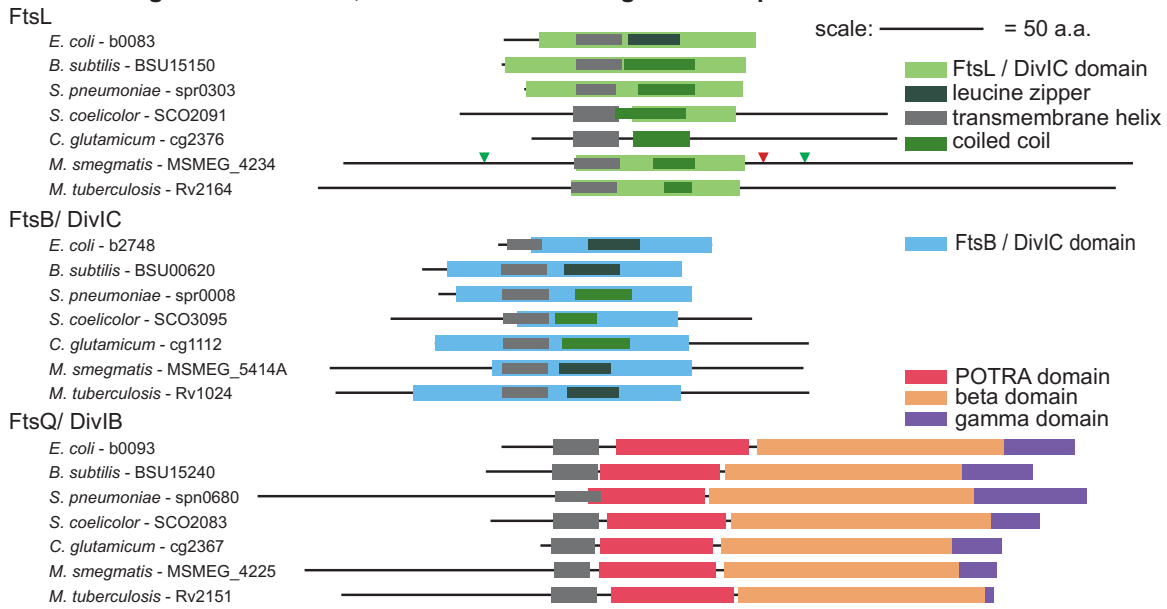
M. smegmatis and *M. tuberculosis* encode homologs of *ftsI* and *ftsQ* (*divIB*), but not annotated homologs for *ftsB* (*divIC*) or *ftsL*. Using HHPred, a Hidden Markov Model-based homology prediction tool (29), we identified putative homologs for both *ftsL* (MSMEG_4234, Rv2164) and *ftsB* (MSMEG_5414A, Rv1024). Although the sequences of the mycobacterial FtsL and FtsB proteins are not similar enough to the proteins from *E. coli* or *B. subtilis* to make a sequence alignment, these proteins share conserved domains that can be detected using a variety of secondary and tertiary structure prediction programs (29-34) (Figure 2.1A). The putative *ftsL* homolog is also highly syntenic: it is in an apparent operon with *ftsI* in evolutionarily distant species, including *Mtb*, *E. coli* and *B. subtilis*.

To determine whether these genes are essential for survival, we built *Msmeg* strains that allow us to repress transcription of putative septal factors. In these strains, the targeted gene was first complemented at the L5 phage attachment site with a tetracycline (tet)-inducible or tet-repressible promoter (35), then the endogenous copy of the gene was deleted using recombineering (36). We found that the depletion strains either died or failed to grow upon depletion of *ftsI*, *ftsQ*, *ftsL* or *ftsB* (Figure 2.1B), confirming predictions from TnSeq experiments in *Mtb* (37, 38) and *Msmeg* that these genes are all essential. To determine whether these genes are involved in septation, we compared the morphology of these depleted strains to that of the FtsZ-depleted strain, described previously (39). Our data show that depletion of *ftsZ*, *ftsI* (MSMEG_4233), *ftsQ*, *ftsL* and *ftsB* all result in elongated, branched cells that are clearly defective for septation (Figure 2.1C).

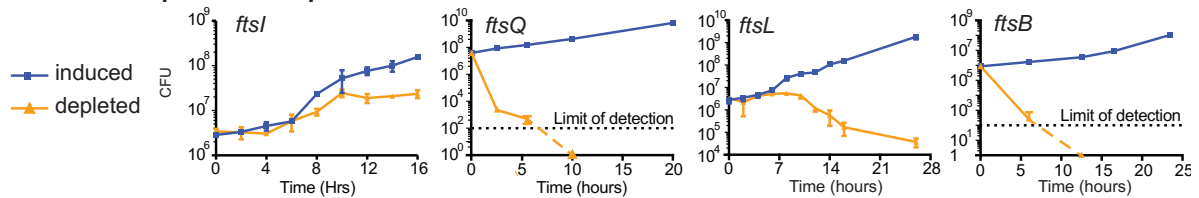
The mycobacterial FtsL homologs have long, non-conserved N- and C-terminal extensions. To determine if these were important for function, we exchanged the wild-type *Msmeg ftsL* allele at the L5 site with alleles truncated at the N or C termini. We found that *ftsL* missing the first 67 codons or the last 158 codons could complement the wild-type *ftsL*, but an allele missing the last 178 codons did not support growth (Figure 2.1A).

To determine whether and when these cell division factors are associated with the divisome, we built strains expressing both 1) a fusion between FtsZ and the mCherry2B protein (FtsZ-mcherry2B) and 2) either *ftsQ*, *ftsL*, *ftsB*, or *ftsK* fused to GFPmut3. This allowed us to simultaneously track the localization of these proteins during the course of the cell cycle using time-lapse microscopy. We found that all four Fts- proteins localize to the site of septation, as defined by co-localization with FtsZ (Figure 2.2A), and that FtsQ, L, B, and K are all recruited to the septal site after FtsZ (Figure 2.2B). We quantified the fluorescence signal at the cell center

A. Domain organization of *ftsL*, *ftsB* and *ftsQ* homologs across species



B. Survival in depletion of septal factors



C. *M. smegmatis* cells induced and depleted for septal factors

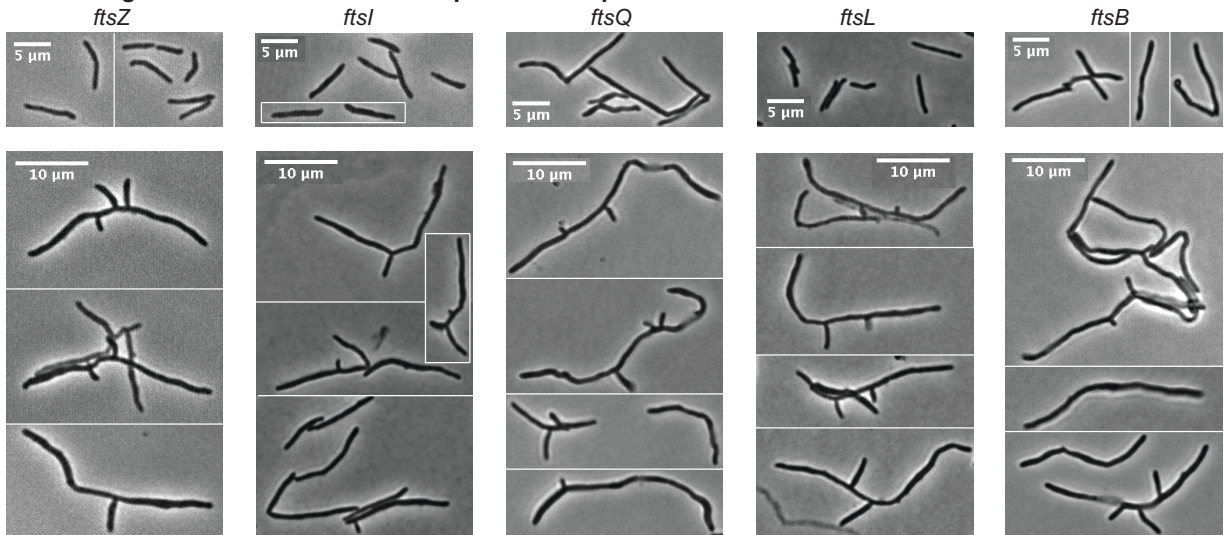


Figure 2.1: Essentiality and cell division function of septal factors. (A) Domain structure diagrams of FtsQ, L and B from mycobacteria and other species in which these genes have been studied. Domains were defined through a number of secondary structure prediction programs.

Figure 2.1 (Continued)

All gene and domain lengths are to scale. The *ftsL* truncation sites that supported growth are indicated with green arrows, the red arrow indicates a truncation site that did not support growth.

(B) Colony forming units (CFU) of strains in which *ftsI*, *Q*, *L* or *B* are under the control of a tetracycline-controlled promoter, during depletion and induction of the indicated gene. **(C)** Phase micrographs of *ftsZ*, *I*, *Q*, *L* and *B* depletion strains during induction of the gene (top) and depletion (bottom). All scale bars are 5 microns.

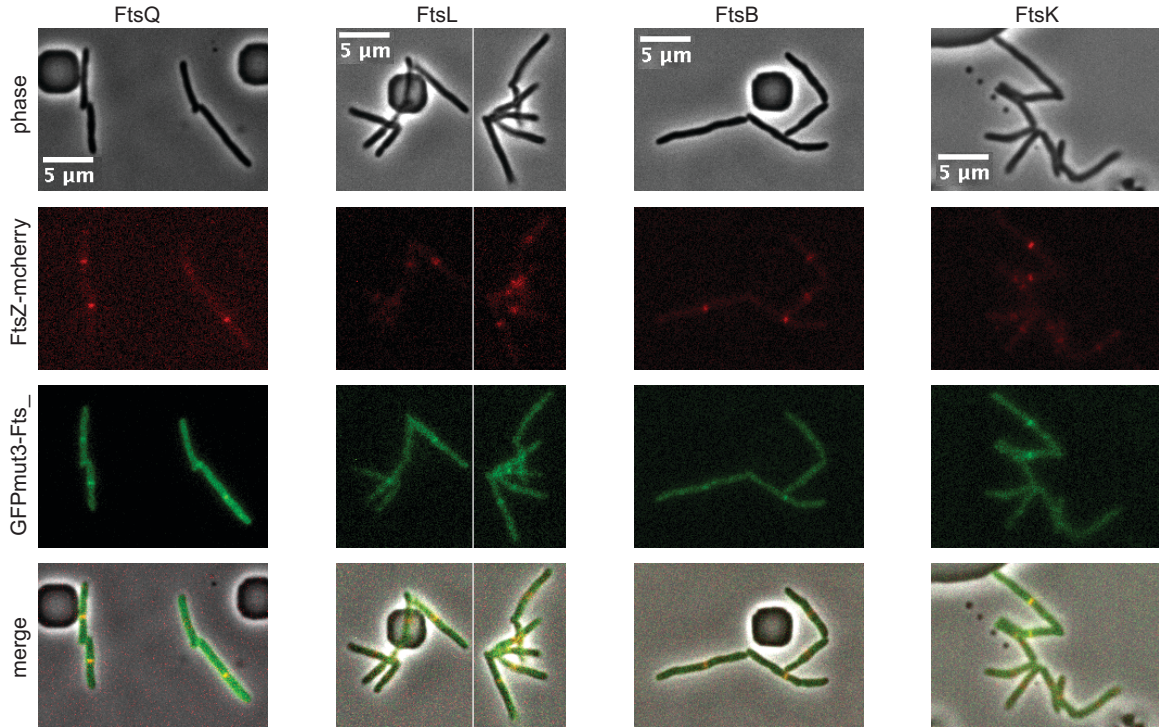
from one division event to the next and observed that the FtsZ signal always peaks ~70-80% of the way through the cell cycle, but that the peak has an earlier shoulder. The signal for FtsL and FtsB fully stabilizes by ~60% of the cell cycle, while the signal for FtsQ and FtsK fully stabilizes by ~70% of the cell cycle. The signal for all four proteins peaks between 70-80% of the cell cycle; these proteins did not exhibit localization during the shoulder period of the weaker localization of FtsZ (Figure 2.2B). Thus, FtsZ precedes FtsL, FtsB, FtsQ, and FtsK to the septation site.

We next sought to determine the dependency of localization of FtsZ, FtsK, FtsQ, FtsL, and FtsB to the mycobacterial septum. In *E. coli*, FtsZ localization to the septum and formation of the Z-ring complex directly precede FtsK recruitment. FtsK and FtsQ physically associate, recruiting FtsQ to the septum, where it brings together FtsL and FtsB to form the FtsQLB complex (40). To test if this model holds true in mycobacteria, we expressed the GFPmut3 fusions of *ftsK*, *ftsQ*, *ftsL*, and *ftsB* in the *ftsZ*, *ftsQ*, *ftsL*, and *ftsB* depletion strains and quantified their localization to the septum, as marked by FtsZ-mcherry2B (except in the *ftsZ* depletion strain). We found that all other tested Fts proteins were dependent on FtsZ. Furthermore, both FtsZ and FtsK could localize in the absence of FtsQ, L, or B, as in *E. coli*. However, while FtsL and FtsB failed to localize in the *ftsQ* depletion, FtsQ successfully localized in 40-70% of cells depleted of *ftsL* and *ftsB* (Figure 2.3A,B and Table 2.1).

To identify new proteins that interact with the mycobacterial divisome, we immunoprecipitated (IP) FtsQ-strep and identified interactors with mass spectrometry (41). We were able to IP several proteins with FtsQ-strep in two independent experiments (Table 2.2).

Because we covalently cross-linked proteins in the cells before IP, we expect that many of the identified interaction partners may not directly interact with FtsQ, but are likely to be associated with the larger divisome complex. We found several proteins that are known to be associated with

A. *M. smegmatis* cells with FtsZ-mcherry and GFP fused to other septal proteins



B. Septal signal during the cell cycle

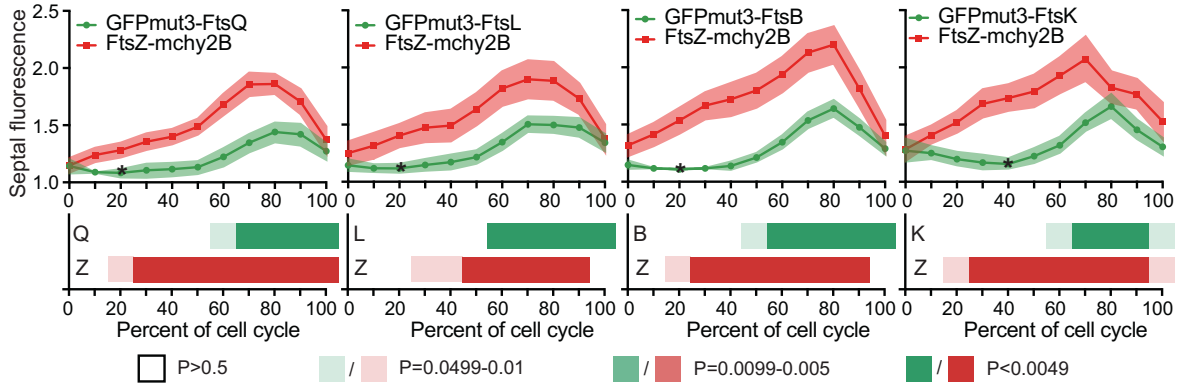


Figure 2.2: Localization of septal factors. (A) Micrographs of strains which express both FtsZ-mcherry2B and either GFPmut3-FtsQ, GFPmut3-FtsL, GFPmut3-FtsB, or FtsK-GFPmut3. **(B)** Analysis of time-lapse movies taken of the strains described in A. Phase, red and green images

Figure 2.2 (Continued)

were taken at 15 minute intervals, and the fluorescence intensity was quantified in each channel for 40-60 cell division events from at least two independent biological replicate cultures. Top: fluorescence intensity at midcell over time, data is normalized to the signal at the dimmest time point for each cell. Error bars are 95% confidence intervals. Bottom: bar graph depicts the p-value of protein localization at the midcell, indicating whether the fluorescent signal at midcell at each time point is significantly different from the fluorescent signal at the time point with the least fluorescence. For FtsZ-mcherry2B, this is always the first time point. For the other fusions, the dimmest time point, to which the others are compared, is indicated with an asterisk. The comparisons in signal intensity were made using an ordinary one-way ANOVA with Dunnet correction for multiple comparisons. The darkly colored boxes indicate that there is high confidence that the protein localized to midcell at that time point.

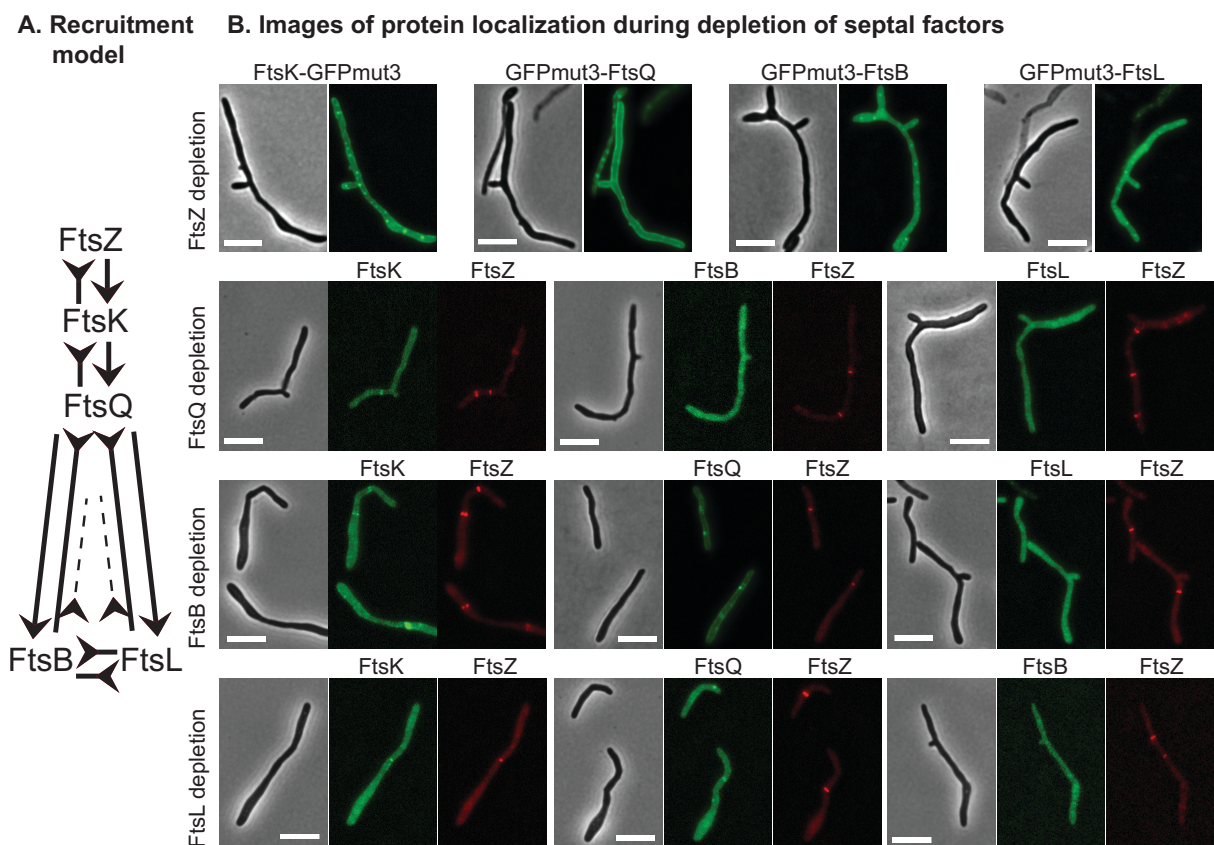


Figure 2.3: Dependency of localization between Fts septal factors. (A) Model for the recruitment of septal factors to the midcell. Regular arrow heads indicate that the protein pointed to is recruited to midcell by the protein on the side of the arrow without a point. Arrows with inverted heads indicate that the protein pointed to is dependent on the other protein for localization to midcell. Dashed lines between FtsQ and FtsB and L indicate that FtsQ is partially dependent on FtsB and L for localization. (B) Micrographs of strains depleted of FtsZ, FtsQ, FtsB, or FtsL, expressing FtsZ-mcherry2B (except in FtsZ depletion) and GFPmut3-FtsQ, GFPmut3-FtsL, GFPmut3-FtsB, or FtsK-GFPmut3. Multiple images from these experiments were used to produce the data in Table 2.1.

Table 2.1: Dependency of Localization. Ratios indicate the number of cells in which the fluorescent protein constructs listed in the left column localized to septa at midcell in strains in which the proteins across the top row were depleted, over the total number of such cells that were imaged. Only cells expressing an FtsZ signal, which served as a reference point for septal localization, were quantified.

Table 2.1. Dependency of Localization				
Localization	Depletion			
FP-Fusion	FtsZ	FtsQ	FtsL	FtsB
FtsZ-mCherry	ND	75/75	75/75	75/75
GFPmut3-FtsQ	0/200	ND	30/75	54/75
GFPmut3-FtsL	0/200	2/75	ND	0/75
GFPmut3-FtsB	1/200	6/75	0/75	ND
FtsK-GFPmut3	0/200	62/75	65/75	66/75

Table 2.2: Proteins whose peptides were pulled down with cross-linked FtsQ-strep. The “Ess TB?” and “Ess SM?” refer to predicted essentiality from TnSeq screens performed in *Mtb* (37) and *Msmeg*: Y=essential, N=non-essential, Y-D=domain essential. The “sum unique peptides” is the sum from the two independent IP experiments. Localization was determined by fusing GFPmut3 to the N (NT) or C (CT) termini of the indicated proteins; representative localization images are shown in Figure 2.4.

Table 2.2. FtsQ pulldown data							
Gene	MSMEG #	TB #	annotation / conserved domains	ESS TB?	ESS Msm?	localization	sum unique peptides
secA1	MSMEG_1881	Rv3240	SecA1 translocase	Y	Y		54
ffh	MSMEG_2430	Rv2916	signal recognition particle	Y	Y		50
	MSMEG_3748	Rv1697	thiamine pyrophosphokinase	Y	Y		32
choD	MSMEG_1604	Rv3409	cholesterol oxidase	N	N		32
	MSMEG_2416	Rv2927	DivIVA domain	Y	Y	NT fusion - septal and PMf	22
subI	MSMEG_4533	Rv2400	sulfate binding lipoprotein	Y	N		22
ftsK	MSMEG_2690	Rv2748	septation factor, DNA translocase	Y	Y		21
	MSMEG_6434	Rv3850	conserved hypothetical	N	N		20
ftsH	MSMEG_6105	Rv3610	membrane protease	Y	N		20
	MSMEG_4287	Rv2219	conserved membrane protein	Y	Y	NT fusion - septal	19
	MSMEG_2410	Rv2969	DsbA family, disulfide isomerase	Y	Y		19
secA2	MSMEG_3654	Rv1821	preprotein translocase ATPase	Y	N		19
	MSMEG_6051	N/A	ABC transporter		N		18
sugC	MSMEG_5058	Rv1238	ABC ATPase - sugar transport	N	N		18
	MSMEG_1642	Rv1747	ABC transporter	N	N		18
ftsY	MSMEG_2424	Rv2921	SRP receptor	Y	Y		16
	MSMEG_3027	Rv2553	MltG - endolytic transglycosylase	Y	Y - D	NT fusion - septal, poles, membrane	16
	MSMEG_5223	Rv1111	conserved membrane protein	Y	Y	CT fusion- septal and polar	15
	MSMEG_0690	Rv0338	iron sulfur reductase?	Y	Y		15
	MSMEG_3655	Rv1819	ABC permease, drug exporter	N	N		15
ftsE	MSMEG_2089	Rv3102	ABC ATPase - cell division	N	N		14
pntA	MSMEG_0110	N/A	NAD(P) transhydrogenase alpha subunit		N		14
pstP	MSMEG_0033	Rv0018	Protein serine threonine phosphatase	Y	N		14
lppW	MSMEG_2439	Rv2905	alanine rich lipoprotein, PBP or beta-lactamase	N	N		14
	MSMEG_5419	N/A	cupredoxin, lipoprotein		N		13
	MSMEG_4254	Rv2187	Fad15 - long chain fatty acid coA ligase	N	N		13
	MSMEG_6394	Rv3802	conserved membrane protein, hydrolase/ esterase	Y	Y	NT fusion - septal and membrane	12
oxaA	MSMEG_6942	Rv3921	membrane protein insertase YidC	Y	Y	CT fusion - septal and membrane	11
pknA	MSMEG_0030	Rv0015	Serine Threonine protein kinase	Y	Y		11
	MSMEG_6725	N/A	ABC transporter, ATPase		N		11
	MSMEG_6282	Rv3718		N	N		9
	MSMEG_2727	N/A	periplasmic binding protein		N		9

Table 2.2 (Continued)

	MSMEG_0736	Rv0383	conserved secreted protein	Y	Y - D	CT fusion - septal, poles, membrane	9
	MSMEG_1353	Rv0647	serine threonine protein kinase	Y	Y	NT fusion - PMf	9
rhIE	MSMEG_1930	Rv3211	RNA helicase rhIE (ribosome maturation)	Y	Y - D		9
ppk	MSMEG_2391	Rv2984	polyphosphate kinase	Y	N		9
deaD	MSMEG_5042	Rv1253	ATP dependent, DEAD box RNA helicase	N	N		9
	MSMEG_1252	N/A			N		9
	MSMEG_4484	Rv2345	conserved membrane protein	N	N		8
	MSMEG_1285	Rv0613	conserved hypothetical	N	N		8
			phosphoribosylformylglycinamide CYCLO-ligase	Y	N		8
purM	MSMEG_5798	Rv0809		Y	N		8
ppiB	MSMEG_2974	Rv2582	prolyl cis-trans isomerase	Y	N		7
fhaA	MSMEG_0035	Rv0020	conserved, forkhead associated domain	Y	Y		7
	MSMEG_0639	N/A	transporter		N		7
	MSMEG_4692	Rv2468	conserved hypothetical	N	N		7
fadD6	MSMEG_5086	Rv1206	very long chain acyl-coA synthetase	N	N		7
	MSMEG_1945	Rv3200	ion channel	N	Y - D		7
dnaJ	MSMEG_4504	Rv2373	co-chaperone	Y	N		6

the divisome in other bacterial species, including FtsE, FtsH and FtsK (42-45). We also found proteins that have previously been shown to localize to the mycobacterial divisome: FhaA (46) and PknA (47). Additionally, we identified proteins involved in the secretion and co-translational insertion of membrane proteins, which is expected because FtsQ is a membrane protein. Finally, we also saw many proteins with unknown functions. Several of these are transmembrane and essential for survival in *Mtb* and *Msmeg* according to TnSeq screens (37). We hypothesize that these could be mediators of cell wall insertion during division or elongation.

To test whether these uncharacterized proteins could be involved in septation or elongation, we constructed *Msmeg* strains in which we expressed each gene tagged at either the C or N terminus with a fluorescent protein. We found that several of these factors appear to localize to the septum, poles, Intracellular Membrane Domain (IMD), or some combination of these sites (Figure 2.4). The IMD is a cytoplasmic polar membrane domain which seems to be the localization site of several cell wall precursor enzymes (48).

Of interest among the novel divisome factors was MSMEG_2416, henceforth called *sepIVA*, which is predicted to be essential in *Mtb* (37), has a conserved DivIVA domain and shares 19.7% amino acid identity and 29.4% similarity with the well-studied mycobacterial DivIVA homolog Wag31 (MSMEG_4217). We attempted to construct a strain in which *sepIVA* could be transcriptionally depleted as in Figure 2.1; however, we were unable to obtain strains in which we could replace the endogenous *sepIVA* with a construct at the L5 phage integrase site with a non-native promoter. Instead, we used Oligo-mediated Recombineering with Bxb1 Integrase Targeting (ORBIT) (49) to integrate a vector with a DAS tag at the C-terminus of *sepIVA*. The DAS tag targets the attached protein for proteolysis by ClpXP upon expression of the adaptor protein SspB

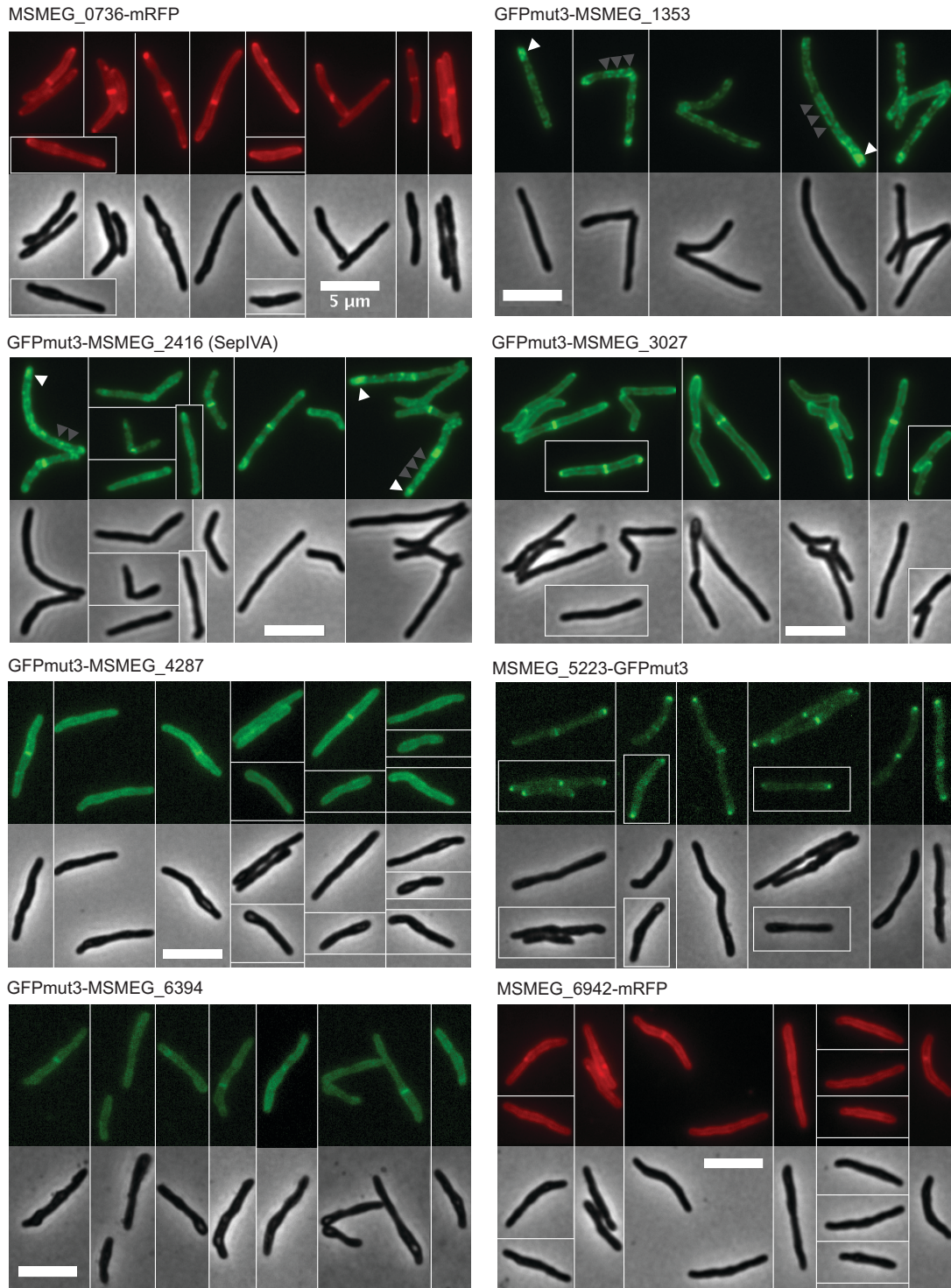


Figure 2.4: Micrographs of merodiploid *Msmeg* cells expressing the indicated fluorescent protein fusions. Fluorescent images on top, phase images on bottom. The white arrows point to

Figure 2.4 (Continued)

the polar localization, and grey arrows point to the patchy side-wall localization that is characteristic of proteins associated with the IMD (Intracellular Membrane Domain) (59).

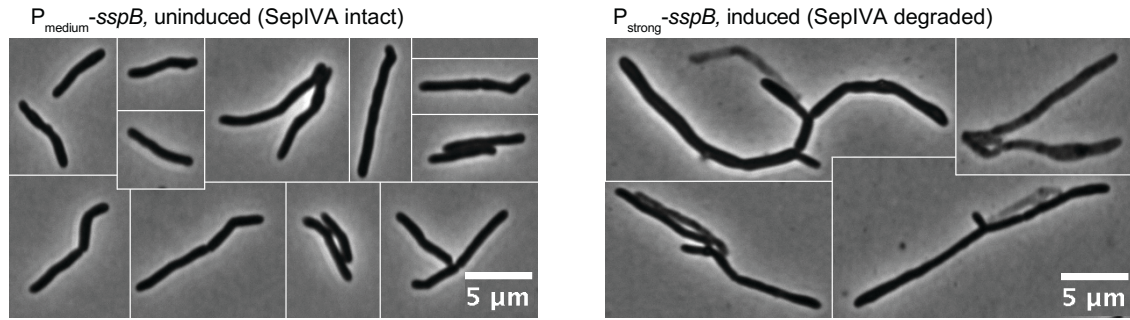
(50). We found that when SepIVA-DAS was degraded by expression of high levels of SspB, *Msmeg* cells continued to elongate but failed to divide, resulting in long, branched filaments (Figure 2.5A) like those seen in the transcriptional depletion of other septal factors (Figure 2.1). These filamenting cells were not viable (Figure 2.5B).

While the previously-studied DivIVA homologs in actinobacteria are all involved in cell elongation (25, 51-53), the DivIVA protein in *B. subtilis* is involved in septation site positioning and cell division (54, 55). DivIVA in *B. subtilis* works by recruiting the septation inhibitors MinC and MinD to the nascent poles at the end of each septation event and anchoring them there through the next cell cycle so that FtsZ rings do not form over the cell poles (56, 57). There are no apparent MinC homologues in *Msmeg*. Nevertheless, if SepIVA has a similar function in mycobacteria as DivIVA has in *B. subtilis*, then we would expect that it would localize to the cell division site after FtsZ, and that FtsZ would form extra Z-rings at the poles upon SepIVA depletion (55, 58).

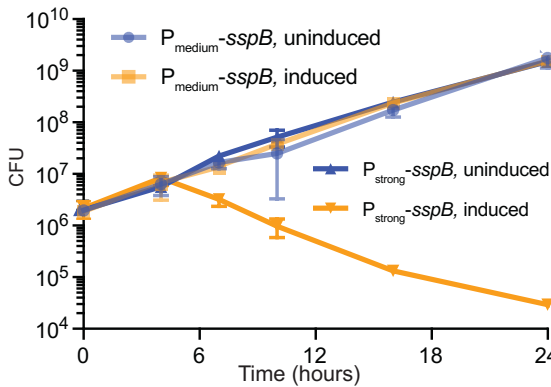
We used time-lapse microscopy of a strain with merodiploid GFPmut3-SepIVA and FtsZ-mcherry2B constructs and found that the septal localization of SepIVA occurred late in septation (Figure 2.5C), well after the localization of FtsZ. However, we find that after depletion of SepIVA, FtsZ-mcherry2B still localizes, and does not form Z-rings near the pole (Figure 2.5D), as we would expect if SepIVA had the same function as the DivIVA homolog from *B. subtilis* (55, 58).

We did not observe consistent polar localization of SepIVA, but did often see a localization pattern that was similar to the IMD localization pattern observed previously (59): the proteins dynamically populate a region near the pole in some cells and are present in patches along the membrane (Figure 2.5E). To assess whether the localization of SepIVA coincides with the IMD, we conducted co-localization analysis on a strain expressing both GFPmut3-SepIVA and mCherry-Glft2, a protein which has previously been shown to be associated with the IMD (59).

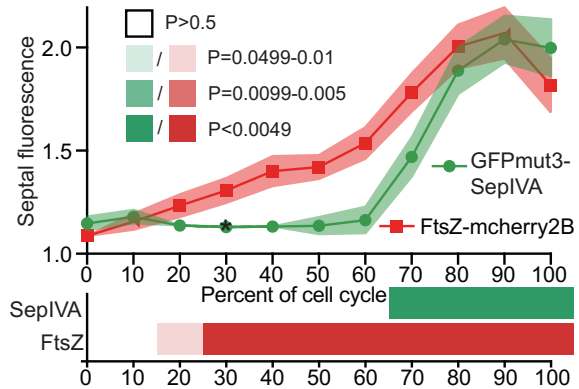
A. Cell morphology during induced degradation of SepIVA



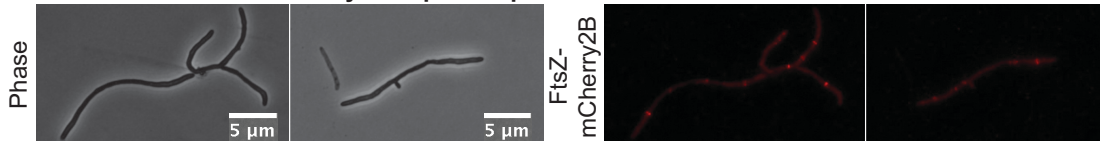
B. Survival in degradation of SepIVA



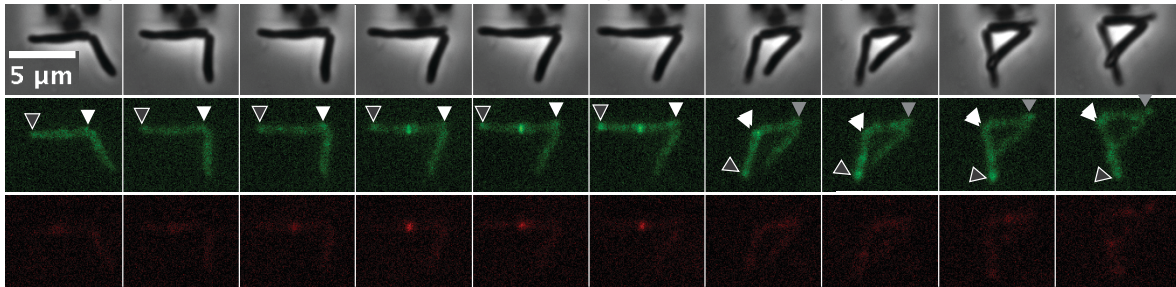
C. Septal signal during the cell cycle



D. Localization of FtsZ-mCherry in SepIVA depletion



E. Micrographs of GFPmut3-SepIVA and FtsZ-mCherry2B across the cell cycle



F. Co-localization of GFPmut3-SepIVA and mCherry-GltF2

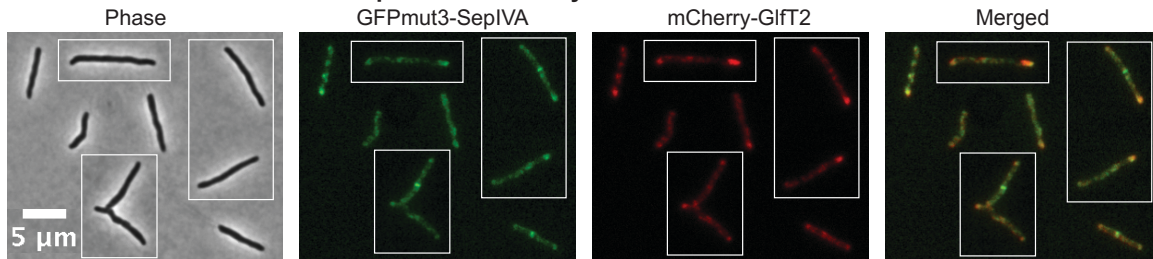


Figure 2.5: Cellular role and localization of SepIVA. (A) Micrographs of SepIVA-DAS depletion strains with very low levels (left) and high levels (right) of the degradation-mediation

Figure 2.5 (Continued)

factor SspB which corresponds to normal levels of SepIVA (left) and low levels of SepIVA (right). **(B)** Colony forming units of SepIVA-DAS depletion strains with SspB expressed at various levels. High levels of SspB expression correspond to low levels of SepIVA (dark orange). **(C)** Analysis of septal localization from time-lapse movies of the strain with GFPmut3-SepIVA and FtsZ-mcherry2B constructs. Phase, red and green images were taken at 15 minute intervals, and the fluorescence intensity was quantified in each channel for 40-60 cell cycles from at least two independent biological replicate cultures. Top: fluorescence intensity at midcell over time. Data are normalized to the signal at the dimmest time point for each cell. Error bars are 95% confidence intervals. Bottom: p-value indicating whether the fluorescent signal at each time point is significantly different from the fluorescent signal at the dimmest time point ($t=0$ for FtsZ and $t=30$ for SepIVA). The darkly colored boxes indicate that there is high confidence that the protein localized to midcell at that time point, see p-value color scale on top panel. **(D)** Images of the SepIVA-DAS *twety2::FtsZ-mcherry2B* strain depleted of SepIVA by SspB expression. Left: phase, right: FtsZ-mcherry2B. **(E)** Selected time-lapse images from one of the movies used in (C), one and a half cell cycles. The dark gray arrows with white outlines indicate the oldest pole, the white arrows indicate the newest pole and the medium gray arrows indicate an intermediate-age pole. Top: phase; middle: GFPmut3-SepIVA; bottom: FtsZ-mcherry2B. **(F)** Representative images of the *mc²155 glfIT2::mCherry-glfIT2 L5::GFPmut3-sepIVA* strain. The Pearson's correlation coefficient between these two protein fusions, calculated from 16 images representing 200-400 cells, is $R=0.87\pm 0.3$.

We find that these two protein fusions significantly co-localize, with a Pearson's R coefficient of 0.87 ± 0.03 . Although the co-localization was significant, it was not perfect. We observed that GFPmut3-SepIVA localized more brightly to the septum and mCherry-GltT2 localized more brightly at the subpolar region. We conclude that SepIVA could be associated with the IMD, but that its association with the septation site could be independent of the IMD.

Discussion

Cell septation in mycobacteria has been shown to involve many factors which are conserved in species as evolutionarily distant as the model organisms *E. coli* and *B. subtilis* (18, 22, 60). However, mycobacterial septation is still poorly understood, both because not all the homologs of conserved septal factors have been studied and identified, and because septation in pole-growing actinomycetes should require additional functionalities that are not required in the lateral wall-growing Gram-positive and Gram-negative species. In this work, we identify and characterize structural homologs of broadly conserved septal factors in *Msmeg*, and describe a new septation factor that appears to have a previously undescribed function.

FtsQ, FtsL and FtsB are septal factors in *E. coli* that do not have enzymatic activity but are involved in cueing the initiation of septation, probably through conformational changes that are propagated to their interaction partners (61). Our work confirms that these proteins are likely to have a similar function in mycobacteria (Figure 2.1, 2.2). We find that FtsQ, L, B and K all localize to the septation site after FtsZ, as has been observed in other species (40, 62); thus, none of them are likely to be involved in early divisome assembly. FtsQ, L, B and K all start to localize significantly to the midcell co-incident with the strengthening of the FtsZ-mcherry2B signal. We observe that FtsL and FtsB seem to brighten at midcell slightly before FtsQ and FtsK. This result

is confusing in light of the dependency of localization data, which shows that FtsK localization is independent of the presence of Q, L and B, and that FtsL and FtsB require FtsQ for localization (Figure 2.3, Table 2.1); one naturally assumes that FtsQ would localize before L and B. While our dependency of localization results mirror those seen in *E. coli* (40, 62), comparable timing of localization experiments have not been done in that organism, to our knowledge. In *B. subtilis*, DivIB (FtsQ) may also localize slightly after FtsL (63). There are several factors that make these data difficult to interpret. Firstly, the signal to noise ratio varies between the GFPmut3 fusion constructs, possibly because of partial mislocalization or proteolysis of some of the fusion proteins. Secondly, the brighter signal could be due to an increase in the number of proteins being recruited to the septal site or to a compaction of the Z ring such that more of those proteins emit their light into a smaller number of pixels in the detector. We suspect that these septal factors may be accumulating near the septal site for a while before we can see them above the noise in the images. The earlier timing of FtsL and FtsB localization, the partial dependency of FtsQ localization on FtsB and FtsL and the interdependency of FtsB and FtsL localization (64, 65) implies that these proteins may all slowly accumulate at midcell and help stabilize each other there. There is precedent in *B. subtilis* for early septal factors to be dependent on later factors for stabilization to the septum (66).

We find that FtsQ associates with known septal factors, and several other factors that are expected to interact with membrane proteins (Table 2.2). The localization patterns of the novel divisome-associated factors (Figure 2.4) corroborate the idea that septal and polar elongative factors are likely to be in close contact during certain times of the mycobacterial cell cycle. We did not find FtsL or FtsB in this IP experiment, however. These negative results are difficult to

interpret: FtsQ, L and B are expected to be present in very low copy numbers (67), and so they are not likely to be identified in the mass spectrometry experiment.

One new septal factor, which we have named SepIVA, is essential for cell division and localizes to the midcell late in the cell cycle (Figure 2.5C). The FtsZ-mcherry2B signal in the GFPmut3-SepIVA, FtsZ-mcherry2B strain peaked later in the cell cycle than the FtsZ-mcherry2B signal in the experiments in Figure 2.2, implying that the two fluorescent protein constructs in this strain may interfere slightly with the timing of divisome assembly. SepIVA appears to dynamically move from the septum to the Intracellular Membrane Domain (IMD) over the course of the cell cycle (Figure 2.5EF). While the exact function of the IMD is still being explored, the available data suggest that it is a site for organizing the enzymes involved in the biosynthesis of cell surface precursor molecules (59). The presence of SepIVA at both the septum and IMD implies that these functional zones may have coordinated functions. Alternatively, the IMD could serve as reservoir to store SepIVA until it is needed in division, or SepIVA may have multiple independent functions, as has been seen in the DivIVA homolog from *Listeria monocytogenes* (68).

Interestingly, SepIVA has a DivIVA domain and shares considerable similarity with Wag31, the well-studied DivIVA homolog in mycobacteria. Wag31 localizes to the poles and is essential for elongation, but how it mediates its role in elongation is not clear. It seems likely that Wag31 is an enzymatic activator of some of the cell wall precursor enzymes with which it interacts (25, 28, 69). SepIVA, like Wag31, does not have apparent enzymatic domains of its own, so it seems likely that it is also a regulator. However, it does not appear to have a function similar to the DivIVA homolog in *B. subtilis*, which regulates inhibitors of Z-ring formation at the cell poles (56, 57): depletion of SepIVA does not lead to misplacement of Z-rings to the pole in *Msmeg* (Figure 2.5D). The GpsB proteins from *B. subtilis* and *Streptococcus pneumoniae* are shortened

DivIVA homologs that are important in regulating septation (70, 71); SepIVA may be more similar to these in function than it is to *B. subtilis* DivIVA proper. In *B. subtilis*, GpsB and EzrA work together to move PBP1 to the septum and then away from the poles after septation (70). In *S. pneumoniae*, GpsB and DivIVA coordinate peptidoglycan synthesis between the septum and periphery, partly by interactions with the septal factor EzrA (71). DivIVA homologs in general seem to be involved in recruiting other proteins to their sites of activity and regulating them (27, 68, 72). Thus, we surmise that SepIVA may recruit and activate cell wall precursor enzymes or transmembrane cell wall enzymes that are required for the construction of the septal cross-wall, similarly to how Wag31 apparently regulates such enzymes during elongation (25, 28, 69).

All of the experiments presented here were done in *Msmeg*. All the genes and proteins studied have close homologs in *M. tuberculosis*. However, close homologs have been shown to have slightly different functions between these two species (73-75), so we cannot be sure that these proteins all behave identically in *M. tuberculosis*.

Although various rod-shaped bacteria may look indistinguishable in the light microscope, there are several different ways to build a rod-shaped cell (11, 76). These different modes of cell morphogenesis have conserved and distinct mechanisms of assembling and arranging the cell wall. Here, we show that the actinomycete *Msmeg* has the conserved septation proteins FtsQ, FtsL and FtsB. We also find that *Msmeg* has a previously undescribed septal factor, SepIVA, which may have a function that is restricted to pole-growing actinomycetes.

Section 2.2: Materials and Methods

Bacterial strains and culture conditions

M. smegmatis mc²155 was cultured in 7H9 (Becton-Dickinson, Franklin Lakes, NJ) media with 5 g/L albumin, 2 g/L glucose, 0.85 g/L NaCl, 0.003 g/L catalase, 0.2% glycerol and 0.05% Tween80 added, or plated on LG agar. *E. coli* DH5 α , TOP10 or XL1 Blue were used for cloning. For *Msmeg*, antibiotic concentrations were: 25 μ g/ml kanamycin, 50 μ g/ml hygromycin, 20 μ g/ml nourseothricin, 20 μ g/ml zeocin. For *E. coli*, antibiotic concentrations were: 50 μ g/ml kanamycin, 100 μ g/ml hygromycin, 50 μ g/ml zeocin, 40 μ g/ml nourseothricin. Anhydrotetracycline was used at between 50 and 250 ng/ml for gene induction or repression. Acetamide was used at 0.2% for *ftsZ* induction.

Strain construction

Gene knockouts of essential genes were made by first integrating a copy of the gene at the L5 site (77) under the control of a promoter with the tet operator. *ftsI* and *ftsL* were cloned into vectors with the tetON repressor, so their expression was tetracycline dependent. *ftsB* and *ftsQ* were cloned into vectors with the tetOFF repressor, so their expression was tetracycline-repressible (35). Once these essential genes were complemented at the L5, the endogenous copies were knocked out using recombineering (36) as described (78). Mutants, epitope-tagged and fluorescent-protein tagged versions of genes were made by swapping L5 integrating vectors with different antibiotic markers (79). We were unable to knock out MSMEG_2416 in any background in which it was complemented with a non-native promoter, so we used ORBIT (49) to introduce a vector that inserts a FLAG-DAS tag at the C-terminus of MSMEG_2416, and induced *sspB* to cause the MSMEG_2416 protein to be proteolyzed (80). The ORBIT primer had a Bxb1 phage integration

site flanked by 70 base pairs of homology before and after the stop codon of MSMEG_2416. Merodiploid expression constructs were integrated at the L5 site, except FtsZ-mcherry2B, which was integrated at the Tweety integrase site (81). All strains used are listed in Supplemental Table 2.1. All plasmids used are listed in Supplemental Table 2. All primers used are listed in Supplemental Table 3.

Bioinformatic protein analysis.

The FtsL/ DivIC and the FtsB/ DivIC domains were defined using the NCBI's Conserved Domain Database (34) or HHPred (29). The transmembrane helices were predicted using the TMHMM server (30). Coiled coils were predicted using the Coils/Pcoils tool in the MPI Bioinformatics Toolkit (31). Leucine zippers are coiled coils that contain four leucines that are each seven residues apart. The *ftsQ* homologs were analyzed in order to find the POTRA, β and γ structural domains defined in (32). Because the sequence homology between *ftsQ* homologs was low, the PredictProtein secondary structure prediction tool (33) was used to define the domains according to secondary structure.

Microscopy and image analysis

Still images were taken of cells immobilized on agar pads on a Nikon Ti inverted widefield epifluorescence microscope with a Photometrics coolSNAP CCD monochrome camera, a 49002 green filter cube, a 49008 red filter cube and a Plan Apo 100X objective with a numerical aperture of 1.4. Images were processed using NIS Elements version 4.3 and ImageJ. Time lapse movies were taken at 15 minute intervals of cells growing in CellASIC microfluidic plates (Millipore Sigma) on a Nikon Eclipse Ti inverted widefield epifluorescence microscope with a Spectra X

LED lightsource and an Andor Zyla sCMOS camera and a Plan Apo 100X objective with a numerical aperture of 1.4. The microscope was equipped with a Prior stage controlled with Nikon Perfect Focus and an In vivo Scientific environmental chamber set at 37. The green images were taken with a 465-495 excitation filter and a 515-555 emission filter. The red fluorescent images were taken with a 528-553 excitation filter and a 590-650 emission filter. Images were processed using NIS Elements version 4.5 and ImageJ. The videos were analyzed by custom semi-automated ImageJ and MATLAB scripts. Briefly, in ImageJ, fluorescence line profiles were measured consistently from new pole to old pole for a single cell at every time point in the cell cycle. These line profiles were then imported into MATLAB, and analyzed by a custom script. The maximum fluorescence intensity from the middle third of the cell was determined at every time point. Then for every cell, each time-point was interpolated to 1/10 of the cell cycle for that cell so as to be able to average many cells consistently. The midcell fluorescent signal values for each cell cycle were divided by the value at the time point with the lowest signal for that cell. These normalized values were averaged to make the top graphs in Figures 2.2B and 2.5C. The time point with the lowest average signal was then compared to the other time points using an ordinary one-way ANOVA with Dunnet correction for multiple comparisons in order to build the P-value graphs at the bottom of Figures 2.2B and 2.5C. These midcell fluorescent values were calculated for between 50 and 70 cells for each strain measured, and the data are presented with error bars representing 95% confidence intervals.

All aTc-dependent depletion strains were depleted by either 1) the addition of 50-250 ng/mL anhydrotetracycline (aTc) or 2) washing of cells in 7H9 lacking aTc and depleted as such for 9

hours. The FtsZ depletions were conducted by washing cells grown in 7H9 + 0.2% acetamide with 7H9 and growing without acetamide for 7 hours before imaging.

The co-localization analysis was performed by taking red (mCherry-GlfT2) and green (GFPmut3-SepIVA) fluorescent and phase images of mc²155 L5::CB910-*sepIVA glfT2*::mCherry-*glfT2* from two independent cultures. The background was subtracted from the fluorescent images. The phase images were used to create a mask, outside of which all pixel data was deleted in the fluorescent images. The coloc2 program in ImageJ was used to calculate the Pearson's correlation coefficient for all the pixels within the cell masks from 16 individual images, representing 100-200 cells from each biological replicate. The Pearson's R values were converted to Fisher's z values, and the mean and 95% confidence interval of the z-values was calculated, then the average R value was calculated from the Fisher's z-values.

Immunoprecipitations

To identify potential interactors of FtsQ, a 1 L cultures of the *ftsQ-strep* strain and a wild-type control were spun down and resuspended in PBS tween 80 + 0.13% paraformaldehyde. The cultures were incubated with the paraformaldehyde for an hour at 37°C, then resuspended in a wash buffer of 100 mM Tris, 150 mM NaCl, 1 mM EDTA, protease inhibitor and 0.1% n-Dodecyl- β -D-maltose (DDM) (Cayman Chemical). The cells were lysed twice using a French press and lysate was pelleted at 15000 rpm for 15 minutes at 4°C. The supernatant was incubated with Streptactin-covered beads (IBA). The beads were washed with the wash buffer, and the protein was eluted with Buffer BX (IBA). The eluted samples were separated on 4-12% NuPAGE Bis Tris precast gel (Invitrogen Novex) and then stained with Coomassie blue. The entire lane of eluted

protein from the FtsQ-strep and control pulldowns were cut out and sent to Harvard Taplin facility for mass spectrometry analysis. The pulldown was performed twice and results were sorted first for hits that appeared in both runs and then for enrichment in the FtsQ pulldown as compared to the wild type control pulldown.

Acknowledgements

This research received no specific grant from any funding agency in the public, commercial, or not-for-profit sectors. We thank the The Microscopy Resources on the North Quad (MicRoN) core at Harvard Medical School for the use of microscopes and assistance with imaging.

Section 2.3: References

1. **Wu KJ, Zhang J, Baranowski C, Leung V, Rego EH, Morita YS, Rubin EJ, Boutte CC.** 2018. Characterization of Conserved and Novel Septal Factors in *Mycobacterium smegmatis*. *Journal of Bacteriology* **200**:e00649–17–15.
2. **Wu LJ, Errington J.** 2011. Nucleoid occlusion and bacterial cell division. *Nat Rev Microbiol* **10**:8–12.
3. **Blaauwen den T, de Pedro MA, Nguyen-Disteche M, Ayala JA.** 2008. Morphogenesis of rod-shaped sacculi. *FEMS Microbiology Reviews* **32**:321–344.
4. **Tsang M-J, Bernhardt TG.** 2015. A role for the FtsQLB complex in cytokinetic ring activation revealed by an *ftsL* allele that accelerates division. *Mol Microbiol* **95**:925–944.
5. **Yang DC, Tan K, Joachimiak A, Bernhardt TG.** 2012. A conformational switch controls cell wall-remodelling enzymes required for bacterial cell division. *Mol Microbiol* **85**:768–781.
6. **Daniel RA, Errington J.** 2003. Control of Cell Morphogenesis in Bacteria. *Cell* **113**:767–776.
7. **Randich AM, Brun YV.** 2015. Molecular mechanisms for the evolution of bacterial morphologies and growth modes. *Front Microbiol* **6**.
8. **Brown PJB, de Pedro MA, Kysela DT, Van der Henst C, Kim J, De Bolle X, Fuqua C, Brun YV.** 2012. Polar growth in the Alphaproteobacterial order Rhizobiales. *Proc Natl Acad Sci USA* **109**:1697–1701.
9. **Thanky NR, Young DB, Robertson BD.** 2007. Unusual features of the cell cycle in mycobacteria: Polar-restricted growth and the snapping-model of cell division. *Tuberculosis* **87**:231–236.
10. **Aldridge BB, Fernandez-Suarez M, Heller D, Ambravaneswaran V, Irimia D, Toner M, Fortune SM.** 2012. Asymmetry and aging of mycobacterial cells lead to variable growth and antibiotic susceptibility. *Science* **335**:100–104.
11. **Howell M, Brown PJ.** 2016. Building the bacterial cell wall at the pole. *Current*

Opinion in Microbiology **34**:53–59.

12. **Kalakoutskii LV, Agre NS.** 1976. Comparative aspects of development and differentiation in actinomycetes. *Bacteriol Rev* **40**:469–524.
13. **Braña A.** 1982. Mode of cell wall growth of *Streptomyces antibioticus*. *FEMS Microbiology Letters* **13**:231–235.
14. **Lohnis F.** 1921. Studies upon the life cycles of the bacteria. National Academy of Sciences.
15. **Gottlieb D.** 1953. The physiology of the actinomycetes. The Sixth International Congress for Microbiology, Rome 122–136.
16. **Pichoff S, Lutkenhaus J.** 2002. Unique and overlapping roles for ZipA and FtsA in septal ring assembly in *Escherichia coli*. *The EMBO Journal* **21**:685–693.
17. **Buss JA, Peters NT, Xiao J, Bernhardt TG.** 2017. ZapA and ZapB form an FtsZ-independent structure at midcell. *Mol Microbiol* **2**:2006.0008–12.
18. **Sharma AK, Chatterjee A, Basu J, Kundu M, Gupta S, Banerjee SK.** 2015. Essential protein SepF of mycobacteria interacts with FtsZ and MurG to regulate cell growth and division. *Microbiology (Reading, Engl)* **161**:1627–1638.
19. **Duman R, Ishikawa S, Celik I, the HS,** 2013. Structural and genetic analyses reveal the protein SepF as a new membrane anchor for the Z ring. *Proceedings of National Academy of Sciences*.
20. **Datta P.** 2002. Interaction between FtsZ and FtsW of *Mycobacterium tuberculosis*. *Journal of Biological Chemistry* **277**:24983–24987.
21. **Rajagopalan M, Maloney E, Dziadek J, Poplawska M, Lofton H, Chauhan A, Madiraju M.** 2005. Genetic evidence that mycobacterial FtsZ and FtsW proteins interact, and colocalize to the division site in *Mycobacterium smegmatis*. *FEMS Microbiology Letters* **250**:9–17.
22. **Datta P, Dasgupta A, Singh AK, Mukherjee P, Kundu M, Basu J.** 2006. Interaction between FtsW and penicillin-binding protein 3 (PBP3) directs PBP3 to mid-cell,

- controls cell septation and mediates the formation of a trimeric complex involving FtsZ, FtsW and PBP3 in mycobacteria. *Mol Microbiol* **62**:1655–1673.
23. **Liu B, Persons L, Lee L, De Boer PAJ.** 2015. Roles for both FtsA and the FtsBLQ subcomplex in FtsN-stimulated cell constriction in *Escherichia coli*. *Mol Microbiol* **95**:945–970.
 24. **Blaauwen den T, de Pedro MA, Nguyen-DistÃ che M, Ayala JA.** 2008. Morphogenesis of rod-shaped sacculi. *FEMS Microbiology Reviews* **32**:321–344.
 25. **Meniche X, Otten R, Siegrist MS, Baer CE, Murphy KC, Bertozzi CR, Sassetti CM.** 2014. Subpolar addition of new cell wall is directed by DivIVA in mycobacteria. *Proc Natl Acad Sci USA* **111**:E3243–51.
 26. **Howell M, Aliashkevich A, Salisbury AK, Cava F, Bowman GR, Brown PJB.** 2017. Absence of the Polar Organizing Protein PopZ Results in Reduced and Asymmetric Cell Division in *Agrobacterium tumefaciens*. *J Bacteriol* **199**:e00101–17–16.
 27. **Kang CM, Nyayapathy S, Lee JY, Suh JW, Husson RN.** 2008. Wag31, a homologue of the cell division protein DivIVA, regulates growth, morphology and polar cell wall synthesis in mycobacteria. *Microbiology* **154**:725–735.
 28. **Xu W-X, Zhang L, Mai J-T, Peng R-C, Yang E-Z, Peng C, Wang H-H.** 2014. The Wag31 protein interacts with AccA3 and coordinates cell wall lipid permeability and lipophilic drug resistance in *Mycobacterium smegmatis*. *Biochemical and Biophysical Research Communications* **448**:255–260.
 29. **Soding J, Biegert A, Lupas AN.** 2005. The HHpred interactive server for protein homology detection and structure prediction. *Nucleic Acids Research* **33**:W244–W248.
 30. **Krogh A, Larsson B, Heijne von G, Sonnhammer ELL.** 2001. Predicting transmembrane protein topology with a hidden markov model: application to complete genomes¹ Edited by F. Cohen. *Journal of Molecular Biology* **305**:567–580.
 31. **Alva V, Nam S-Z, Soding J, Lupas AN.** 2016. The MPI bioinformatics Toolkit as an integrative platform for advanced protein sequence and structure analysis. *Nucleic Acids Research* **44**:W410–W415.

32. **Robson SA, King GF.** 2006. Domain architecture and structure of the bacterial cell division protein DivIB. *Proceedings of the National Academy of Sciences* **103**:6700–6705.
33. **Rost B, Yachdav G, Liu J.** 2004. The PredictProtein server. *Nucleic Acids Research* **32**:W321–W326.
34. **Marchler-Bauer A, Derbyshire MK, Gonzales NR, Lu S, Chitsaz F, Geer LY, Geer RC, He J, Gwadz M, Hurwitz DI, Lanczycki CJ, Lu F, Marchler GH, Song JS, Thanki N, Wang Z, Yamashita RA, Zhang D, Zheng C, Bryant SH.** 2015. CDD: NCBI's conserved domain database. *Nucleic Acids Research* **43**:D222–D226.
35. **Klotzsche M, Ehrt S, Schnappinger D.** 2009. Improved tetracycline repressors for gene silencing in mycobacteria. *Nucleic Acids Research* **37**:1778–1788.
36. **van Kessel JC, Hatfull GF.** 2008. Mycobacterial recombineering. *Methods Mol Biol* **435**:203–215.
37. **Griffin JE, Gawronski JD, DeJesus MA, Ioerger TR, Akerley BJ, Sassetti CM.** 2011. High-Resolution Phenotypic Profiling Defines Genes Essential for Mycobacterial Growth and Cholesterol Catabolism. *PLoS Pathog* **7**:e1002251.
38. **Zhang YJ, Ioerger TR, Huttenhower C, Long JE, Sassetti CM, Sacchettini JC, Rubin EJ.** 2012. Global Assessment of Genomic Regions Required for Growth in *Mycobacterium tuberculosis*. *PLoS Pathog* **8**:e1002946.
39. **Dziadek J.** 2003. Conditional expression of *Mycobacterium smegmatis* *ftsZ*, an essential cell division gene. *Microbiology* **149**:1593–1603.
40. **Goehring NW, Gonzalez MD, Beckwith J.** 2006. Premature targeting of cell division proteins to midcell reveals hierarchies of protein interactions involved in divisome assembly. *Mol Microbiol* **61**:33–45.
41. **Schmidt TG, Skerra A.** 2007. The Strep-tag system for one-step purification and high-affinity detection or capturing of proteins. *Nat Protoc* **2**:1528–1535.
42. **Yang DC, Peters NT, Parzych KR, Uehara T, Markovski M, Bernhardt TG.** 2011. An ATP-binding cassette transporter-like complex governs cell-wall hydrolysis at the bacterial cytokinetic ring. *Proc Natl Acad Sci USA* **108**:E1052–60.

43. **Meisner J, Montero Llopis P, Sham L-T, Garner E, Bernhardt TG, Rudner DZ.** 2013. FtsEX is required for CwlO peptidoglycan hydrolase activity during cell wall elongation in *Bacillus subtilis*. *Mol Microbiol* **89**:1069–1083.
44. **Vicente M, Rico AI, Martinez-Arteaga R, Mingorance J.** 2005. Septum Enlightenment: Assembly of Bacterial Division Proteins. *J Bacteriol* **188**:19–27.
45. **Wang L, Lutkenhaus J.** 1998. FtsK is an essential cell division protein that is localized to the septum and induced as part of the SOS response. *Mol Microbiol* **29**:731–740.
46. **Gee CL, Papavinasasundaram KG, Blair SR, Baer CE, Falick AM, King DS, Griffin JE, Venghatakrishnan H, Zukauskas A, Wei JR, Dhiman RK, Crick DC, Rubin EJ, Sassetti CM, Alber T.** 2012. A Phosphorylated Pseudokinase Complex Controls Cell Wall Synthesis in Mycobacteria. *Science Signaling* **5**:ra7–ra7.
47. **Nagarajan SN, Upadhyay S, Chawla Y, Khan S, Naz S, Subramanian J, Gandotra S, Nandicoori VK.** 2015. Protein Kinase A (PknA) of *Mycobacterium tuberculosis* Is Independently Activated and Is Critical for Growth in Vitro and Survival of the Pathogen in the Host. *J Biol Chem* **290**:9626–9645.
48. **Hayashi JM, Luo C-Y, Mayfield JA, Hsu T, Fukuda T, Walfield AL, Giffen SR, Leszyk JD, Baer CE, Bennion OT, Madduri A, Shaffer SA, Aldridge BB, Sassetti CM, Sandler SJ, Kinoshita T, Moody DB, Morita YS.** 2016. Spatially distinct and metabolically active membrane domain in mycobacteria. *Proc Natl Acad Sci USA* **201525165**.
49. **Murphy KC, Nelson S, Nambi S, Papavinasasundaram K, Baer CE, Sassetti CM.** ORBIT: a new paradigm for genetic engineering of mycobacterial chromosomes. www.biorxiv.org.
50. **Kim J-H, Wei J-R, Wallach JB, Robbins RS, Rubin EJ, Schnappinger D.** 2010. Protein inactivation in mycobacteria by controlled proteolysis and its application to deplete the beta subunit of RNA polymerase. *Nucleic Acids Research* **39**:2210–2220.
51. **Letek M, Ordonez E, Vaquera J, Margolin W, Flardh K, Mateos LM, Gil JA.** 2008. DivIVA Is Required for Polar Growth in the MreB-Lacking Rod-Shaped Actinomycete *Corynebacterium glutamicum*. *J Bacteriol* **190**:3283–3292.
52. **Hempel AM, Wang SB, Letek M, Gil JA, Flardh K.** 2008. Assemblies of DivIVA

- Mark Sites for Hyphal Branching and Can Establish New Zones of Cell Wall Growth in *Streptomyces coelicolor*. *J Bacteriol* **190**:7579–7583.
53. **Flårdh K.** 2003. Essential role of DivIVA in polar growth and morphogenesis in *Streptomyces coelicolor* A3(2). *Mol Microbiol* **49**:1523–1536.
 54. **Cha JH, Stewart GC.** 1997. The divIVA minicell locus of *Bacillus subtilis*. *J Bacteriol* **179**:1671–1683.
 55. **Edwards DH, Errington J.** 1997. The *Bacillus subtilis* DivIVA protein targets to the division septum and controls the site specificity of cell division. *Mol Microbiol* **24**:905–915.
 56. **Marston AL, Thomaidis HB, Edwards DH, Sharpe ME, Errington J.** 1998. Polar localization of the MinD protein of *Bacillus subtilis* and its role in selection of the mid-cell division site. *Genes & Development* **12**:3419–3430.
 57. **Marston AL, Errington J.** 1999. Selection of the midcell division site in *Bacillus subtilis* through MinD-dependent polar localization and activation of MinC. *Mol Microbiol* **33**:84–96.
 58. **Eswaramoorthy P, Winter PW, Wawrzusin P, York AG, Shroff H, Ramamurthi KS.** 2014. Asymmetric division and differential gene expression during a bacterial developmental program requires DivIVA. *PLoS Genet* **10**:e1004526.
 59. **Hayashi JM, Luo C-Y, Mayfield JA, Hsu T, Fukuda T, Walfield AL, Giffen SR, Leszyk JD, Baer CE, Bennion OT, Madduri A, Shaffer SA, Aldridge BB, Sassetti CM, Sandler SJ, Kinoshita T, Moody DB, Morita YS.** 2016. Spatially distinct and metabolically active membrane domain in mycobacteria. *Proceedings of the National Academy of Sciences* **113**:5400–5405.
 60. **Kieser KJ, Rubin EJ.** 2014. How sisters grow apart: mycobacterial growth and division. *Nat Rev Microbiol* **12**:550–562.
 61. **Tsang M-J, Bernhardt TG.** 2015. A role for the FtsQLB complex in cytokinetic ring activation revealed by an ftsL allele that accelerates division. *Mol Microbiol* **95**:925–944.
 62. **Goehring NW, Beckwith J.** 2005. Diverse Paths to Midcell: Assembly of the

Bacterial Cell Division Machinery. *Current Biology* **15**:R514–R526.

63. **Gamba P, Veening JW, Saunders NJ, Hamoen LW, Daniel RA.** 2009. Two-Step Assembly Dynamics of the Bacillus subtilis Divisome. *J Bacteriol* **191**:4186–4194.
64. **Buddelmeijer N, Judson N, Boyd D, Mekalanos JJ, Beckwith J.** 2002. YgbQ, a cell division protein in Escherichia coli and Vibrio cholerae, localizes in codependent fashion with FtsL to the division site. *Proceedings of the National Academy of Sciences* **99**:6316–6321.
65. **Wadenpohl I, Bramkamp M.** 2010. DivIC Stabilizes FtsL against RasP Cleavage. *J Bacteriol* **192**:5260–5263.
66. **Gamba P, Hamoen LW, Daniel RA.** 2016. Cooperative Recruitment of FtsW to the Division Site of Bacillus subtilis. *Front Microbiol* **7**:642–9.
67. **Guzman L-M, Barondess JJ, Beckwith J.** 1992. FtsL, an Essential Cytoplasmic Membrane Protein Involved in Cell Division in Escherichia coli. *J Bacteriol* **174**:7717–7728.
68. **Kaval KG, Hauf S, Rismondo J, Hahn B, Halbedel S.** 2017. Genetic Dissection of DivIVA Functions in Listeria monocytogenes. *J Bacteriol* **199**:e00421–17–16.
69. **Jani C, Eoh H, Lee JJ, Hamasha K, Sahana MB, Han J-S, Nyayapathy S, Lee J-Y, Suh J-W, Lee SH, Rehse SJ, Crick DC, Kang C-M.** 2010. Regulation of Polar Peptidoglycan Biosynthesis by Wag31 Phosphorylation in Mycobacteria. *BMC Microbiology* **10**:327.
70. **Claessen D, Emmins R, Hamoen LW, Daniel RA, Errington J, Edwards DH.** 2008. Control of the cell elongation–division cycle by shuttling of PBP1 protein in Bacillus subtilis. *Mol Microbiol* **68**:1029–1046.
71. **Fleurie A, Manuse S, Zhao C, Campo N, Cluzel C, Lavergne J-P, Freton C, Combet C, Guiral S, Soufi B, Macek B, Kuru E, VanNieuwenhze MS, Brun YV, Di Guilmi A-M, Claverys J-P, Galinier A, Grangeasse C.** 2014. Interplay of the Serine/Threonine-Kinase StkP and the Paralogs DivIVA and GpsB in Pneumococcal Cell Elongation and Division. *PLoS Genet* **10**:e1004275.
72. **Hamoen LW, Errington J.** 2003. Polar Targeting of DivIVA in Bacillus subtilis Is

Not Directly Dependent on FtsZ or PBP 2B. *J Bacteriol* **185**:693–697.

73. **Hett EC, Chao MC, Deng LL, Rubin EJ.** 2008. A Mycobacterial Enzyme Essential for Cell Division Synergizes with Resuscitation-Promoting Factor. *PLoS Pathog* **4**:e1000001.
74. **Kieser KJ, Baranowski C, Chao MC, Long JE, Sasseti CM, Waldor MK, Sacchettini JC, Ioegeer TR, Rubin EJ.** 2015. Peptidoglycan synthesis in *Mycobacterium tuberculosis* is organized into networks with varying drug susceptibility. *Proc Natl Acad Sci USA* **112**:13087–13092.
75. **Chao MC, Kieser KJ, Minami S, Mavrici D, Aldridge BB, Fortune SM, Alber T, Rubin EJ.** 2013. Protein Complexes and Proteolytic Activation of the Cell Wall Hydrolase RipA Regulate Septal Resolution in Mycobacteria. *PLoS Pathog* **9**:e1003197–16.
76. **Randich AM, Brun YV.** 2015. Molecular mechanisms for the evolution of bacterial morphologies and growth modes. *Front Microbiol* **6**:938–13.
77. **Lewis JA, Hatfull GF.** 2003. Control of Directionality in L5 Integrase-mediated Site-specific Recombination. *Journal of Molecular Biology* **326**:805–821.
78. **Boutte CC, Baer CE, Papavinasasundaram K, Liu W, Chase MR, Meniche X, Fortune SM, Sasseti CM, Ioegeer TR, Rubin EJ, Laub M.** 2016. A cytoplasmic peptidoglycan amidase homologue controls mycobacterial cell wall synthesis. *eLife* **5**:e14590.
79. **Pashley CA, Parish T.** 2003. Efficient switching of mycobacteriophage L5-based integrating plasmids in *Mycobacterium tuberculosis*. *FEMS Microbiology Letters* **229**:211–215.
80. **Kim J-H, Wei J-R, Wallach JB, Robbins RS, Rubin EJ, Schnappinger D.** 2010. Protein inactivation in mycobacteria by controlled proteolysis and its application to deplete the beta subunit of RNA polymerase. *Nucleic Acids Research* **39**:2210–2220.
81. **Pham TT, Jacobs-Sera D, Pedulla ML, Hendrix RW, Hatfull GF.** 2007. Comparative genomic analysis of mycobacteriophage Tweety: evolutionary insights and construction of compatible site-specific integration vectors for mycobacteria. *Microbiology* **153**:2711–2723.

Chapter 3: Mycobacterial peptidoglycan synthesis and the role of L,D-transpeptidase mediated crosslinks in rod shape maintenance

Section 3.1: Overview of peptidoglycan synthesis and L,D-transpeptidases in mycobacteria

Bacteria separate their cytoplasm from the environment with a membrane and cell wall whose foundational layer is called peptidoglycan (PG). PG and the process of its synthesis determine bacterial cell shape (1-4) and are necessary for protecting the cell from osmotic lysis (5, 6). As a critical bacterial polymer, PG is the target of very successful antibiotics like β -lactams. Though the cell wall of mycobacteria, a genus including the human pathogen *Mycobacterium tuberculosis* (the causative agents of tuberculosis, hereafter referred to as Mtb), contains PG, this layer is not currently targeted by first-line treatments (7).

β -lactams (penicillins, cephalosporins and carbapenems) are antibiotics known to target PG synthesis enzymes by mimicking their substrate. β -lactams have historically been found ineffective against Mtb due to the presence of an active β -lactamase enzyme that cleaves to inactivate these drugs (8, 9). This has been overcome by use of a β -lactamase inhibitor called clavulanate (10). Thus, there is renewed interest in β -lactams for Mtb treatment (11). By targeting PG synthesis enzymes, exposing bacteria to β -lactams results in a disruption of growth and division (12-14).

PG synthesis begins in the cytoplasm with the construction and transport of the precursor, lipid II (15). Once flipped over the membrane, lipid II is integrated into the existing PG structure via two reactions- transglycosylation to polymerize the glycan chains, and transpeptidation to crosslink the peptide side chains (6).

PG is a meshwork of linear glycan strands that are linked by short peptide side chains. Glycan strands are repeating disaccharide units of *N*-acetylmuramic acid (NAM) — *N*-acetylglucosamine (NAG), with peptide side chains attached to NAM (6). In mycobacteria, NAM is modified with a glycol resulting in *N*-glycolylmuramic acid (NGM) (16) (Figure 3.1). Newly

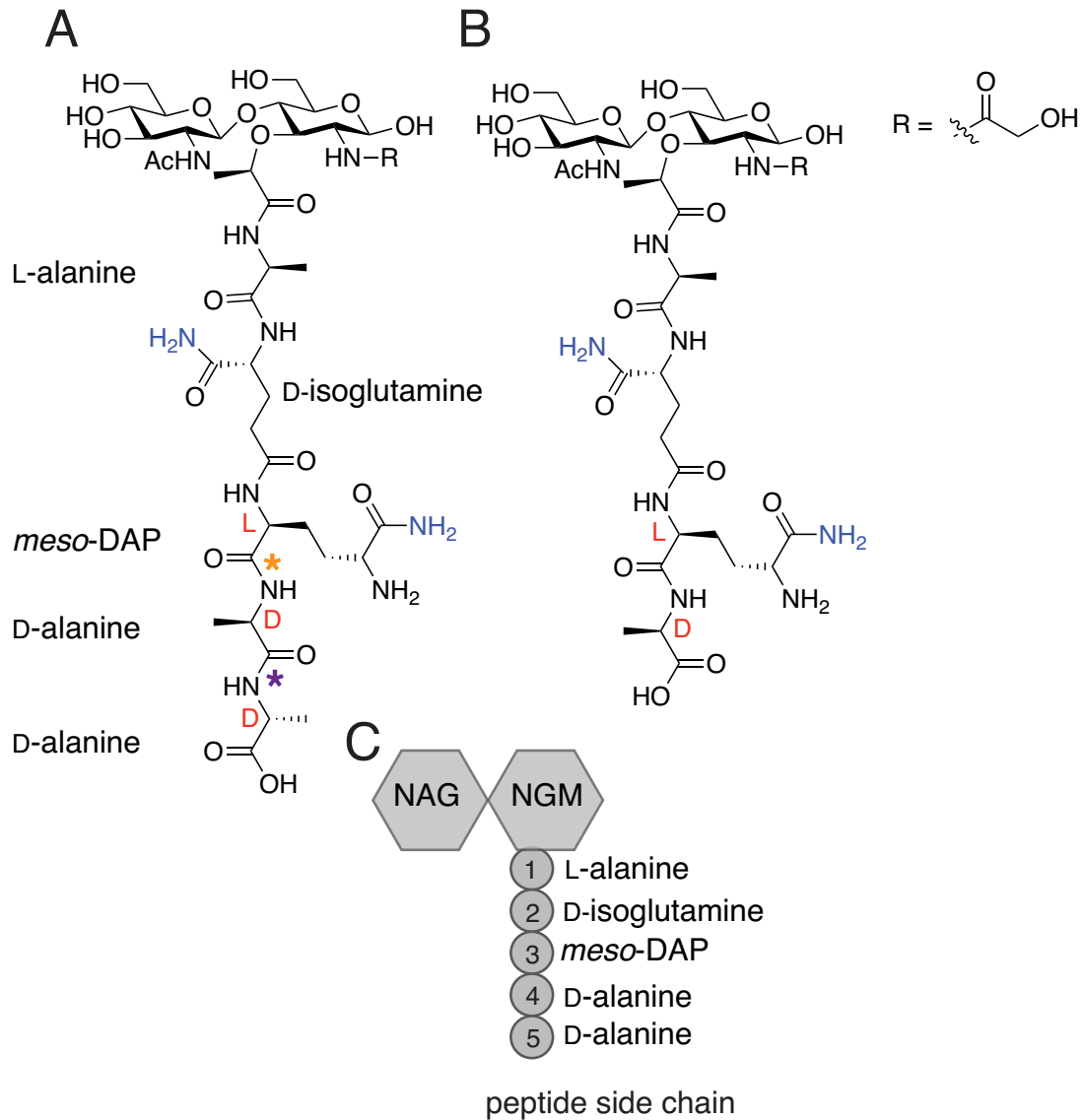


Figure 3.1: Structure of mycobacterial peptidoglycan. (A) Structure of the peptidoglycan (PG) pentapeptide including NAM-NGM. Amino acids are labeled and red letters indicate amino acid configuration. The orange asterisk indicates the L,D peptide bond that is cleaved during 3-3 crosslink formation by L,D-transpeptidases (LDTs). The purple asterisk indicates the D,D peptide bond that is cleaved during 4-3 crosslink formation by D,D-transpeptidases (aPBPs, bPBPs).

Figure 3.1 (Continued)

Blue NH₂ groups indicate amidation of D-glu and *m*-DAP. **(B)** PG tetrapeptide structure. **(C)**

Schematic of PG pentapeptide on NAG-NGM.

synthesized mycobacterial PG side chains consist of: [1] L-alanine (L-ala), [2] D-isoglutamate (D-glu), [3] *meso*-diaminopimelic acid (*m*-DAP), [4] D-alanine (D-ala), [5] D-alanine and are referred to as pentapeptides. Mycobacterial D-glu and *m*-DAP are often amidated (resulting in D-isoglutamine, D-isoglu) (17, 18) (Figure 3.1A-C). To covalently close the PG network and form a continuous molecular cage surrounding the plasma membrane, the peptide side chains are crosslinked between either the 4th and 3rd ([4] D-ala—[3]*m*-DAP) or the 3rd and 3rd ([3]*m*-DAP—[3]*m*-DAP) residues of proximal PG strands resulting in what are known as 4-3 or 3-3 crosslinks respectively (Figure 3.2).

As was discussed in Chapter 1, bi-functional (Class A) penicillin binding proteins, aPBPs, can both polymerize the glycan chains (transglycosylation) and utilize pentapeptide side chains to create 4-3 crosslinks (transpeptidation) (19). Mono-functional (Class B) PBPs, bPBPs, only harbor transpeptidase function. PG that has been processed by aPBP/bPBPs (or D,D-carboxypeptidase enzymes that cleave the terminal D-ala from pentapeptides) contains a tetrapeptide side chain because the terminal [5]D-ala is removed by the action of these enzymes (Figure 3.1B). PG tetrapeptides are substrates for L,D-transpeptidases (LDTs) to catalyze 3-3 crosslinks (20). Importantly, PBPs and LDTs have different substrates (penta- vs. tetra- peptides (21)) and active sites (PBPs contain an active site serine while LDTs have a cysteine (20)).

LDTs are of specific interest to mycobacteriologists. First, carbapenem antibiotics (a class of β -lactam), those shown to bind and inhibit purified LDTs *in vitro* (see below), are active against drug resistant Mtb *in vitro* (both in aerobic and persistence mimicking anaerobic conditions (22)) and have been shown to be effective against drug sensitive Mtb in patients (11). Second, mycobacterial PG, in contrast to that of other rod-shaped bacteria like *Escherichia coli*, is rich in LDT catalyzed 3-3 crosslinks (18, 23, 24). These two points suggest that 3-3 crosslinks

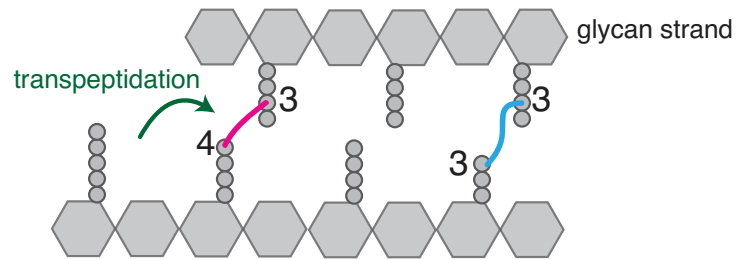


Figure 3.2: Cartoon of 4-3 and 3-3 peptidoglycan crosslinks. Schematic of 4-3 and 3-3 crosslinking.

are both abundant and critical for robust mycobacterial survival. Further, these data highlight that LDTs could be viable drug targets for the treatment of Mtb.

The existence of 3-3 crosslinks in mycobacterial PG has been known for decades (25). However, the enzymes that catalyze them were only identified recently. They were first characterized in *Enterococcus faecium* as part of a β -lactam resistance mechanism (20, 26). Because mycobacterial PG is rich in 3-3 crosslinks there has been a heavy focus on mycobacterial LDTs. Many of these studies have used purified enzymes and *in vitro* assays. Intriguingly, it has been shown *in vitro* that LDTs are bound and inactivated efficiently by carbapenems (i.e.-meropenem) when compared to the relatively ineffective or partial inhibition by non-carbapenem β -lactams (hereafter N-C β -lactams) (21, 23, 27-29). With purified enzymes and artificial substrates, it has been shown that LDTs in Mtb utilize PG tetrapeptides (not pentapeptides) to catalyze 3-3 crosslinks (21).

Structural studies have found that carbapenems, analogously to the N-C β -lactams against PBPs, covalently bind the active site of the LDT enzymes despite their low affinities (30). This mirrors the acyl-enzyme intermediate established during the crosslinking reaction (31).

It is important to note that carbapenems have been shown *in vitro* to inhibit various PBPs in *E. coli* and *Pseudomonas aeruginosa* (32-35). Though *in vitro* data supports the notion that carbapenems, rather than N-C β -lactams, are better at inhibiting mycobacterial LDTs, this does not exclude mycobacterial PBPs as targets of carbapenems.

Due to the primarily *in vitro* nature of LDT studies, the role of LDTs and 3-3 crosslinks in the context of the mycobacterial cell is poorly understood. In Mtb, deletion of the most highly expressed LDT, *ldtB* (*Ldt_{M12}/Rv2518c*), results in shorter cells, as well as both growth attenuation and increased susceptibility to a β -lactam (combined with the β -lactamase inhibitor clavulanate),

in a mouse model of Mtb (36, 37). Genetic deletion of both *ldtA* and *ldtB* ($\Delta ldt_{M1}\Delta ldt_{M2}$, $\Delta Rv0116c\Delta Rv2518c$) results in slight deformation of the tubercle bacillus and an increased susceptibility to β -lactams (with clavulanate) (37). It has also been shown in *Mycobacterium smegmatis*, a non-pathogenic model for Mtb (hereafter Msm), that cells disrupted for *ldtC* alone or in combination with knock-outs of *ldtB* and *ldtF* ($\Delta ldtBCF$) are more susceptible to the carbapenem antibiotic, imipenem. Further, those cells exhibit bulbous morphology (38). Despite these studies, the general role of LDTs within the mycobacterial cell is unknown.

In rod-shaped bacteria that incorporate new peptidoglycan along the lateral cell wall (like *E. coli* and *B. subtilis*) nearly all PG crosslinks are PBP catalyzed 4-3 (24, 39, 40). In the asymmetrically polar-elongating mycobacteria (41), where the majority of PG crosslinks are 3-3 (18), we are left with the question: what is the role of 3-3 crosslinks?

The following manuscript (Section 3.2) describes the role of LDT catalyzed 3-3 crosslinks in mycobacterial rod shape maintenance at sites of aging cell wall. Section 3.3 provides further characterization of the fluorescent D-amino acid probes utilized in Section 3.2.

Section 3.2: Maturing mycobacterial peptidoglycan requires non-canonical crosslinks to maintain shape

Overview: This section consists of a manuscript to be submitted shortly.

Attributions: CB generated all strains except the Msm-Wag31 strain (Figure 3.4C,D (HAE)) and the Mtb strain expressing the *lux* operon (JCW). CB performed all experiments except Figure 3.4C, D done by HAE (HAE wrote AFM methods). TRI sequenced transposon libraries and performed analysis for Figure 3.5A. MAW provided DacB2 purification methods. HCL wrote custom Matlab scripts for image analysis in Figure 3.3C. KJK made the ponA1-RFP strain used in Figure 3.6A. EHR wrote FIJI and Matlab scripts for analysis in Figure 3.6B and was instrumental in data interpretation, inspiration and editing. CB wrote this manuscript with input from all authors.

Authors: Catherine Baranowski,¹ Lok-To Sham,² Haig A. Eskandarian,^{3,4} , Michael A. Welsh,² Karen J. Kieser,¹ Hoong C. Lim,² Jeffrey C. Wagner,¹ Suzanne Walker,² John D. McKinney,³ Georg E. Fantner,⁴ Thomas G. Bernhardt,² Thomas R. Ioerger,⁵ Eric J. Rubin^{1,2*}, E. Hesper Rego^{6*}

¹ Department of Immunology and Infectious Disease, Harvard T. H. Chan School of Public Health, Boston, MA 02115, USA. ² Department of Microbiology and Immunobiology, Harvard Medical School, Boston, MA 02115, USA. ³ School of Life Sciences, Swiss Federal Institute of Technology in Lausanne (EPFL), 1015 Lausanne, Switzerland. ⁴ School of Engineering, Swiss Federal Institute of Technology in Lausanne (EPFL), 1015 Lausanne, Switzerland. ⁵ Department of Computer Science and Engineering, Texas A&M University, College Station, Texas, USA. ⁶ Department of Microbial Pathogenesis, Yale University School of Medicine, New Haven, Connecticut, 06510,

USA. * to whom correspondence should be addressed: erubin@hsph.harvard.edu;
hesper.rego@yale.edu

Abstract

In most well-studied rod-shaped bacteria, peptidoglycan is primarily crosslinked by penicillin binding proteins (PBPs). However, in mycobacteria L,D-transpeptidase (LDT)-mediated crosslinks are highly abundant. To elucidate the role of these unusual crosslinks, we characterized mycobacterial cells lacking all LDTs. We find that LDT-mediated crosslinks are required for rod shape maintenance specifically at sites of aging cell wall, a byproduct of polar elongation. Asymmetric polar growth leads to a non-uniform distribution of these two types of crosslinks in a single cell. Consequently, in the absence of LDT-mediated crosslinks, PBP-catalyzed crosslinks become more important. Because of this, *Mycobacterium tuberculosis* is more rapidly killed using a combination of drugs capable of PBP and LDT inhibition. Thus, knowledge about the single-cell distribution of drug targets can be exploited to more effectively treat this pathogen.

Main Text

Peptidoglycan (PG) is an essential component of all bacterial cells (6), and the target of many antibiotics. PG consists of linear glycan strands crosslinked by short peptides to form a continuous molecular cage surrounding the plasma membrane. This structure maintains cell shape and protects the plasma membrane from rupture. Our understanding of PG is largely derived from studies on laterally-growing model rod-shaped bacteria like *Escherichia coli* and *Bacillus subtilis* (Figure S1A). However, there are important differences between these bacteria and the mycobacteria, a genus that includes the major human pathogen *Mycobacterium tuberculosis* (Mtb).

For example, new PG in mycobacteria is inserted at the cell poles (at unequal amounts based on pole age), rather than along the lateral side walls (Figure 3.3A). In addition, the abundance of various PG linkages is substantially different in mycobacteria versus other rod-shaped bacteria. In model rod-shaped bacteria like *E. coli*, PBP-mediated crosslinks make up a vast majority of the PG linkages (24, 39). PBPs, the targets of most β -lactams, catalyze the peptide links between adjacent strands. They join the third amino acid of one PG peptide to the fourth amino acid of another, resulting in 4-3 crosslinks (Figure S1B). However, in mycobacteria, non-canonical 3-3 crosslinks are abundant (~60% of linkages) (18, 23). These 3-3 crosslinks are formed by L,D-transpeptidases (LDTs), which link the third positions of two adjacent PG side chains (Figure S1B). Because PG has been studied most in bacteria where 3-3 crosslinks are rare, the role of this linkage - and the enzymes that catalyze it - is not understood. Importantly, carbapenems, a class of β -lactam that potently inhibit LDTs *in vitro*, are effective against *Mtb in vitro* and in patients (11, 22). Thus, we sought to understand the role of 3-3 crosslinks in mycobacterial physiology.

PG uniquely contains D-amino acids; this was recently exploited to design fluorescent probes (fluorescent D-amino acids, FDAAs) to visualize PG synthesis in live bacterial cells (42). When we incubated *Msm* with FDAAs for a short 2-minute pulse (< 2% of *Msm*'s generation time), we observed a striking pattern. While we saw incorporation at both poles, the sites of new PG insertion in mycobacteria (Figure 3.3A) (41), we also saw a gradient extending from the old pole (the previously established growth pole) that fades to a minimum at roughly mid-cell as it reaches the new pole (the pole formed at the last cell division) (Figure 3.3B).

To identify the enzymes responsible for this unexpected pattern of lateral cell wall FDAAs incorporation, we performed a fluorescence-activated cell sorting (FACS)-based transposon screen (Figure S1C). Briefly, we stained an *Msm* transposon library with FDAAs and sorted the least

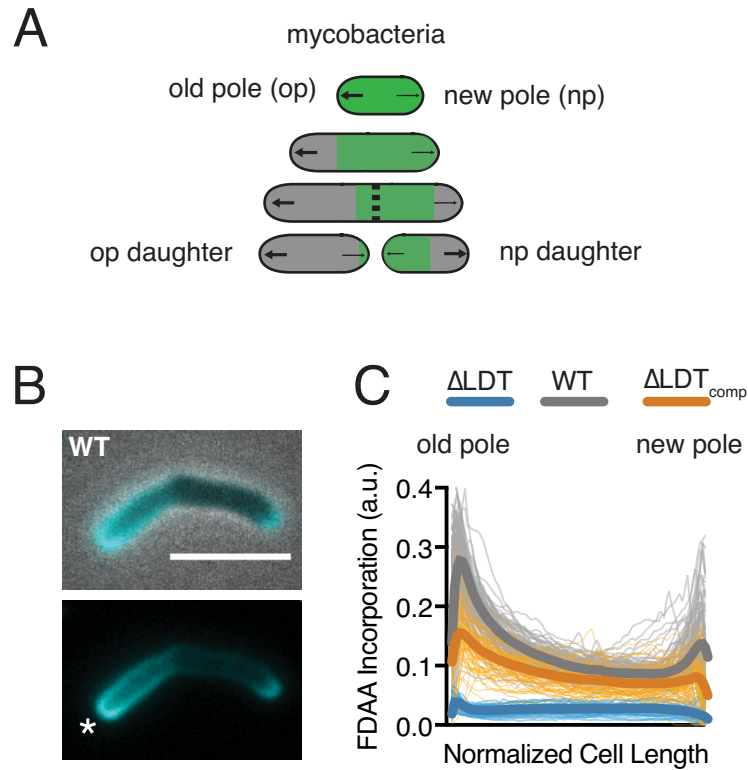


Figure 3.3: FDAAs are incorporated asymmetrically by LD-transpeptidases. (A) Schematic of mycobacterial asymmetric polar growth. Green portion represents old cell wall, grey portion represents new material. Dotted line represents septum. Arrows reflect relative amounts of polar growth where small arrows reflect new pole and large arrows reflect old pole growth. (B) FdAA incorporation in log-phase WT Msm cell after 2-minute incubation with FdAA. Scale bar=5 μ m. Old pole marked with (*). (C) Profiles of FdAA incorporation in log-phase WT (N=98), Δ LDT (N=40), and Δ LDT_{comp} (N=77) cells. Thick lines represent mean incorporation profile, while thin lines are FdAA incorporation in single cells.

fluorescent 12.5% of the population by FACS. We repeated this to enrich for mutants that were less fluorescent than WT cells. After each sort we regrew cells, extracted gDNA and used deep sequencing to map the location of the transposons found in the low staining population.

From this screen, we identified three LDTs (*ldtA-MSMEG_3528*, *ldtB-MSMEG_4745*, *ldtE-MSMEG_0233*) (Figure S1D) that were primarily responsible for FDAA incorporation. Deleting these three LDTs significantly reduced FDAA incorporation (Figure S2A,B). To further investigate the physiological role of LDTs, we constructed a strain lacking all 6 LDTs (Δ *ldtAEBCGF*, hereafter Δ LDT). FDAA incorporation and 3-3 crosslinking is nearly abolished in Δ LDT cells and can be partially restored by complementation with a single LDT (*ldtE*-mRFP; Δ LDT_{comp}) (Figure 3.3C, S2C,D, S3). Thus, FDAA incorporation in Msm is primarily LDT dependent. This is similar to findings made recently in *Bdellovibrio*, where LDTs are also responsible for FDAA incorporation (42, 43). LDTs can also exchange non-canonical D-amino acids onto PG tetrapeptides in *Vibrio cholera* (44).

While partial knock-outs of LDTs in Msm have been implicated in cell shape previously, their role in shape maintenance has not been investigated (38). To examine this, we visualized Δ LDT cells by time-lapse microscopy. We observed that a subpopulation of cells loses rod shape progressively over time, resulting in localized spherical blebbing (Figure 3.4A-top, S4A). Complemented cells are able to maintain rod shape (Figure S4B).

We reasoned that localized loss of rod shape may occur for two reasons: 1) a spatially specific loss of cell wall integrity and/or 2) a cell wall deformation due to uncontrolled, local PG synthesis. To test the first hypothesis, we tested if high osmolarity would protect cells against forming blebs. Indeed, switching cells from iso- to high-osmolarity prevented bleb formation over time (Figure 3.4A, bottom). These results indicate that 3-3 crosslinks are required to counteract

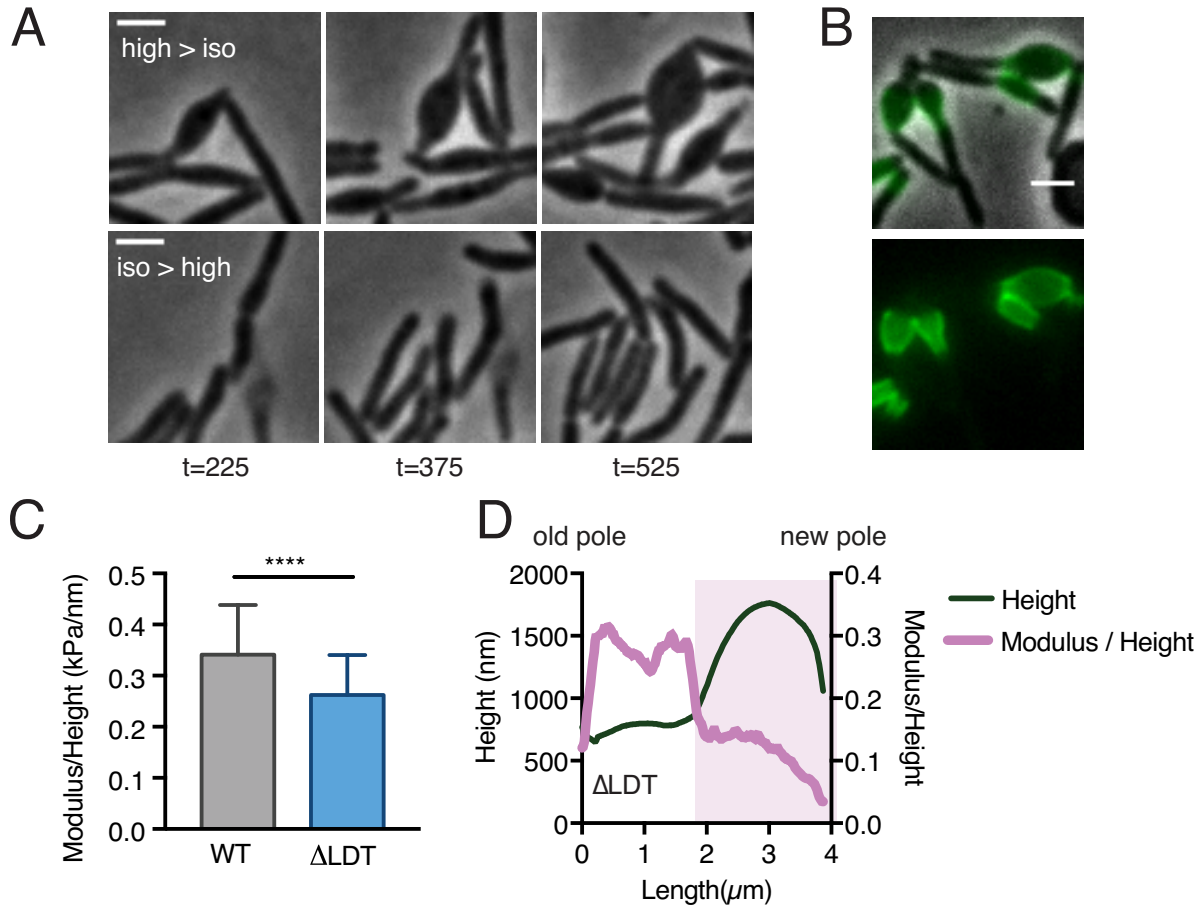


Figure 3.4: LDT catalyzed 3-3 crosslinks are required for rod shape maintenance at aging cell wall. (A) Msm Δ LDT time-lapse microscopy of cells switched from high- to iso- (top) osmolar media, or iso- to high osmolar media (bottom). (high=7H9+150mM sorbitol; iso=7H9). t= time in minutes post osmolarity switch. (B) Oldest cell wall (Alexa 488 NHS-ester stained in green) localization in Δ LDT cells. New cell wall material is unstained and visualized after outgrowth. Scale bar=2 μ m. (C) Average stiffness of WT (N=73) and Δ LDT (N=47) Msm cells as measured by atomic force microscopy. Mann-Whitney U P-Value **** < 0.0001. (D) Representative profile of cell height (nm) and height normalized stiffness (modulus/height) in a single Δ LDT cell. Pink shaded portion highlights location of a bleb.

turgor pressure and maintain the rod shape of mycobacteria. To test the second hypothesis, we stained Δ LDT cells with an amine reactive dye, and observed outgrowth of new, unstained material (Figure 3.4B). The bleb maintained the stain, indicating that no new growth occurred there. We, therefore, hypothesized that 3-3 crosslinks are required to maintain the structural stability necessary for the rod shape of mycobacteria.

To directly test cell wall rigidity, we used atomic force microscopy (AFM) on live Δ LDT and WT cells. We measured the rigidity of cells in relation to their height. Generally, WT cells are stiffer than Δ LDT cells (Figure 3.4C). Blebs in Δ LDT cells can be identified by a sharp increase in height found towards the new pole (Figure 3.4C). The circumferential stress of the rod measured by AFM is proportional to the radius of the cell, and inversely proportional to the thickness of the cell wall. While we cannot measure cell wall thickness but can measure cell height, a proxy for radius, we normalized the stiffness measurement (modulus in kPa) by cell height (nm) to decouple this relationship. The difference in stiffness along the profile of a representative Δ LDT cell shows lower rigidity at the location of the bleb (Figure 3.4D, pink shaded). Together, these data suggest that localized PG reinforcement through the action of LDTs is required to maintain rod shape in a sub-population of Msm cells (Figure S4C).

Why does loss of rod shape occur only in a sub-population of cells? Mycobacterial polar growth and division results in daughter cells with phenotypic differences (41). For example, the oldest cell wall is specifically inherited by the new pole daughter (Figure S5A,(41)). We hypothesized that the loss of rod shape might occur in specific progeny generated during cell division. Indeed, the daughter which inherited the new pole from the previous round of division, and the oldest cell wall, consistently lost rod shape over time, while the old pole daughter maintained rod shape (Figure S5B). In addition, the bleb was localized to the oldest cell wall

(Figure 3.4B). Thus, 3-3 crosslinking is likely occurring in the oldest cell wall, which is non-uniformly distributed in the population via asymmetric polar growth and division.

Our observations lead to the following model (Figure 3.6C): PBP-catalyzed 4-3 crosslinks are formed at the poles where new PG is inserted. These newly synthesized 4-3 crosslinks are then gradually cleaved (by D-D endopeptidases) as PG ages and moves toward the middle of the cell, leaving tetrapeptide substrates for LDTs to create 3-3 crosslinks. This is consistent with our initial observation of LDT-dependent FDAA staining along the side walls in WT cells (Figure 3.3C), because staining can only occur at available tetrapeptide substrates, which get progressively consumed as the cell wall ages. In the absence of LDTs to reinforce this processed, older, PG, the cell wall loses integrity and turgor pressure causes bleb formation over time.

This model predicts that: 1) Δ LDT cells should be even more dependent on 4-3 crosslinking than wild type cells; 2) enzymes that make different types of crosslinks (PBPs vs LDT) should be differentially localized or active along the length of the cell; and 3) D,D-endopeptidases, which can putatively create LDT substrates by cleaving 4-3 crosslinks, should be localized at sites of aging PG.

To test the first prediction, we used TnSeq (45) to identify genes required for growth in cells lacking LDTs (Figure 3.5A). We found that mutants of two PBPs, *pbpA* (*MSMEG_0031c*) and *ponA2* (*MSMEG_6201*), were recovered at significantly lower frequencies in Δ LDT cells (Figure 3.5B). Likewise, we directly tested the essentiality of the transpeptidase (TP) activity of PonA1, the major PG synthase in Msm, by allele swapping (46) (Figure S6A). The transpeptidase activity of PonA1 is non-essential in WT cells (46), but becomes essential in Δ LDT cells (Figure S6B). Thus, 4-3 crosslinking is more important to cell viability in cells lacking 3-3 crosslinks. To test whether 3-3 and 4-3 crosslinkers localize differently, we visualized fluorescent fusions of a

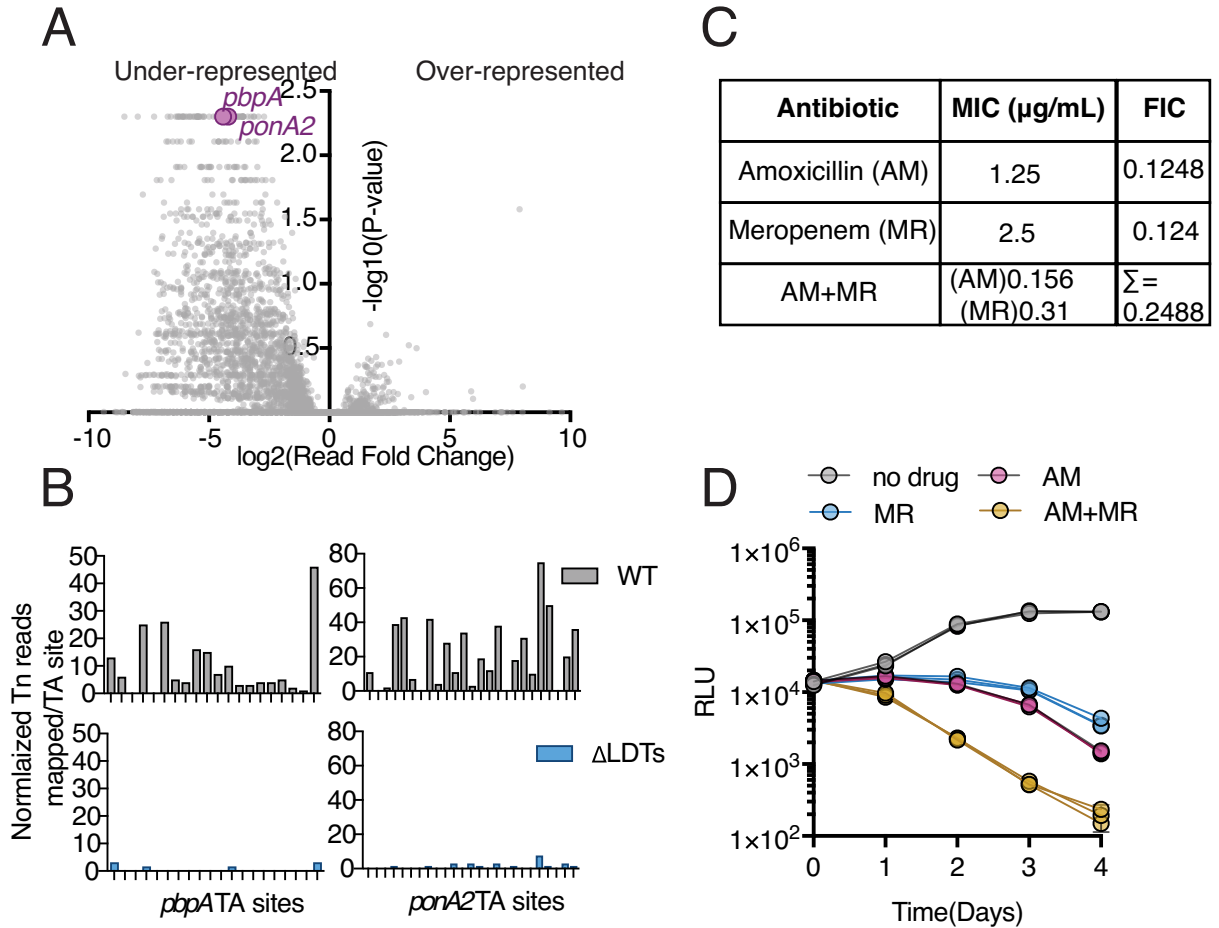


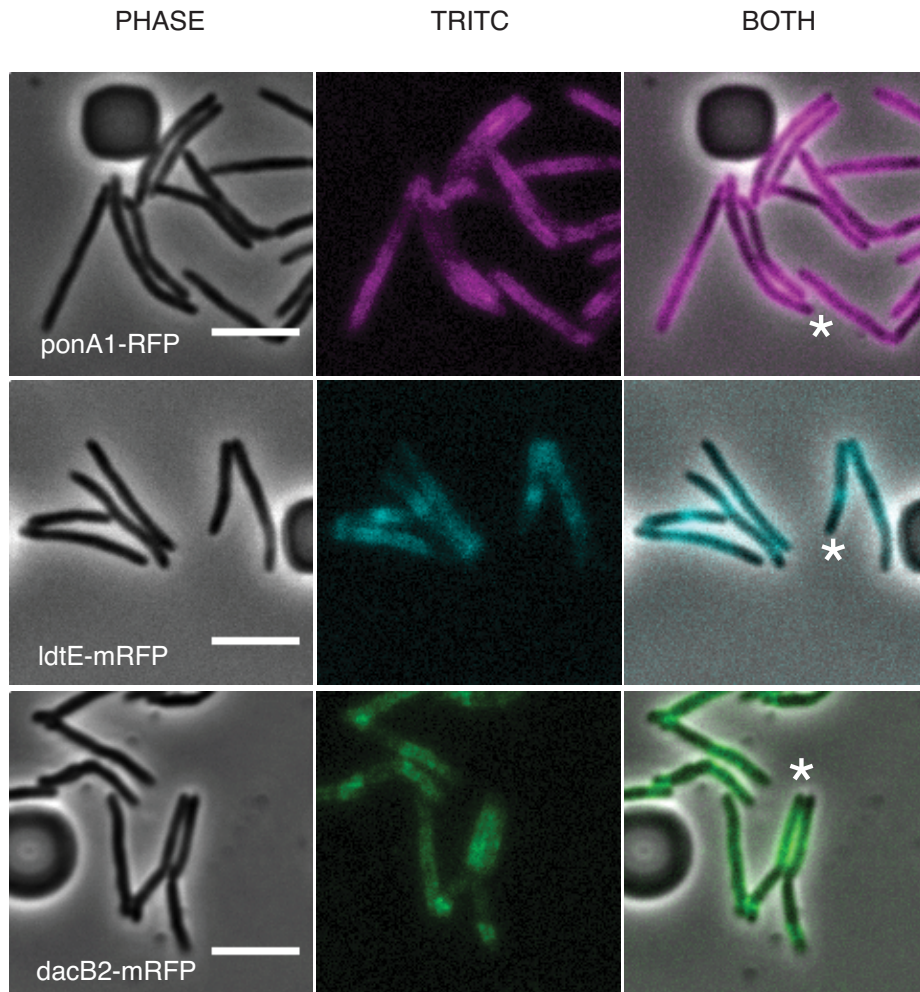
Figure 3.5: Mycobacteria are hypersensitive to PBP inactivation in the absence of LDTs. (A) Fold change in the number of reads for transposon insertion counts in Δ LDT cells compared to WT Msm. P-value is derived from a rank sum test. **(B)** Transposon insertion read count profile at each TA site in *pbpA* and *ponA2* in WT and Δ LDT cells. **(C)** Minimum inhibitory concentration (MIC) of amoxicillin, meropenem or the combination against *M. tuberculosis*. FIC (fractional inhibitory concentration) = MIC of drug in combination/MIC of drug alone. Synergy is defined as $\Sigma \text{ FIC} \leq 0.5$. **(D)** Killing dynamics of 5X MIC amoxicillin, 5X MIC meropenem or the combination against *M. tuberculosis* (expressing the *luxABCDE* operon from *Phototrhhabdus luminescens*) measured via luciferase production (RLU=relative light units). Biological triplicate are plotted. All drugs in Fig 3.5 were used in combination with 5 $\mu\text{g/mL}$ clavulanate.

PBP (PonA1), and an LDT (LdtE), (Figure 3.6A). We found that PonA1-RFP largely localized to the old pole, where new PG is inserted (Figure 3.6A, B). On the other hand, LdtE-mRFP localized farther from the poles, the sites of older PG (Figure 3.6A, B). Collectively, these data demonstrate that enzymes responsible for 4-3 and 3-3 crosslinks exhibit distinctive subcellular localizations, consistent with the model that they act on differentially-aged PG

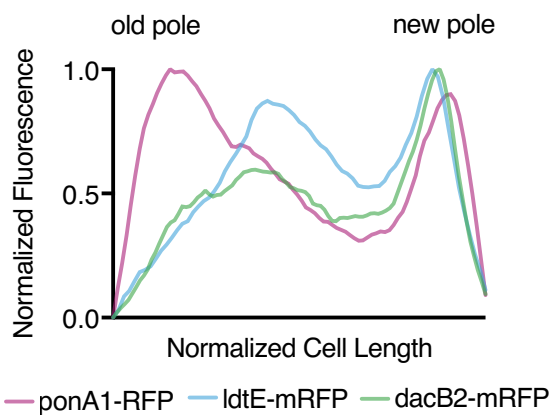
To test our third hypothesis, we sought to localize a D,D-endopeptidase in Msm. As no D,D-endopeptidase has been experimentally verified in Msm, we used the homology search algorithm HHPRED (47) to identify a candidate. We found dacB2 (MSMEG_2433), a protein shown to harbor D,D-carboxypeptidase activity in Msm (48), as a candidate by homology to the *E. coli* protein AmpH, an enzyme with both D,D-carboxy- and endopeptidase activity (49). We expressed and purified DacB2 and found that it had both D,D-carboxy- and D,D-endopeptidase activity on substrate generated *in vitro* (Figure S7). Consistent with our model, we find that DacB2-mRFP localizes closer to LDT-mRFP, further from the poles, at sites of older PG (Figure 3.6A, B). Thus, bleb formation may be the result of unchecked D,D-endopeptidase activity in Δ LDT cells.

The importance of 3-3 crosslinks in mycobacteria suggests a unique vulnerability. While mycobacteria can be killed by most non-carbapenem (N-C) β -lactams, which largely target the PBPs, carbapenems, which target LDTs more specifically than N-C β -lactams *in vitro* (27) (and may also target mycobacterial PBPs), are also effective against *Mycobacterium tuberculosis* (11, 22). As has been previously postulated (27, 36, 50), our data suggest that faster Mtb killing could be achieved with drug combinations that target both PBPs and LDTs. In fact, we find that amoxicillin (a N-C β -lactam) and meropenem (a carbapenem), in combination, exhibit synergism in minimal inhibitory concentration (Σ Fractional Inhibitory Concentration < 0.5) (51) (Figure S8),

A



B



C

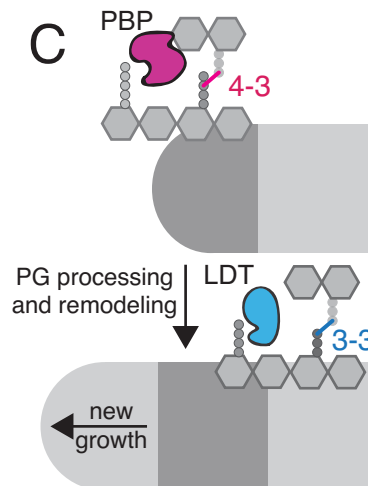


Figure 3.6: Peptidoglycan synthesizing enzymes localize to differentially aged cell wall. (A)

Representative fluorescence images of PonA1-RFP (false colored magenta), LdtE- mRFP (false

Figure 3.6 (Continued)

colored cyan) or DacB2-mRFP (false colored green). Scale bars=5 μ m. **(B)** Average PonA1-RFP (N=24), LdtE-mRFP (N=23) or DacB2-mRFP (N=23) distribution in cells before cell division **(C)** A model for PG age and crosslink segregation via polar growth in mycobacteria.

and lead to faster killing of Mtb via luminescence as a reporter of survival (Figure 3.5C, D, Figure S9) (52).

In well-studied rod-shaped bacteria like *E. coli* and *B. subtilis* shape is maintained by MreB-directed PG synthesis (53-55). On the other hand, mycobacteria, must maintain structural stability in the absence of an obvious MreB homolog. Further, in contrast to lateral-elongating bacteria, in which new and old cell wall are constantly intermingled during growth (Figure S4A), polar growth segregates new and old cell wall (Figure S10). Mycobacteria appear to utilize 3-3 crosslinks at asymmetrically-distributed aging cell wall to provide stability along the lateral body, something that may not be required in the presence of MreB-directed PG synthesis. Thus, drug combinations that target both 4-3 and 3-3 crosslinks could lead to better treatment of tuberculosis. In fact, a clinical trial to test meropenem with amoxicillin/clavulanate with and without the first line drug rifampin for the treatment of tuberculosis is currently recruiting (56).

Section 3.3: Characterization of fluorescent D-amino acid probes in *Mycobacterium smegmatis*

FDAAs can be incorporated into the PG peptide side chains through periplasmic remodeling or new cytoplasmic synthesis (42, 43). Importantly, FDAAs are not incorporated via a “one size fits all” route. Thus, their incorporation must be characterized in each bacterial species. Here, I will describe experiments performed to further characterize FDA incorporation in Msm. Intellectual contributions from Erkin Kuru, Hoong Lim (data analysis) and Sloan Siegrist were instrumental for these experiments. We found that FDA incorporation in Msm is primarily LDT dependent rather than intracellular, and furthermore, that LDTs themselves are not completely identical in terms of FDA incorporation capacity.

Results

FDAAs with various fluorescent moieties are incorporated in the same pattern in WT Msm

FDAAs can be synthesized with various fluorescent moieties leading to different dyes: NADA (3-[7-nitrobenzofurazan]-carboxamide-D-alanine), HADA (3-[7-hydroxycoumarin]-carboxamide-D-alanine) and TADA (RADA) (3-[5-carboxytetramethylrhodamine]-carboxamide-D-alanine) (57). Incorporation of the different FDAAs (NADA, HADA, RADA) shows a wide range of brightness however, the pattern of their incorporation is very similar (Figure 3.7). Thus, we concluded that these dyes are being incorporated via the same route.

Contributions to FDA incorporation vary by LDT

In Section 3.2 we identified LDTs as the primary enzymes responsible for most FDA incorporation in Msm. The FDA incorporation ability of various LDT knock out combinations

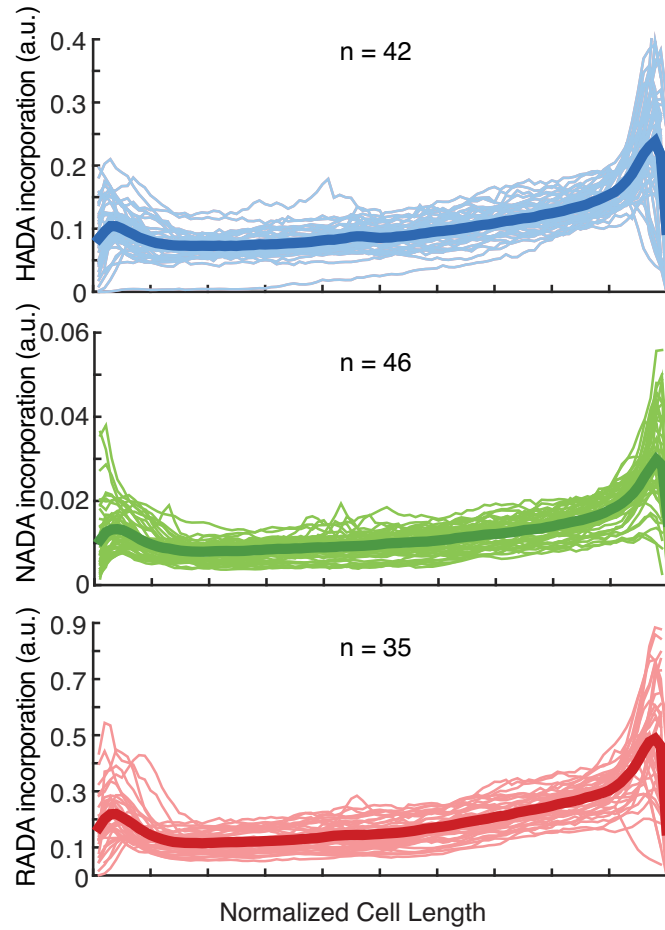


Figure 3.7: Different FDAAs incorporate in the same pattern in WT Msm.

HADA, NADA or RADA incorporation profiles in WT Msm after a 2-minute short pulse. (top) HADA incorporation (blue lines), (middle) NADA incorporation (green lines), (bottom) RADA incorporation (red lines). Note the Y-axis is different for each dye given the intensity of fluorescence.

was assessed. Intriguingly, different combinations of mutants result in varying amounts of FDAA incorporation (Figure 3.8A, B). For example $\Delta ldtAEB$, $\Delta ldtAEC$ and $\Delta ldtAEF$ cells do not have the same defect in FDAA incorporation. This suggests that the LDTs are not perfectly interchangeable. Perhaps various LDTs work in distinct complexes or with specific regulators or they may have preferences for substrates. Notably, these mutants (except $\Delta ldtAEC$ which is slightly longer than WT) do not have length defects suggesting that the decrease observed in FDAA incorporation is growth independent (Figure 3.8C).

Meropenem treatment inhibits FDAA incorporation

Since Mycobacterial LDTs are known to be potently inhibited *in vitro* by carbapenem antibiotics (21, 23, 27, 28, 31), we hypothesized that treatment of Msm with a carbapenem could inhibit FDAA incorporation via LDT inhibition. To test this, cells were treated with 12.5ug/mL of meropenem (~10X the minimum inhibitory concentration MIC) for 60 minutes. Cells were then stained with FDAA (RADA) for a short 2-minute pulse and imaged. The incorporation was substantially inhibited (Figure 3.9A). This data supports an LDT dependent mechanism of incorporation for the FDAAs. However, two caveats to the interpretation of this experiment are that meropenem likely also targets mycobacterial PBPs (as has been shown in other bacterial species (33, 34)) and treatment with carbapenems can halt growth quickly leading to a decrease in substrate for dye incorporation (58).

FDAAs cannot substitute for D-alanine to rescue an alanine racemase mutant

PG synthesis begins in the cytoplasm where UDP-MurNac-tripeptide is generated and then a D-ala-D-ala dipeptide is ligated to create the pentapeptide (15). To make the D-ala-D-ala

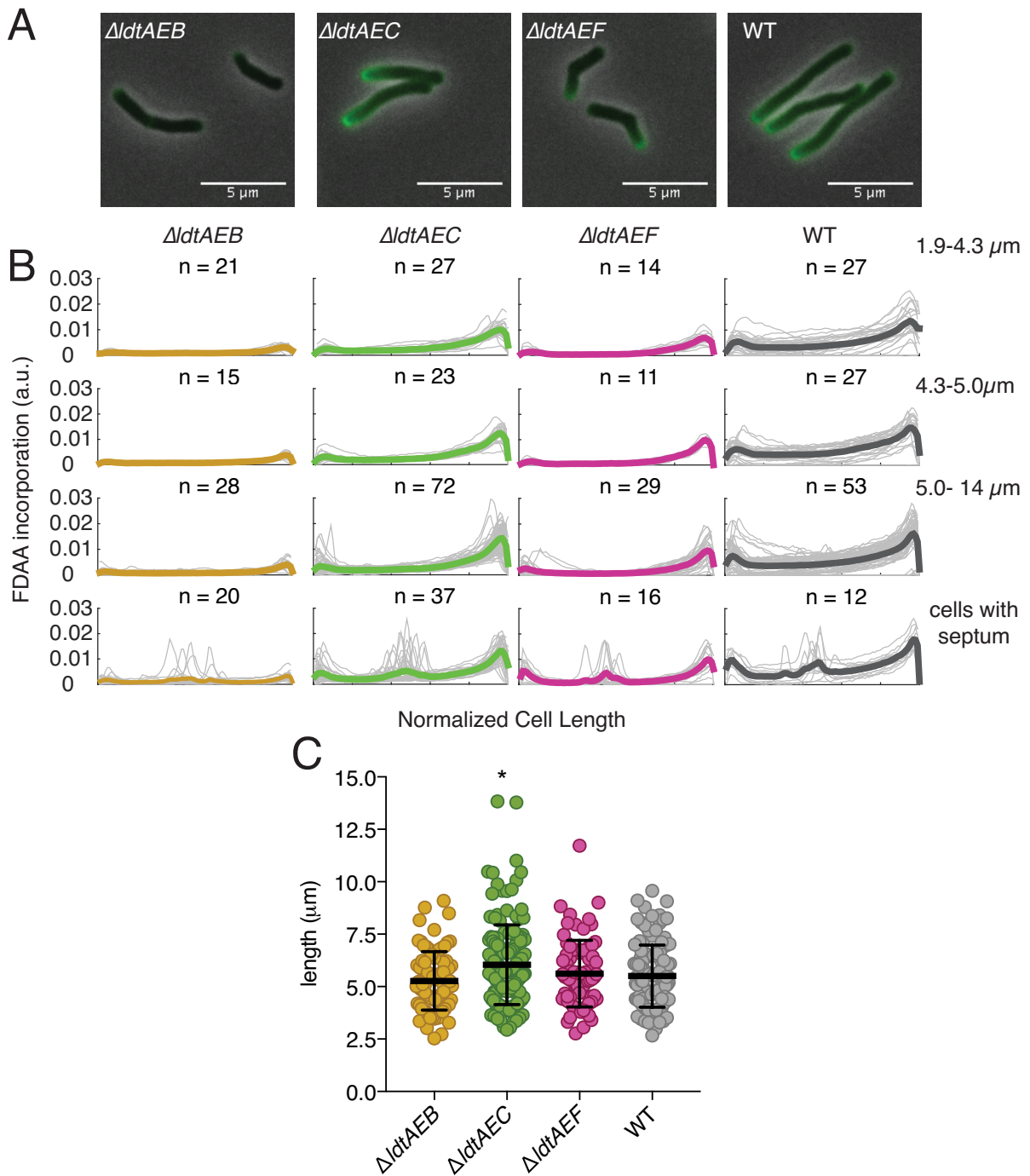


Figure 3.8: LDT homologs in Msm are not equal in their ability to incorporated FDAAs. (A) images of ΔldtAEB , ΔldtAEC , ΔldtAEF and WT Msm cells after a 2-minute pulse with FDAA (NADA). Scale bars are 5 μm . **(B)** Quantification of FDAA incorporation in ΔldtAEB ,

Figure 3.8 (Continued)

ΔldtAEC, *ΔldtAEF* and WT Msm cells. Each row represents cells binned by length (bins of cell lengths are 1.9-4.3μm, 4.3-5.0μm, and 5.0-14 μm). The last row is cells with FDAA stained septa. Thin grey lines in each plot represent FDAA incorporation of a single cell, thick colored lines represented the average FDAA incorporation. (C) Length of *ΔldtAEB*, *ΔldtAEC*, *ΔldtAEF* and WT Msm cells. *ΔldtAEC* was statistically significantly longer than WT cells (* Mann-Whitney U P-Value < 0.05).

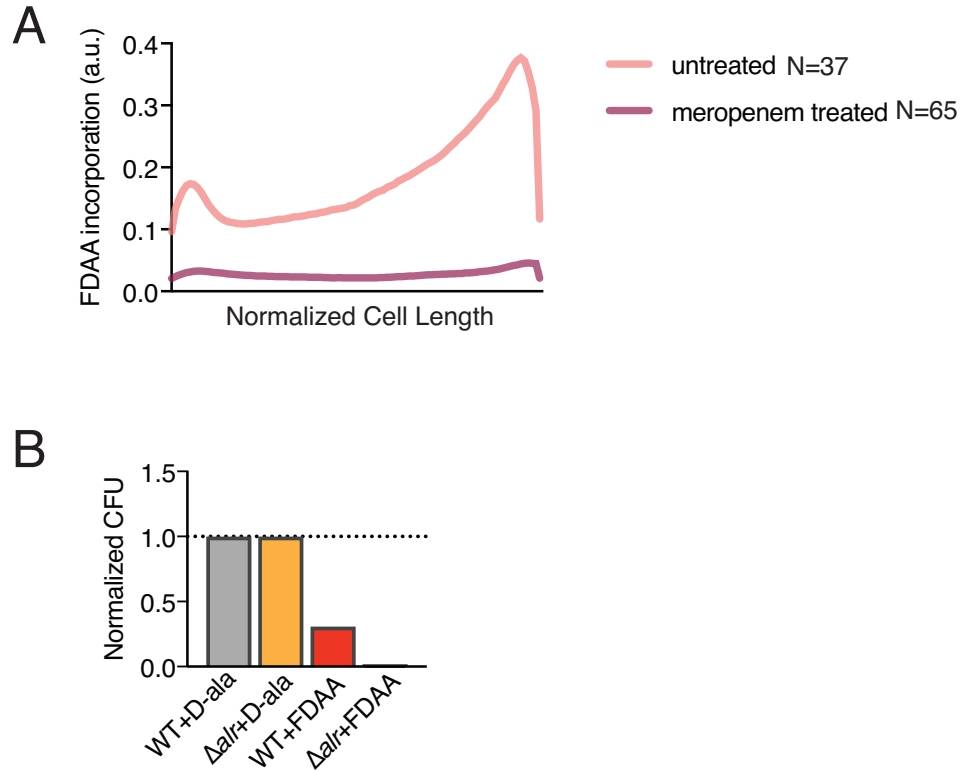


Figure 3.9: Evidence for extracellular incorporation of FDAAs in Msm. (A) Mean line profiles of FDAA incorporation (RADA) in WT Msm with or without exposure to meropenem. Line profiles were calculated from microscopy images. (B) Colony forming units of WT or Δalr Msm normalized to growth in 1mM D-alanine.

dipeptide, L-alanine must be converted into D-alanine by the essential protein Alr (alanine racemase) (15, 59). Cells lacking Alr die unless they are supplemented with D-alanine. To test whether FDAAs could incorporate into PG during its synthesis in the cytoplasm, survival of a D-alanine auxotrophic alanine racemase mutant was used. WT or Δalr cells were grown in media containing D-alanine (1mM) to log phase. Cells were washed and subcultured into media containing either D-alanine (2mM) or FDAA (2mM RADA) and plated for colony forming units 96 hours later on LB containing D-alanine. FDAAs could not rescue growth of the Δalr mutant (Figure 3.9B). This suggests that FDAAs cannot substitute for D-alanine during intracellular PG synthesis. Large chemical moieties are ligated to D-alanine to make the FDAAs therefore, it is plausible that these may not be suitable substrates for the intracellular PG synthesis enzymes.

Taken together, the inability of LDT mutants to incorporate FDAAs, (presented here and in Section 3.2) along with the meropenem pre-treatment results suggest strongly that most FDAA signal Msm is attributable to LDT dependent extracellular exchange of D-alanine for FDAA. Furthermore, the inability of FDAAs to rescue growth of the alanine racemase mutant supports an extracellular, rather than cytoplasmic, route of FDAA incorporation in Msm.

Section 3.4: Materials and Methods

Bacterial strains and culture conditions

Unless otherwise stated, *Mycobacterium smegmatis* (mc²155) was grown shaking at 37°C in liquid 7H9 media consisting of Middlebrook 7H9 salts with 0.2% glycerol, 0.85g/L NaCl, ADC (5g/L albumin, 2g/L dextrose, 0.003g/L catalase), and 0.05% Tween 80 and plated on LB agar. *Mycobacterium tuberculosis* (H37Rv) was grown in liquid 7H9 with OADC (oleic acid, albumin, dextrose, catalase) with 0.2% glycerol and 0.05% Tween 80. Antibiotic selection for *M. smegmatis* and *M. tuberculosis* were done at the following concentrations in broth and on agar: 25µg/mL kanamycin, 50µg/mL hygromycin, 20µg/mL zeocin and 20µg/mL nourseothricin and, twice those concentrations for cloning in *Escherichia coli* (TOP10, XL1-Blue and DH5α).

Strain construction

M. smegmatis mc²155 (Msm) mutants lacking *ldtABECFG* (Δ LDT) was constructed using recombineering to replace endogenous copies with zeocin or hygromycin resistance cassettes flanked by lox sites as previously described (60). Briefly, 500 base pairs of upstream and downstream sequence surrounding the gene of interest were amplified via PCR (KOD XtremeTM Hot Start DNA polymerase (EMD Millipore, Billerica, MA)). These flanking regions were amplified with overlaps to either a zeocin or hygromycin resistance cassette flanked by loxP sites and these pieces were assembled into a knock-out construct via isothermal assembly (61). Each knock-out cassette was transformed into Msm expressing inducible copies of RecET for recombination (60, 62, 63). Once deletions were verified by PCR using and sequencing, the antibiotic resistance cassettes were removed by the expression of Cre recombinase. The order of

deletion construction in the Δ LDT strain was as follows (where arrows represent transformation of a Cre-recombinase plasmid, followed by curing of the Cre-recombinase plasmid as it contains the *sacB* gene for sucrose counter selection on LB supplemented with 10% sucrose, and strain names are listed in parenthesis). This resulted in the removal of antibiotic cassettes flanked by loxP sites:

- 1) $mc^2155\Delta ldtA::zeo^R$ (KB103) \rightarrow $mc^2155\Delta ldtA::loxP$ (KB134)
- 2) $mc^2155\Delta ldtA::loxP + \Delta ldtE::zeo^R$ (KB156)
- 3) $mc^2155\Delta ldtA::loxP \Delta ldtE::zeo^R + \Delta ldtB::hyg^R$ (KB200) \rightarrow $mc^2155\Delta ldtA::loxP \Delta ldtE::loxP \Delta ldtB::loxP$ (KB207)
- 4) $mc^2155\Delta ldtA::loxP \Delta ldtE::loxP \Delta ldtB::loxP + \Delta ldtC::hyg^R$ (KB209)
- 5) $mc^2155\Delta ldtA::loxP \Delta ldtE::loxP \Delta ldtB::loxP \Delta ldtC::hyg^R \Delta ldtG::zeo^R$ (KB222) \rightarrow $mc^2155\Delta ldtA::loxP \Delta ldtE::loxP \Delta ldtB::loxP \Delta ldtC::loxP \Delta ldtG::loxP$ (KB241)
- 6) $mc^2155\Delta ldtA::loxP \Delta ldtE::loxP \Delta ldtB::loxP \Delta ldtC::loxP \Delta ldtG::loxP \Delta ldtF::hyg^R$ (KB303 referred to as Δ LDT) .

M. tuberculosis H37Rv was transformed with a vector expressing the codon optimized *Photobacterium luminescens luxABCDE* operon (pMV306hsp+LuxG13 –Addgene #26161)(64). This strain is referred to as Mtb Lux.

Refer to Supplemental Table 1 for oligonucleotides, and Supplemental Table 2 for a complete strain list.

Δ LDT complementation plasmid construction

To complement Δ LDT we placed a copy of *ldtE* (*MSMEG_0233*) under the constitutive TetO promoter (a UV15 derivative within a pMC1s plasmid that is inducible with anhydrous tetracycline in the presence of a tet-repressor TetR, which the Δ LDT_{comp} strain lacks (46, 65)) on vector that integrates at the L5 phage integration site of the chromosome of the Δ LDT strain (the vector is marked with kanamycin resistance). A glycine, glycine, serine linker was cloned between *ldtE* and mRFP in this complementation construct.

PonA1 transpeptidase essentiality L5 allele swapping

To test essentiality of transpeptidation by PonA1 in the Δ LDT cells, L5 allele swapping as described in (46) and figure S9 was performed. The plasmids used in this experiment were previously published in (46). Briefly, a wild-type copy of PonA1 (TetO driven expression, L5 integrating and kanamycin marked) was transformed into Δ LDT. Then, the endogenous copy of *ponA1* was replaced with zeocin using the above mentioned recombineering technique (amplifying the construct from a previously published deletion mutant of *ponA1*(46)). Swapping efficiency of either wildtype or transpeptidase mutant PonA1 marked with nourseothricin was tested with a transformation into Δ LDT//L5-TetO-ponA1 (WT)-kanamycin.

M. tuberculosis minimum inhibitory concentration (MIC) determination

Mtb Lux was grown to log phase and diluted to an OD₆₀₀=0.006 in each well of non-treated 96 well plates (Genessee Scientific) containing 100 μ L of meropenem (Sigma Aldrich) and/or amoxicillin (Sigma Aldrich) diluted in 7H9+OADC+5 μ g/mL clavulanate (Sigma Aldrich). Cells were incubated in drug at 37°C shaking for 7 days, 0.002% resazurin (Sigma Aldrich) was added

to each well, and the plates were incubated for 24 hours before MICs were determined. Pink wells signify metabolic activity and blue signify no metabolic activity (66). Checkerboard MIC plates and fractional inhibitory concentrations were calculated as described in (51).

M. tuberculosis drug killing assays

Mtb Lux was grown to log phase (kanamycin 25 μ g/mL) and diluted in 30mL inkwells (Corning Lifesciences) to an OD₆₀₀=0.05 in 7H9+OADC+5 μ g/mL clavulanate with varying concentrations of amoxicillin, meropenem, or both. 100 μ L of these cultures were pipetted in duplicate into a white 96-well polystyrene plate (Greiner Bio-One) and luminescence was read in a Synergy H1 microplate reader from BioTek Instruments, Inc. using the Gen5 Software (2.02.11 Installation version). The correlation between relative light units (RLU) and colony forming units (CFU) has been previously shown in drug killing (52), and is shown in Msm in supplemental figure S11.

Fluorescent D-amino acid labeling

NADA (3-[7-nitrobenzofurazan]-carboxamide-D-alanine), HADA (3-[7-hydroxycoumarin]-carboxamide-D-alanine) and TADA (RADA) (3-[5-carboxytetramethylrhodamine]-carboxamide-D-alanine) were synthesized by Tocris following the published protocol (57). To 1mL of exponentially growing cells 0.1mM of FDAA final was added and incubated for 2 minutes before washing in 7H9 twice. For still imaging, after the second wash, cells were fixed in 7H9 + 1% paraformaldehyde before imaging. For pulse chase experiments, cells were stained, washed with 7H9 and allowed to grow out for 40 minutes before being stained with a second dye and imaged.

Flow cytometry

An *M. smegmatis* transposon library was grown to mid-log phase, and stained with 2 µg/mL NADA for 2 minutes. Cells were centrifuged and half of the supernatant was discarded. The pellet was resuspended in the remaining supernatant, passed through a 10µm filter and taken to be sorted (FACS Aria; Excitation: 488nm; Emission filter: 530/30). Two bins were drawn at the lowest and highest staining end of the population, representing 12.5% of the population. 600,000 cells from these bins were sorted into 7H9 medium. Half of this was directly plated onto LB agar supplemented with kanamycin to select for cells harboring the transposon. The remaining 300,000 cells were grown out in 7H9 to log phase, stained with FDAA and sorted again to enrich the populations.

Transposon sequencing, mapping and FDAA flow cytometry enrichment analysis.

Genomic DNA (gDNA) was harvested from the sorted transposon library colonies and transposon-gDNA junction libraries were constructed and sequenced using the Illumina Hi-Seq platform (45). Reads were mapped on the *M. smegmatis* genome, tallied and reads at each TA site for the bins (low/high incorporating sort 1 and 2) were imported into MATLAB and processed by a custom scripts as described in (67).

Microscopy

Both still imaging and time lapse microscopy were performed on an inverted Nikon TI-E microscope at 60x magnification. Time lapse was done using a CellASIC (B04A plate) with constant liquid 7H9 flow in a 37°C chamber. For turgor experiment (Figure 3.4A), cells were

grown in either 7H9 or 7H9 500mM sorbitol overnight, and then switched to either 7H9 with 150mM sorbitol (high osmolar) or to 7H9 alone (iso-osmolar).

Atomic force microscopy

AFM experimentation was conducted as previously(68). In short, polydimethylsiloxane (PDMS) – coated coverslips were prepared by spin-coating a mixture of PDMS at a ratio of 15:1 (elastomer:curing agent) with hexane (Sigma 296090) at a ratio of 1:10 (PDMS:hexane) (69, 70). A 50 μ l filtered (0.5 μ m pore size PVDF filter – Millipore) aliquot of bacteria grown to mid-log phase and concentrate from 2-5 ml of culture was put onto the hydrophobic surface of the PDMS-coated coverslip and incubated for ~20 min to increase surface interactions between the bacteria and the coverslip. 7H9 (~3 ml) was supplied to the sample so as to immerse the bacterial sample and the AFM cantilever in fluid. The AFM imaging mode, Peak Force QNM, was used to image bacteria with a Nanoscope 5 controller (Veeco Metrology) at a scan rate of 0.5 Hz and a maximum Z-range of 12 μ m. A ScanAsyst fluid cantilever (Bruker) was used. Height, peak force error, DMT modulus, and log DMT modulus were recorded for all scanned images in the trace and retrace directions. Images were processed with Gwyddion (Department of Nanometrology, Czech Metrology Institute). ImageJ was used for extracting bacterial cell profiles in a tabular form.

Correlated optical fluorescence and AFM

Correlated optical fluorescence and AFM images were acquired as described (68). Briefly, optical fluorescence images were acquired with an electron-multiplying charge-coupled device (EMCCD) iXon Ultra 897 camera (Andor) mounted onto an IX81 inverted optical microscope (Olympus) with an UPLFLN100XO2PH x 100 oil immersion objective (Olympus). Transmitted light was

delivered by a 12V/100W AHS-LAMP halogen lamp. An U-MGFPHQ fluorescence filter cube for GFP (HQ-Ion-coated filters) was used for GFP fluorescence detection. The AFM was mounted atop the inverted microscope. Images were acquired with a Dimension Icon scan head (Bruker) using ScanAsyst fluid cantilevers (Bruker) with a nominal spring constant of 0.7 N m^{-1} in Peak Force QNM mode at a force setpoint $\sim 1 \text{ nN}$ and typical scan rates of 0.5 Hz . Indentation on the cell surface was estimated to be $\sim 10 \text{ nm}$ in the Z-axis. Optical fluorescence microscopy was used to identify Wag31-GFP puncta expressed in a wild-type background (71) in order to distinguish them from cells of the ΔLDT mutant strains.

Calculating cell surface rigidity

A cell profile was extracted from AFM Height and DMT Modulus image channels as sequentially connected linear segments following the midline of an individual cell. A background correction was conducted to by dividing the DMT modulus values of the cell surface by the mean value of the PDMS surface and rescaled to compare the cell surface rigidity between individual cells from different experiments. The DMT modulus reflects the elastic modulus (stress-strain relationship) for each cross-sectional increment along the cell length.

Analysis of fluorescent protein distribution

Using a segmented line, profiles of cells from new to old pole were created at the frame “pre-division” based on physical cell separation of the phase image. A custom FIJI (72) script (written by E. Hesper Rego) was run to extract fluorescence line profiles of each cell and save them as .csv files. These .csv files were imported to Matlab where a custom script (written by E. Hesper Rego)

was applied to normalize the fluorescence line profile to fractional cell length and to interpolate the fluorescence values to allow for averaging.

Analysis of cell wall distribution

Cells were stained with Alexa488 NHS ester as described previously (41) and followed via time-lapse microscopy in the CellASIC device. Briefly, 1mL of log phase cells was pelleted at 8,000 rpm for 1 minute and washed with 1mL PBST. The pellet was resuspended in 100uL of PBST and 10uL Alexa Fluor 488 carboxylic acid succinimidyl ester was added for a final concentration of 0.05mg/mL. This was incubated for 3 minutes at room temperature. Stained cells were pelleted for 1 minute at 13,000 rpm and washed with 500 μ L PBST. They were spun again and resuspended in 7H9 for outgrowth observation over time in the CellASIC device.

Analysis of FDAAs

Images were analyzed using a combination of Oufi (73) for cell selection followed by custom coded Matlab scripts to plot FDAA fluorescence over normalized cell length, calculate cell length and bin cells by existence of an FDAA labeled septum (custom scripts written by Hoong C. Lim).

Generation of transposon libraries

M. smegmatis cells were transduced at (OD_{600} 1.1-1.7) with ϕ MycoMarT7 phage (temperature sensitive) that has a Kanamycin marked Mariner transposon as previously described (45, 74). Briefly, mutagenized cells were plated at 37°C on LB plates supplemented with Kanamycin to select for phage transduced cells. Roughly 100,000 colonies per library were scraped, and genomic DNA was extracted. Sequencing libraries were generated specifically containing transposon

disrupted DNA as previously described (74). Libraries were sequenced on the Illumina platform. Data were analyzed using the TRANSIT pipeline (75).

Peptidoglycan isolation and analysis

600mLs of wildtype and Δ LDT cells were grown to log phase and collected via centrifugation at 5000 x g for 10 minutes at 4°C. The resulting pellet was resuspended in PBS and cells were lysed using a cell disruptor at 35,000psi twice. Lysed cells were boiled in 10% SDS (sodium dodecyl sulfate) for 30 minutes and peptidoglycan was collected via centrifugation at 17,000 x g. Pellets were washed with 0.01% DDM (*n*-Dodecyl β -D-maltoside) to remove SDS and resuspended in 1XPBS + 0.01% DDM. PG was digested with alpha amylase (Sigma A-6380) and alpha chymotrypsin (Amersco 0164) overnight. The samples were again boiled in 10% SDS and washed in 0.01% DDM. The resulting pellet was resuspended in 400 μ L 25mM sodium phosphate pH6, 0.5mM MgCl₂, 0.01% DDM. 20 μ L of lysozyme (10mg/mL) and 20 μ L 5U/ μ L mutanolysin (Sigma M9901) were added and incubated overnight at 37°C. Samples were heated at 100°C and centrifuged at 100,000 x g. 128 μ L of ammonium hydroxide was added and incubated for 5 hours at 37°C. This reaction was neutralized with 122 μ L of glacial acetic acid. Samples were lyophilized, resuspended in 300 μ L 0.1% formic acid and subjected to analysis by LC-MS/MS. Peptide fragments were separated with an Agilent Technologies 1200 series HPLC on a Nucleosil C18 column (5 μ m 100A 4.6 x 250mm) at 0.5mL/min flow rate with the following method: Buffer A= 0.1% Formic Acid; Buffer B=0.1% Formic Acid in acetonitrile; 0% B from 0-10 minutes, 0-20% B from 10-100 minutes, 20% B from 100-120 minutes, 20-80% B from 120-130 minutes, 80% B

from 130-140 minutes, 80%-0% B from 140- 150minutes, 0% B from 150-170 minutes. MS/MS was conducted in positive ion mode using electrospray ionization on an Agilent Q-TOF (6520).

Expression and purification of MSMEG_2433 (DacB2)

MSMEG_2433 was expressed and purified using a modified method for purification of low molecular weight PBPs that was previously published (76). An N-terminally truncated MSMEG_2433₍₂₉₋₂₉₆₎ was cloned into the pET28b vector for isopropyl β -D-1-thiogalactopyranoside (IPTG) inducible expression in *E. coli* BL21 (DE3). 10mLs of overnight culture grown in LB with Kanamycin (50 μ g/mL) were diluted 1:100 into 1L of LB with Kanamycin (50 μ g/mL) and grown at 37°C until an OD₆₀₀ of 0.5. The culture was allowed to cool to room temperature. It was then induced with 0.5mM IPTG and allowed to grow at 16°C overnight with shaking. Cells were pelleted via centrifugation at 4,000rpm for 20 min at 4°C. The pellet was suspended in 20mL binding buffer (20mM Tris pH8, 10mM MgCl₂, 160mM NaCl, 20mM imidazole) with 1mM phenylmethylsulfonylfluoride (PMSF) and 500 μ g/mL DNase. Cells were then lysed with a cell disrupter at 25,000psi (twice). Lysate was pelleted by ultracentrifugation (90,000 \times g, 30 min, 4°C). To this resulting supernatant, 1.0mL of washed Ni-NTA resin (Qiagen) was added and this mixture was rocked at 4°C for 40 min. This was loaded onto a gravity column and the resin was washed with 20mL wash buffer (20mM Tris pH 8, 500mM NaCl, 20mM imidazole, 0.1% Triton X-100). The protein was eluted in 10mL of elution buffer (20 mM Tris pH8, 150mM NaCl, 300mM imidazole, 0.1% reduced Triton X-100) and was concentrated to 1 mL with a 10kD MWCO Amicon Ultra Centrifuge Filter. The final protein concentration was measured via Nanodrop using the estimated extinction coefficient (29459 M⁻¹cm⁻¹). The protein was diluted to 200 μ M in elution buffer, aliquoted in 10% glycerol, and stored at -80°C. Proper

folding of purified MSMEG_2433₍₂₉₋₂₉₆₎ was tested via Bocillin-FL binding. Briefly, 20 μ M of purified protein was added to penicillin G (100, 1000 U/mL in 20mM K₂HPO₄, 140mM NaCl, pH7.5) in a 9 μ L reaction. The reaction was incubated at 37°C for 1hour. 10 μ M Bocillin-FL was added and incubated at 37°C for 30 minutes. SDS loading dye was added to quench the reaction and samples were loaded onto a 4-20% gel. MSMEG_2433₍₂₉₋₂₉₆₎ bound by Bocillin-FL was imaged using a Typhoon 9400 Variable Mode Imager (GE Healthcare) (Alexa Excitation-488nm Emission-526nm).

Lipid II extraction.

B. subtilis Lipid II was extracted as previously published (77).

SgtB purification.

SgtB was purified as previously published (78).

Purification of *B. subtilis* PBP1 and *in vitro* Lipid II crosslinking.

Purification of *B. subtilis* PBP1 and *in vitro* Lipid II crosslinking were carried out as previously described (79).

In vitro Lipid II polymerization and crosslinking.

20 μ M purified BS Lipid II was incubated with TGase buffer (10X-500mM HEPES pH7.5, 100mM CaCl₂) and either 5 μ M PBP1(final) or 0.33 μ M SgtB for 1 hour at room temperature. A PBP1 buffer (20mM Tris pH7.6, 0.5M NaCl, 0.1% reduced Triton X-100, 10% glycerol) control consisting of Lipid II + SgtB + PBP1a buffer was included. The enzymes were heat denatured at

95°C for 5 minutes. Then, purified MSMEG_2433₍₂₉₋₂₉₆₎ was added (20uM) and the reaction was incubated at room temperature for 1 hour. Mutanolysin (1μL of 4000U/mL) was then added and incubated for 1.5 hours at 37°C (twice). The resulting mucopeptides were reduced with 30μL of NaBH₄ (10mg/mL) for 20 minutes at room temperature with tube flicking every 5 minutes to mix. The pH was adjusted to 4 using ~5μL of 20% H₃PO₄. The resulting product was lyophilized and then resuspended in 18μL of water and analyzed via LC-MS on a QTOF.

Section 3.5: References

1. **Salton MRJ.** 1952. Cell wall of *Micrococcus lysodeikticus* as the substrate of lysozyme. *Nature* **170**:746–747.
2. **Salton MR.** 1958. The lysis of micro-organisms by lysozyme and related enzymes. *J Gen Microbiol* **18**:481–490.
3. **Martin HH.** 1964. Composition of the mucopolymer in cell walls of the unstable and stable L-form of *Proteus mirabilis*. *J Gen Microbiol* **36**:441–450.
4. **Weidel W, Frank H, Martin HH.** 1960. The rigid layer of the cell wall of *Escherichia coli* strain B. *J Gen Microbiol* **22**:158–166.
5. **Whatmore AM, Reed RH.** 1990. Determination of turgor pressure in *Bacillus subtilis*: a possible role for K⁺ in turgor regulation. *J Gen Microbiol* **136**:2521–2526.
6. **Vollmer W, Blanot D, de Pedro MA.** 2008. Peptidoglycan structure and architecture. *FEMS Microbiol Rev* **32**:149–167.
7. **Horsburgh CR, Barry CE, Lange C.** 2015. Treatment of Tuberculosis. *N Engl J Med* **373**:2149–2160.
8. **Flores AR, Parsons LM, Pavelka MS.** 2005. Genetic analysis of the beta-lactamases of *Mycobacterium tuberculosis* and *Mycobacterium smegmatis* and susceptibility to beta-lactam antibiotics. *Microbiology* **151**:521–532.
9. **Wivagg CN, Bhattacharyya RP, Hung DT.** 2014. Mechanisms of β -lactam killing and resistance in the context of *Mycobacterium tuberculosis*. *The Journal of Antibiotics* **67**:645–654.
10. **Hugonnet J-E, Blanchard JS.** 2007. Irreversible inhibition of the *Mycobacterium tuberculosis* beta-lactamase by clavulanate. *Biochemistry* **46**:11998–12004.
11. **Diacon AH, van der Merwe L, Barnard M, Groote-Bidlingmaier von F, Lange C, García-Basteiro AL, Sevene E, Ballell L, Barros-Aguirre D.** 2016. β -Lactams against Tuberculosis--New Trick for an Old Dog? *N Engl J Med* **375**:393–394.

12. **Tipper DJ, Strominger JL.** 1965. Mechanism of action of penicillins: a proposal based on their structural similarity to acyl-D-alanyl-D-alanine. *Proc Natl Acad Sci USA* **54**:1133–1141.
13. **Spratt BG.** 1975. Distinct penicillin binding proteins involved in the division, elongation, and shape of *Escherichia coli* K12. *Proc Natl Acad Sci USA* **72**:2999–3003.
14. **Spratt BG, Pardee AB.** 1975. Penicillin-binding proteins and cell shape in *E. coli*. *Nature* **254**:516–517.
15. **Typas A, Banzhaf M, Gross CA, Vollmer W.** 2011. From the regulation of peptidoglycan synthesis to bacterial growth and morphology. *Nature Publishing Group* **10**:123–136.
16. **Azuma I, Thomas DW, Adam A, Ghuysen JM, Bonaly R, Petit JF, Lederer E.** 1970. Occurrence of N-glycolylmuramic acid in bacterial cell walls. A preliminary survey. *Biochim Biophys Acta* **208**:444–451.
17. **Mahapatra S, Yagi T, Belisle JT, Espinosa BJ, Hill PJ, McNeil MR, Brennan PJ, Crick DC.** 2005. Mycobacterial lipid II is composed of a complex mixture of modified muramyl and peptide moieties linked to decaprenyl phosphate. *Journal of Bacteriology* **187**:2747–2757.
18. **Kumar P, Arora K, Lloyd JR, Lee IY, Nair V, Fischer E, Boshoff HIM, Barry CE III.** 2012. Meropenem inhibits D,D-carboxypeptidase activity in *Mycobacterium tuberculosis*. *Molecular Microbiology* **86**:367–381.
19. **Ghuysen JM.** 1991. Serine beta-lactamases and penicillin-binding proteins. *Annu Rev Microbiol* **45**:37–67.
20. **Mainardi J-L, Fourgeaud M, Hugonnet J-E, Dubost L, Brouard J-P, Ouazzani J, Rice LB, Gutmann L, Arthur M.** 2005. A novel peptidoglycan cross-linking enzyme for a beta-lactam-resistant transpeptidation pathway. *Journal of Biological Chemistry* **280**:38146–38152.
21. **Cordillot M, Dubee V, Triboulet S, Dubost L, Marie A, Hugonnet JE, Arthur M, Mainardi JL.** 2013. In Vitro Cross-Linking of *Mycobacterium tuberculosis* Peptidoglycan by L,D-Transpeptidases and Inactivation of These Enzymes by Carbapenems. *Antimicrobial Agents and Chemotherapy* **57**:5940–5945.

22. **Hugonnet J-E, Tremblay LW, Boshoff HI, Barry CE, Blanchard JS.** 2009. Meropenem-clavulanate is effective against extensively drug-resistant *Mycobacterium tuberculosis*. *Science* **323**:1215–1218.
23. **Lavollay M, Arthur M, Fourgeaud M, Dubost L, Marie A, Veziris N, Blanot D, Gutmann L, Mainardi JL.** 2008. The Peptidoglycan of Stationary-Phase *Mycobacterium tuberculosis* Predominantly Contains Cross-Links Generated by L,D-Transpeptidation. *Journal of Bacteriology* **190**:4360–4366.
24. **Glauner B, Höltje JV, Schwarz U.** 1988. The composition of the murein of *Escherichia coli*. *Journal of Biological Chemistry* **263**:10088–10095.
25. **Wietzerbin J, Das BC, Petit JF, Lederer E, Leyh-Bouille M, Ghuysen JM.** 1974. Occurrence of D-alanyl-(D)-meso-diaminopimelic acid and meso-diaminopimelyl-meso-diaminopimelic acid interpeptide linkages in the peptidoglycan of *Mycobacteria*. *Biochemistry* **13**:3471–3476.
26. **Mainardi JL, Legrand R, Arthur M, Schoot B, van Heijenoort J, Gutmann L.** 2000. Novel mechanism of beta-lactam resistance due to bypass of DD-transpeptidation in *Enterococcus faecium*. *Journal of Biological Chemistry* **275**:16490–16496.
27. **Mainardi J-L, Hugonnet J-E, Rusconi F, Fourgeaud M, Dubost L, Moumi AN, Delfosse V, Mayer C, Gutmann L, Rice LB, Arthur M.** 2007. Unexpected inhibition of peptidoglycan LD-transpeptidase from *Enterococcus faecium* by the beta-lactam imipenem. *Journal of Biological Chemistry* **282**:30414–30422.
28. **Dubee V, Triboulet S, Mainardi JL, Etheve-Quelquejeu M, Gutmann L, Marie A, Dubost L, Hugonnet JE, Arthur M.** 2012. Inactivation of *Mycobacterium tuberculosis* L,D-Transpeptidase LdtMt1 by Carbapenems and Cephalosporins. *Antimicrobial Agents and Chemotherapy* **56**:4189–4195.
29. **Triboulet S, Dubée V, Lecoq L, Bougault C, Mainardi J-L, Rice LB, Ethève-Quelquejeu M, Gutmann L, Marie A, Dubost L, Hugonnet J-E, Simorre J-P, Arthur M.** 2013. Kinetic features of L,D-transpeptidase inactivation critical for β -lactam antibacterial activity. *PLoS ONE* **8**:e67831.
30. **Lecoq L, Bougault C, Hugonnet J-E, Veckerlé C, Pessey O, Arthur M, Simorre J-P.** 2012. Dynamics induced by β -lactam antibiotics in the active site of *Bacillus subtilis* L,D-transpeptidase. *Structure* **20**:850–861.

31. **Kim HS, Kim J, Im HN, Yoon JY, An DR, Yoon HJ, Kim JY, Min HK, Kim SJ, Lee JY, Han BW, Suh SW.** 2013. Structural basis for the inhibition of Mycobacterium tuberculosis L,D-transpeptidase by meropenem, a drug effective against extensively drug-resistant strains. *Acta Cryst* (2013) **D69**, 420-431 [doi:10.1107/S0907444912048998] 1–12.
32. **Sumita Y, Fukasawa M, Okuda T.** 1990. Comparison of two carbapenems, SM-7338 and imipenem: affinities for penicillin-binding proteins and morphological changes. *The Journal of Antibiotics* **43**:314–320.
33. **Sumita Y, Fukasawa M.** 1995. Potent activity of meropenem against Escherichia coli arising from its simultaneous binding to penicillin-binding proteins 2 and 3. *Journal of Antimicrobial Chemotherapy* **36**:53–64.
34. **Davies TA, Shang W, Bush K, Flamm RK.** 2008. Affinity of doripenem and comparators to penicillin-binding proteins in Escherichia coli and Pseudomonas aeruginosa. *Antimicrobial Agents and Chemotherapy* **52**:1510–1512.
35. **Davies TA, Page MGP, Shang W, Andrew T, Kania M, Bush K.** 2007. Binding of ceftobiprole and comparators to the penicillin-binding proteins of Escherichia coli, Pseudomonas aeruginosa, Staphylococcus aureus, and Streptococcus pneumoniae. *Antimicrobial Agents and Chemotherapy* **51**:2621–2624.
36. **Gupta R, Lavollay M, Mainardi J-L, Arthur M, Bishai WR, Lamichhane G.** 2010. The Mycobacterium tuberculosis protein LdtMt2 is a nonclassical transpeptidase required for virulence and resistance to amoxicillin. *Nature Medicine* **16**:466–469.
37. **Schoonmaker MK, Bishai WR, Lamichhane G.** 2014. Nonclassical transpeptidases of Mycobacterium tuberculosis alter cell size, morphology, the cytosolic matrix, protein localization, virulence, and resistance to β -lactams. *Journal of Bacteriology* **196**:1394–1402.
38. **Sanders AN, Wright LF, Pavelka MS.** 2014. Genetic characterization of mycobacterial L,D-transpeptidases. *Microbiology (Reading, Engl)* **160**:1795–1806.
39. **Pisabarro AG, de Pedro MA, Vázquez D.** 1985. Structural modifications in the peptidoglycan of Escherichia coli associated with changes in the state of growth of the culture. *Journal of Bacteriology* **161**:238–242.

40. **Atrih A, Bacher G, Allmaier G, Williamson MP, Foster SJ.** 1999. Analysis of peptidoglycan structure from vegetative cells of *Bacillus subtilis* 168 and role of PBP 5 in peptidoglycan maturation. *Journal of Bacteriology* **181**:3956–3966.
41. **Aldridge BB, Fernandez-Suarez M, Heller D, Ambravaneswaran V, Irimia D, Toner M, Fortune SM.** 2012. Asymmetry and aging of mycobacterial cells lead to variable growth and antibiotic susceptibility. *Science* **335**:100–104.
42. **Kuru E, Hughes HV, Brown PJ, Hall E, Tekkam S, Cava F, de Pedro MA, Brun YV, VanNieuwenhze MS.** 2012. In Situ Probing of Newly Synthesized Peptidoglycan in Live Bacteria with Fluorescent D-Amino Acids. *Angew Chem Int Ed* **51**:12519–12523.
43. **Kuru E, Lambert C, Rittichier J, Till R, Ducret A, Derouaux A, Gray J, Biboy J, Vollmer W, VanNieuwenhze M, Brun YV, Sockett RE.** 2017. Fluorescent D-amino-acids reveal bi-cellular cell wall modifications important for *Bdellovibrio bacteriovorus* predation. *Nat Microbiol* **2**:1648–1657.
44. **Cava F, de Pedro MA, Lam H, Davis BM, Waldor MK.** 2011. Distinct pathways for modification of the bacterial cell wall by non-canonical D-amino acids. *The EMBO Journal* **30**:3442–3453.
45. **Long JE, DeJesus M, Ward D, Baker RE, Ioerger T, Sassetti CM.** 2015. Identifying Essential Genes in *Mycobacterium tuberculosis* by Global Phenotypic Profiling, pp. 79–95. *In* Gene Essentiality. Humana Press, New York, NY, New York, NY.
46. **Kieser KJ, Boutte CC, Kester JC, Baer CE, Barczak AK, Meniche X, Chao MC, Rego EH, Sassetti CM, Fortune SM, Rubin EJ.** 2015. Phosphorylation of the Peptidoglycan Synthase PonA1 Governs the Rate of Polar Elongation in Mycobacteria. *PLoS Pathog* **11**:e1005010.
47. **Zimmermann L, Stephens A, Nam S-Z, Rau D, Kübler J, Lozajic M, Gabler F, Söding J, Lupas AN, Alva V.** 2017. A Completely Reimplemented MPI Bioinformatics Toolkit with a New HHpred Server at its Core. *J Mol Biol*.
48. **Bansal A, Kar D, Murugan RA, Mallick S, Dutta M, Pandey SD, Chowdhury C, Ghosh AS.** 2015. A putative low-molecular-mass penicillin-binding protein (PBP) of *Mycobacterium smegmatis* exhibits prominent physiological characteristics of DD-carboxypeptidase and beta-lactamase. *Microbiology (Reading, Engl)* **161**:1081–1091.

49. **González-Leiza SM, de Pedro MA, Ayala JA.** 2011. AmpH, a bifunctional DD-endopeptidase and DD-carboxypeptidase of *Escherichia coli*. *Journal of Bacteriology* **193**:6887–6894.
50. **Gonzalo X, Drobniewski F.** 2013. Is there a place for β -lactams in the treatment of multidrug-resistant/extensively drug-resistant tuberculosis? Synergy between meropenem and amoxicillin/clavulanate. *J Antimicrob Chemother* **68**:366–369.
51. 2016. Synergism Testing: Broth Microdilution Checkerboard and Broth Macrodilution Methods, pp. 5.16.1–5.16.23. *In* *Clinical Microbiology Procedures Handbook*, Fourth Edition. American Society of Microbiology.
52. **Andreu N, Fletcher T, Krishnan N, Wiles S, Robertson BD.** 2012. Rapid measurement of antituberculosis drug activity in vitro and in macrophages using bioluminescence. *J Antimicrob Chemother* **67**:404–414.
53. **Ursell TS, Nguyen J, Monds RD, Colavin A, Billings G, Ouzounov N, Gitai Z, Shaevitz JW, Huang KC.** 2014. Rod-like bacterial shape is maintained by feedback between cell curvature and cytoskeletal localization. *Proc Natl Acad Sci USA* **111**:E1025–34.
54. **Garner EC, Bernard R, Wang W, Zhuang X, Rudner DZ, Mitchison T.** 2011. Coupled, Circumferential Motions of the Cell Wall Synthesis Machinery and MreB Filaments in *B. subtilis*. *Science* **333**:222–225.
55. **Hussain S, Wivagg CN, Szwedziak P, Wong F, Schaefer K, Izore T, Renner LD, Sun Y, Bisson Filho AW, Walker S, Amir A, Löwe J, Garner EC.** 2017. MreB Filaments Create Rod Shape By Aligning Along Principal Membrane Curvature.
56. **Dooley, K.** Early Bactericidal Activity of Rifampin + Meropenem + Amoxicillin/Clavulanate in Adults With Pulmonary TB - clinicaltrials.gov/ct2/show/NCT03174184
57. **Kuru E, Tekkam S, Hall E, Brun YV, Van Nieuwenhze MS.** 2014. Synthesis of fluorescent D-amino acids and their use for probing peptidoglycan synthesis and bacterial growth in situ. *Nat Protoc* **10**:33–52.
58. **Dhar N, Dubée V, Ballell L, Cuinet G, Hugonnet J-E, Signorino-Gelo F, Barros D, Arthur M, McKinney JD.** 2015. Rapid cytolysis of *Mycobacterium tuberculosis* by faropenem, an orally bioavailable β -lactam antibiotic. *Antimicrobial Agents and Chemotherapy* **59**:1308–1319.

59. **Hett EC, Rubin EJ.** 2008. Bacterial growth and cell division: a mycobacterial perspective. *Microbiol Mol Biol Rev* **72**:126–56– table of contents.
60. **Boutte CC, Baer CE, Papavinasundaram K, Liu W, Chase MR, Meniche X, Fortune SM, Sasseti CM, Ioerger TR, Rubin EJ.** 2016. A cytoplasmic peptidoglycan amidase homologue controls mycobacterial cell wall synthesis. *eLife* **5**:a021113.
61. **Gibson DG, Young L, Chuang R-Y, Venter JC, Hutchison CA, Smith HO.** 2009. Enzymatic assembly of DNA molecules up to several hundred kilobases. *Nature Methods* **6**:343–345.
62. **van Kessel JC, Marinelli LJ, Hatfull GF.** 2008. Recombineering mycobacteria and their phages. *Nature Publishing Group* **6**:851–857.
63. **Murphy KC, Papavinasundaram K, Sasseti CM.** 2015. Mycobacterial recombineering. *Methods Mol Biol* **1285**:177–199.
64. **Andreu N, Zelmer A, Fletcher T, Elkington PT, Ward TH, Ripoll J, Parish T, Bancroft GJ, Schaible U, Robertson BD, Wiles S.** 2010. Optimisation of bioluminescent reporters for use with mycobacteria. *PLoS ONE* **5**:e10777.
65. **Ehrt S, Guo XV, Hickey CM, Ryou M, Monteleone M, Riley LW, Schnappinger D.** 2005. Controlling gene expression in mycobacteria with anhydrotetracycline and Tet repressor. *Nucleic Acids Research* **33**:e21.
66. **Kieser KJ, Baranowski C, Chao MC, Long JE, Sasseti CM, Waldor MK, Sacchettini JC, Ioerger TR, Rubin EJ.** 2015. Peptidoglycan synthesis in *Mycobacterium tuberculosis* is organized into networks with varying drug susceptibility. *Proc Natl Acad Sci USA* **112**:13087–13092.
67. **Rego EH, Audette RE, Rubin EJ.** 2017. Deletion of a mycobacterial divisome factor collapses single-cell phenotypic heterogeneity. *Nature* **546**:153–157.
68. **Eskandarian HA, Odermatt PD, Ven JXY, Hannebelle MTM, Nievergelt AP, Dhar N, McKinney JD, Fantner GE.** 2017. Division site selection linked to inherited cell surface wave troughs in mycobacteria. *Nat Microbiol* **2**:17094.
69. **Koschwanetz JH, Carlson RH, Meldrum DR.** 2009. Thin PDMS films using long spin times or tert-butyl alcohol as a solvent. *PLoS ONE* **4**:e4572.

70. **Thangawng AL, Ruoff RS, Swartz MA, Glucksberg MR.** 2007. An ultra-thin PDMS membrane as a bio/micro-nano interface: fabrication and characterization. *Biomed Microdevices* **9**:587–595.
71. **Dhar N, Bousbaine D, Wakamoto Y, McKinney JD, Santi I.** 2013. Single-cell dynamics of the chromosome replication and cell division cycles in mycobacteria. *Nature Communications* **4**:1–10.
72. **Schindelin J, Arganda-Carreras I, Frise E, Kaynig V, Longair M, Pietzsch T, Preibisch S, Rueden C, Saalfeld S, Schmid B, Tinevez J-Y, White DJ, Hartenstein V, Eliceiri K, Tomancak P, Cardona A.** 2012. Fiji: an open-source platform for biological-image analysis. *Nature Methods* **9**:676–682.
73. **Paintdakhi A, Parry B, Campos M, Irnov I, Elf J, Surovtsev I, Jacobs-Wagner C.** 2016. Oufiti: an integrated software package for high-accuracy, high-throughput quantitative microscopy analysis. *Molecular Microbiology* **99**:767–777.
74. **Zhang YJ, Ioerger TR, Huttenhower C, Long JE, Sassetti CM, Sacchettini JC, Rubin EJ.** 2012. Global Assessment of Genomic Regions Required for Growth in *Mycobacterium tuberculosis*. *PLoS Pathog* **8**:e1002946–9.
75. **DeJesus MA, Ambadipudi C, Baker R, Sassetti C, Ioerger TR.** 2015. TRANSIT - A Software Tool for Himar1 TnSeq Analysis. *PLoS Comput Biol* **11**:e1004401–17.
76. **Qiao Y, Lebar MD, Schirner K, Schaefer K, Tsukamoto H, Kahne D, Walker S.** 2014. Detection of lipid-linked peptidoglycan precursors by exploiting an unexpected transpeptidase reaction. *J Am Chem Soc* **136**:14678–14681.
77. **Qiao Y, Srisuknimit V, Rubino F, Schaefer K, Ruiz N, Walker S, Kahne D.** 2017. Lipid II overproduction allows direct assay of transpeptidase inhibition by β -lactams. *Nature Chemical Biology* **13**:793–798.
78. **Rebets Y, Lupoli T, Qiao Y, Schirner K, Villet R, Hooper D, Kahne D, Walker S.** 2014. Moenomycin resistance mutations in *Staphylococcus aureus* reduce peptidoglycan chain length and cause aberrant cell division. *ACS Chem Biol* **9**:459–467.

79. **Lebar MD, May JM, Meeske AJ, Leiman SA, Lupoli TJ, Tsukamoto H, Losick R, Rudner DZ, Walker S, Kahne D.** 2014. Reconstitution of peptidoglycan cross-linking leads to improved fluorescent probes of cell wall synthesis. *J Am Chem Soc* **136**:10874–10877.

**Chapter 4: Pathways and networks of peptidoglycan synthesis in
*Mycobacterium tuberculosis***

Section 4.1: Peptidoglycan synthesis in *Mycobacterium tuberculosis* is organized into networks with varying drug susceptibility

Overview: This chapter consists of a manuscript published in PNAS in October 2015 (1).

Attributions: CB performed transposon mutagenesis in $\Delta ponA2$ and $\Delta ldtB$ strains of *M. tuberculosis* and subsequently generated the transposon sequencing libraries for these two transposon screens. CB and KJK sequenced and analyzed these libraries (along with the $\Delta ponA1$ library) using a pipeline that CB was involved in creating prior to this publication. KJK wrote the manuscript and CB provided edits.

Authors: Karen J. Kieser¹, Catherine Baranowski¹, Michael C. Chao², Jarukit E. Long³, Christopher M. Sassetti^{3,4}, Matthew K. Waldor^{2,4,5}, James C. Sacchettini⁶, Thomas R. Ioerger⁷, Eric J. Rubin^{1,5†}

¹ Department of Immunology and Infectious Disease, Harvard T.H. Chan School of Public Health, Boston, MA 02115, USA

² Division of Infectious Diseases, Brigham & Women's Hospital, Boston, MA 02115, USA

³ Department of Microbiology and Physiological Systems, University of Massachusetts Medical School, 55 Lake Avenue N., Worcester MA 01655, USA

⁴ Howard Hughes Medical Institute, 4000 Jones Bridge Road, Chevy Chase, MD 20815, USA

⁵ Department of Microbiology and Immunobiology, Harvard Medical School, Boston, MA 02115, USA

⁶ Department of Biochemistry and Biophysics and Department of Chemistry, Texas A&M University, College Station, TX 77843, USA

⁷ Department of Computer Science, Texas A&M University, College Station, TX 77843, USA

‡ **Corresponding Author Contact:**

erubin@hsph.harvard.edu

Harvard Institutes of Medicine, Room 1007A

4 Blackfan Circle

Boston, MA 02115

Phone: 617-432-3335

Abstract

Peptidoglycan (PG), a complex polymer composed of saccharide chains crosslinked by short peptides, is a critical component of the bacterial cell wall. PG synthesis has been extensively studied in model organisms but remains poorly understood in mycobacteria, a genus that includes the important human pathogen *Mycobacterium tuberculosis* (*Mtb*). The principle PG synthetic enzymes have similar and, at times, overlapping functions. To determine how these are functionally organized, we carried out whole genome transposon mutagenesis screens in *Mtb* strains deleted for *ponA1*, *ponA2*, and *ldtB*, major PG synthetic enzymes. We identified distinct factors required to sustain bacterial growth in the absence of each of these enzymes. We find that even the homologues PonA1 and PonA2 have unique sets of genetic interactions, suggesting there are distinct PG synthesis pathways in *Mtb*. Either PonA1 or PonA2 is required for growth of *Mtb*, but both genetically interact with LdtB, which has its own distinct genetic network. We further

provide evidence that each interaction network is differentially susceptible to antibiotics. Thus, *Mtb* uses alternative pathways to produce PG, each with its own biochemical characteristics and vulnerabilities.

Significance Statement

The rise of drug resistant *Mycobacterium tuberculosis* (*Mtb*) underscores the critical need for a better understanding of essential physiological processes. Among these is cell wall synthesis, the target of many antibiotics. To understand how *Mtb* orchestrates synthesis of its cell wall, we performed whole genome interaction studies in cells with different peptidoglycan synthesis mutations. We found that different enzymes become required for bacterial growth in Δ *ponA1*, Δ *ponA2*, or Δ *ldtB* cells, suggesting that discrete cell envelope biogenesis networks exist in *Mtb*. Furthermore, we show that these network's enzymes are differentially susceptible to cell wall active drugs. Our data provide insight into the essential processes of cell wall synthesis in *Mtb* and highlight the role of different synthesis networks in antibiotic tolerance.

Introduction

Mycobacterium tuberculosis (*Mtb*) is the etiologic agent of tuberculosis (TB), one of the leading causes of infectious disease deaths worldwide. One third of the human population is thought to harbor *Mtb* and ~1.5 million individuals died of TB last year (2). *Mtb*'s success as a pathogen is due in part to its unusual cell wall, which is notorious for its complexity and is implicated in *Mtb*'s innate resistance to many commonly used antibiotics (3). A critical component of the bacterial cell wall (including *Mtb*'s) is PG, a complex polymer that provides structural

support and counteracts turgor pressure (4). PG is essential for cell survival, and its synthesis is targeted by many potent antibiotics (3).

PG consists of long glycan chains composed of two different sugars (Figure 4.1A) that are crosslinked via short peptide side chains that extend from the glycan chains. Notably, generation of mature PG occurs outside of the cell membrane and is mediated by enzymes that incorporate new PG subunits, which are formed in the cytoplasm, into the PG polymer. PonA1 and PonA2 are the two enzymes in *Mtb* that can both polymerize glycan strands and crosslink peptides (known as bifunctional penicillin binding proteins [PBPs], Figure 4.1A). The predominant peptide crosslinks in mycobacteria join the third amino acids (3–3) of adjacent stem peptides (5, 6), which are synthesized by L,D-transpeptidases (Ldts) such as LdtB, one of the major Ldts in *Mtb* (Figure 4.1A). The peptides can also be joined by crosslinking the fourth and third amino acids (4–3) (Figure 4.1A) through the action of bifunctional or monofunctional (capable of only peptide crosslinking) PBPs. The activity of these distinct factors must be coordinated to ensure proper cell wall synthesis. One method of coordination is the use of large protein complexes, the elongation complex and divisome, which mediate cell wall biogenesis during cell elongation or division, respectively (3). The essential activity of these enzymes makes them prime drug targets; indeed, PBPs and Ldts are inhibited by carbapenems and penicillin (7, 8), which remains one of the most clinically important drugs in use.

Although the biosynthesis and structure of PG have been investigated for decades, predominantly in organisms like *Escherichia coli* or *Bacillus subtilis*, the mechanisms that coordinate the biochemical activities required to polymerize and modify the cell wall remain incompletely understood. Moreover, much less is known about PG synthesis in many pathogenic organisms, including *Mtb* (3). However, previous studies in *Mtb* suggest that PG synthesis in this

pathogen does not strictly conform to the *E. coli* paradigm. For example, *E. coli* has three bifunctional PBPs (PBP1A, PBP1B, PBP1C (4)) whereas *Mtb* has just two (PonA1 and PonA2 (9)). Additionally, PBP2 (known as PBPA in mycobacteria) is a monofunctional PBP and is required for cell elongation in *E. coli*, but instead appears to function in cell septation in mycobacteria (4, 10).

The structure of PG is also different in *Mtb* than in *E. coli*: mycobacterial PG has an unusual prevalence of 3–3 peptide linkages. The abundance of 3–3 crosslinks in mycobacterial PG throughout different growth stages (6) suggests that Ldts are active during normal growth; however, their cellular roles or regulation during growth and PG biogenesis remain largely unknown. While penicillins and cephalosporins target only enzymes that produce 4–3 crosslinks, Ldts can be targeted by carbapenems (8). Recent work suggests that these agents might be far more efficacious against both dividing and non-dividing bacteria (11). While little is known about *Mtb*'s five encoded Ldts (12), one, LdtB, is implicated in antibiotic tolerance (12-14), is required for normal virulence in a mouse model of TB (13), and is important for normal cell shape (14).

Previous studies have also revealed that PG biosynthesis differs between *Mtb* and the related saprophytic *Mycobacterium smegmatis* (*Msm*). As opposed to *Mtb*, *Msm* has three bifunctional PBPs: PonA1, PonA2, and PonA3 (15). PonA1 is required for *Msm* but not *Mtb* growth in culture (16, 17); however, *ponA1* is required for robust growth of *Mtb* during infection (17). In contrast, *Mtb* and *Msm ponA2* mutants do not have growth defects in culture (15, 18). However, *Mtb* strains with inactivated *ponA1* or *ponA2* exhibit similar survival defects during growth in a host (17, 19), suggesting that these two similar bifunctional enzymes have non-redundant and important contributions to PG synthesis during infection. Collectively, the

differences in PG synthase functionality may imply that different PG synthetic pathways exist across species, which may have consequences for a pathogen's virulence during infection.

Here, we interrogated PG synthesis in *Mtb* by investigating the genetic interactions of *ponA1*, *ponA2*, and *ldtB*, which encode three PG synthases critical for *Mtb*'s growth during infection. To identify these interactions, we performed genome-wide transposon mutagenesis screens in *Mtb* mutant strains that lacked one of these enzymes. Advances in highthroughput sequencing technology coupled with the power of whole genome studies provide unique insights into key bacterial processes, such as cell wall biosynthesis. Such studies have been performed to a limited extent in bacteria, and further work would substantially expand our understanding of the organization of prokaryotic metabolic processes. In this study, we identified diverse genetic interaction networks for *ponA1*, *ponA2*, and *ldtB*, suggesting that these synthases are embedded within distinct cellular networks for assembling *Mtb*'s PG. We found that either *ponA1* or *ponA2* is required for cell growth, and that *ldtB* interacts with both *ponA1* and *ponA2*. Moreover, mutants that lack these enzymes have differential susceptibility to agents that interfere with cell wall biogenesis. Thus, the *Mtb* cell wall is synthesized using multiple interacting networks that are both overlapping and unique.

Results

PonA1, PonA2, and LdtB are individually dispensable for growth of *M. tuberculosis*

PonA1, its homologue PonA2, and LdtB can generate bonds between new PG subunits and those in the existing PG polymer (Figure 4.1A). We generated independent *ponA2* and *ldtB* deletion mutants and assessed their growth. As suggested by previous studies (15, 19) absence of either gene did not substantially impact *Mtb*'s exponential growth, although loss of LdtB

diminishes population density in stationary phase (Figure 4.1B). However, $\Delta ponA2$ cells were moderately wider than wildtype *Mtb* (Figure 4.1C). In contrast, $\Delta ponA1$ cells are longer than wildtype cells (17), suggesting these two homologous enzymes have distinct roles in PG synthesis in *Mtb*. Mutant cells that lack LdtB were significantly shorter (as previously reported (14)) and wider than wildtype cells (Figure 4.1D), indicating that LdtB impacts cell wall synthesis and cell shape in a manner distinct from the two bifunctional PBPs. Thus, even though deletion of *ponA1* (17), *ponA2* or *ldtB* is compatible with cell growth, their individual deletions have detectable and distinct physiological effects.

Whole genome mutagenesis identifies PG biogenesis pathways in *M. tuberculosis*

In *E. coli*, the PonA1 and PonA2 homologues, PBP1a and PBP1b, seem to function in different subcellular complexes and have been shown to have distinct interaction partners (4). We hypothesized that, in a similar fashion, PonA1 and PonA2 genetically interact with different pathways. To elucidate the shared and distinct roles of PonA1, PonA2, and LdtB in *Mtb* PG biogenesis, we used transposon mutagenesis and high-throughput sequencing in $\Delta ponA1$, $\Delta ponA2$, and $\Delta ldtB$ *Mtb* strains to define the genetic interactions of these enzymes on a genome-wide scale (20, 21) (Figure S13). These experiments measure bacterial fitness across a population. Genes that contain fewer than expected transposon insertions have a growth disadvantage (here termed “essential”) while those with larger numbers of insertions have an advantage (“enriched”). Comparisons of the transposon insertion profiles (22, 23) of the wildtype and mutant strains revealed both essential and enriched genes – two types of genetic interaction – in each strain (Figure 4.2).

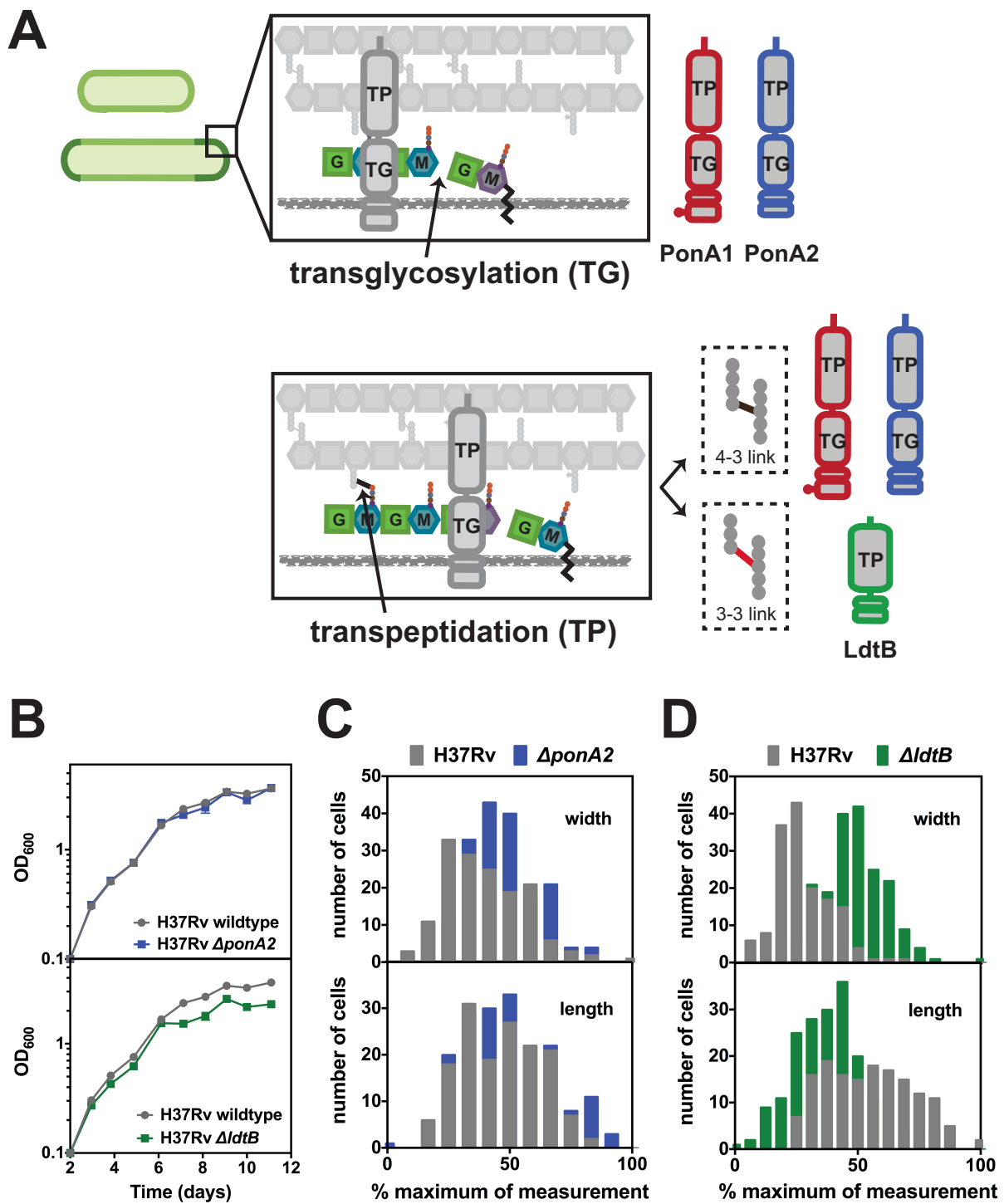


Figure 4.1: Deletion of PG synthases influences growth and morphology of *M. tuberculosis*.

(A) Transglycosylation (TG) and transpeptidation (TP) reactions incorporate new peptidoglycan

Figure 4.1 (Continued)

(PG) subunits into the cell wall. PonA1 and PonA2 carry out both TG and 4–3 TP reactions. LdtB only mediates 3–3 TP reactions. M, N-acetylmuramic acid. G, N-acetylglucosamine. **(B)** Deletion of either *ponA2* or *ldtB* does not greatly impact *Mtb* growth during log phase, although loss of *ldtB* reduces population density in stationary phase. Error bars are often too small to see. **(C)** *ponA2* mutant cells (N=179) have increased width compared to wildtype cells (N=153) (approximate p-value < 0.0001 by the Kolmogorov-Smirnov test). **(D)** *ldtB* mutant cells (N=193) have increased width and decreased length compared to wildtype cells (N=153) (approximate p-value < 0.0001 by the Kolmogorov-Smirnov test for both length and width).

We identified ten factors required in cells that lack PonA1 (Figure 4.2A, “essential” factors). Most of these factors are associated with or predicted to be involved in cell wall synthesis. For example, factors involved in peptidoglycan (PonA2), mycolic acid (MmaA4), and, potentially, arabinogalactan (CpsY) synthesis in addition to cell wall precursor production (*rv1086*) were found to be required in Δ *ponA1* cells (Figure 4.2A). These data suggest that the cell requires either PonA1 or PonA2 for PG synthesis, analogous to the situation in *E. coli* (4). We also identified eight factors whose disruption in the Δ *ponA1* mutant appeared beneficial to the cell (Figure 4.2A, “enriched”). For example, the transcription factor EspR (*rv3849*) had higher levels of transposon insertions in cells that lack *ponA1* compared to wildtype *Mtb*, suggesting that cells that lack EspR may grow more rapidly than wildtype cells under these conditions. This could indicate that EspR regulates *ponA1* transcription. Indeed, we found multiple canonical EspR binding sites (24) in the *ponA1* promoter region (Figure S14).

Our screen identified widely different genetic connections for *ponA2* compared to *ponA1*. As predicted from the screen performed in Δ *ponA1* cells, *ponA1* was required in Δ *ponA2* cells (Figure 4.2B). Relatively few factors were shared between Δ *ponA1* and Δ *ponA2* cells. For example, *rv3490* and *rv1248c* were required in both backgrounds. However, there were many differences, such as *cpsY*, *rv1086*, *pra* and *fadB*, and the differences were in both the “essential” and “enriched” classes (Figure 4.2A,B). Thus, while either PonA1 or PonA2 is required for *Mtb* growth, both enzymes have predominantly different genetic interactions.

ldtB also interacts with a number of loci including some, such as *ponA2*, that overlap with *ponA1* interactions (Figure 4.2C). In the absence of either of the bifunctional enzymes that form 4–3 crosslinks, 3–3 crosslinking may become more important for maintaining cell integrity. In addition, *ldtB* interacts with genes involved in cell wall precursor synthesis (*treS*) and other steps

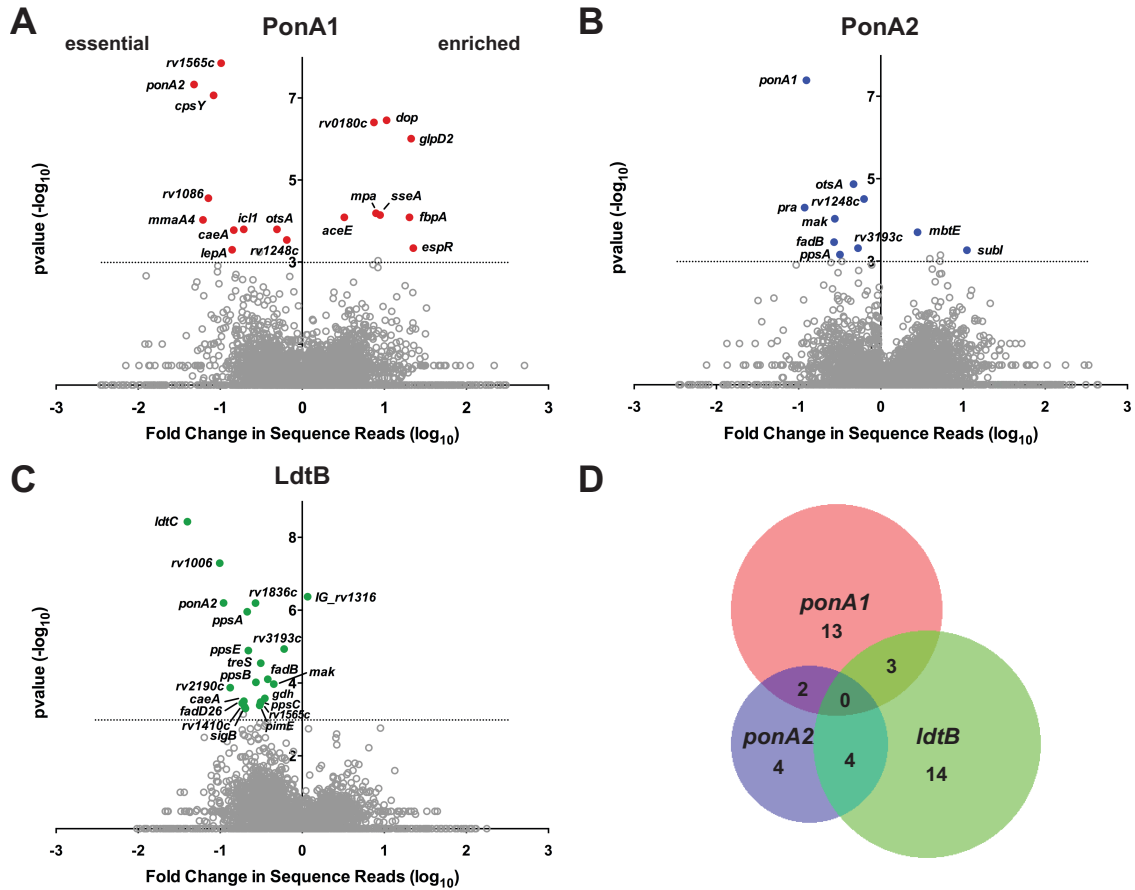


Figure 4.2: *ponA1*, *ponA2*, and *ldtB* have largely distinct genetic interactions. Loci whose sequence reads were significantly different between wildtype and mutant cells ((**A**) Δ *ponA1*, red circles; (**B**) Δ *ponA2*, blue circles; (**C**) Δ *ldtB*, green circles) with a p-value < 0.001 (represented by the dotted line) by the Mann-Whitney U test are plotted according to their p-value and fold change in sequence reads from wildtype (calculated from the geometric mean). Gray circles, non-significant loci. Gray circles above the dotted line are loci that are $< 90\%$ significant in the simulations (see Supplementary Methods). (**D**) Venn diagram representation of the distinct interaction networks of *ponA1*, *ponA2*, and *ldtB*.

in peptidoglycan metabolism, including the NlpP60 hydrolase *rv2190c* (25). Collectively, these data show that the PG synthases PonA1, PonA2, and LdtB participate in largely distinct genetic networks (Figure 4.2D).

PG synthases are variably required in *ponA1*, *ponA2*, or *ldtB* mutant cells

We took advantage of the depth and saturation of the mutant libraries to establish the relative contributions of PBPs and Ldts to bacterial fitness in the different mutant strain backgrounds. We analyzed the frequency of transposon insertions in the four PBP and five Ldt loci as well as a putative penicillin binding protein (*Rv2864c*) in each mutant strain. We found that particular PG synthases had differential insertion profiles in cells that lack *ponA1*, *ponA2*, or *ldtB* (Figure 4.3). For example, *pbpA* had a relative growth disadvantage in *ponA1* mutant cells compared to wildtype whereas *pbpA* exhibited growth advantages in *ponA2* and *ldtB* mutant cells. These data suggest that PBPA may be more important for PG synthesis in cells without PonA1 than in cells without PonA2 or LdtB. Our data also support a role for *rv2864c* in PG synthesis. In *ponA1* mutant cells, *rv2864c* was disrupted at just 15% of the wildtype frequency but was disrupted at 82% or 51% of the wildtype frequency in *ponA2* or *ldtB* mutant cells, respectively (Figure 4.3).

PonA2 is required for PG synthesis in the absence of PonA1

We chose selected genes for individual validation of essentiality using a previously described allelic exchange method (17, 26) (Figure 4.4A, S15). For example, we generated a *ponA2* deletion in a strain whose only copy of *ponA1* is at the L5 phage integration site (Δ *ponA1* L5::*ponA1*_{wt}). We also generated a *ponA2* deletion in wildtype H37Rv *Mtb* as a control. We assessed the impact of *ponA2* loss in the mutant background and found that Δ *ponA1* L5::*ponA1*_{wt}

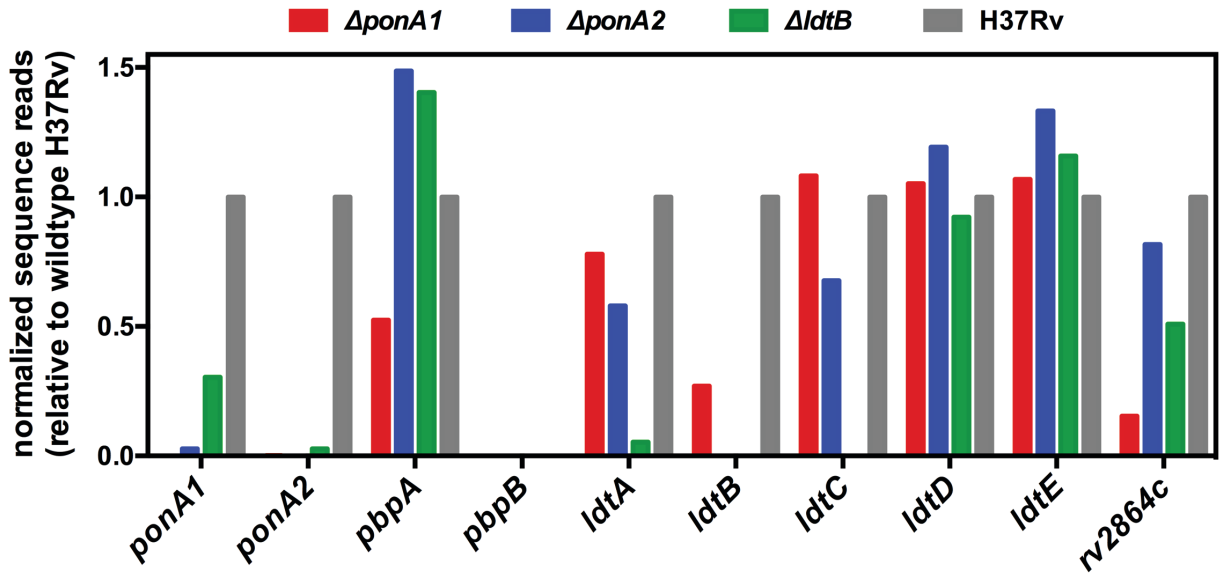


Figure 4.3: Importance of PG synthases in *ponA1*, *ponA2*, or *ldtB* mutant cells. Sequence reads corresponding to transposon insertions at the indicated loci in the $\Delta ponA1$, $\Delta ponA2$, and $\Delta ldtB$ mutant cells. Sequence reads at each locus are normalized to the respective locus in wildtype H37Rv cells.

ΔponA2 cells grew at rates similar to and exhibited similar rod-shaped morphology as wildtype *Mtb* (Figure S16A,B). However, while we could integrate a wildtype *ponA1* copy into the L5 site in *ΔponA2* or *ΔponA1* L5::*ponA1*_{wt} *ΔponA2* backgrounds (Figure 4.4B, S17A), when we transformed an L5 empty vector, we only obtained a significant number of colonies in the *ΔponA2* cells that still encode *ponA1* at the original locus (Figure 4.4B, S17A). This confirms that PonA2 is required in the absence of PonA1 in *Mtb* and that even though these enzymes participate in largely distinct genetic networks, they have at least partially complementary roles in PG biogenesis in *Mtb*.

Rv1086 is required for cell wall synthesis in cells that lack PonA1

Rv1086, a Z-isoprenyl diphosphate synthase, carries out the first committed step in the synthesis of the lipid carrier for cell wall precursors (27). As with *ponA2*, we used allelic exchange to test whether *rv1086* was required in cells that lack *ponA1* (Figure 4.4C). Indeed, we obtained robust growth only when we transformed *ΔponA1* L5::*ponA1*_{wt} *Δrv1086* cells (which grew similarly to and exhibited similar cell shape as wildtype *Mtb* [Figure S16C,D,E]) with another *ponA1* copy (Figure 4.4D). These data demonstrate that *rv1086* is required in cells that lack *ponA1* and may indicate that PonA2 requires a dedicated pool of precursors.

LdtB is critical for normal bacterial fitness in cells without PonA1

An important prediction of the findings from our *ΔponA1* and *ΔponA2* screens is that both strains require *ldtB* for optimal growth (Figure 4E, Figure S6). While bifunctional PBPs are critical in many bacterial species (4), mycobacterial PG exhibits very different architecture with its prevalence of 3–3 crosslinks (5, 6). Using allelic exchange, we found that only tiny *ΔponA1* *ΔldtB*

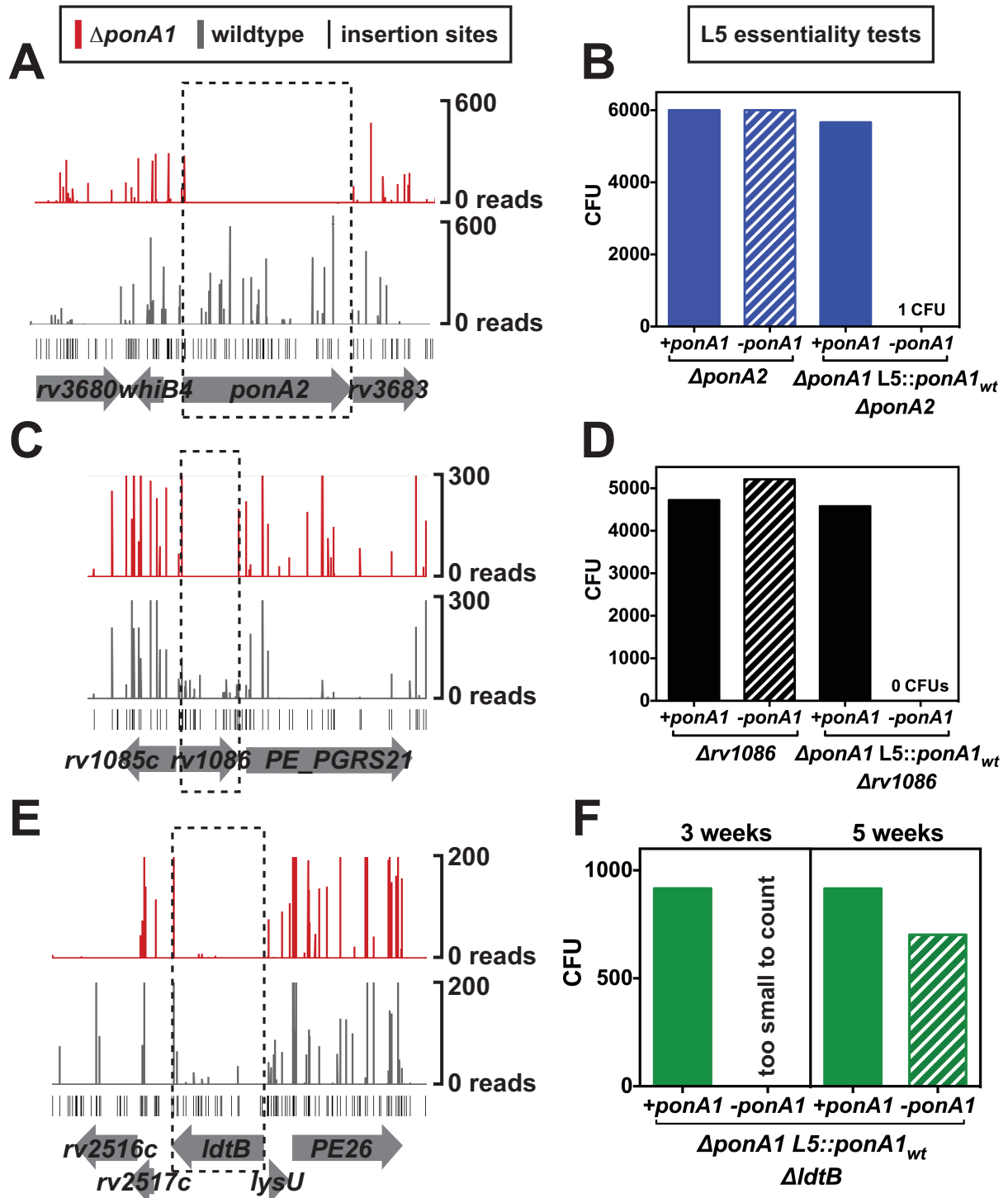


Figure 4.4: Diverse cell wall synthesis factors become required in $\Delta ponA1$ cells. (A) Transposon insertions (vertical bars), determined from highthroughput sequencing, are visualized at the *ponA2* locus in either wildtype (gray) or $\Delta ponA1$ (red) cells. **(B)** Colony forming units

Figure 4.4 (Continued)

(CFUs) were counted from allelic exchanges with L5-integrating vectors that do or do not encode *ponA1* in the experimental $\Delta ponA1$ L5::*ponA1*_{wt} $\Delta ponA2$ strain or the control $\Delta ponA2$ strain (both control strain transformations had lawn growth, and CFUs were arbitrarily set to 6000). **(C)** Transposon insertions at the *rv1086* locus in wildtype (gray) and $\Delta ponA1$ (red) cells. **(D)** CFU counts from L5 allelic exchanges in the experimental $\Delta ponA1$ L5::*ponA1*_{wt} $\Delta rv1086$ strain or the control $\Delta rv1086$ strain. **(E)** Transposon insertions at the *ldtB* locus in wildtype (gray) or $\Delta ponA1$ (red) cells. **(F)** CFU counts from L5 allelic exchanges in the experimental $\Delta ponA1$ L5::*ponA1*_{wt} $\Delta ldtB$ strain.

colonies could be seen after 21 days of growth, when *ΔldtB* colonies were already large (Figure 4.4F, S17C); these colonies required 35 days to reach a similar size (Figure S17D). Thus, *ldtB* is required for robust growth in the absence of *ponA1*.

Distinct cell wall synthesis networks exhibit differential tolerance to cell wall active drugs

Our data suggest that PonA1, PonA2, and LdtB participate in distinct genetic networks with partially overlapping but largely unique genetic interactions for each enzyme. We hypothesized that these networks would have different cellular activity and could therefore be differentially susceptible to drugs that target cell wall synthesis. To test this hypothesis, we treated cells that lack *ponA1*, *ponA2*, *ldtB* or other members of their interaction networks with drugs that inhibit the various components of *Mtb*'s cell wall, including meropenem, which blocks PG transpeptidases, and teicoplanin, which binds directly to PG to prevent further crosslinking (11, 28), ethambutol, which targets arabinogalactan synthesis, and isoniazid, which targets mycolic acid synthesis. We found that *ΔponA1* cells had the same minimum inhibitory concentration (MIC) for meropenem and teicoplanin as wildtype *Mtb* (Figure 4.5); however, *ΔponA2* and *ΔldtB* cells were 4- to 8-fold more susceptible to both meropenem and teicoplanin. Furthermore, mutants that lack *ponA1* exhibit a 4-fold increased susceptibility to ethambutol. But the *ΔponA2* or *ΔldtB* mutants do not exhibit heightened sensitivity to this antibiotic. *ΔponA1*, *ΔponA2* or *ΔldtB* cells exhibited no change in MIC when treated with SDS, and only *ΔldtB* cells were slightly more sensitive to isoniazid. The *Δrv1086* mutant was 8-fold more sensitive to teicoplanin and 4-fold more sensitive to meropenem and ethambutol compared to wildtype *Mtb* (Figure 4.5). Together, these data suggest that the enzymes that comprise distinct PG synthetic networks have different roles in antibiotic tolerance in *Mtb*.

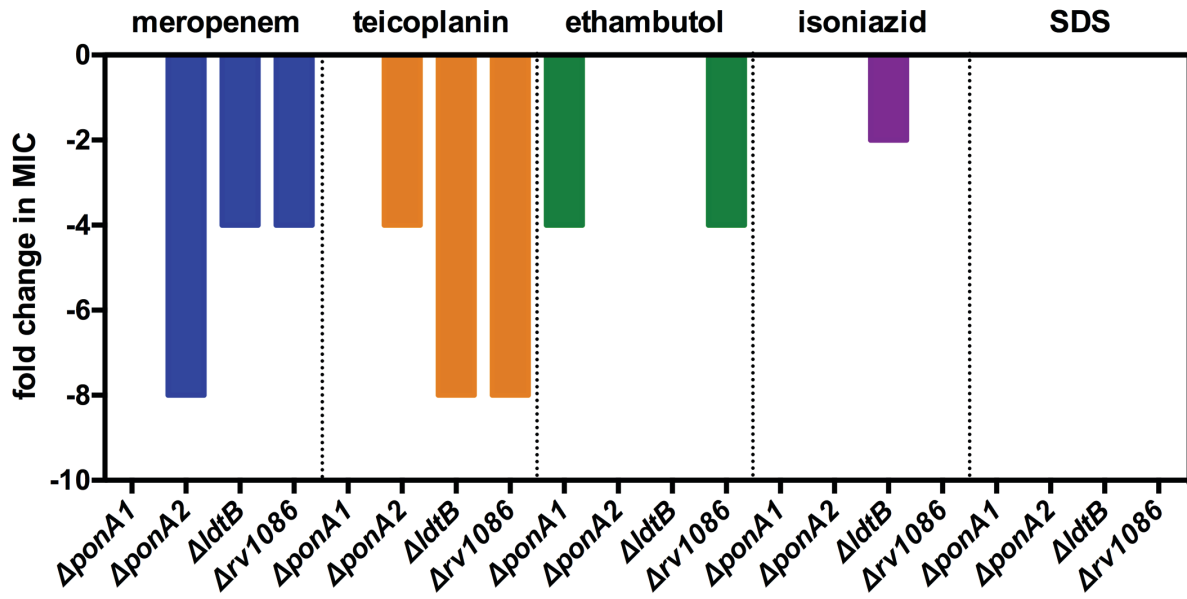


Figure 4.5: Differential susceptibility of *Mtb* cell wall mutants to cell wall active antibiotics.

The fold change in minimum inhibitory concentration (MIC) for the indicated drugs and sodium dodecyl sulfate (SDS) were calculated compared to wildtype *Mtb* for the indicated strains.

Discussion

Cell wall synthesis requires the collaboration of multiple enzymes. In most bacterial species, individual PBPs are dispensable. This is generally interpreted as evidence of functional redundancy, suggesting that enzymes have overlapping functions. Clearly, this is not entirely true in both *Msm* and *Mtb*. In *Msm*, a single bifunctional PBP, PonA1, is essential for normal growth, but *ponA1* and *ponA2* are both required for robust growth of *Mtb* during infection. Our network analysis suggests that PonA1 and PonA2 are not identical – each is genetically associated with overlapping and, importantly, unique factors. This may suggest that although PonA1 and PonA2 mediate similar reactions, the pathways by which each synthesizes PG are different. This likely has functional consequences for bacterial growth in specific conditions. Indeed, we found that mutant cells exhibit differential survival under antibiotic treatment, suggesting that cell wall synthesis enzymes, even closely related homologues, exhibit different functionality during mycobacterial growth. This is likely true for other bacterial species as well. Furthermore, we found that both *ponA1* and *ponA2* are genetically associated with *ldtB*. This suggests that the bifunctional PBPs function together with this major 3–3 transpeptidase to synthesize new PG during growth.

What do these genetic interactions mean? They may imply separate biochemical pathways that, for example, provide precursors to PonA1 and PonA2. Several pieces of evidence indicate that PonA1 and PonA2 have distinct cellular roles, including their susceptibilities to host-like stresses or infection (15) as well as structural differences (29) and different impacts on cell shape (Figure 4.1) (17). These data may support a model wherein PonA1 and PonA2 exist in different subcellular complexes (4). Our genetic analyses also support different cellular roles for PonA1 and PonA2. Notably, few interactions were identical for *ponA1* and *ponA2*, suggesting their cellular activities are not truly redundant (Figure 4.6). As a fully redundant system would unlikely be

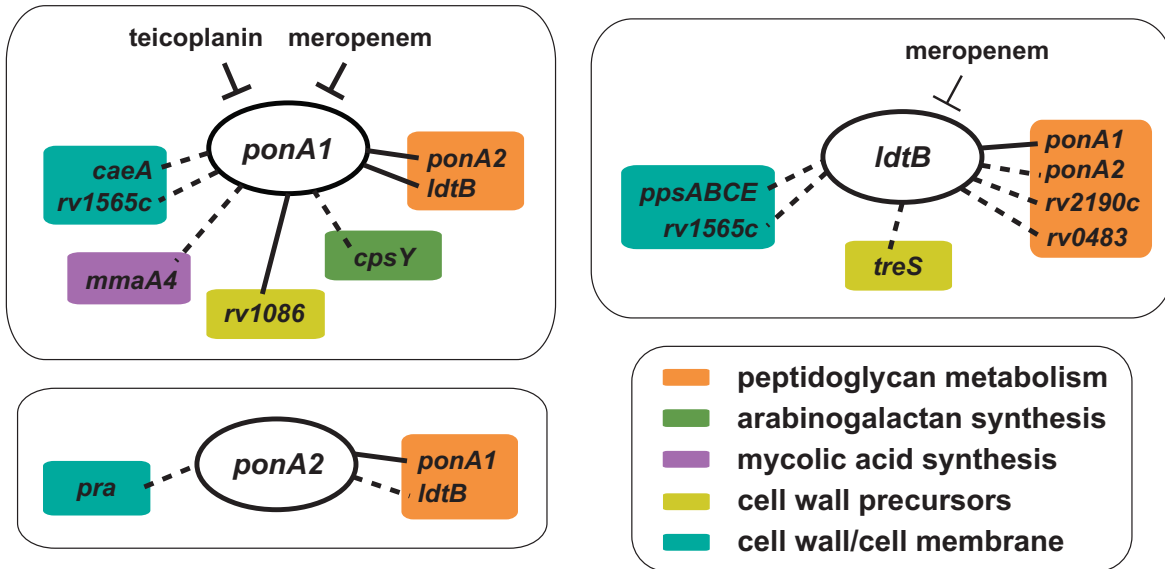


Figure 4.6: *ponA1*, *ponA2*, and *ldtB* are hubs of distinct cell wall synthesis networks. Selected interactions with cell wall synthesis genes discovered in whole genome screens (dashed lines) and/or by directed knockouts (solid lines) for *ponA1*, *ponA2*, and *ldtB*. The members of these networks respond differently to specific cell wall drugs, such as teicoplanin and meropenem. For example, meropenem may target PonA1 more (thicker ‘T’) than LdtB (thinner ‘T’).

maintained through evolution, there is likely some selective advantage to having multiple independent systems for PG synthesis (in *Mtb* and other organisms). There could be several reasons for this. For example, these proteins could be individually regulated, either transcriptionally or by substrate availability provided by proteins lying within dedicated synthesis pathways. This could result in altered rates of PG formation and, consequently, growth, or could result in a different structure of PG. For example, loss of 4–3 crosslinks could increase the importance of 3–3 crosslinks for cell wall integrity. This model is consistent with the relative importance of *ldtB*, one of the major 3–3 crosslinking enzymes, with loss of either *ponA1* or *ponA2*.

ldtB is the single Ldt that becomes critical for growth in the absence of *ponA1* or *ponA2* (Figure 4.3). The genetic interaction between the bifunctional PBPs and *ldtB* suggests that these enzymes together promote new cell wall synthesis during growth. This may indicate that new glycan strands (synthesized by PonA1 or PonA2) are predominantly first crosslinked in a 3–3 manner (for example, by LdtB). This model is supported by the prevalence of 3–3 crosslinks in mycobacterial PG at all growth stages (6). Our data also show that LdtB is critical for the maintenance of normal cell shape (Figure 4.1), which suggests that LdtB holds a key role in cell wall synthesis. Such 3–3 peptide crosslinks, which also exist in other bacteria, may provide increased structural integrity to the cell during adverse conditions.

While the cellular changes brought about by mutation are the ends of the spectrum, it is likely that the balance between PonA1 and PonA2 activity is altered under different growth conditions. This produces bacilli that can closely adapt to particular growth conditions. For example, while there is little effect on growth rate in culture, loss of PonA1 or PonA2 results in attenuation during murine infection. This could be associated with changes in cell morphology that

are observed even in culture or could be specific for interactions between the cell wall and the host.

A specific example of adaptation is the presence of antibiotics. Mutant cells have altered susceptibility to some antibiotics (Figures 4.5, 4.6). It is possible that this is due to altered bacterial permeability. However, these differences are mainly specific for drugs that affect the synthesis of cell wall components and not the detergent SDS, suggesting that increased susceptibility is actually caused by changes in the requirement for specific cell wall synthetic enzymes in the presence of mutations. The differential antibiotic response of *ponA1* and *ponA2* mutant cells further supports a model wherein they exist in separate PG synthesis pathways. For example, *ponA2* mutant cells are more sensitive to meropenem and teicoplanin than *ponA1* mutant cells. This suggests that these drugs may more efficiently inhibit the active enzymes in Δ *ponA2* cells (including *ponA1*) than the remaining enzymes in Δ *ponA1* cells. These observations suggest that inhibition of PG synthesis by transpeptidase inhibitors such as β -lactam or glycopeptide antibiotics could synergize with other cell wall biosynthesis inhibitors and increase their efficacy. Understanding the pathways involved could help to design such synergistic pairs of inhibitors – for *Mtb* as well as other bacterial pathogens, many of which have not been subjected to similar studies. Efforts to target these pathogens could ultimately profit from similar strategies to identify novel members of key metabolic pathways and define individual contributions to antibiotic tolerance.

Section 4.2: Materials and Methods

Bacterial Strains and Growth Conditions

M. tuberculosis H37Rv and *E. coli* Top10 (Invitrogen; used for cloning) were cultured as in (17).

The construction of the $\Delta ponA1$ and $\Delta ponA1$ L5::*ponA1*_{wt} *Mtb* strains was described in (17).

Transposon Mutagenesis

The H37Rv transposon libraries were generated using the ϕ MycoMarT7 phagemid as previously described (30).

Genomic Library Construction and Highthroughput Sequencing

Genomic DNA (gDNA) was harvested from the transposon libraries and prepared for PCR amplification as described(20). PCR-amplified transposon-gDNA junctions were then subjected to highthroughput sequencing (Illumina, San Diego, CA). For additional details of library preparation and data analysis, see Supplementary Methods.

Mapping and Counting Transposon Insertions

Sequence data were filtered for transposon-specific information and trimmed of transposon sequence except for the TA dinucleotide insertion site with custom Python scripts (S13 Text, #1, #2, #3). Trimmed reads were mapped to the H37Rv genome using Bowtie2 (31). Insertions at each genomic TA site were counted with custom Python scripts (S13 Text, #4, #5).

Analysis of Differentially Inserted Genes

Loci that were differentially disrupted between wildtype and mutant cells were assessed as in (23) (S1 Dataset). We used the Mann-Whitney U-test and simulation-based normalization without the Hidden Markov Model(23). For each library's locus, the geometric mean of the sequence reads was calculated (S2 Dataset) with a custom Matlab script using the encoded geomean function (S1 Text, #10).

Recombinant DNA Constructs and Gene Knockouts

ponA1 was subcloned into the L5 pMC1s vector as in (17). The *ponA2* knockout cassette was amplified by PCR from a custom phage (32). The *rv1086* and *ldtB* knockout cassettes consisted of 500 nucleotides 5' or 3' of *rv1086* or *ldtB* flanking a hygromycin cassette with *PmeI* sites at each end (Gen9, Cambridge, MA). Digestion with *PmeI* (New England Biolabs, Ipswich, MA) generated linear recombineering products. The *ponA2*, *ldtB*, and *rv1086* deletions were generated in the Δ_{ponA1} L5::*ponA1*_{wt} strain (17) via recombineering (for more details, see Supplementary Methods).

Allelic Exchange in *M. tuberculosis*

Allelic exchange occurs as described (17, 24). The Δ_{ponA1} L5::*ponA1*_{wt} loxed strain wherein *ponA2*, *rv1086*, or *ldtB* were deleted was used for allelic exchange. Simultaneous control transformations with the same L5 vectors were performed in Δ_{ponA2} , Δ_{rv1086} , and Δ_{ldtB} cells. Colony forming units were counted at 21 days, except for the Δ_{ponA1} L5::*tetR* Δ_{ldtB} plate that was counted at 35 days.

Optical Density Measurements

Population growth curves for *Mtb* strains were performed as in (17).

Light Microscopy and Image Analysis

Cells were fixed overnight in 1% formalin at 4°C in the Biosafety Level 3 facility. Cells were imaged and morphology analyzed as in . Final images were prepared in FIJI (33).

Antibiotic Minimum Inhibitory Concentration Assays

The antibacterial effects of meropenem, teicoplanin, ethambutol, isoniazid, and SDS (Sigma Aldrich, St. Louis, MO) were determined as in (17).

Data Representation and Statistical Analysis

Prism 6.0 (GraphPad Software, La Jolla, CA) was used to graph and analyze numerical data. Statistical tests in Prism calculated significance of measurements as reported in figure legends. The Venn diagram was generated with BioVenn (34). Transposon insertions were visualized in DNAPlotter (35) or Artemis (36) by converting the insertion counts to appropriate data structures with custom Python scripts (S1 Text, #8, #9).

Acknowledgements

We thank the Rubin and Fortune labs for thoughtful discussions and technical expertise, and M. Larsen for the phage encoding the *ponA2* knockout cassette. This work was supported by the National Institutes of Health (U19 AI107774 to EJR, TRI, CMS, and JCS; U01 GM094568 to EJR; F32 GM108355-02 to MCC; and F32 A1093049 to JEL), the Howard Hughes Medical

Institute (to CMS and MKW), and a National Science Foundation Graduate Research Fellowship (DGE1144152 and DGE0946799 to KJK).

Section 4.3: References

1. **Kieser KJ, Baranowski C, Chao MC, Long JE, Sasseti CM, Waldor MK, Sacchetti JC, Ioerger TR, Rubin EJ.** 2015. Peptidoglycan synthesis in *Mycobacterium tuberculosis* is organized into networks with varying drug susceptibility. *Proc Natl Acad Sci USA* **112**:13087–13092.
2. 2017. Global Tuberculosis Report 2017 1–262.
3. **Kieser KJ, Rubin EJ.** 2014. How sisters grow apart: mycobacterial growth and division. *Nature Publishing Group* **12**:550–562.
4. **Typas A, Banzhaf M, Gross CA, Vollmer W.** 2011. From the regulation of peptidoglycan synthesis to bacterial growth and morphology. *Nature Publishing Group* **10**:123–136.
5. **Lavollay M, Arthur M, Fourgeaud M, Dubost L, Marie A, Veziris N, Blanot D, Gutmann L, Mainardi JL.** 2008. The Peptidoglycan of Stationary-Phase *Mycobacterium tuberculosis* Predominantly Contains Cross-Links Generated by L,D-Transpeptidation. *Journal of Bacteriology* **190**:4360–4366.
6. **Kumar P, Arora K, Lloyd JR, Lee IY, Nair V, Fischer E, Boshoff HIM, Barry CE III.** 2012. Meropenem inhibits D,D-carboxypeptidase activity in *Mycobacterium tuberculosis*. *Molecular Microbiology* **86**:367–381.
7. **Dubee V, Triboulet S, Mainardi JL, Etheve-Quellejeu M, Gutmann L, Marie A, Dubost L, Hugonnet JE, Arthur M.** 2012. Inactivation of *Mycobacterium tuberculosis* L,D-Transpeptidase LdtMt1 by Carbapenems and Cephalosporins. *Antimicrobial Agents and Chemotherapy* **56**:4189–4195.
8. **Wivagg CN, Bhattacharyya RP, Hung DT.** 2014. Mechanisms of β -lactam killing and resistance in the context of *Mycobacterium tuberculosis*. *The Journal of Antibiotics* **67**:645–654.
9. **Cole ST, Brosch R, Parkhill J, Garnier T, Churcher C, Harris D, Gordon SV, Eiglmeier K, Gas S, Barry CE, Tekaiia F, Badcock K, Basham D, Brown D, Chillingworth T, Connor R, Davies R, Devlin K, Feltwell T, Gentles S, Hamlin N, Holroyd S, Hornsby T, Jagels K, Krogh A, McLean J, Moule S, Murphy L, Oliver K, Osborne J, Quail MA, Rajandream MA, Rogers J, Rutter S, Seeger K, Skelton J, Squares R, Squares S, Sulston JE, Taylor K, Whitehead S, Barrell BG.** 1998.

- Deciphering the biology of *Mycobacterium tuberculosis* from the complete genome sequence. *Nature* **393**:537–544.
10. **Dasgupta A, Datta P, Kundu M, Basu J.** 2006. The serine/threonine kinase PknB of *Mycobacterium tuberculosis* phosphorylates PBPA, a penicillin-binding protein required for cell division. *Microbiology* **152**:493–504.
 11. **Hugonnet J-E, Tremblay LW, Boshoff HI, Barry CE, Blanchard JS.** 2009. Meropenem-clavulanate is effective against extensively drug-resistant *Mycobacterium tuberculosis*. *Science* **323**:1215–1218.
 12. **Sanders AN, Wright LF, Pavelka MS.** 2014. Genetic characterization of mycobacterial L,D-transpeptidases. *Microbiology (Reading, Engl)* **160**:1795–1806.
 13. **Gupta R, Lavollay M, Mainardi J-L, Arthur M, Bishai WR, Lamichhane G.** 2010. The *Mycobacterium tuberculosis* protein LdtMt2 is a nonclassical transpeptidase required for virulence and resistance to amoxicillin. *Nature Medicine* **16**:466–469.
 14. **Schoonmaker MK, Bishai WR, Lamichhane G.** 2014. Nonclassical transpeptidases of *Mycobacterium tuberculosis* alter cell size, morphology, the cytosolic matrix, protein localization, virulence, and resistance to β -lactams. *Journal of Bacteriology* **196**:1394–1402.
 15. **Patru MM, Pavelka MS.** 2010. A Role for the Class A Penicillin-Binding Protein PonA2 in the Survival of *Mycobacterium smegmatis* under Conditions of Nonreplication. *Journal of Bacteriology* **192**:3043–3054.
 16. **Hett EC, Chao MC, Rubin EJ.** 2010. Interaction and Modulation of Two Antagonistic Cell Wall Enzymes of *Mycobacteria*. *PLoS Pathog* **6**:e1001020–14.
 17. **Kieser KJ, Boutte CC, Kester JC, Baer CE, Barczak AK, Meniche X, Chao MC, Rego EH, Sasseti CM, Fortune SM, Rubin EJ.** 2015. Phosphorylation of the Peptidoglycan Synthase PonA1 Governs the Rate of Polar Elongation in *Mycobacteria*. *PLoS Pathog* **11**:e1005010.
 18. **Vandal OH, Pierini LM, Schnappinger D, Nathan CF, Ehrt S.** 2008. A membrane protein preserves intrabacterial pH in intraphagosomal *Mycobacterium tuberculosis*. *Nature Medicine* **14**:849–854.

19. **Vandal OH, Roberts JA, Odaira T, Schnappinger D, Nathan CF, Ehrt S.** 2009. Acid-susceptible mutants of *Mycobacterium tuberculosis* share hypersusceptibility to cell wall and oxidative stress and to the host environment. *Journal of Bacteriology* **191**:625–631.
20. **Long JE, DeJesus M, Ward D, Baker RE, Ioerger T, Sassetti CM.** 2015. Identifying Essential Genes in *Mycobacterium tuberculosis* by Global Phenotypic Profiling, pp. 79–95. *In* *Gene Essentiality*. Humana Press, New York, NY, New York, NY.
21. **Joshi SM, Pandey AK, Capite N, Fortune SM, Rubin EJ, Sassetti CM.** 2006. Characterization of mycobacterial virulence genes through genetic interaction mapping. *Proc Natl Acad Sci USA* **103**:11760–11765.
22. **Chao MC, Pritchard JR, Zhang YJ, Rubin EJ, Livny J, Davis BM, Waldor MK.** 2013. High-resolution definition of the *Vibrio cholerae* essential gene set with hidden Markov model-based analyses of transposon-insertion sequencing data. *Nucleic Acids Research* **41**:9033–9048.
23. **Pritchard JR, Chao MC, Abel S, Davis BM, Baranowski C, Zhang YJ, Rubin EJ, Waldor MK.** 2014. ARTIST: High-Resolution Genome-Wide Assessment of Fitness Using Transposon-Insertion Sequencing. *PLoS Genet* **10**:e1004782–15.
24. **Blasco B, Chen JM, Hartkoorn R, Sala C, Uplekar S, Rougemont J, Pojer F, Cole ST.** 2012. Virulence regulator EspR of *Mycobacterium tuberculosis* is a nucleoid-associated protein. *PLoS Pathog* **8**:e1002621.
25. **Parthasarathy G, Lun S, Guo H, Ammerman NC, Geiman DE, Bishai WR.** 2012. Rv2190c, an NlpC/P60 family protein, is required for full virulence of *Mycobacterium tuberculosis*. *PLoS ONE* **7**:e43429.
26. **Pashley CA, Parish T.** 2003. Efficient switching of mycobacteriophage L5-based integrating plasmids in *Mycobacterium tuberculosis*. *FEMS Microbiology Letters* **229**:211–215.
27. **Schulbach MC, MAHAPATRA S, Macchia M, Barontini S, Papi C, Minutolo F, Bertini S, Brennan PJ, Crick DC.** 2001. Purification, enzymatic characterization, and inhibition of the Z-farnesyl diphosphate synthase from *Mycobacterium tuberculosis*. *Journal of Biological Chemistry* **276**:11624–11630.

28. **Dong SD, Oberthür M, Losey HC, Anderson JW, Eggert US, Peczuh MW, Walsh CT, Kahne D.** 2002. The structural basis for induction of VanB resistance. *J Am Chem Soc* **124**:9064–9065.
29. **Calvanese L, Falcigno L, Maglione C, Marasco D, Ruggiero A, Squeglia F, Berisio R, D'Auria G.** 2014. Structural and binding properties of the PASTA domain of PonA2, a key penicillin binding protein from *Mycobacterium tuberculosis*. *Biopolymers* **101**:712–719.
30. **Sassetti CM, Boyd DH, Rubin EJ.** 2001. Comprehensive identification of conditionally essential genes in mycobacteria. *Proc Natl Acad Sci USA* **98**:12712–12717.
31. **Langmead B, Salzberg SL.** 2012. Fast gapped-read alignment with Bowtie 2. *Nature Methods* **9**:357–359.
32. **Jain P, Hsu T, Arai M, Biermann K, Thaler DS, Nguyen A, González PA, Tufariello JM, Kriakov J, Chen B, Larsen MH, Jacobs WR.** 2014. Specialized transduction designed for precise high-throughput unmarked deletions in *Mycobacterium tuberculosis*. *mBio* **5**:e01245–14.
33. **Schindelin J, Arganda-Carreras I, Frise E, Kaynig V, Longair M, Pietzsch T, Preibisch S, Rueden C, Saalfeld S, Schmid B, Tinevez J-Y, White DJ, Hartenstein V, Eliceiri K, Tomancak P, Cardona A.** 2012. Fiji: an open-source platform for biological-image analysis. *Nature Methods* **9**:676–682.
34. **Hulsen T, de Vlieg J, Alkema W.** 2008. BioVenn - a web application for the comparison and visualization of biological lists using area-proportional Venn diagrams. *BMC Genomics* **9**:488.
35. **Carver T, Thomson N, Bleasby A, Berriman M, Parkhill J.** 2009. DNAPlotter: circular and linear interactive genome visualization. *Bioinformatics* **25**:119–120.
36. **Carver T, Harris SR, Berriman M, Parkhill J, McQuillan JA.** 2012. Artemis: an integrated platform for visualization and analysis of high-throughput sequence-based experimental data. *Bioinformatics* **28**:464–469.

Chapter 5: Discussion

Section 5.1: Abstract

Tuberculosis, the bacterial infection caused by *Mycobacterium tuberculosis* (Mtb), is an ancient human disease and yet, it continues to evade our efforts of eradication. The World Health Organization (WHO) estimates that 1.6 million people died of Mtb in 2016, and that 10 million became sick (1). To effectively treat Mtb, we must “know thy enemy”. What do we know about Mtb? Mycobacteria are unique in comparison to other bacteria in many ways, and in my dissertation, I have mainly focused on two of these characteristics- their distinct mode of growth and their “non-canonical” cell wall.

In contrast to the lateral cell body elongation of many well studied rod-shaped bacteria (like *Escherichia coli* and *Bacillus subtilis*), mycobacteria grow via insertion of new cell wall at their proximal ends known as the poles of the bacillus. Lateral cell wall insertion mixes new and old cell wall material. However, polar growth spatially segregates material based on age. Intriguingly, this leads to areas of aging cell wall localized toward mid-cell.

After some polar growth, the mycobacterial cell divides, and each daughter cell inherits a new pole, created at the site of division, and an old pole, that which was already existing. The old pole grows throughout the cell cycle. In contrast, the new pole is not thought to begin growth immediately after its founding at cell division. While rates of growth from these poles may be the same, the delay in elongation from the new pole has obvious consequences such as, an asymmetry of the total amount of nascent material produced from each pole.

In this Chapter I will delve into the implications of our findings regarding mycobacterial cell division, the spatiotemporal distributions of different peptidoglycan chemistries and enzymes in single cells, the role of non-canonical crosslinks for rod shape maintenance in mycobacteria,

and lastly, how we can potentially leverage our understanding of the asymmetric distribution of cell wall factors for treatment of Mtb.

Section 5.2: Summary of results and implications for understanding and targeting mycobacterial growth

Mycobacterial growth and division are complex processes requiring coordination of numerous factors (i.e. cell wall synthases) to ultimately achieve the creation of two daughter cells following polar elongation. In Chapter 2, we identified and characterized conserved proteins involved in division, and then utilized them as a tool to discover novel factors for this process. Work presented in Chapter 3 elucidated the function of mycobacterial L,D-transpeptidases, cell wall enzymes that catalyze a crosslink uniquely enriched in this genus, as well as proposing a distribution of cell wall chemistries based on polar growth. Finally, Chapter 4 focused on genetic interaction networks between cell wall enzymes in Mtb.

While cell division has been extensively studied in bacteria like *E. coli*, less is known about this process and the proteins involved in mycobacteria. Thus, in Chapter 2 we utilized computational tools to identify two unannotated but conserved septal proteins- FtsL and FtsB in mycobacteria. In other bacteria, FtsL and B work in concert with FtsQ and this complex is believed to both recruit proteins, and work in divisome maturation (2, 3). We found that depletion of FtsL or FtsB phenocopied that of known septal factors, and that they localized to the septum. Using FtsQ in a pulldown, we identified novel septal factors including one we named SepIVA, which shows homology to Wag31, a mycobacterial protein required for the transition of the septum to a new pole. SepIVA was found to be required for division and it also localized to the septum. Thus, SepIVA is likely an essential, novel component of the mycobacterial divisome. Taken together,

these data suggest that while conserved septal factors are present in mycobacteria, there exist unique factors that can be discovered through interactions with these known division proteins.

Before a mycobacterial cell divides, it first elongates (at least during exponential growth *in vitro*). The field generally agrees that mycobacteria do not elongate by adding new material along the sidewall, however more nuanced theories about where exactly at the polar region new material is incorporated have been postulated. The two models are that mycobacteria either grow at the apex of the pole (4), or that they grow at the peripolar region (5).

To probe new growth in mycobacteria, Hesper Rego and I utilized fluorescent D-amino acid (FDAA) probes. Peptidoglycan (PG), the innermost layer of the cell wall, uniquely contains D-amino acids and this was recently exploited to design fluorescent probes (or probes amenable to click chemistry addition of fluorescent molecules) to visualize new PG synthesis in bacteria (6-8). While it is more clearly understood now that these probes are not necessarily ligated to new PG in the cytoplasm (lipid II), it was postulated when they were first published that these dyes could report on new peptidoglycan synthesis. Intriguingly, when we incubated *Mycobacterium smegmatis* (a non-pathogenic model for Mtb, referred to hereafter as Msm) for < 2% of its life cycle with an FDAA we saw a pattern of incorporation which suggested that either Msm grew along the lateral cell wall or that these dyes were reporting some other process occurring there.

In Chapter 3, we undertook a screen to identify the enzymes responsible for the incorporation of FDAAs in Msm. We found L,D-transpeptidases (LDTs) as the most likely candidates. These enzymes catalyze 3-3 crosslinks in PG, and have been shown to exchange non-canonical D-amino acids onto PG tetrapeptides (9). They have also been found to attach Braun's lipoprotein (10, 11). I systematically deleted all 6 of the LDTs in Msm (*ΔldtABCEFG*) to test whether these enzymes were responsible for the incorporation of FDAAs. We found that nearly

all FDAA incorporation was LDT dependent. LDTs are extracellular enzymes that require processed PG containing a tetra- rather than nascent penta- peptide side chains as a substrate. Therefore, these data support a model where FDAA incorporation in Msm is likely a reflection of available PG tetrapeptides for exchange with FDAAs, and not visualization of newly flipped FDAA labeled lipid II.

The pattern of FDAA incorporation in Msm (an asymmetric gradient) lead to the hypothesis that PG chemistries along a single mycobacterial cell are non-uniformly distributed. Further, the correlation of FDAA incorporation to polar identity (the old pole incorporates far more FDAA and the gradient emanates from the old pole specifically) suggested that this asymmetric tetrapeptide distribution was a result of unequal polar growth where the new pole grows less (as described by others (4, 12)).

The Msm strain lacking all LDTs (Δ LDT) showed phenotypes beyond decrease of FDAA incorporation. We found that these cells displayed morphological defects. Specifically, we observed that Δ LDT cells lose rod shape over time (in a turgor dependent manner) at the oldest cell wall- that which is specifically inherited by the new pole daughter cell.

Because LDTs are known to catalyze 3-3 crosslinks, we concluded that 3-3 crosslinks in Msm cells localized to the aging cell wall, a feature unique to polar growth, to maintain integrity (and therefore shape) and counterbalance turgor pressure. Why might this strategy be utilized to maintain rod shape in mycobacteria?

PG, an elastic and flexible polymer (13), maintains bacterial cell shape in the face of turgor pressure. PG is formed into a structure and the force of turgor pressure evenly expands this structure (14). It has recently been found through osmotically shocking and then observing *E. coli*

grow, that the force of turgor is not required for the expansion of the PG structure, but specifically for the inflation of it (15).

But, what dictates where and in what shape PG is made? The backbone of PG is composed of linear glycan strands-how are these linear strands formed into a rod-shaped structure? What are the forces required to shape the cell? If you imagine holding a spherical balloon (one where the thickness and composition of the balloon itself is identical along the sphere and where the pressure inside the balloon is constant in all directions) clamping down on the middle of it would effectively squeeze it into a rod shape (Figure 5.1)¹. Thus, the symmetry of the sphere is broken via force along the lateral wall to create a rod shape (14). Existing as a rod shape has physical consequences. For instance, the stress along the circumference (or hoop stress) is twice that compared to the stress along the long axis (longitudinal stress) (14). Bacterial rod shape creation is similar. In bacterial rods, the amount of stretch along the long axis (from tip to tip) is greater than that around the hoop therefore, the hoop is stiffer (15). This also agrees with observations that the less flexible portion of PG, the glycan strands, are likely oriented in hoops around the short axis of the rod (16), likely to handle the stress there.

In our most well studied rod-shaped bacteria, *E. coli* and *B. subtilis*, the shape establishment and maintenance force along the lateral wall is thought to be provided by membrane bound proteins coupled to PG synthesis machinery. An example of this is the actin like protein, MreB. MreB polymerizes into short, discontinuous hoops (17, 18) at regions of membrane curvature (19). Its motion around the hoop of the cell requires and directs PG synthesis, though the details of this mechanism remain an area of active research (20, 21). MreB has also been shown to induce curvature in lipid membranes suggesting it may provide force inwards (22-24).

¹ This analogy was created by Hesper Rego.

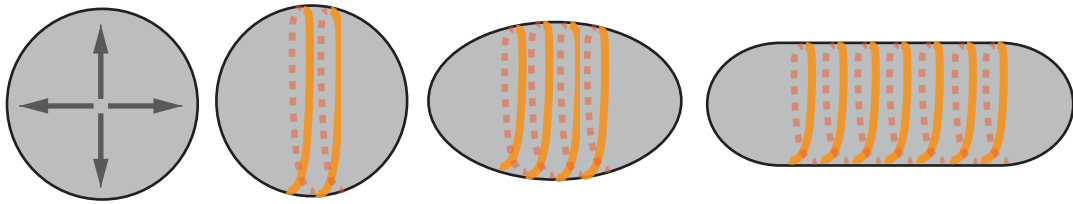


Figure 5.1: Formation of a rod shape requires symmetry breaking forces along the lateral cell wall.

Bacterial rod shape requires a force along the lateral cell wall (orange hoops). The asymmetry of rod shape also leads to different stresses, namely the hoop stress is twice that of the longitudinal stress.

Unlike these lateral growing rods, polar elongating mycobacteria lack homologs of proteins like MreB. The data presented in Chapter 3 suggest that in the absence of active lateral growth and this “canonical” rod shape maintenance strategy, perhaps “non-canonical” LDT catalyzed 3-3 crosslinks are fulfilling this role in mycobacteria. These 3-3 crosslinks are referred to as “non-canonical” because they are rare in the well-studied lateral growing rods. They are however the most highly abundant crosslink in mycobacteria and other polar growing bacteria like *Agrobacterium tumefaciens* and *Sinorhizobium meliloti* (Figure 5.2) suggesting that 3-3 crosslinks located at aging cell wall to maintain rod shape could be a mechanism broadly applicable to other polar growing rod-shaped bacteria (25-29).

How could a 3-3 crosslink stabilize shape? One theory is that the shorter length of the peptides participating in the 3-3 crosslink, compared to those in a 4-3 crosslink, leads to a more rigid crosslink. Furthermore, one could speculate that the distance between the glycan strands would be shorter and as these are the more rigid portion of PG, that areas of 3-3 crosslinks could provide localized stability.

One spatially targeted and cell wall perturbing process is cell division. Bacterial cell division (covered in Chapter 1) requires both the breakdown and synthesis of the cell wall at roughly mid-cell to produce two daughter cells from one mother cell.

Mycobacteria have a very complex multi-layered cell wall (covalently attached to PG is a carbohydrate polymer called arabinogalactan, and attached to that is the mycolic acid layer, and then outside of that is the capsule) (30). It is feasible that to cleave these layers for the separation of daughter cells takes more time in mycobacteria (perhaps longer than a single generation) than in bacteria with simpler cell walls. This longer timeframe, where the cell is susceptible to lysis,

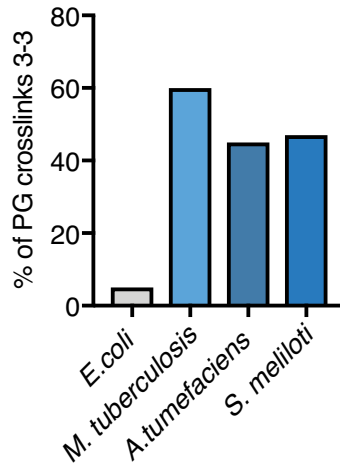


Figure 5.2: The percentage of peptidoglycan crosslinks that are LDT catalyzed 3-3 crosslinks in various bacterial species. Analysis of peptidoglycan has found that the crosslinks found in peptidoglycan of lateral growing *E. coli* contains ~5-10% of the 3-3 variety, while in the polar growing *M. tuberculosis*, *A. tumefaciens* and *S. meliloti*, 3-3 crosslinks make up nearly half of the peptidoglycan crosslinks.

may require mycobacteria to employ special fortification at the division site. Perhaps this fortification comes in the form of 3-3 crosslinks for the highest probability of successful daughter cell separation without rupturing.

In Chapter 3, we hypothesized that as new cell wall (pentapeptide containing PG) incorporates at the poles, it is first 4-3 crosslinked by PBPs (resulting in tetrapeptides) and then, these crosslinks are cut by enzymes (D,D-endopeptidases) leaving tetrapeptides for LDTs to bind and create 3-3 crosslinks at this “aging”, processed PG. As new cell wall is continuously inserted at the poles, we postulated that these processes (4-3 crosslinking, 4-3 cleavage and 3-3 crosslinking) would be occurring at different portions of the cell since these processes occur in a linear dependency over time. Given this, we tagged a PBP (PonA1 courtesy of Karen Kieser), an LDT (LdtE) and a putative D,D-endopeptidase (DacB2) with fluorescent proteins to track their localization over time. We saw that these enzymes do in fact localize to their putative substrate distribution, as governed directly by unequal polar growth.

Using Tn-seq, we also found that typically non-essential PBPs sustained significantly fewer transposon insertions in Δ LDT cells suggesting that 4-3 crosslinking may be more important when 3-3 crosslinks are absent. I directly tested the essentiality of 4-3 crosslinking by PonA1 in Δ LDT cells and found that it was required for cells to survive. This finding was extremely exciting in the framework of tuberculosis treatment.

The first line treatment for drug susceptible Mtb consists of isoniazid, rifampicin, pyrazinamide and ethambutol. Two of these drugs, isoniazid and ethambutol, target the cell wall (mycolic acids and arabinogalactan respectively). (31) While these drugs are effective, resistance is a continued problem. In 2016, there were nearly 500,000 cases of multi-drug-resistant Mtb

(resistant to rifampicin and isoniazid). (1) These figures underscore the urgent need for the use of new drugs to treat Mtb.

Noticeably absent from the list of drugs to treat Mtb are agents that are common in the treatment of most bacterial infections: the PG targeting β -lactams. Why isn't the PG layer of the Mtb cell wall currently targeted?² For many years, β -lactams were not effective against Mtb due to its active and promiscuous β -lactamase enzyme (an enzyme that cleaves to inactivate β -lactams) (33, 34). This has been overcome by use of a β -lactamase inhibitor, clavulanate (33, 35). Recently, the combination of amoxicillin (a non-carbapenem (N-C) β -lactam) with clavulanate and meropenem (a carbapenem β -lactam that targets LDTs with a much higher efficiency than N-C β -lactams *in vitro* (27, 28, 36)) has shown promise in killing drug sensitive Mtb in people (37). This treatment will be explored further in combination with (and without) rifampicin in an upcoming clinical trial (38).

Why does the combination of a carbapenem and a N-C β -lactam (with β -lactamase inhibitor) work? Our data from Chapter 3 provide two mechanistic explanations. First, when we removed LDTs genetically, PBPs became more important (this is also supported by our Mtb Tn-seq findings, discussed below, from Chapter 4). The inhibition of LDTs with carbapenems may also lead to this effect, which we can exploit with the PBP inhibiting N-C β -lactam (mycobacterial PBPs may also be targets of carbapenems). Second, the asymmetric distribution of enzymes and PG chemistries along a single cell predict that daughter cells will inherit cell walls with different characteristics. This may contribute to phenotypic heterogeneity in the face of drugs. Therefore,

² PG targeting drugs have been used to treat drug resistant Mtb anecdotally (32)

understanding and targeting both daughter cell phenotypes (for instance with the combination mentioned above) would lead to more complete killing.

In Chapter 4 we found that in Mtb cells lacking both the aPBP *ponA1* and the LDT *ldtB* display a growth defect, suggesting that in the absence of the 4-3 crosslinking PBP, the 3-3 crosslinking LDT is required for optimal fitness. Furthermore, we found that the *ldtB* gene sustained fewer transposon insertions in the Δ *ponA1* and Δ *ponA2* (an aPBP) cells than in WT. The reciprocal was also true- *ponA1* and *ponA2* had fewer transposon insertions mapped in the Δ *ldtB* strain suggesting that these genes are less dispensable in this genetic background. This data is in concordance with the Msm Tn-seq in Chapter 3 where we found that in the absence of LDTs, non-essential PBPs appear essential, and that the transpeptidase domain of *ponA1* is required for survival. In conclusion, these data argue that in the absence of one type of crosslink, the other becomes more important and thus supports targeting Mtb with a combination of PBP- (4-3 crosslinkers) and LDT- (3-3 crosslinkers) inhibiting drugs, such as a β -lactam with a carbapenem.

Our data (Chapter 3) also suggest that the distribution of PG substrates is different across a single cell and can lead to variance in daughter cells post-division that can be exploited with combination drug treatment. For instance, the new pole daughter cell will inherit most of the 3-3 crosslinked, older PG. Therefore, as these crosslinks are already established in this daughter cell, a carbapenem may be less effective. In agreement with this prediction, work by Aldridge *et al* found that the new pole daughter cell survives carbapenem treatment better than the old pole daughter cell (4).

Taking all these data into account, we hypothesized that the combination of inhibiting PBPs and LDTs (using a N-C β -lactam, a carbapenem and a β -lactamase inhibitor) would lead to more rapid killing of Mtb. Excitingly, we verified this prediction *in vitro* showing drug synergism (39)

with respect to the kinetics of Mtb killing. Though we are not the first to show that this combination is more effective than these drugs alone (40), the mechanistic insight provided through our work is new. These single cell details will be imperative in understanding the mechanism of action for this treatment as well as lending a springboard to identifying putative mechanisms of resistance as this drug combination moves towards becoming a treatment option for tuberculosis.

Section 5.3: Future Directions

There remain many questions about mycobacterial growth and division-*What? Where? Who? When? How? Why?* First, I will discuss the future directions of studies related specifically to LDTs and 3-3 crosslinks (*What* is the function of 3-3 crosslinks?) and then I will focus on questions related more broadly to mycobacterial growth and division- *Where* do mycobacteria grow? What proteins (*who*) are involved in growth and division? *When* is the site of septation determined? *How* is the expansion of the cell coordinated between the layers of the cell wall? *Why* grow asymmetrically?

What is the function of 3-3 crosslinks?

Given our data in Msm, it appears that 3-3 crosslinks are required for rod shape maintenance at sites of aging cell wall. But, what is the role of 3-3 crosslinking in Mtb? Single, double and even triple knock-outs of LDTs in Msm had no gross growth defects. This is in contrast to data in Mtb where the deletion of two LDTs shows significant defects in growth (41), and where in the absence of one LDT, the gene predicted most essential was another LDT (42) suggesting that a double knock-out of these two genes would not be viable. While Msm doubles every ~2.5 hours, Mtb doubles every ~20 hours. This may be key to the apparent difference in LDT

essentiality between these two related organisms. With a quick doubling time, PG ages much less in Msm than in Mtb. Therefore, perhaps the role of LDTs for maintenance of old PG is magnified in Mtb. One other obvious difference is that Msm is not a pathogen, and Mtb must survive in the host. This suggests that 3-3 crosslinks are specifically required during infection.

During latent infection, Mtb is believed to enter a state of dormancy with halted growth and decreased metabolism (43). When this occurs, there is likely few or no new PG pentapeptides for 4-3 crosslinking and thus, 3-3 crosslinking would be the only transpeptidation option. In agreement with this, expression data shows that at least one LDT is highly upregulated (17-fold) during an *in vitro* model of dormancy (28, 44) and that during stationary phase of growth, ~80% of Mtb PG crosslinks are of the 3-3 variety (28). Also, it has been shown that Mtb lacking a single or combination of two LDTs is attenuated in a mouse model of Mtb infection (41, 45). Lastly, meropenem was shown to be effective against Mtb in an *in vitro* model of persistence (46). While stationary phase peptidoglycan from Mtb shows high 3-3 crosslinking, it will be critical to determine whether 3-3 crosslinking is enriched in Mtb during infection by performing PG analysis on cells harvested from macrophages or mice infected with Mtb.

Where do mycobacteria grow?

The seemingly simplest questions can be the most challenging to answer. Does new PG get inserted at the very polar cap or at the peripolar region? There is evidence for both of these possibilities (4, 5, 47). But, is it critical to distinguish them? These are geometrically distinct locations (the polar cap is a hemisphere while the peripolar region is cylindrical) and the forces at these sites are different (14). Therefore, it is likely that the mode of cell wall incorporation would not be equivalent at these two sites and could be susceptible to different drugs.

First, it is important to define growth. PG synthesis begins in the cytoplasm where the final product is the disaccharide with the pentapeptide attached to a lipid (lipid II). Lipid II is flipped over the membrane, new PG is polymerized into the existing PG structure and the lipid is recycled (48). It is possible that newly flipped PG is not immediately inserted into the cell wall, and therefore not contributing to growth. Therefore, for the purposes of the following discussion “new growth” will be defined as the addition of newly flipped PG into the existing structure.

The incorporation of FDAAs into the polar apex of the mycobacterial cell suggests that both the substrate and the enzymes for incorporation are localized there. While we have shown that most FDAA incorporation in Msm is primarily LDT dependent, there remains faint polar incorporation of these dyes in cells lacking LDTs. This polar incorporation could be pentapeptide exchange by PBPs (6). This is intimately correlated to newly synthesized PG, as pentapeptides only exist on unprocessed, nascent PG.

Perhaps localizing enzymes, like PonA1, responsible for the incorporation of newly flipped PG could aid in our understanding of where mycobacteria elongate. PonA1-RFP does not localize to the very tip of the mycobacterial bacillus (Figure 3.6A, B) suggesting peripolar elongation. However, this localization could be a consequence of fluorescent protein maturation.³ It has been shown recently that monomeric red fluorescent protein (mRFP) takes ~20 minutes to mature at 37°C (49). Our time-lapse microscopy experiments in Chapter 3 were performed at 37°C so, the RFP tagged PonA1 that we can visualize was translated at least 20 minutes prior. If new PG is continuously being inserted at the pole, previously inserted PonA1-RFP only becomes visible slightly inward from this as the fluorescent protein matures. Therefore, it is plausible that PonA1 is inserted at the very tip of the pole working to insert new PG into the existing PG structure there.

³ These ideas were generated through correspondence and data with Hesper Rego.

Again however, this data does not directly test where new cell wall is inserted as the localization of an enzyme does not prove its functions at this location.

Where does new PG get inserted into existing PG? At the core, what we are asking first is: where does lipid II get flipped from the cytoplasm? To test this directly, one could utilize a PG probe that incorporates solely into lipid II (in the cytoplasm). There is a D-alanine dipeptide probe, ethynyl-D-alanyl-D-alanine (E-DADA) (50), that has been used to show new growth in other bacterial species (50). Some preliminary experiments I have done in collaboration with Sloan Siegrist (University of Massachusetts) suggest however, that E-DADA can incorporate into lipid II via a cytoplasmic route, as well as through an extracellular LDT dependent route in mycobacteria.

I found that E-DADA can rescue an alanine racemase mutant (*Msm Δ alr⁴*), a strain that requires D-alanine for PG synthesis to grow (Figure 5.3A). Alanine racemase works in the cytoplasm to change L-alanine to D-alanine specifically for the PG pentapeptide (51). This data suggests that E-DADA can enter the cytoplasm and be utilized there for PG synthesis. One caveat to this interpretation is that E-DADA may be cleaved into its constituent parts, and these may be incorporated extracellularly as well as by cytoplasmic enzymes.

To elucidate whether E-DADA incorporation occurs through extracellular PG enzymes, I tested if it could be inhibited by carbapenem antibiotics. I exposed cells to 2X or 50X the minimum inhibitory concentration (MIC) of imipenem (a carbapenem) for a short 3-minute or long 30-minute incubation. We reasoned that the short incubation was not enough time for Msm to completely halt PG synthesis and further, that available substrates would not be depleted entirely. Conversely, in the 30-minute treatment it is plausible that cells halted PG synthesis and that

⁴ Strain provided courtesy of Jeff Wagner, Rubin lab.

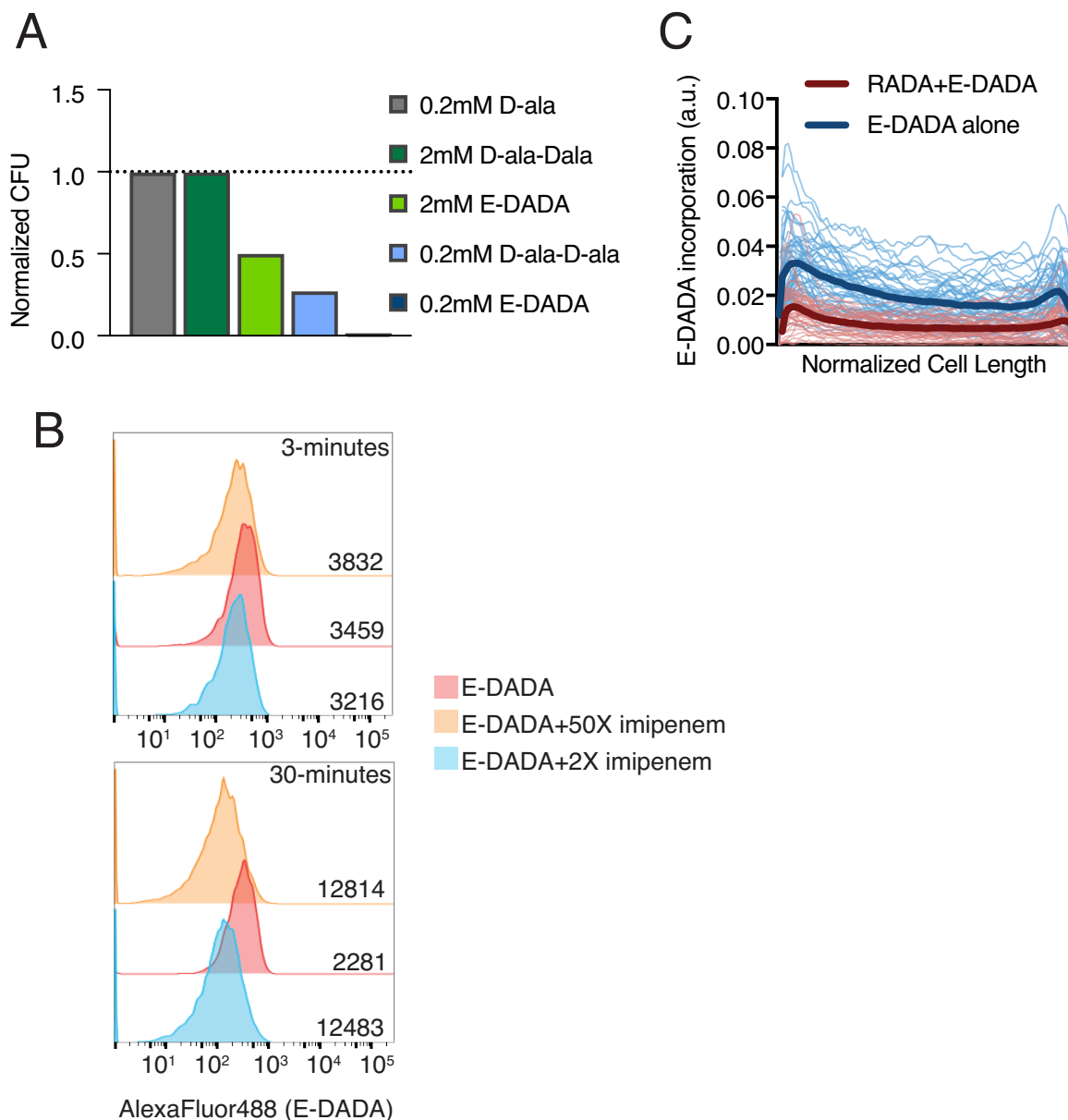


Figure 5.3: Probing incorporation routes of the D-alanine dipeptide probe: ethynyl-D-alanyl-D-alanine. (A) Colony forming units (CFU) of wild-type or an alanine racemase mutant of Msm given either 0.2 or 2.0 mM of D-alanine (D-ala), D-alanine-D-alanine dipeptide (D-ala-D-ala) or ethynyl-D-alanyl-D-alanine (E-DADA). Data are shown as CFU normalized to growth on D-alanine alone. **(B)** E-DADA incorporation into WT Msm after imipenem treatment. Plots are histograms of fluorescence normalized to mode, measured via FACs. Number of events per is

Figure 5.3 (Continued)

listed in the top right of each panel. **(C)** FDAA (RADA) competition of E-DADA incorporation into WT Msm. E-DADA alone (N=49 cells), RADA+E-DADA (competition) (N=43 cells). Thin lines represent E-DADA incorporation in single cells and thick lines represent the mean incorporation for that condition.

substrate availability for dye incorporation would be greatly reduced. E-DADA incorporation was inhibited by both 3- and 30- minute incubation in either 2X or 50X MIC of imipenem (Figure 5.3B). These data support a model where imipenem inhibits extracellular enzymes (i.e. LDTs, PBPs) and prevents E-DADA incorporation extracellularly.

Given that we have shown that FDAA incorporation is primarily due to LDTs, we reasoned that if E-DADA was also utilizing this route that we could compete these two probes. Briefly, I mixed FDAA (1mM RADA) with E-DADA (1mM) and added this to log phase WT Msm cells (8-minutes). I compared this to cells stained with only E-DADA. I found that E-DADA incorporation in Msm can be competed with FDAAs (Figure 5.3C), suggesting these utilize the same route. However, it remains unclear whether all E-DADA incorporation can be competed with FDAAs.

Taken together, these data suggest a model where E-DADA can be incorporated via both a cytoplasmic and LDT dependent extracellular route. However, direct biochemical experiments, such as characterization of lipid II, will be required to determine the routes of probe incorporation. These results will be critical to our interpretation of data derived from PG probe experiments. Furthermore, if we can identify a probe that solely incorporates into lipid II, it would illuminate the location of newly flipped PG. As was discussed before, the location of newly flipped PG however, isn't necessarily where this molecule is incorporated into the structure. Thus, a dye that can be visualized only upon the crosslinking of new PG into existing PG would show us where new growth occurs.

FDAA incorporation, PG synthase localization and E-DADA incorporation data presented here do not rule out either peripolar elongation or polar apex growth. It is possible that the

mycobacterial bacillus elongates at both regions. Future studies utilizing diverse probes of PG synthesis are required to elucidate exactly where new growth occurs in mycobacteria.

What proteins (*who*) are involved in growth and division?

Aside from where exactly growth occurs, the identity of proteins involved in cell growth and division are largely unknown (see Chapters 1, 2). The elongasome, the complex of proteins for elongation, and the divisome, those required for cell division, are considered separate complexes in most bacteria. In mycobacteria however, since the septum will become the growth pole, it is challenging to distinguish proteins involved in these separate processes.

Are the elongasome and divisome separate complexes in mycobacteria? Are these processes coupled? It has been shown that when division is blocked, ectopic poles form and elongate (Chapter 2) (52), suggesting that these processes are not dependent on one another. If this is the case, why would the cell utilize different complexes to build a septum than to elongate? Here again we must consider the geometry of cell wall synthesis. The septal cell wall is built orthogonally to the existing PG. It has been shown in *B. subtilis* that the septal cell wall is built inward in a spiraling fashion (53). If growth is occurring at the peripolar region for example, enzymes would likely be inserting new material in a hoop circling around the cell (similar to MreB driven PG synthesis), but not enclosing inward. Perhaps then, the divisome would contain a distinct set of proteins from the elongasome with specificity for the geometry of septal synthesis or factors that regulate the spatial orientation of PG synthases. More work in this area is required to distinguish these possibilities.

My work has shown that LDTs are required to maintain cell shape in mycobacteria. However, it remains unknown whether these enzymes work in concert with other cell wall

enzymes for elongation or division. Protein pulldowns (like the FtsQ pulldown in Chapter 2) would identify interacting partners, and could illuminate the separation (or lack thereof) between complexes. For example, given our model that PBPs create a substrate for D,D-endopeptidases, that then provide the substrate for LDTs, do these three classes of PG proteins physically interact? Perhaps LDTs interact with other factors required for rod shape in polar growing bacteria.

When is the site of septation determined?

Mycobacteria lack systems (like Min and Noc) for FtsZ ring and septal site placement (51). It remains unclear how the Z-ring is placed in mycobacteria. However, there is growing evidence that the spatial information for septum placement may be encoded in the cell wall, and that polar growth may itself be instrumental in mid-cell septal site placement. Atomic force microscopy studies by Eskandarian *et al* found troughs on the mycobacterial cell surface that appear at the poles and through polar growth travel to the mid-cell where they eventually become the site of septation (54). Furthermore, it has been shown that layers of the mycobacterial cell wall are not freely diffusible (55). This suggests that information created at the pole during growth can travel through polar elongation to mid-cell where cell division will occur.

In our studies of fluorescently tagged PG enzymes and FDAA incorporation, we observe a distinct gradient of signal that is highest at the old pole with a sharp decline toward mid-cell where the minimum of signal (a divot) is located. This divot is beguilingly located near mid-cell where the septum will eventually be placed. What creates this gradient and this divot?

Considering the distribution of PG enzymes, if these proteins are inserted and “stuck”, their distribution should be linear along the cell. The gradient observed suggests that they are removed from specific portions of the cell, most noticeably at the divot (mid-cell). Perhaps, these enzymes

are inserted at sites of new substrate, and remain at these sites until their substrate is utilized. When they are no longer processing PG, they are targeted for degradation. I hypothesize that there could be a protease helping to establish the gradient of protein localization along the cell. Again, protein pulldowns of PG enzymes like LDTs and PBPs to identify interacting partners would elucidate key regulators of both spatial organization and activity of these proteins. I hypothesize that this divot has characteristics (like aging PG enriched in 3-3 crosslinks) which may act as a marker for FtsZ placement in the absence of other systems to do so. Identifying mutants that mis-localize the gradient would allow us to test whether septum site placement is correlated to the divot. One way to identify these genes would be to perform a high-throughput microscopy screen of a transposon mutant library stained with FDAAs to identify genes whose disruption changes the pattern of FDAA incorporation. This would lead to data different from the FACs based FDAA screen in Chapter 3 because there we could only distinguish mutants with increased or decreased incorporation.

How is the expansion of the cell coordinated between the layers of the cell wall?

My thesis work has focused on the innermost PG layer of the mycobacterial cell wall. However, the mycobacterial cell wall is far more complex than this first layer alone. Covalently attached to the PG is a polysaccharide known as arabinogalactan (AG), and covalently attached to the AG is a layer of fatty acids called mycolic acids (30). Beyond the mycolic acid layer is a non-covalently connected capsule composed of proteins, glycans and lipids (30, 51, 56). How mycobacteria coordinate (or don't) the synthesis of the PG, AG, MA and capsule remains enigmatic. There is evidence, though limited, that construction of the layers is synchronized. For example, Wag31, a non-enzymatic orchestrator of polar growth, interacts with both PG and

mycolic acid synthesis enzymes suggesting coordination between these layers (5, 57-60). Co-localization of the putative septal factor SepIVA with the AG synthesis protein GlfT2 illustrates a potential link between cell division, a process we know is intimately tied to PG synthesis, and the synthesis of the AG layer (Chapter 2) (52). Lastly, genetic interactions in Mtb between PG synthesis and putative AG enzymes supports communication between the creation of these layers (Chapter 4) (42).

Analysis of PG isolated from Msm cells lacking detectable 3-3 crosslinks (Chapter 3) showed an increase in a putative anhydrous disaccharide tripeptide PG species whose creation is thought to be catalyzed by lytic transglycosylases (Figure 5.4A, B). Lytic transglycosylases are enzymes that cleave PG to prevent further glycan polymerization. Thus, they dictate the length of the glycan strands (61). This finding is interesting in light of cell wall layer coordination because the cleavage of PG and subsequent creation of the 1,6 anhydro ring blocks the attachment site of AG (62, 63). Therefore, in cells that lack detectable 3-3 crosslinks it is possible that there are fewer AG attachment sites leading to less AG. Less AG means that there would be fewer MA attachment sites, and therefore less MA, consequently altering the entire cell envelope.

Because there are putatively fewer attachment sites for AG (and as a result for MA), the synthesis of these layers may be downregulated and could lead to less effective targeting by drugs like ethambutol and isoniazid. Future experiments like characterizing the amount of AG and MA in the Δ LDT strain (chemical probes for these layers exist (55)) , testing the susceptibility of cells lacking detectable 3-3 crosslinks to AG and MA inhibiting drugs will be required to understand whether this relationship is physiologically meaningful. Furthermore, identifying proteins that physically interact with LDTs could reveal AG and MA synthesis enzymes suggesting physical

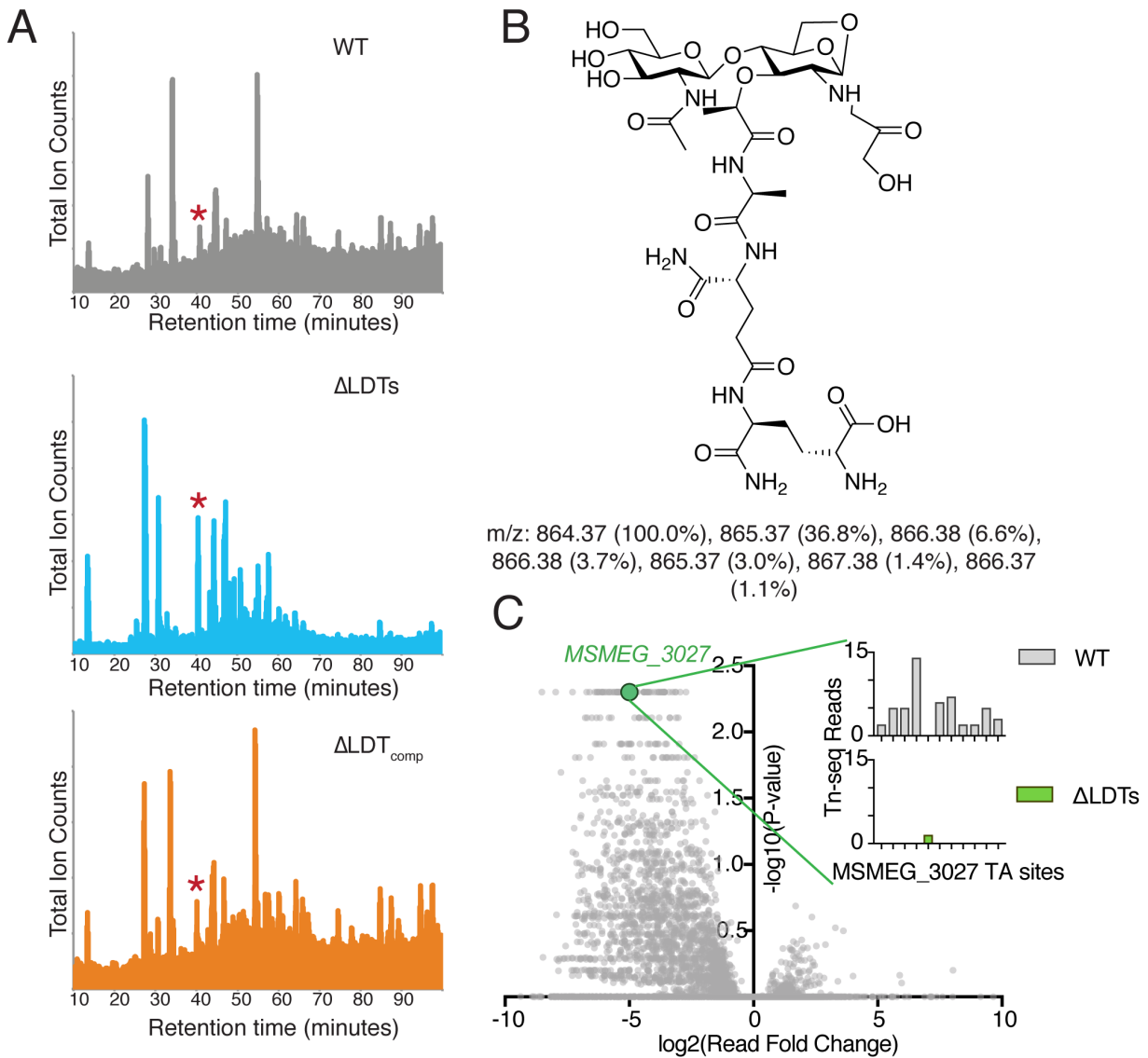


Figure 5.4: Putative response of a predicted lytic transglycosylase in cells lacking detectable 3-3 crosslinks. (A) Total ion chromatograms of WT, Δ LDT and Δ LDT_{comp} peptidoglycan analyzed via mass spectrometry. The red asterisk indicates the peak corresponding to the anhydrous tripeptide species depicted in **(B)**. **(B)** Putative anhydrous disaccharide tripeptide peptidoglycan species generated by lytic transglycosylases. **(C)** Transposon read fold change in Δ LDT cells compared to WT Msm. (Data presented in Figure 3.5A). Inset shows the number of transposon

Figure 5.4 (Continued)

reads mapped to each TA site in *MSMEG_3027* in WT (top, grey bars) and Δ LDT (bottom, green bars).

links between the complexes that synthesize each layer as has been shown for the PG and outer membrane in *E.coli* (64).

Besides the biochemical evidence for a change in lytic transglycosylase activity, we also found genetic evidence of this in data from Chapter 3. One gene predicted to sustain significantly fewer transposon insertions in Δ LDT cells was *MSMEG_3027* (Figure 5.4C), a gene of unknown function with homology to LytG, a lytic transglycosylase (61) (homology to LytG was found using HHPRED (65)). This candidate gene product may be responsible for the relative increase in anhydrous disaccharide tripeptide. Given its predicted essentiality in Tn-seq, it will be interesting to test whether *MSMEG_3027* is essential in Δ LDT cells. Its putative essentiality might hint at an attempt by the cell at reinforcing the cell wall through regulation of glycan strand length.

Why grow asymmetrically?

The benefits of asymmetric growth and division in bacteria are poorly understood (66). Producing progeny with a range of phenotypes can increase the probability of survival in a variety of environments. Moreover, the asymmetric partitioning of aging or damaged material (like old PG) to specific daughter cells leads to a population of cells that are both relatively “young” and relatively “old” (66). For instance, since the mycobacterial old pole grows more than the new pole, after septation, most of the old pole daughter cell PG is younger than that found in the new pole daughter cell. In mycobacteria specifically, asymmetry has been shown beneficial in response to drug treatment, where one daughter cell preferentially survives treatment, and where loss of asymmetry leads to more uniform killing (4, 12). The molecular details of phenotypic heterogeneity are not yet fully understood.

The gradient and divot of PG enzymes and FDAAs discussed above are one source of asymmetry in each mycobacterial cell that appears correlated to the relative amount of asymmetric growth from the poles. Recent work by Rego *et al* has shown that asymmetry in growth from the poles is actively created in mycobacteria. Specifically, it was found that a protein of unknown function, LamA, works at the new pole to inhibit growth (12). The precedent set by active asymmetry via LamA's function supports the notion that the gradient of PG enzymes and substrates can be actively established and maintained. Furthermore, the disruption of the asymmetric gradient is likely to have phenotypic consequences.

Section 5.4: References

1. 2017. Global Tuberculosis Report 2017 1–262.
2. **Tsang M-J, Bernhardt TG.** 2015. A role for the FtsQLB complex in cytokinetic ring activation revealed by an ftsL allele that accelerates division. *Molecular Microbiology* **95**:925–944.
3. **Egan AJF, Vollmer W.** 2012. The physiology of bacterial cell division. *Annals of the New York Academy of Sciences* **1277**:8–28.
4. **Aldridge BB, Fernandez-Suarez M, Heller D, Ambravaneswaran V, Irimia D, Toner M, Fortune SM.** 2012. Asymmetry and aging of mycobacterial cells lead to variable growth and antibiotic susceptibility. *Science* **335**:100–104.
5. **Meniche X, Otten R, Siegrist MS, Baer CE, Murphy KC, Bertozzi CR, Sasseti CM.** 2014. Subpolar addition of new cell wall is directed by DivIVA in mycobacteria. *Proc Natl Acad Sci USA* **111**:E3243–51.
6. **Kuru E, Hughes HV, Brown PJ, Hall E, Tekkam S, Cava F, de Pedro MA, Brun YV, VanNieuwenhze MS.** 2012. In Situ Probing of Newly Synthesized Peptidoglycan in Live Bacteria with Fluorescent D-Amino Acids. *Angew Chem Int Ed* **51**:12519–12523.
7. **Kuru E, Tekkam S, Hall E, Brun YV, Van Nieuwenhze MS.** 2014. Synthesis of fluorescent D-amino acids and their use for probing peptidoglycan synthesis and bacterial growth in situ. *Nat Protoc* **10**:33–52.
8. **Siegrist MS, Whiteside S, Jewett JC, Aditham A, Cava F, Bertozzi CR.** 2013. d-Amino Acid Chemical Reporters Reveal Peptidoglycan Dynamics of an Intracellular Pathogen. *ACS Chem Biol* **8**:500–505.
9. **Cava F, de Pedro MA, Lam H, Davis BM, Waldor MK.** 2011. Distinct pathways for modification of the bacterial cell wall by non-canonical D-amino acids. *The EMBO Journal* **30**:3442–3453.
10. **Mainardi J-L, Fourgeaud M, Hugonnet J-E, Dubost L, Brouard J-P, Ouazzani J, Rice LB, Gutmann L, Arthur M.** 2005. A novel peptidoglycan cross-linking enzyme for a beta-lactam-resistant transpeptidation pathway. *Journal of Biological Chemistry* **280**:38146–38152.

11. **Magnet S, Bellais S, Dubost L, Fourgeaud M, Mainardi J-L, Petit-Frère S, Marie A, Mengin-Lecreulx D, Arthur M, Gutmann L.** 2007. Identification of the L,D-transpeptidases responsible for attachment of the Braun lipoprotein to Escherichia coli peptidoglycan. *Journal of Bacteriology* **189**:3927–3931.
12. **Rego EH, Audette RE, Rubin EJ.** 2017. Deletion of a mycobacterial divisome factor collapses single-cell phenotypic heterogeneity. *Nature* **546**:153–157.
13. **Cabeen MT, Jacobs-Wagner C.** 2005. Bacterial cell shape. *Nat Rev Micro* **3**:601–610.
14. **Chang F, Huang KC.** 2014. How and why cells grow as rods. *BMC Biol* **12**:2102–11.
15. **Rojas E, Theriot JA, Huang KC.** 2014. Response of Escherichia coli growth rate to osmotic shock. *Proc Natl Acad Sci USA* **111**:7807–7812.
16. **Gan L, Chen S, Jensen GJ.** 2008. Molecular organization of Gram-negative peptidoglycan. *Proc Natl Acad Sci USA* **105**:18953–18957.
17. **Garner EC, Bernard R, Wang W, Zhuang X, Rudner DZ, Mitchison T.** 2011. Coupled, Circumferential Motions of the Cell Wall Synthesis Machinery and MreB Filaments in *B. subtilis*. *Science* **333**:222–225.
18. **Domínguez-Escobar J, Chastanet A, Crevenna AH, Fromion V, Wedlich-Söldner R, Carballido-López R.** 2011. Processive movement of MreB-associated cell wall biosynthetic complexes in bacteria. *Science* **333**:225–228.
19. **Ursell TS, Nguyen J, Monds RD, Colavin A, Billings G, Ouzounov N, Gitai Z, Shaevitz JW, Huang KC.** 2014. Rod-like bacterial shape is maintained by feedback between cell curvature and cytoskeletal localization. *Proc Natl Acad Sci USA* **111**:E1025–34.
20. **Cho H, Wivagg CN, Kapoor M, Barry Z, Rohs PDA, Suh H, Marto JA, Garner EC, Bernhardt TG.** 2016. Bacterial cell wall biogenesis is mediated by SEDS and PBP polymerase families functioning semi-autonomously. *Nat Microbiol* **1**:16172.
21. **Lee TK, Meng K, Shi H, Huang KC.** 2016. Single-molecule imaging reveals modulation of cell wall synthesis dynamics in live bacterial cells. *Nature Communications* **7**:13170.

22. **Hussain S, Wivagg CN, Szwedziak P, Wong F, Schaefer K, Izore T, Renner LD, Sun Y, Bisson Filho AW, Walker S, Amir A, Löwe J, Garner EC.** 2017. MreB Filaments Create Rod Shape By Aligning Along Principal Membrane Curvature.
23. **Salje J, van den Ent F, de Boer P, Löwe J.** 2011. Direct membrane binding by bacterial actin MreB. *Mol Cell* **43**:478–487.
24. **van den Ent F, Izore T, Bharat TA, Johnson CM, Löwe J.** 2014. Bacterial actin MreB forms antiparallel double filaments. *eLife* **3**:e02634.
25. **Brown PJB, de Pedro MA, Kysela DT, Van der Henst C, Kim J, De Bolle X, Fuqua C, Brun YV.** 2012. Polar growth in the Alphaproteobacterial order Rhizobiales. *Proc Natl Acad Sci USA* **109**:1697–1701.
26. **Glauner B, Höltje JV, Schwarz U.** 1988. The composition of the murein of *Escherichia coli*. *Journal of Biological Chemistry* **263**:10088–10095.
27. **Kumar P, Arora K, Lloyd JR, Lee IY, Nair V, Fischer E, Boshoff HIM, Barry CE III.** 2012. Meropenem inhibits D,D-carboxypeptidase activity in *Mycobacterium tuberculosis*. *Molecular Microbiology* **86**:367–381.
28. **Lavollay M, Arthur M, Fourgeaud M, Dubost L, Marie A, Veziris N, Blanot D, Gutmann L, Mainardi JL.** 2008. The Peptidoglycan of Stationary-Phase *Mycobacterium tuberculosis* Predominantly Contains Cross-Links Generated by L,D-Transpeptidation. *Journal of Bacteriology* **190**:4360–4366.
29. **Cameron TA, Zupan JR, Zambryski PC.** 2015. The essential features and modes of bacterial polar growth. *Trends Microbiol* **23**:347–353.
30. **Kieser KJ, Rubin EJ.** 2014. How sisters grow apart: mycobacterial growth and division. *Nature Publishing Group* **12**:550–562.
31. **Horsburgh CR, Barry CE, Lange C.** 2015. Treatment of Tuberculosis. *N Engl J Med* **373**:2149–2160.
32. **Sotgiu G, D'Ambrosio L, Centis R, Tiberi S, Esposito S, Dore S, Spanevello A, Migliori GB.** 2016. Carbapenems to Treat Multidrug and Extensively Drug-Resistant Tuberculosis: A Systematic Review. *Int J Mol Sci* **17**:373.

33. **Wivagg CN, Bhattacharyya RP, Hung DT.** 2014. Mechanisms of β -lactam killing and resistance in the context of *Mycobacterium tuberculosis*. *The Journal of Antibiotics* **67**:645–654.
34. **Flores AR, Parsons LM, Pavelka MS.** 2005. Genetic analysis of the beta-lactamases of *Mycobacterium tuberculosis* and *Mycobacterium smegmatis* and susceptibility to beta-lactam antibiotics. *Microbiology* **151**:521–532.
35. **Hugonnet J-E, Blanchard JS.** 2007. Irreversible inhibition of the *Mycobacterium tuberculosis* beta-lactamase by clavulanate. *Biochemistry* **46**:11998–12004.
36. **Mainardi J-L, Hugonnet J-E, Rusconi F, Fourgeaud M, Dubost L, Moumi AN, Delfosse V, Mayer C, Gutmann L, Rice LB, Arthur M.** 2007. Unexpected inhibition of peptidoglycan LD-transpeptidase from *Enterococcus faecium* by the beta-lactam imipenem. *Journal of Biological Chemistry* **282**:30414–30422.
37. **Diacon AH, van der Merwe L, Barnard M, Groote-Bidlingmaier von F, Lange C, García-Basteiro AL, Sevene E, Ballell L, Barros-Aguirre D.** 2016. β -Lactams against Tuberculosis--New Trick for an Old Dog? *N Engl J Med* **375**:393–394.
38. **Dooley, K.** Early Bactericidal Activity of Rifampin + Meropenem + Amoxicillin/Clavulanate in Adults With Pulmonary TB - clinicaltrials.gov/ct2/show/NCT03174184
39. 2016. Synergism Testing: Broth Microdilution Checkerboard and Broth Macrodilution Methods, pp. 5.16.1–5.16.23. *In* *Clinical Microbiology Procedures Handbook*, Fourth Edition. American Society of Microbiology.
40. **Gonzalo X, Drobniewski F.** 2013. Is there a place for β -lactams in the treatment of multidrug-resistant/extensively drug-resistant tuberculosis? Synergy between meropenem and amoxicillin/clavulanate. *J Antimicrob Chemother* **68**:366–369.
41. **Schoonmaker MK, Bishai WR, Lamichhane G.** 2014. Nonclassical transpeptidases of *Mycobacterium tuberculosis* alter cell size, morphology, the cytosolic matrix, protein localization, virulence, and resistance to β -lactams. *Journal of Bacteriology* **196**:1394–1402.
42. **Kieser KJ, Baranowski C, Chao MC, Long JE, Sassetti CM, Waldor MK, Sacchettini JC, Iøerger TR, Rubin EJ.** 2015. Peptidoglycan synthesis in *Mycobacterium tuberculosis*

is organized into networks with varying drug susceptibility. *Proc Natl Acad Sci USA* **112**:13087–13092.

43. **Gengenbacher M, Kaufmann SHE.** 2012. Mycobacterium tuberculosis: success through dormancy. *FEMS Microbiol Rev* **36**:514–532.
44. **Betts JC, Lukey PT, Robb LC, McAdam RA, Duncan K.** 2002. Evaluation of a nutrient starvation model of Mycobacterium tuberculosis persistence by gene and protein expression profiling. *Molecular Microbiology* **43**:717–731.
45. **Gupta R, Lavollay M, Mainardi J-L, Arthur M, Bishai WR, Lamichhane G.** 2010. The Mycobacterium tuberculosis protein LdtMt2 is a nonclassical transpeptidase required for virulence and resistance to amoxicillin. *Nature Medicine* **16**:466–469.
46. **Hugonnet J-E, Tremblay LW, Boshoff HI, Barry CE, Blanchard JS.** 2009. Meropenem-clavulanate is effective against extensively drug-resistant Mycobacterium tuberculosis. *Science* **323**:1215–1218.
47. **Botella H, Yang G, Ouerfelli O, Ehrt S, Nathan CF, Vaubourgeix J.** 2017. Distinct Spatiotemporal Dynamics of Peptidoglycan Synthesis between Mycobacterium smegmatis and Mycobacterium tuberculosis. *mBio* **8**:e01183–17.
48. **Typas A, Banzhaf M, Gross CA, Vollmer W.** 2011. From the regulation of peptidoglycan synthesis to bacterial growth and morphology. *Nature Publishing Group* **10**:123–136.
49. **Balleza E, Kim JM, Cluzel P.** 2017. Systematic characterization of maturation time of fluorescent proteins in living cells. *Nat Meth* **15**:47–51.
50. **Liechti GW, Kuru E, Hall E, Kalinda A, Brun YV, VanNieuwenhze M, Maurelli AT.** 2013. A new metabolic cell-wall labelling method reveals peptidoglycan in Chlamydia trachomatis. *Nature* **506**:507–510.
51. **Hett EC, Rubin EJ.** 2008. Bacterial growth and cell division: a mycobacterial perspective. *Microbiol Mol Biol Rev* **72**:126–56– table of contents.
52. **Wu KJ, Zhang J, Baranowski C, Leung V, Rego EH, Morita YS, Rubin EJ, Boutte CC.** 2018. Characterization of conserved and novel septal factors in Mycobacterium smegmatis. *Journal of Bacteriology* **JB.00649–17**.

53. **Bisson-Filho AW, Hsu Y-P, Squyres GR, Kuru E, Wu F, Jukes C, Sun Y, Dekker C, Holden S, VanNieuwenhze MS, Brun YV, Garner EC.** 2017. Treadmilling by FtsZ filaments drives peptidoglycan synthesis and bacterial cell division. *Science* **355**:739–743.
54. **Eskandarian HA, Odermatt PD, Ven JXY, Hannebelle MTM, Nievergelt AP, Dhar N, McKinney JD, Fantner GE.** 2017. Division site selection linked to inherited cell surface wave troughs in mycobacteria. *Nat Microbiol* **2**:17094.
55. **Rodriguez-Rivera FP, Zhou X, Theriot JA, Bertozzi CR.** 2017. Visualization of mycobacterial membrane dynamics in live cells. *J Am Chem Soc* **139**:3488–3495.
56. **Sani M, Houben ENG, Geurtsen J, Pierson J, de Punder K, van Zon M, Wever B, Piersma SR, Jiménez CR, Daffé M, Appelmelk BJ, Bitter W, van der Wel N, Peters PJ.** 2010. Direct visualization by cryo-EM of the mycobacterial capsular layer: a labile structure containing ESX-1-secreted proteins. *PLoS Pathog* **6**:e1000794.
57. **Plocinski P, Arora N, Sarva K, Blaszczyk E, Qin H, Das N, Plocinska R, Ziolkiewicz M, Dziadek J, Kiran M, Gorla P, Cross TA, Madiraju M, Rajagopalan M.** 2012. Mycobacterium tuberculosis CwsA interacts with CrgA and Wag31, and the CrgA-CwsA complex is involved in peptidoglycan synthesis and cell shape determination. *Journal of Bacteriology* **194**:6398–6409.
58. **Plocinska R, Martinez L, Gorla P, Pandeeti E, Sarva K, Blaszczyk E, Dziadek J, Madiraju MV, Rajagopalan M.** 2014. Mycobacterium tuberculosis MtrB sensor kinase interactions with FtsI and Wag31 proteins reveal a role for MtrB distinct from that regulating MtrA activities. *Journal of Bacteriology* **196**:4120–4129.
59. **Mukherjee P, Sureka K, Datta P, Hossain T, Barik S, Das KP, Kundu M, Basu J.** 2009. Novel role of Wag31 in protection of mycobacteria under oxidative stress. *Molecular Microbiology* **73**:103–119.
60. **Jani C, Eoh H, Lee JJ, Hamasha K, Sahana MB, Han J-S, Nyayapathy S, Lee J-Y, Suh J-W, Lee SH, Rehse SJ, Crick DC, Kang C-M.** 2010. Regulation of polar peptidoglycan biosynthesis by Wag31 phosphorylation in mycobacteria. *BMC Microbiol* **10**:327.
61. **Vollmer W, Joris B, Charlier P, Foster S.** 2008. Bacterial peptidoglycan (murein) hydrolases. *FEMS Microbiol Rev* **32**:259–286.

62. **McNeil M, Daffe M, Brennan PJ.** 1990. Evidence for the nature of the link between the arabinogalactan and peptidoglycan of mycobacterial cell walls. *Journal of Biological Chemistry* **265**:18200–18206.
63. **Alderwick LJ, Harrison J, Lloyd GS, Birch HL.** 2015. The Mycobacterial Cell Wall--Peptidoglycan and Arabinogalactan. *Cold Spring Harb Perspect Med* **5**:a021113.
64. **Gray AN, Egan AJF, Van't Veer IL, Verheul J, Colavin A, Koumoutsi A, Biboy J, Altelaar AFM, Damen MJ, Huang KC, Simorre J-P, Breukink E, Blaauwen den T, Typas A, Gross CA, Vollmer W.** 2015. Coordination of peptidoglycan synthesis and outer membrane constriction during *Escherichia coli* cell division. *eLife* **4**:e07118.
65. **Zimmermann L, Stephens A, Nam S-Z, Rau D, Kübler J, Lozajic M, Gabler F, Söding J, Lupas AN, Alva V.** 2017. A Completely Reimplemented MPI Bioinformatics Toolkit with a New HHpred Server at its Core. *J Mol Biol.*
66. **Kysela DT, Brown PJB, Huang KC, Brun YV.** 2013. Biological consequences and advantages of asymmetric bacterial growth. *Annu Rev Microbiol* **67**:417–435.

Appendices

Appendix 1: Supplementary Data for Chapter 3

Overview: These are the supplemental data for the manuscript (to be submitted) presented in Chapter 3.2.

Attributions: CB and EHR performed the experiments for Figures S1C, D. CB generated the transposon libraries, EHR conceived of the screen and analyzed the data. CB performed the experiments in Figure S2. HCL wrote scripts for and guided data analysis presented in Figure S2A, B. CB and LTS performed the experiments and analyzed data in Figure S3. CB performed the experiments in Figures S5A, B. Data analysis in Figure S5B was done by CB but inspired by EHR. CB performed the experiments in Figure S6 with constructs made by KJK. CB generated strains for Figure S7. MAW performed experiments for Figure S7 with help from CB. CB performed experiments for Figure S8. JCW created strains and performed the experiments in Figure S9. EHR performed the experiment in S10. CB generated all *M.smegmatis* strains except for the one used in S9 (JCW).

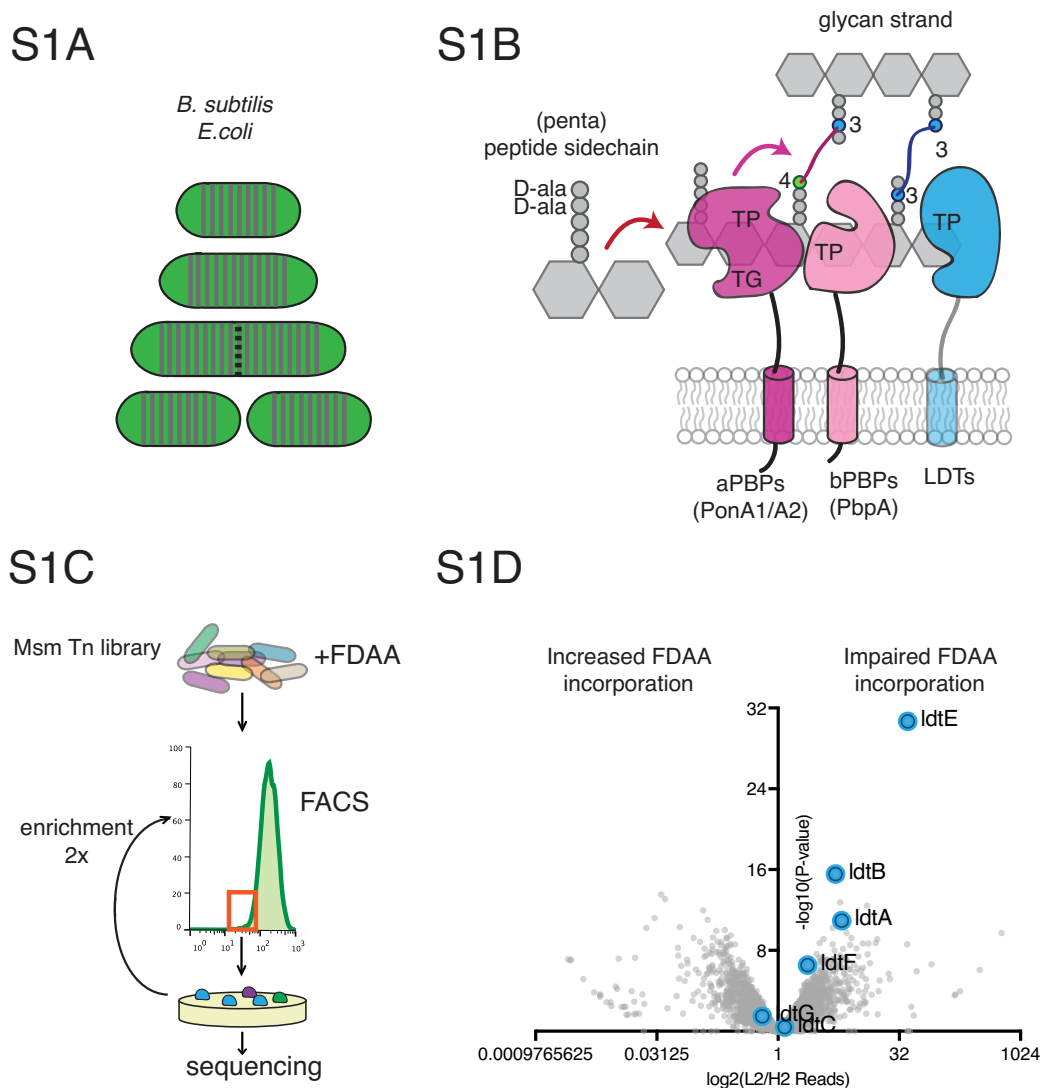


Figure S1: Peptidoglycan synthesis and FDAA screen overview. (A) *E. coli/B. subtilis* lateral cell wall growth. Unlike mycobacteria, *E. coli/B. subtilis* insert new cell wall along the lateral cell body, constantly mixing old and new peptidoglycan. Green portion represents old cell wall, grey portion represents new material. **(B)** Cartoon of penicillin binding proteins (PBPs), L,D-transpeptidases (LDTs), and both 4-3 and 3-3 crosslinking. PBPs utilize a pentapeptide substrate found on new peptidoglycan, ending in D-alanine-D-alanine. LDTs utilize a tetrapeptide substrate found on processed peptidoglycan. **(C)** Schematic of FACs based FDAA transposon

Figure S1 (Continued)

library enrichment. A *Mycobacterium smegmatis* transposon library was stained with FDAAs, and the dimmest cells were sorted, grown, sorted again to enrich for transposon mutants that are unable to incorporate FDAA. **(D)** Results from S1C screen- Ratio (\log_2) of transposon reads per gene in the second sort low FDAA staining (L2) over the second sort high FDAA staining (H2) compared to the Mann-Whitney U P-value.

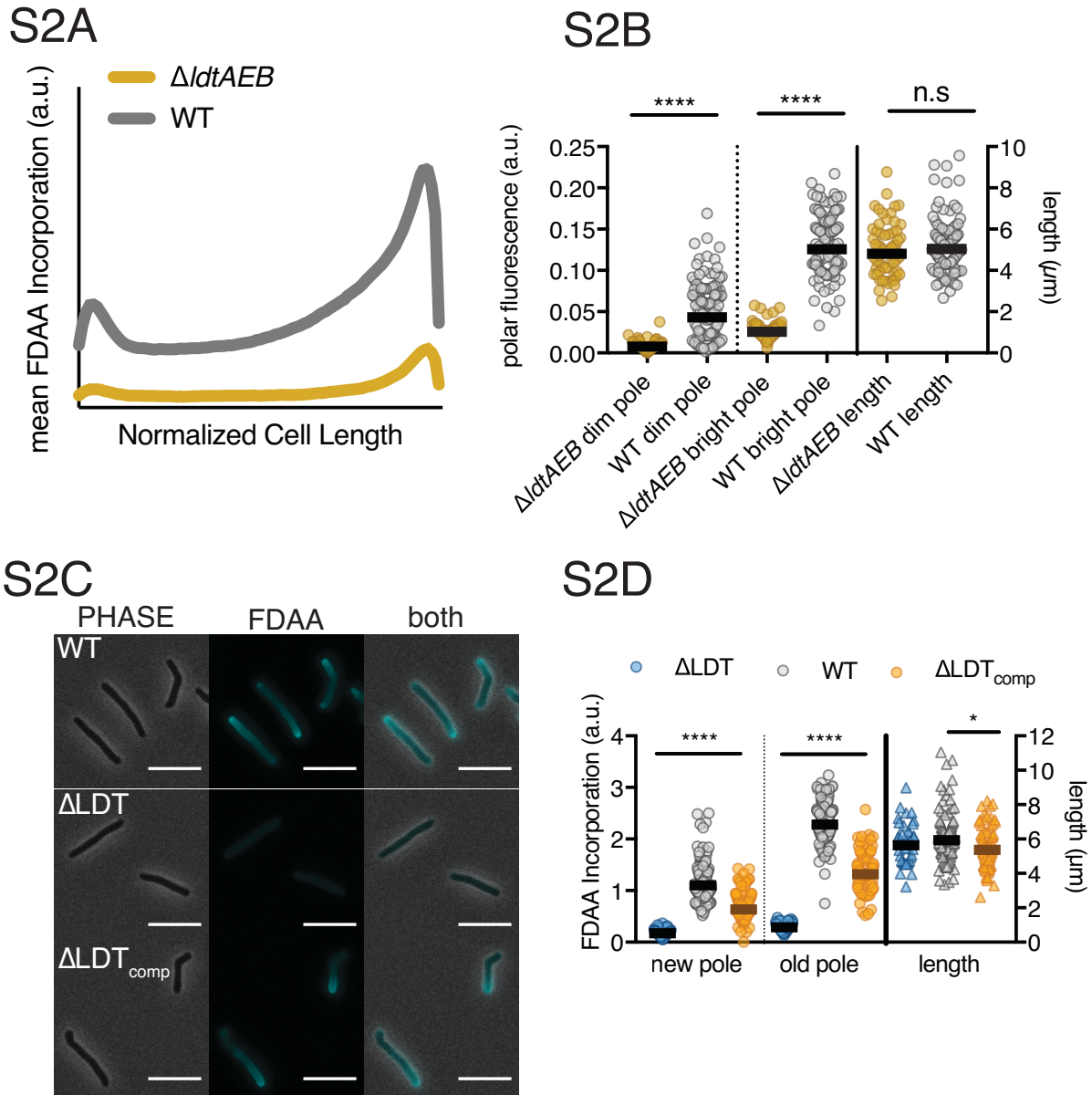


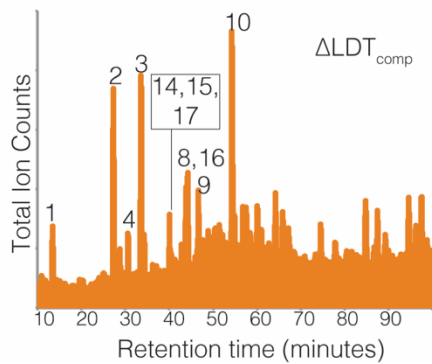
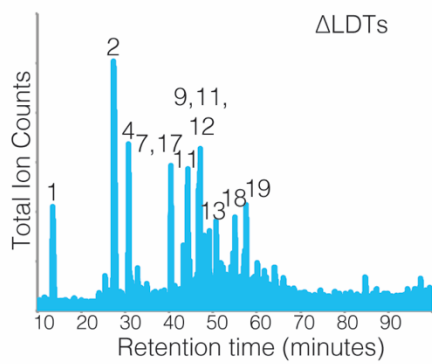
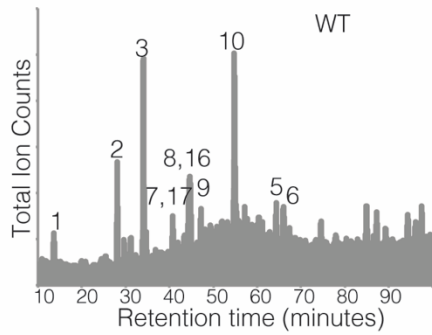
Figure S2: Fluorescent D-amino acid screen validation. (A) Mean line profiles (from new to old pole) of FDAA incorporation in log-phase WT (N=97), $\Delta ldtABE$ (N=64). (B) Quantification of FDAA incorporation at cell poles and quantification of cell length. Mann-Whitney U P-Value shown (**** P-Value < 0.0001). (C) Representative image of FDAA incorporation in log-phase WT, ΔLDT and ΔLDT_{comp} cells. Scale bar= 5 μm . (D) Quantification of FDAA incorporation at

Figure S2 (Continued)

poles and cell lengths of WT, Δ LDT and Δ LDT_{comp} cells shown in S2C and whose mean incorporation is shown in Figure 3.3C.

S3A

S3B



PEAK	Tripeptides observed	Description*
1	461.2	
Tetrapeptides observed		
2	532.3	Tetra (2 NH ₂)
3	534.2	Tetra (OH)
4	533.2	Tetra (NH ₂)
pentapeptides observed		
5	604.3	Penta (OH)
6	602.3	Penta(2 NH ₂)
4-3 observed		
7	974.5	4--3 (2 NH ₂)
8	1045.4	4--4 (4 NH ₂)
9	1046.5	4--4 (3 NH ₂)
10	1049.4	4--4
11	975.4	4--3 (NH ₂)
12	974.3	4--3 (2 NH ₂)
13	1047.5	4--4 (2 NH ₂)
3-3 observed		
14	974.4	4--3 (4 NH ₂)
15	904.4	3--3 (3 NH ₂)
16	975.5	4--3 (3 NH ₂)
Tripeptide(anhydrous)		
17	865.4	
4--4--4		
18	1559.7	
19	1560.0	

S3C

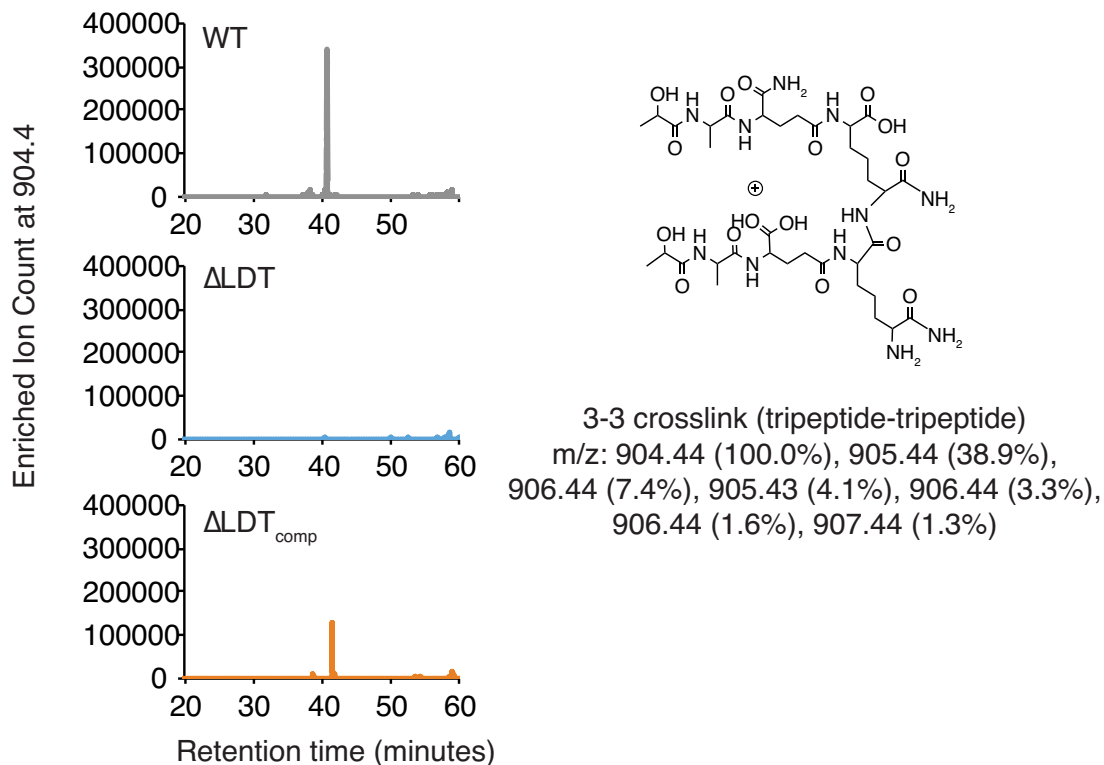


Figure S3: 3-3 crosslinks are not detectable in Δ LDT cells. (A) Total ion chromatograms of WT, Δ LDT and Δ LDT_{comp} peptidoglycan. (B) Table of muropeptide masses (Da) observed in (S6A). The molecular weight difference by one of the identified peptides is due to differential amidation. The descriptions include the peptide lengths in the crosslink (4= tetra-, 3= tri- peptide) and the following parenthesis specifies the number of amidation in the species according to mass. (C) Extracted ion chromatograms from WT, Δ LDT and Δ LDT_{comp} for a representative 3-3 crosslink with a m/z=904.4.

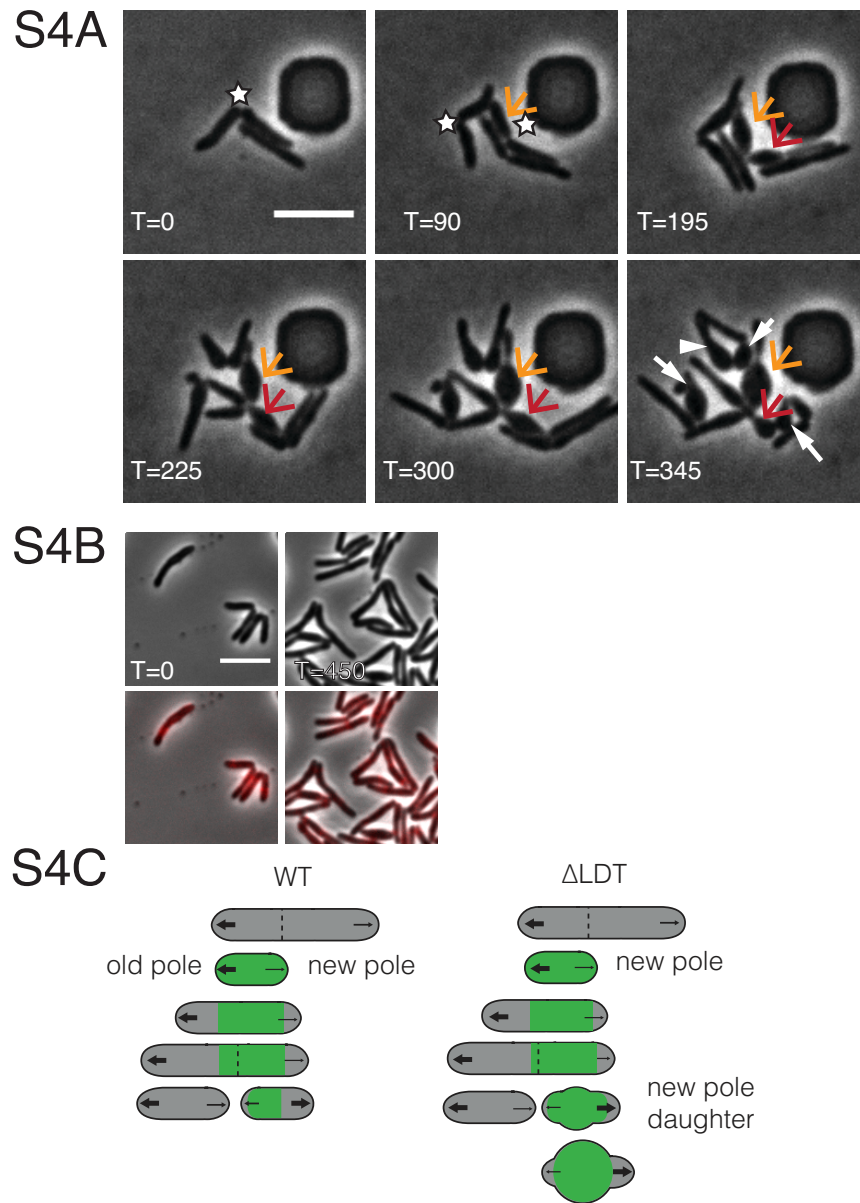
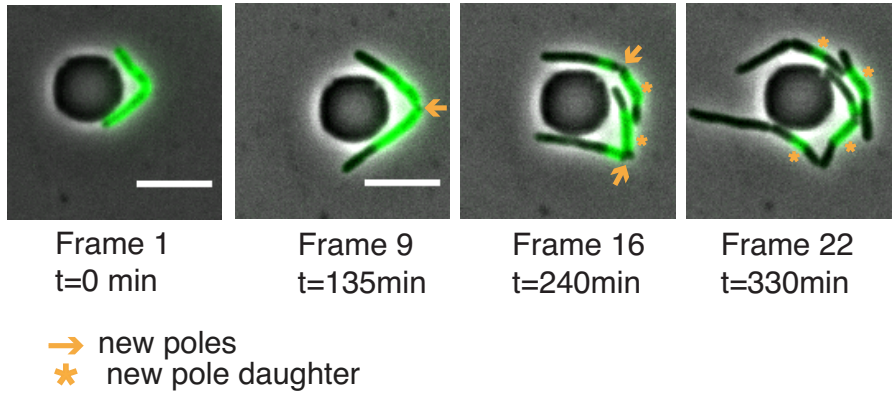


Figure S4: Δ LDT cell morphological characteristics. (A) Time-lapse microscopy montage of Δ LDT cells. The white stars mark new poles. The orange arrow points to the first new pole daughter cell of this series. The red arrow indicates the second resulting new pole daughter cell. In the last frame, white arrows point to all new pole daughter cells (besides the orange arrow and red arrow). (B) Time-lapse microscopy of Δ LDT_{comp} cells expressing TetO-ldtE-mRFP. (C)

Figure S4 (Continued)

Model of rod shape loss in old cell wall of Δ LDT cells compared to WT. Green portions of the cell represents old cell wall, grey portion represents new cell wall. The larger arrows indicate more growth from the old pole, while smaller arrows show less relative growth from the new pole. Dotted lines represent septa. All scale bars=5 μ m

S5A



S5B

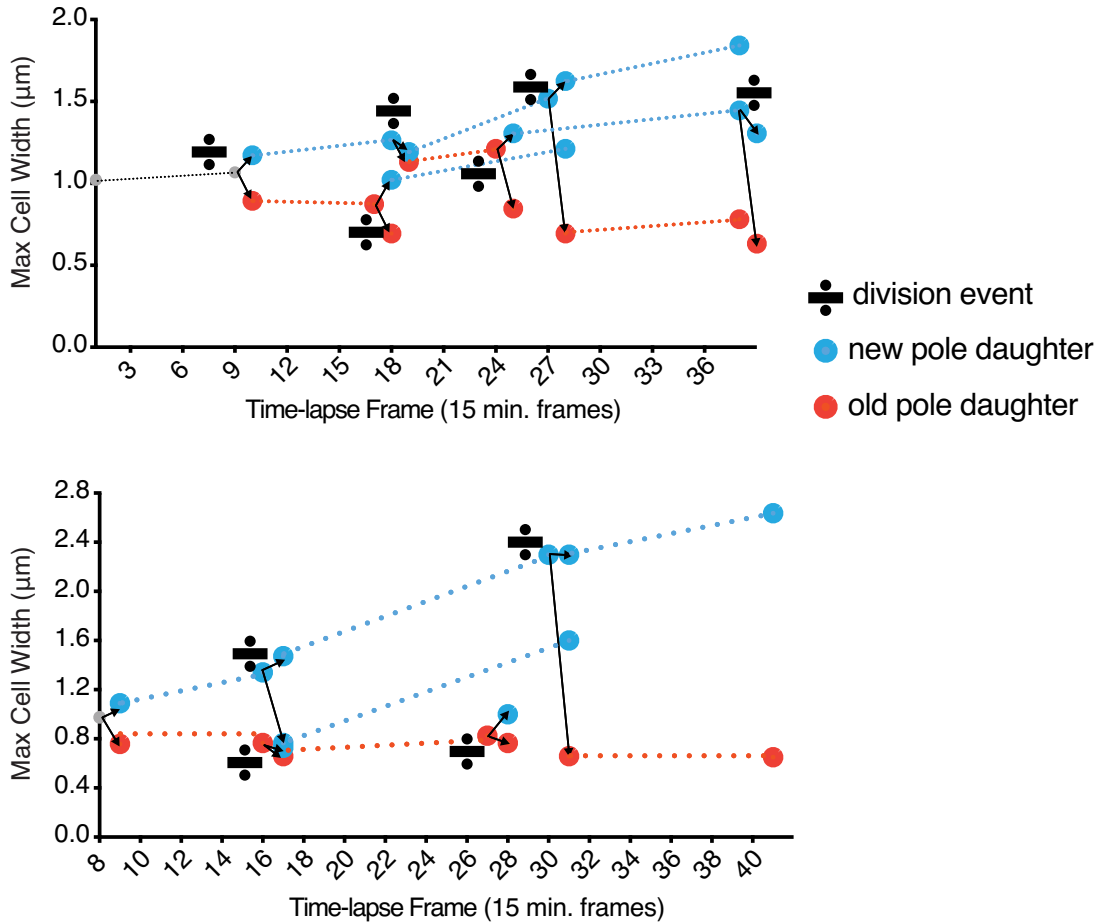


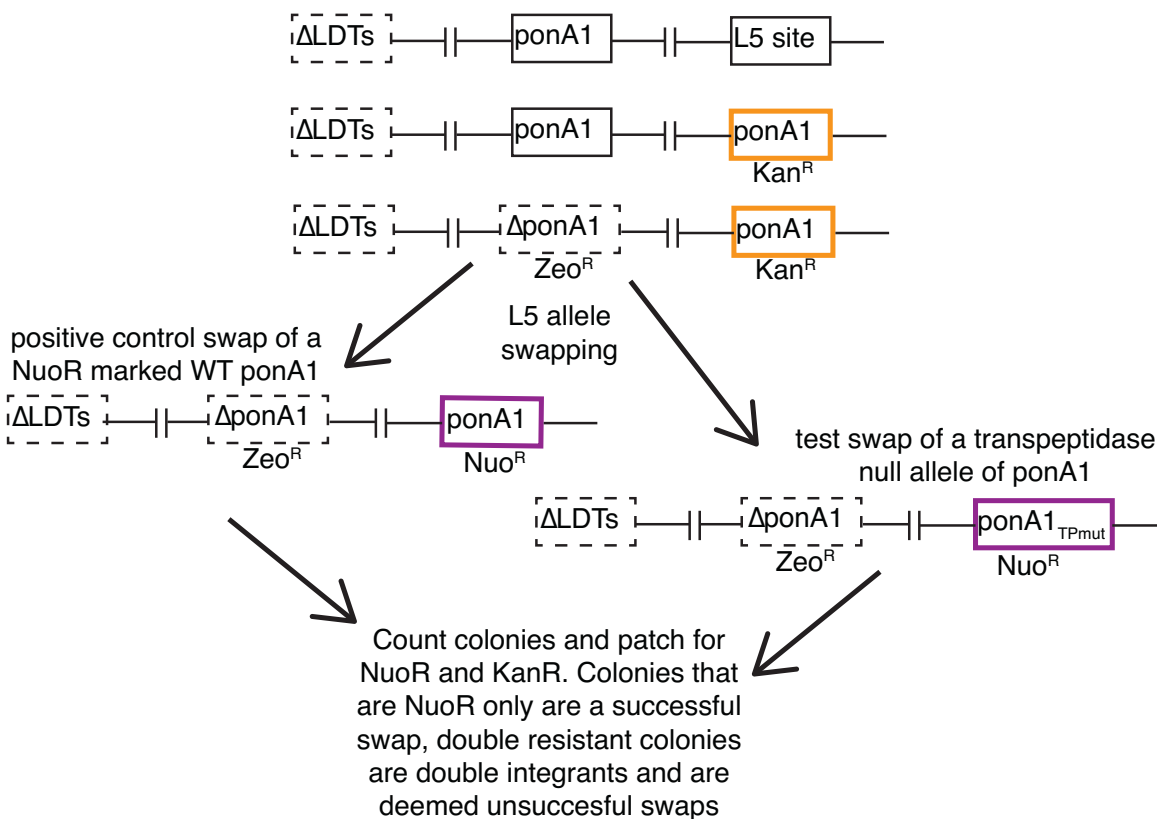
Figure S5: Inheritance of old cell wall and occurrence of blebs in new pole daughter cells.

(A) WT *Mycobacterium smegmatis* stained with Alexa Fluor™ 488 NHS ester, washed and

Figure S5 (Continued)

visualized over time. New material is unstained, old material is stained green. Orange arrows indicate a new pole. Orange stars mark new pole daughter cells. All scale bars=5 μ m **(B)** Maximum cell width of Δ LDT cell lineages over time. Width of new pole daughters is plotted as a blue circle and width of old pole daughters is an orange circle. Division signs denote a division event. At each division, there are two arrows from the dividing cell leading to the resulting new and old pole daughter cell widths (blue and orange respectively).

S6A



S6B

Genetic Background: Δ LDT Δ ponA1 // L5 TetO-ponA1 WT (KanR)	Number of colonies	Proportion of true swaps
SWAP: L5 TetO-ponA1 WT (NuoR)	249	26/50
SWAP: L5 TetO-ponA1 TP mutant (NuoR)	0	

Figure S6: L5 allele swapping to test essentiality of ponA1's ability to form 4-3 crosslinks (transpeptidation). (A) Schematic of L5 allele swapping experiment. Adapted from Kieser *et al* 2015. (B) Results of *ponA1* allele swapping experiment in Δ LDT cells.

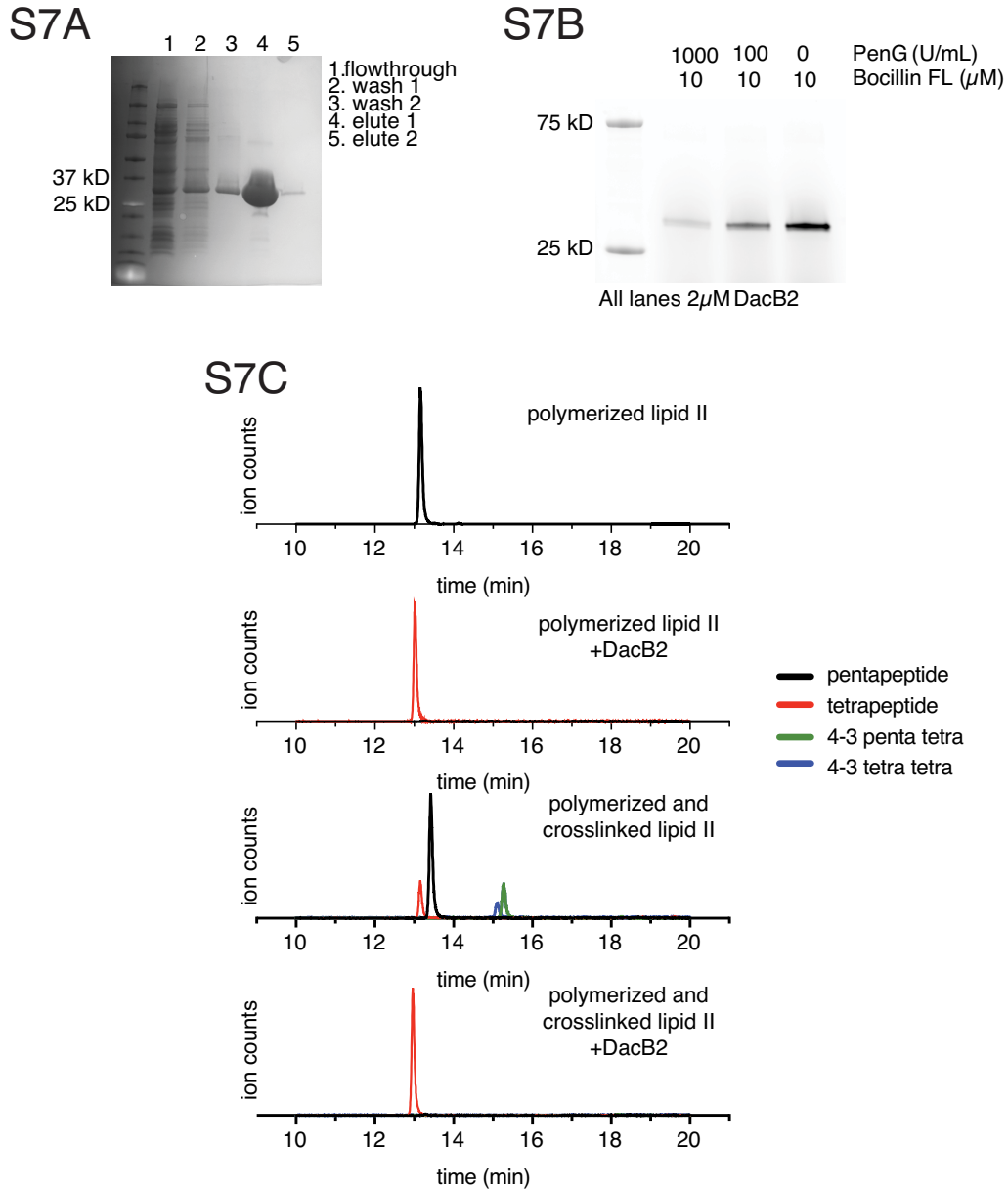
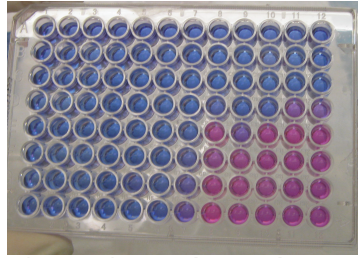


Figure S7: MSMEG_2433 (DacB2) functions as a D,D-carboxypeptidase and D,D-endopeptidase *in vitro*. (A) Coomassie gel of purified 6XHIS-DacB2. (B) Bocillin-FL and Penicillin G binding assay of purified DacB2. (C) Extracted ion chromatograms of the substrates (polymerized lipid II, polymerized and crosslinked lipid II for D,D-carboxy- or D,D-endopeptidase activity respectively) and of the products of substrate incubation with DacB2.

S8A



	1	2	3	4	5	6	7	8	9	10	11	12
A	10.00	10.00	10.00	10.00	10.00	10.00	10.00	10.00	10.00	10.00	10.00	
	10.00	5.00	2.50	1.25	0.63	0.31	0.16	0.08	0.04	0.02	0.01	
B	5.00	5.00	5.00	5.00	5.00	5.00	5.00	5.00	5.00	5.00	5.00	
	10.00	5.00	2.50	1.25	0.63	0.31	0.16	0.08	0.04	0.02	0.01	
C	2.50	2.50	2.50	2.50	2.50	2.50	2.50	2.50	2.50	2.50	2.50	
	10.00	5.00	2.50	1.25	0.63	0.31	0.16	0.08	0.04	0.02	0.01	
D	1.25	1.25	1.25	1.25	1.25	1.25	1.25	1.25	1.25	1.25	1.25	
	10.00	5.00	2.50	1.25	0.63	0.31	0.16	0.08	0.04	0.02	0.01	
E	0.63	0.63	0.63	0.63	0.63	0.63	0.63	0.63	0.63	0.63	0.63	
	10.00	5.00	2.50	1.25	0.63	0.31	0.16	0.08	0.04	0.02	0.01	
F	0.31	0.31	0.31	0.31	0.31	0.31	0.31	0.31	0.31	0.31	0.31	
	10.00	5.00	2.50	1.25	0.63	0.31	0.16	0.08	0.04	0.02	0.01	
G	0.16	0.16	0.16	0.16	0.16	0.16	0.16	0.16	0.16	0.16	0.16	
	10.00	5.00	2.50	1.25	0.63	0.31	0.16	0.08	0.04	0.02	0.01	
H	0.08	0.08	0.08	0.08	0.08	0.08	0.08	0.08	0.08	0.08	0.08	
	10.00	5.00	2.50	1.25	0.63	0.31	0.16	0.08	0.04	0.02	0.01	

S8B

	1	2	3	4	5	6	7	8	9	10	11	12	
A													
	40.00	20.00	10.00	5.00	2.50	1.25	0.63	0.31	0.16	0.08	0.04	0.02	amoxicillin
B													
	40.00	20.00	10.00	5.00	2.50	1.25	0.63	0.31	0.16	0.08	0.04	0.02	
C													
	40.00	20.00	10.00	5.00	2.50	1.25	0.63	0.31	0.16	0.08	0.04	0.02	
D													
	40.00	20.00	10.00	5.00	2.50	1.25	0.63	0.31	0.16	0.08	0.04	0.02	meropenem

Figure S8: Minimum inhibitory concentration (MIC) of amoxicillin or meropenem alone or in combination against *Mycobacterium tuberculosis*. (A) Resazurin MIC plate and dilution

Figure S8 (Continued)

matrix of amoxicillin and meropenem in combination in a checkerboard MIC plate. The table below shows the concentration of each drug per well in $\mu\text{g/mL}$. The concentration of meropenem is in black text and the concentration of amoxicillin is in red text in each well. **(B)** Dilution matrix of amoxicillin or meropenem (alone). The concentrations of drugs are shown in the table. Pink indicates metabolically active cells, blue indicates not metabolically active. In both single drug and checkerboard MIC plates, $5\mu\text{g/mL}$ clavulanate was used.

S9

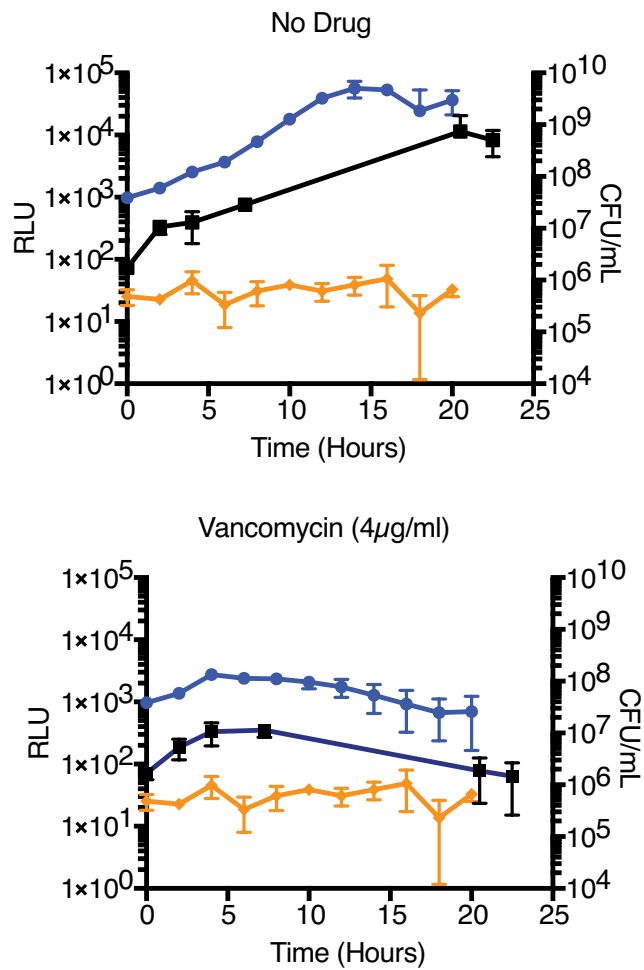
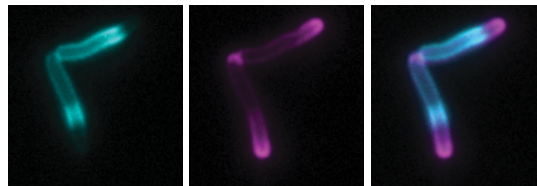
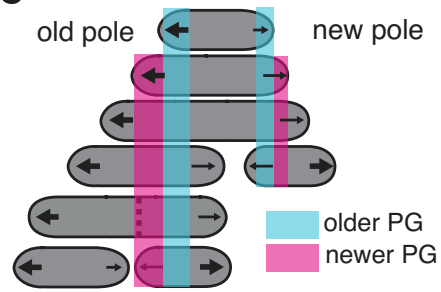


Figure S9: Light production (RLU) correlated to colony forming units (CFU) in mycobacterial cells expressing *luxABCDE* in drug treatment. (A) *Mycobacterium smegmatis* colony forming units (CFU) and luminescence (RLU) during drug treatment.

S10



PULSE CHASE BOTH

Figure S10: New and old cell wall are spatially segregated in mycobacteria. 2-minute FDAA pulse (cyan), 45-minute outgrowth, followed by 2-minute FDAA chase (magenta) in WT *Mycobacterium smegmatis* cells. Newest cell wall (magenta), older cell wall (cyan).

Supplemental Table 1: Strains

Strain	Description	Primers
KB134	mc2155 Δ ldtA::loxP	208/209; 210/211
KB156	mc2155 Δ ldtA::loxP + Δ ldtE::zeoR	220/221; 222/223
KB200	mc2155 Δ ldtA::loxP Δ ldtE::zeoR + Δ ldtB::hygR	444/445; 446/447
KB209	mc2155 Δ ldtA::loxP Δ ldtE::loxP Δ ldtB::loxP + Δ ldtC::hygR	216/448; 449/219 (create original hyg KO) but used 507/508; (amplify KO from strain within the flanks)
KB222	mc2155 Δ ldtA::loxP Δ ldtE::loxP Δ ldtB::loxP Δ ldtC::hygR Δ ldtG::zeoR	228/454; 455/231 (create original hyg KO) but used 513/514; (amplify KO from strain within the flanks)
KB303 (Δ LDT)	mc2155 Δ ldtA::loxP Δ ldtE::loxP Δ ldtB::loxP Δ ldtC::loxP Δ ldtG::loxP Δ ldtF::hygR	224/452; 453/227 (create hyg KO) but used 511/512 (amplify KO from strain or gibson)
KB302	pTetO-ldtE(MSMEG_0233)-linker-mRFP in CT94 XH (XL1-Blue)	323A/351; 352/353
KB316 (Δ LDTcomp)	[mc2155 Δ ldtA::loxP Δ ldtE::loxP Δ ldtB::loxP Δ ldtC::loxP Δ ldtG::loxP Δ ldtF::hygR] + KB302	
KB428	<i>E. coli</i> BL21 + pet28b (dacB2)	662/663

Supplemental Table 2: Primers.

Primer description	Primer Sequence	5' or 3' features	Primer #
MSMEG_3528 (ldtA) upstream flanking region FOR	CGTTGTAAAACGACGGCCAG TGATGGCGGGCGTGATCTG GAATCTCT	pUC57 overlap	208
MSMEG_3528 (ldtA) upstream flanking region REV	ACCCAACCTTAATCGCCTTGC AGCTCTTCCAGTGTAGGTTG TCGAAACG	Zeo cassette overlap	209
MSMEG_3528 (ldtA) downstream flanking region FOR	TAATCATGGTCATAGCTGTTT TCATCGTGCAGGCGTGACGT GCAG	Zeo cassette overlap	210
MSMEG_3528 (ldtA) downstream flanking region REV	CAGTCGACGGGCCCGGGAT CCGCGGTGGTGCCCTTGGT GATGGTC	pUC57 overlap	211
MSMEG_0233 (ldtE) upstream flanking region FOR	CGTTGTAAAACGACGGCCAG TGGCTGTCCGCCAGCCCC GGGCC	pUC57 overlap	220
MSMEG_0233 (ldtE) upstream flanking region REV	CCAACCTTAATCGCCTTGCAG CGTGGTACCTCCAGAGCACAA ACTG	Zeo cassette overlap	221
MSMEG_0233 (ldtE) downstream flanking region FOR	GTAATCATGGTCATAGCTGT TTCCGGACGTCATACGAAGA ACCCCC	Zeo cassette overlap	222
MSMEG_0233 (ldtE) downstream flanking region REV	GCAGTCGACGGGCCCGGGA TCTGGACCGACGCCGACCG CACCG	pUC57 overlap	223
MSMEG_4745 (ldtB) upstream flanking region FOR	GGTCGAGATGCTCCTGGAA GAGGCCG		444
MSMEG_4745 (ldtB) upstream flanking region REV	GAGCTCCAATTCGCCCTACG TCGTTACCTGCCCATCACG	hyg cassette overlap	445
MSMEG_4745 (ldtB) downstream flanking region FOR	GTACCTCGAGTCTAGAAGTA GCGCTATCGCACCGCGCGG TCCAG	hyg cassette overlap	446
MSMEG_4745 (ldtB) downstream flanking region REV	CGACCCGGCCCGTCACAAG GACACCGAAC		447
MSMEG_0929 (ldtC) upstream flanking region FOR	CGTTGTAAAACGACGGCCAG TGAAGTGGCGACGGCGCTG GGCGTGG	pUC57 overlap	216

Supplemental Table 2: Primers (Continued)

MSMEG_0929 (ldtC) upstream flanking region REV	TGGAGCTCCAATTCGCCCTA GTGGATCTAGGGTACCGACA GCACGC	hyg cassette overlap	448
MSMEG_0929 (ldtC) downstream flanking region FOR	GGTACCTCGAGTCTAGAAGT AGTCCGGCGGCTAGGTCCG GCGGTTGAAG	hyg cassette overlap	449
MSMEG_0929 (ldtC) downstream flanking region REV	CAGTCGACGGGCCCGGGAT CCCAAGGGACTCGCGCCGG TCTCC	pUC57 overlap	219
MSMEG_0929 (ldtC) upstream flanking region FOR	GGCTCGTTCTTCACCAACC		507
MSMEG_0929 (ldtC) downstream flanking region REV	CTGCCCAAGCTCATCGAC		508
MSMEG_0674 (ldtG) upstream flanking region FOR	GTTGTAAAACGACGGCCAGT GCGGCGTTCGACCTCCCGGC CGGGTC	pUC57 overlap	228
MSMEG_0674 (ldtG) upstream flanking region REV	GTGGAGCTCCAATTCGCCCT AGCGCATTGGCTTCCGATTT CCCTCG	hyg cassette overlap	454
MSMEG_0674 (ldtG) downstream flanking region FOR	CGGTACCTCGAGTCTAGAAG TACGCCGACGTGTATGCCCA CCCCCGCG	hyg cassette overlap	455
MSMEG_0674 (ldtG) downstream flanking region REV	GCAGTCGACGGGCCCGGGA TCGCCTGCGCCCGCGGGAG CGCCTGCC	pUC57 overlap	231
MSMEG_0674 (ldtG) upstream flanking region FOR	GCATCTGAGTTTCGGCAAG		513
MSMEG_0674 (ldtG) downstream flanking region REV	CAACTACCCCGCAGTTGAAT		514
MSMEG_1322 (ldtF) upstream flanking region FOR	GTTGTAAAACGACGGCCAGT GCGAGGTAAGGGTCTCGAC GGTTTCT	pUC57 overlap	224
MSMEG_1322 (ldtF) upstream flanking region REV	GTGGAGCTCCAATTCGCCCT ATCCAATGTGCTTCGGCGAA AGCCAGTTTG	hyg cassette overlap	452
MSMEG_1322 (ldtF) downstream flanking region FOR	GTACCTCGAGTCTAGAAGTA GTTCCCCCGGCCACATAT GTCTGGACG	hyg cassette overlap	453

Supplemental Table 2: Primers (Continued)

MSMEG_1322 (ldtF) downstream flanking region REV	GCAGTCGACGGGCCCGGGA TCCACGACAACGCCAGCGC GAT	pUC57 overlap	227
MSMEG_1322 (ldtF) upstream flanking region FOR	GGTCGACGACGAACTGGT		511
MSMEG_1322 (ldtF) downstream flanking region REV	AACGGCACGTACATCAGGAC		512
MSMEG_0233 (ldtE) FOR with TetO overlap (vector)	CATGCTTAATTAAGAAGGAG ATATACAATGCCGAAATCGG CAAACGCAG		323A
MSMEG_0233 (ldtE) REV (no stop codon) with ser-ser-gly linker	GATGACGTCCTCGGAGGAG GCCGAGCCGCCAACATCT GCCAGTCGGATG		351
mRFP FOR with ser-ser-gly linker	CATCCGACTGGCAGATGTTC GGCGGCTCGGCCTCCTCCG AGGACGTCATC		352
mRFP REV with vector overlap	GTCCCAATTAATTAGCTAA GTGATGGTGGTGGTGGTGGT AGGCG		353
MSMEG_2433 (dacB2) FOR (first 27 amino acids truncated)	GGCCTGGTGCCGCGCGGCA GCCATCGCGCGGACGCCGA CATCCAG	with 5' overlaps to pet28b cut with NdeI	662
MSMEG_2433 (dacB2) REV	GCTGTCCACCAGTCATGCTA GCCATCAGAGCGCCCGAT GCTCG	with 3' overlaps to pet28b cut with NdeI	663

Appendix 2: BlaR, a protein canonically implicated in β -lactam sensing, is critical for *Mycobacterium tuberculosis* fitness in low iron conditions

Overview: These are data in a manuscript in preparation titled, “Genome-wide Phenotypic Profiling Identifies *blaR* as Required for Mycobacterial Fitness in Low Iron.”

Attributions: CB constructed the *M. tuberculosis* *blaR* knock-out strain, as well as the *M. smegmatis* *blaR* knock-out and tagged *blaI* strain. CB performed the experiments and data analysis in the below presented figures. Alex Meeske helped build the phylogenetic tree. MSD wrote the abstract, significance statement and compiled the materials and methods below. CB edited these materials.

Authors: Marte S. Dragset^{a,b,c}, Catherine Baranowski^b, Thomas R. Ioerger^d, Yanjia J. Zhang^b, Mali Mærk^a, Zekarias Ginbot^a, Trude H. Flo^a, Magnus Steigedal^{a,b,c,e,*}, Eric J. Rubin^{b,*}.

Centre of Molecular Inflammation Research, Department of Cancer Research and Molecular Medicine, NTNU Norwegian University of Science and Technology, 7491 Trondheim, Norway^a; Department of Immunology and Infectious Diseases, Harvard T.H. Chan School of Public Health, Boston, MA 02115, USA^b; Department of Biotechnology, NTNU Norwegian University of Science and Technology, 7491 Trondheim, Norway^c; Department of Computer Science, Texas A&M University, College Station, TX 77843, USA^d; Central Norway Regional Health Authority, 7501 Stjørdal, Norway^e

* The authors contributed equally to this work.

Abstract

Iron is vital for nearly all living organisms but during infection not readily available to pathogens. Infectious organisms therefore depend on specialized mechanisms to survive when iron is limited. *Mycobacterium tuberculosis* (*Mtb*), the causative agent of tuberculosis (TB), can scavenge host-sequestered iron by high-affinity iron chelators called siderophores. Here, by transposon insertion sequencing, we take advantage of siderophore redundancy within the non-pathogenic mycobacterial model organism *M. smegmatis* (*Msmeg*) to identify and categorize mycobacterial genetic requirements for fitness in low iron. We also provide the *Msmeg* essential gene set. Among genes with a potential function in recognition, transport or utilization of mycobacterial siderophores, we identify novel low iron survival strategies separate from siderophores. We find that the putative signal transduction protein BlaR is essential for mycobacterial fitness in low iron (Figure S11), independently of siderophores, and that BlaR regulates its operonic transcriptional repressor protein BlaI in response to iron levels (Figure S12). Our findings support a hitherto undescribed crucial role of BlaR and the downstream BlaI regulon for *Mtb* low iron fitness. This is the first time this regulon has been directly implicated in pathogen fitness via an iron specific mechanism.

Significance

Mechanisms that promote pathogen proliferation within the iron-scarce host environment are attractive targets for new drugs. By genome-wide phenotypic profiling, we identify and categorize novel mycobacterial genetic requirements for low iron fitness. We demonstrate that the gene encoding the putative transducer BlaR is required for low iron growth in the important human pathogen *Mycobacterium tuberculosis* (Figure S11). BlaR is in some pathogens implicated in β -

lactam sensing and resistance via control of transcriptional repressor BlaI. Mycobacterial BlaR lacks an apparent β -lactam sensing domain and we show that BlaR controls BlaI in response to iron (Figure S12). Actually, BlaR lacking the β -lactam receptor domain appears more widespread among bacteria than the full-length protein (Figure S13). This may suggest a role for BlaR in low iron fitness beyond mycobacteria.

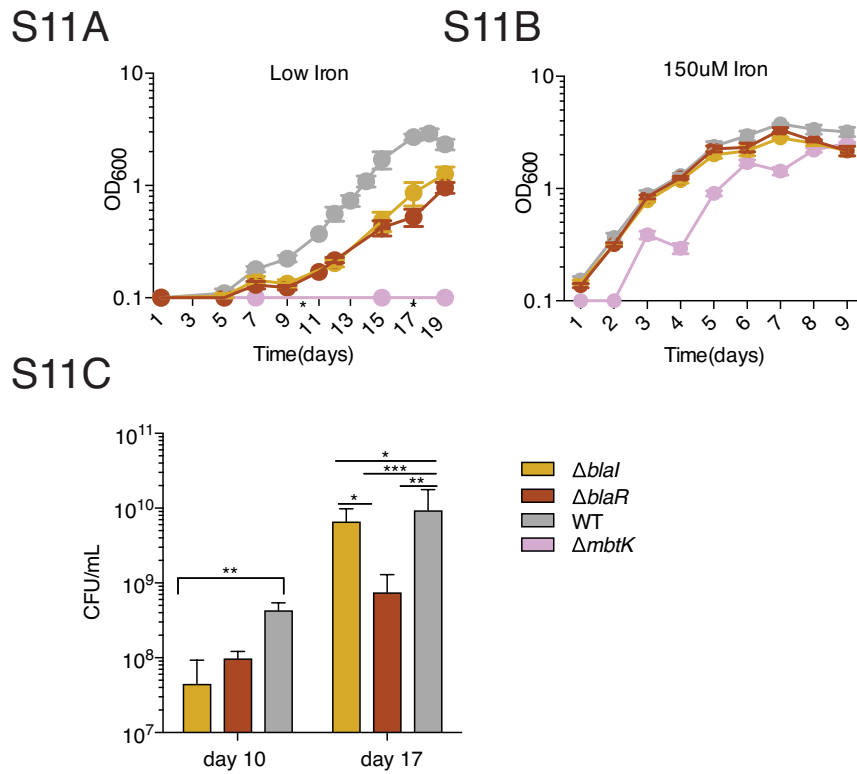


Figure S11: *blaR* is required for optimal Mtb growth in low iron. (A) Optical density measurements (OD₆₀₀) of WT and $\Delta blaR$ Mtb strains in low (A) or high (B) iron media. (C) CFU counts of WT, $\Delta blaI$ or $\Delta blaR$ Mtb measured at day 10 and 17 of low iron growth. Significance determined by T-test. *P-Value < 0.05, **P-Value < 0.005, *** 0.0005 < P-Value > 0.005.

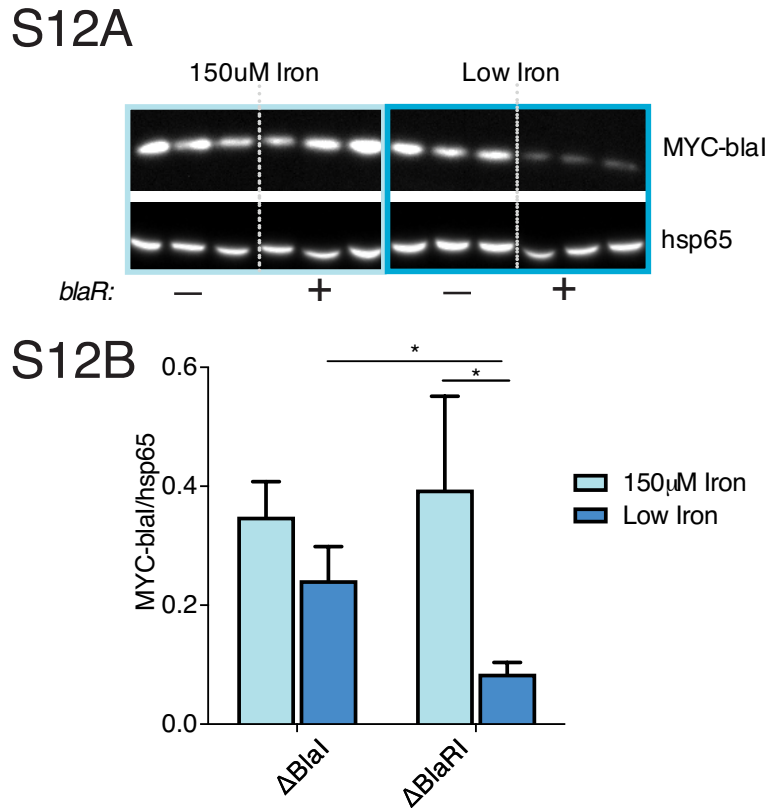


Figure S12: BlaR regulates BlaI levels in response to iron. (A) Levels of myc-tagged BlaI in *Msm* Δ *blaI* strains constitutively expressing myc-tagged BlaI (MYC-BlaI) from an integrating plasmid with the *blaR* gene either intact (+) or knocked out (-), grown in triplicate in high or low iron before proteins were isolated for western blotting. Hsp65 is used as a loading control. **(B)** The quantity of MYC-BlaI normalized to the quantity of hsp65. * denotes T-test P-Value < 0.05. Error bars represent standard deviation of three biological replicas.

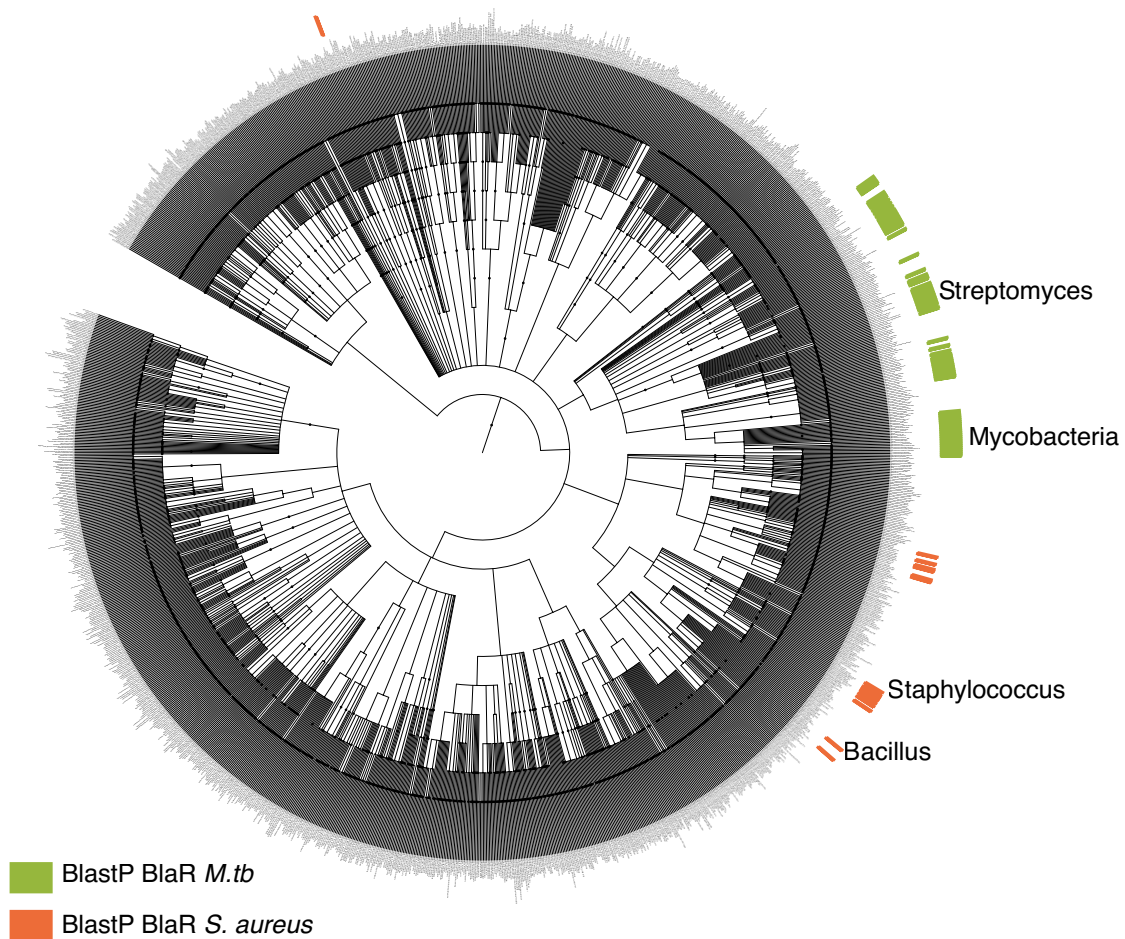


Figure S13: BlaR lacking the β -lactam receptor domain appears more widespread among bacterial species than the full-length protein.

Mtb BlaR and *S. aureus* BlaR protein sequences were used in a BlastP search against the non-redundant database. The results were mapped onto NCBI's Representative Genomes (bacterial taxa), and the tree was generated with phyloT and visualized with iTOL.

Materials and methods

M. smegmatis strain construction

Knockouts of *blaI*, *blaR* and the *blaRI* operon were made via recombineering. A zeocin resistance marker flanked by loxP sites was ligated via isothermal assembly to the 500 base pairs up- and down-stream of the genes to be replaced. This linear knockout cassette was amplified via PCR, gel-purified and transformed into Msm expressing inducible copies of RecET. After PCR screening knockout colonies, the zeocin marker was removed by transforming a Cre recombinase plasmid. For Western blotting, *blaI* was tagged on the N-terminus with a myc tag. This was expressed from a constitutive TetO promoter (UV15 derivative) on an L5 integrating vector.

M. tuberculosis strain construction

The *blaR* (*rv1845c*) deletion mutant was generated as described above for Msm knockouts. Briefly, *blaR* was replaced with a hygromycin resistance cassette via recombineering. The *blaR* KO strain was verified via whole genome sequencing.

Western blot

Msm cells were spun at 5000 rpm for 5 minutes. The pellet was resuspended in 500 µl PBS + protease inhibitor cocktail. The cells were lysed via bead-beating. Laemmli buffer was added to the lysate and boiled for 10 minutes. The proteins were run on a 4–12% NuPAGE Bis Tris precast gel (Life Technologies, Beverley, MA) and transferred to a PVDF membrane. This was incubated with either anti-MYC antibody (1:5000 dilution) or anti-hsp65 antibody (1: 2000) (loading control) overnight at 4 °C. The membrane was washed three times with TBST (0.1% Tween20) and incubated in secondary HRP-linked antibody (1:5000) for 1 hour at room temperature. The

membranes were washed and incubated with SuperSignal chemiluminescent reagent (Thermo Fisher Scientific, Rockford, IL) for five minutes before imaging on a Protein Simple. Background was subtracted from 16-bit western blot images based on the mean background value. The integrated density of each lane was measured using FIJI. MYC-BlaI values were normalized to control hsp65 values for each sample. The mean and standard deviation of triplicate samples was calculated. An unpaired 2-sided T-test with equal SD was used to compare normalized MYC-BlaI signal (Graphpad Prism 7).

Phylogenetic Tree Construction

Mycobacterium tuberculosis BlaR (UniProt accession P95164) and *Staphylococcus aureus* BlaR (UniProt accession P18357), MTB and STAAU hereafter, protein sequences were used in a BLASTp search against the nr database. We used a query coverage cutoff of 72% to ensure hits were true homologs covering both domains of STAAU. This cutoff was applied to MTB blaR as well. We used an evalue cutoff of $1e-4$. The results were mapped onto a phylogenetic tree of 1773 bacterial taxa. The tree was generated with phyloT (<http://phylot.biobyte.de/index.html>) and visualized with iTOL(<http://itol.embl.de/>). Hits that significantly mapped to MTB BlaR are in green, while those that mapped to STAAU blaR are in orange.